Lecture Notes in Civil Engineering

Sunil Kumar
Makarand M. Ghangrekar
Abhijit Kundu *Editors*

Sustainable Environmental Engineering and Sciences

Select Proceedings of SEES 2021

Springer

Lecture Notes in Civil Engineering

Volume 323

Series Editors

Marco di Prisco, Politecnico di Milano, Milano, Italy

Sheng-Hong Chen, School of Water Resources and Hydropower Engineering, Wuhan University, Wuhan, China

Ioannis Vayas, Institute of Steel Structures, National Technical University of Athens, Athens, Greece

Sanjay Kumar Shukla, School of Engineering, Edith Cowan University, Joondalup, WA, Australia

Anuj Sharma, Iowa State University, Ames, IA, USA

Nagesh Kumar, Department of Civil Engineering, Indian Institute of Science Bangalore, Bengaluru, Karnataka, India

Chien Ming Wang, School of Civil Engineering, The University of Queensland, Brisbane, QLD, Australia

Lecture Notes in Civil Engineering (LNCE) publishes the latest developments in Civil Engineering—quickly, informally and in top quality. Though original research reported in proceedings and post-proceedings represents the core of LNCE, edited volumes of exceptionally high quality and interest may also be considered for publication. Volumes published in LNCE embrace all aspects and subfields of, as well as new challenges in, Civil Engineering. Topics in the series include:

- Construction and Structural Mechanics
- Building Materials
- Concrete, Steel and Timber Structures
- Geotechnical Engineering
- Earthquake Engineering
- Coastal Engineering
- Ocean and Offshore Engineering; Ships and Floating Structures
- Hydraulics, Hydrology and Water Resources Engineering
- Environmental Engineering and Sustainability
- Structural Health and Monitoring
- Surveying and Geographical Information Systems
- Indoor Environments
- Transportation and Traffic
- Risk Analysis
- Safety and Security

To submit a proposal or request further information, please contact the appropriate Springer Editor:

– Pierpaolo Riva at pierpaolo.riva@springer.com (Europe and Americas);
– Swati Meherishi at swati.meherishi@springer.com (Asia—except China, Australia, and New Zealand);
– Wayne Hu at wayne.hu@springer.com (China).

All books in the series now indexed by Scopus and EI Compendex database!

Sunil Kumar · Makarand M. Ghangrekar · Abhijit Kundu
Editors

Sustainable Environmental Engineering and Sciences

Select Proceedings of SEES 2021

Springer

Editors
Sunil Kumar
Waste Reprocessing Division
CSIR-National Environmental Engineering Research Institute (CSIR-NEERI)
Nagpur, Maharashtra, India

Abhijit Kundu
Department of Civil Engineering
Dr. Sudhir Chandra Sur Institute of Technology and Sports Complex
Kolkata, West Bengal, India

Makarand M. Ghangrekar
Department of Civil Engineering
Indian Institute of Technology Kharagpur
West Bengal, India

ISSN 2366-2557 ISSN 2366-2565 (electronic)
Lecture Notes in Civil Engineering
ISBN 978-981-99-0822-6 ISBN 978-981-99-0823-3 (eBook)
https://doi.org/10.1007/978-981-99-0823-3

© The Editor(s) (if applicable) and The Author(s), under exclusive license to Springer Nature Singapore Pte Ltd. 2023
This work is subject to copyright. All rights are solely and exclusively licensed by the Publisher, whether the whole or part of the material is concerned, specifically the rights of translation, reprinting, reuse of illustrations, recitation, broadcasting, reproduction on microfilms or in any other physical way, and transmission or information storage and retrieval, electronic adaptation, computer software, or by similar or dissimilar methodology now known or hereafter developed.
The use of general descriptive names, registered names, trademarks, service marks, etc. in this publication does not imply, even in the absence of a specific statement, that such names are exempt from the relevant protective laws and regulations and therefore free for general use.
The publisher, the authors, and the editors are safe to assume that the advice and information in this book are believed to be true and accurate at the date of publication. Neither the publisher nor the authors or the editors give a warranty, expressed or implied, with respect to the material contained herein or for any errors or omissions that may have been made. The publisher remains neutral with regard to jurisdictional claims in published maps and institutional affiliations.

This Springer imprint is published by the registered company Springer Nature Singapore Pte Ltd.
The registered company address is: 152 Beach Road, #21-01/04 Gateway East, Singapore 189721, Singapore

Contents

A Feasibility Case Study of Storm and Sewer Drainage Systems of Rajarhat Gopalpur Municipality 1
Biprodip Mukherjee, Prasun Mukherjee, Kuntal Chaudhuri, and Subhasish Das

Micro-irrigation: An Unsustainable Race to Achieve Higher Irrigation Efficiency 11
Prasun Mukherjee, Subhasish Das, and Asis Mazumdar

Prioritization of Groundwater Quality Parameters for Drinking and Irrigation Purposes: A Perspective Analysis 19
Chinmoy Ranjan Das and Subhasish Das

Regional Ocean Modeling System (ROMS) Simulations to Identify the Sensitivity of Forcing Conditions on the Thermohaline Features of the Bay of Bengal 33
Tarumay Ghoshal and Arun Chakraborty

Variation of Clearwater Scouring Geometry at Isolated Structures Obliging in Sediment Shifting 45
Priyanka Chowdhury, Subhasish Das, Buddhadev Nandi, and Rajib Das

Flow Kinematics Around Two Submerged Inline Eccentric Rectangular Vanes Under Clearwater Scouring 57
Priyanka Roy, Subhasish Das, Rajib Das, and Chakit Samanta

Electrical Conductivity as an Indicator of Sea Water Intrusion in South 24 Parganas, West Bengal, India 67
Souvik Chakraborty, Baibaswata Das, Souradeep Roy, Sourav Kumar Singha, and Anindya Mukherjee

Evaluation of River Health Status Based on Water Quality Index and Multiple Linear Regression Analysis 77
Suyog Gupta and Sunil Kumar Gupta

Assessment of Air Quality with Respect to Particulate Matter (PM_{10}, $PM_{2.5}$) in Mining Industrial Areas of Keonjhar District, Odisha, and Its Public Health Implications 87
Soumyak Palei, Sreetama Das, Rajasree Sarkar, Amrita Chaudhuri, Subhankar Dutta, and Sumanta Nayek

Development of Nutrient Stocks and Soil Properties of Restored Solid Waste Dump After 5 Years of Afforestation with Guava Fruit Orchard 97
Sneha Bandyopadhyay and Subodh Kumar Maiti

Measurement of Noise Levels Inside and Outside Environment of Roadside Schools in Urban Area: A Case Study of Surat, India 111
Ramesh B. Ranpise and B. N. Tandel

Quality Assessment of Various Curd Samples Based on Their Microbiological and Biochemical Properties 123
Argha Dutta, Sushmit Bauldas, Arpan Roy, Chandrani Dutta, and Fatema Calcuttawala

Role of Fly Ash as an Alternative Filler Material in Asphalt Concrete Road 131
Krishnendu Kundu, Sudipta Adhikary, Sanglappaul Chowdhury, and Sahana Ray

Consequences of Flow Fields and Vortices Around Crossway Cylinder with Flow Obstructing Downstream Plate 139
Asim Kuila, Subhasish Das, and Biprodip Mukherjee

Assessment of Mitigation Plan for Arsenic and Fluoride in Groundwater by Artificial Recharge of Rainwater 151
Prasun Mukherjee and Priyanka Roy

Spatio-temporal Diversity Exploration of Closed Surface Water Bodies in Borough 1 of Kolkata Using Satellite Images 161
Bernadette John, Subhasish Das, and Rajib Das

An Overview of Energy Efficient Optimization and Green Networking 171
Rinku Supakar, Madhusmita Mishra, Md. Shafi Hussain, and Parthasarathi Satvaya

Development of Wireless Communication-Based Intelligent Outdoor Lighting System Using Light Emitting Diodes 181
Parthasarathi Satvaya, Indraneel Mondal, and Saswati Mazumdar

Comparative Analysis of Water Storage Change in Ganga–Brahmaputra Basin Based on GLDAS Model Using QGIS Software 191
Sourav Kumar Singha, Souvik Chakraborty, Arnab Chanda, and Moumita Das

About the Editors

Dr. Sunil Kumar is a Senior Principal Scientist and Professor with over 20 years of experience in leading, supervising and undertaking research in the broader field of Environmental Engineering and Science with a focus on solid and hazardous waste management. Dr. Kumar secured 1025 rank worldwide in the subject-wise ranking of top 2% of Scientist from India which is published recently by Stanford University. His contributions since inception at CSIR-NEERI in 2000 include 267 refered publications, 4 books and 35 book chapters, 8 edited volumes and numerous project reports to various governmental and private, local and international academic/research bodies. Dr. Kumar was awarded with the prestigious Alexander von Humboldt-Stiftung Jean-Paul-Str.12 D-53173 Bonn, Germany as a Senior Researcher for developing a Global Network and Excellence for more advanced research and technology innovation. He was also awarded as an Outstanding Scientist twice by CSIR-NEERI, India.

Prof. Makarand M. Ghangrekar is a Professor in the Department of Civil Engineering, Institute Chair Professor and Head of School of Environmental Science and Engineering and Head of PK Sinha Centre for Bioenergy at Indian Institute of Technology (IIT) Kharagpur. He had been a visiting Scientist at Ben Gurion University, Israel and University of Newcastle upon Tyne, UK under Marie Curie fellowship by European Union. He has recognized worldwide in scientific community for his research contribution in the development of bioelectrochemical processes and his research group stands among the top three research labs in the world in terms of scientific publications. He has guided 21 Ph.D. research scholars and 50 master students' projects. He has contributed 203 research papers in journals of international repute and contributed 44 book chapters. His research work has been presented at more than 250 conferences in India and abroad. He has delivered invited lectures in the various reputed universities in the world to name a few, Newcastle upon Tyne, UK; Bremen, Germany; University of Tartu, Estonia, University of California, Berkeley, USA, Hong Kong University, etc. He has received recognition for his research contribution by getting elected as a Fellow, INAE; Member ASCE; receiving Swachha Bharat Award 2017; Gandhian Young Technology Innovation awards; National Design Award; Best paper Award by IEI, etc.

Dr. Abhijit Kundu is currently an Assistant Professor in the Department of Civil Engineering, Dr. Sudhir Chandra Sur Institute of Technology and Sports Complex, Kolkata (Under Maulana Abul Kalam Azad University of Technology (MAKAUT), West Bengal). He obtained his B.E. (Hons) (Civil Engineering) from Indian Institute of Engineering Science and Technology Shibpur (IIEST Shibpur) (Formerly Bengal Engineering and Science University Shibpur). He obtained his M.Tech (Civil Engineering) and Ph.D. (Engineering) from Indian Institute of Technology Kanpur (IIT Kanpur). His All India Rank (AIR) in GATE 2011 examination was 475 and he got a fellowship for M.Tech and Ph.D. from the Ministry of Education, Government of India. His major areas of research interest are Soil Dynamics and Geotechnical Earthquake Engineering. He has published 2 papers in respected International journals.

A Feasibility Case Study of Storm and Sewer Drainage Systems of Rajarhat Gopalpur Municipality

Biprodip Mukherjee, Prasun Mukherjee, Kuntal Chaudhuri, and Subhasish Das

Abstract Drainage systems play a vital role in the framework of any well-functioning society. From a hydraulic design perspective, a drainage network is just the opposite of a water supply distribution network. This study focuses specifically on evaluating and properly designing the existing drainage system which may help the relevant government body in planning, implementing, operating, and maintaining the stormwater drainage systems to solve the problem of wastewater logging like in the study area, along with sustainability that contributes to better service in drainage schemes. According to the results obtained from this study, the existing storm and sewer drainage facility in ward number four of Rajarhat Gopalpur Municipality, West Bengal is observed to be insufficient to transport the peak stormwater discharge during the essential design period. Several drains are found overflowing that cause wastewater-logged flooding and misbalances the day-to-day life of the citizens, especially during the rainy season. The hydraulic analysis for the drainage system had been carried out using SewerGEMS software by dividing the area into seven sub-catchments for better management of the flow of wastewater. From the analysis, it is observed that in some drains, the velocity is very low to negligible in comparison to the self-cleansing velocity. Other parameters such as flow and hydraulic grade line were also computed from the existing network. From the study, a few modifications are advised such as how to achieve a minimum velocity that should be developed in all stormwater-sewer drains so as not to allow any deposition in the drains.

Keywords SewerGEMS · Hydrology · Drainage networks

B. Mukherjee (✉) · P. Mukherjee · K. Chaudhuri · S. Das
School of Water Resources Engineering, Jadavpur University, Kolkata, India
e-mail: biprodip87@gmail.com

© The Author(s), under exclusive license to Springer Nature Singapore Pte Ltd. 2023

S. Kumar et al. (eds.), *Sustainable Environmental Engineering and Sciences*,
Lecture Notes in Civil Engineering 323, https://doi.org/10.1007/978-981-99-0823-3_1

1 Introduction

A drainage network's primary use is to transport wastewater and stormwater in a manner so as to not cause any public health issues in a municipal area. The drainage framework transports wastewater from residential, commercial, and even industrial establishments to wastewater treatment facilities, eventually returning to the environment. The hydraulic pathway of the drainage system can be simplified as an inverse of the supply-water system. In developed and developing countries with extensive urban infrastructure, the drainage system has now become a significant aspect of urban planning and development. The extent of funds essential to build, operate, and sustain the urban stormwater drainage services and the probable potential for substantial adversative societal and environmental effects dictate the utilization of the best conceivable means for the scrutiny, planning, and design. A comparison of the drainage systems of the past and the present had been done, which undoubtedly points to the fact that proper design and planning of drainage systems is inevitable for a healthy environment, especially in cities [1]. In Australia, Water-Sensitive-Urban-Design (WSUD) was used as an approach to sustainable urban water resource management in order to minimize the influence of urban expansion on the complex irreparable natural water cycle of a region [2]. The adoption of best planning practices (BPP) is essential to the application of WSUD. The WSUD empowers proper land use necessities, including layout and the arrangement of stormwater management structure, to be coordinated to the land use features. The Curve Number (CN) procedure is largely and worldwide used for easy application, allowing to estimate the capacity of direct runoff for a specified precipitation occurrence using a single parameter, CN, representing the storage of the basin infiltration and depending on the soil type, land use, and landcover [3]. In the Addis Ketema sub-city of Ethiopia, a study had been conducted on the urban stormwater drainage system amalgamation [4]. A study was also conducted on the rational method design of stormwater drains [5]. The research concluded that in those places where space constraints are acute, trapezoidal sections may be replaced with existing rectangular sections.

A strategy was presented for stormwater drainage in the Jodhpur Tekra region of Gujarat, India [6]. The proposal was based on rainfall records of the past 20 years. The scheme was planned considering an overall 65% of the area as impervious. Several approaches were taken to calculate runoff estimates. The rational method was used here for estimating the stormwater runoff. The excess from the system was directed to certain proposed waterbodies. A study was conducted in Surat City on the issue of stormwater drainage [7]. Their research showed that the problem of stormwater flowing back into river Tapti under high flood conditions when the drainage passages for the city were closed was a major issue. It shows that the city's drainage system during flood conditions is not adequate in certain low-lying parts of the city. A study was conducted in Vijayawada on stormwater drainage design [8]. The rational method was successfully used for Vijayawada city with a good determination coefficient of 0.871 to estimate storm-wise discharge. A study was conducted in Kemise town in Ethiopia to gauge the stormwater drainage facility [9]. According

to the results obtained, the system was insufficient to convey the peak discharge through the essential design period, and the system was affected by sediment and other types of wastes, primarily owing to the plan and the execution which was implemented overlooking hydrological and hydraulic scrutiny. A study analyzed the existing drain condition and proposed the appropriate drain size and effective drainage system for the Yangon city area [10]. Increased frequency and intensity of heavy storm events predicted by climate change effect will amplify the impact of urbanization on stormwater runoff. The existing stormwater drainage network of Ahmedabad was analyzed in 2018 [11]. SewerGEMS software was applied for conducting hydraulic simulations and modeling the wastewater collection system of Kabul [12]. StormCAD software was used to simulate the existing stormwater drainage network for a small part of central Hyderabad [13]. The amalgamation of the prevailing stormwater drainage (SWD) system of the city was evaluated, following in-depth investigation, planning, and design. The study area is categorized by the prolonged and medium quantity of precipitation. Among access roads, almost all part was provided rectangular drainage system. The average annual rainfall received by the area is about 511.30 mm, and rainfall is high in the month of July.

Lack of urban SWD management and sewer drainage are some of the most common causes of residential complaints from various urban centers of Kolkata, and with the increasing rate of rapid urbanization, this problem is getting worse and worse. Population in the Rajarhat area is rapidly growing in the last decades, and massive development work has been done in this area as high-rise buildings, complexes, and commercial buildings had been constructed but the drainage system wasn't relatively developed. The existing drainage system fails to convey the design yield. The issue is now escalating owing to the unforeseen flooding which ascends due to climate change [14].

This study focuses specifically on evaluating and properly designing the existing drainage system which may help the relevant government body in planning, implementing, operating, and maintaining these drainage systems, and also for sustainability that contributes to better service in drainage schemes. Except for the category and size of the drainage structures, this study does not contain all the structural designs as it is beyond the scope of this manuscript.

2 Study Area

Rajarhat, ward number four is in North 24 Parganas under Bidhannagar Municipal Corporation (BMC), Rajarhat. It is situated at 4 m above mean sea level with an area of 1.75 km^2. The geographic coordinates are 22°38′37.03″ N and 88°26′42.41″ E. According to the BMC population of 2015, ward 4 had a population of 15,234. From this data, the population of the year 2045 has been calculated by the Arithmetic Increase method and Geometric Increase method and the largest value of the two has been considered which is 21,425.

Fig. 1 Catchment area of ward number four at Rajarhat demarcated in red color

The study area map extracted from Google Earth software is shown in Fig. 1. Rajarhat has a climate of heavy tropical monsoons followed by a relatively colder winter followed by an extremely hot summer. Between March and June, the summers of Rajarhat experience average temperatures ranging 30–40 °C. The monsoon peak rain ranges 100–150 mm/day, while the winter dry maximizes at 1.2 mm/day.

More than 10% of the Town's Planning Area is in the form of green areas and open spaces with several water bodies and adequate green zones (parks, playgrounds, etc.). Each land use sector has enough green and open spaces to maintain an environment that is environmentally friendly or sustainable. Rajarhat consists of alluvial filling, which includes clay, silt, fine to coarse sand clay bed, and top clay bed. The thickness of the upper clay bed is usually 40 m having a physical character from plastic to semi-plastic.

3 Methodology

The key steps followed to achieve the explicit aims of the study are

- To chalk out the map of ward four under the BMC.
- To superimpose the ward map in Google Earth and draw the ward boundary.
- To analyze the total catchment area and divide it into sub-catchments in Google Earth.
- To select the catchment drawing in SewerGEMS software as a background layer.
- To draw the drainage network in SewerGEMS software.

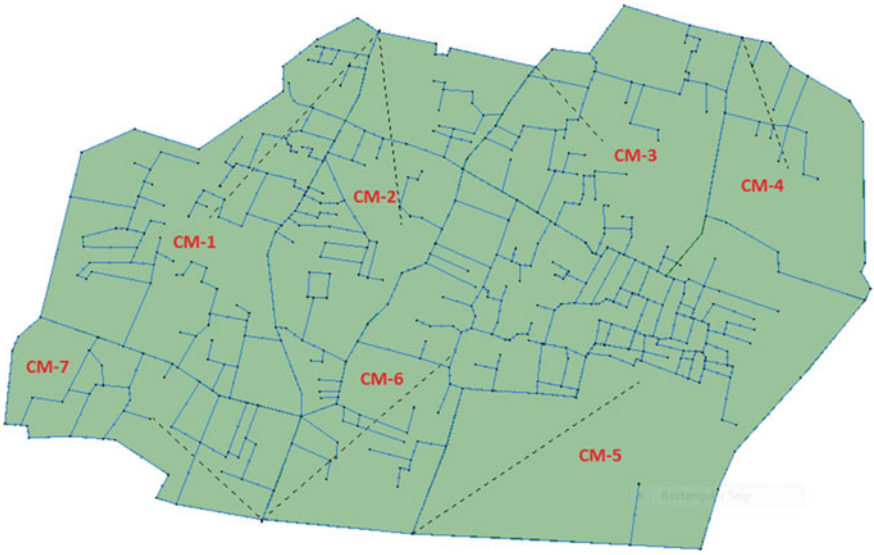

Fig. 2 Demarcation of sub-catchments of ward 4 at Rajarhat in SewerGEMS software

- To survey the study area and measure the drainage depths, widths, and ground elevations by Global Positioning System (GPS).
- To enter the previous data in SewerGEMS and to determine the invert elevations.
- To enter the rainfall data for preparing the Time-Depth curve considering a flood return period of 11 years.
- To calculate future population and calculate fixed load as per population in the different sub-catchment areas and put the data in the software.
- To determine the time of concentration by using the Kirpich equation (1940).
- To select the unit hydrograph method and estimate the SCS CN value by using the SCS-CN method of estimating runoff volume.
- To select two outfalls in the catchment and select the outfall in each sub-catchment.
- To analyze the problem of the ward based on the software outcomes and present field conditions and thereafter recommend mitigation measures, if required.

Figure 2 shows the catchment area of ward number four at Rajarhat. The total catchment area has been demarcated into seven sub-catchments (CM-1 to CM-7).

4 Results and Discussions

After applying the methodology, the result and discussions were bifurcated and reflected in the following subsections as follows.

4.1 Existing Drainage Facilities

Existing drainage facilities in ward 4, Rajarhat, are categorized into open drainage and closed drainage. Closed drains are seen in areas along the main road, while open drains are seen along the by-roads and lanes. It is observed that the drains are of rectangular shape. It is seen that in several sections, the access roads, during flooding periods, even aid as wide-open channels. Rajarhat's ward number four drainage management system is not efficient now. Consequently, rectified drainage design is essential. The drainage system and the catchment area division as input in SewerGEMS are shown in Fig. 2.

The primary issue of the present drainage network is the incapability of conveying large quantities of water, resulting in overflow. According to the observations, problems are primarily due to the clogging of garbage and solid waste materials, the improper slope of the drains, improper usage of manhole covers at various stretches, inappropriate drainage planning, and infrastructure construction practices implemented by overlooking the mandatory hydraulics and hydrology of the region. This also causes different adverse impacts on the public throughout the year like dengue, malaria, and other water-borne diseases.

4.2 Results for Channels

After providing all the input data to SewerGEMS software, the maximum flow, maximum flow width, maximum hydraulic grade, and velocity (maximum) are computed for each stormwater drain as reflected in the profiles of Figs. 3, 4 and 5. The results show that in some stormwater drains the flow is either stagnant to low or moderate. In some other stormwater drains, the flow is very high. But according to CPHEEO manual criterion, this flow velocity should be upto 3 m/s.

Figure 3 depicts that in most channels the flow is equal and near zero though there being the computed value of hydraulic grade as shown in Fig. 4. This depicts water loggings in those channel cross-sections thus leading to flooding of the areas. In some places in Fig. 5, the velocity is below the permissible range of the CPHEEO manual, i.e. 0.6 m/s.

Hydraulic grade line (HGL) is one of the important points to be discussed when it comes to the design of the optimal size of drains. It is defined as the line that gives the sum of the potential head (y) and the datum head (z) of a flowing fluid in the stormwater-sewer drains with respect to some reference, or it is a line that is obtained by joining the top of all vertical ordinates, showing the potential head (y) of a flowing fluid in a stormwater-sewer drain from the center of the stormwater-sewer drain. HGL helps to determine the system's acceptability by setting the elevations of a system from which the water level will increase once the system runs at the designed flood frequency.

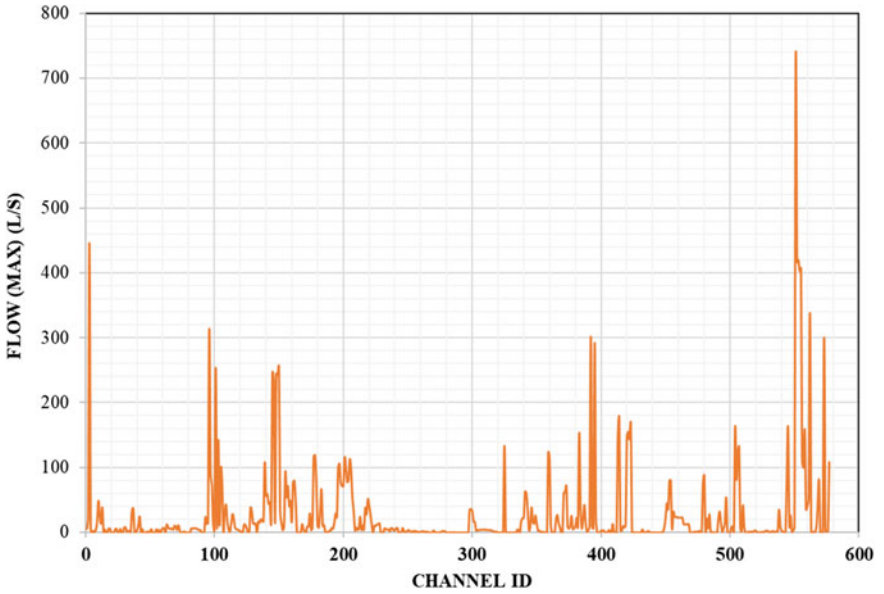

Fig. 3 Maximum flow profile in each channel

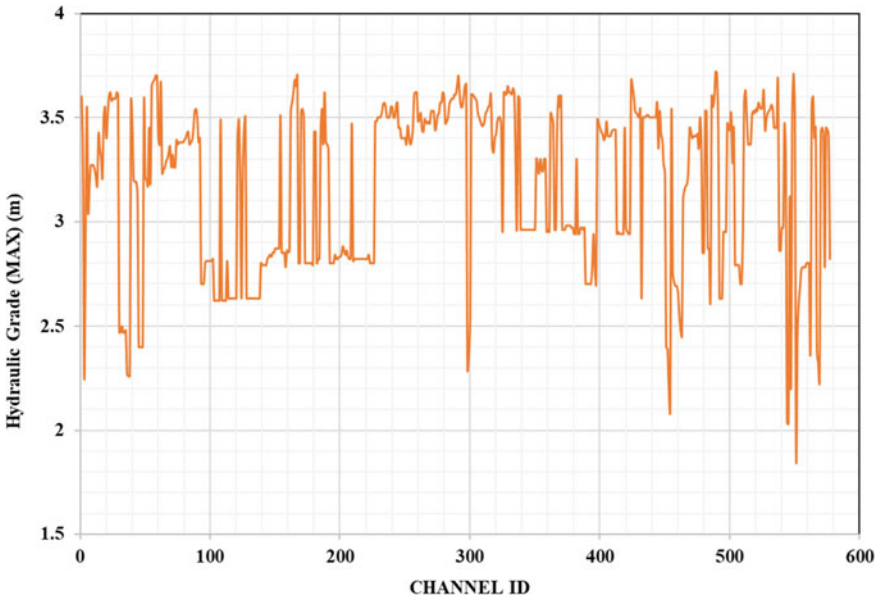

Fig. 4 Hydraulic grade line profile in each channel depicting maximum 1.5 m water depth prevails in drainage system

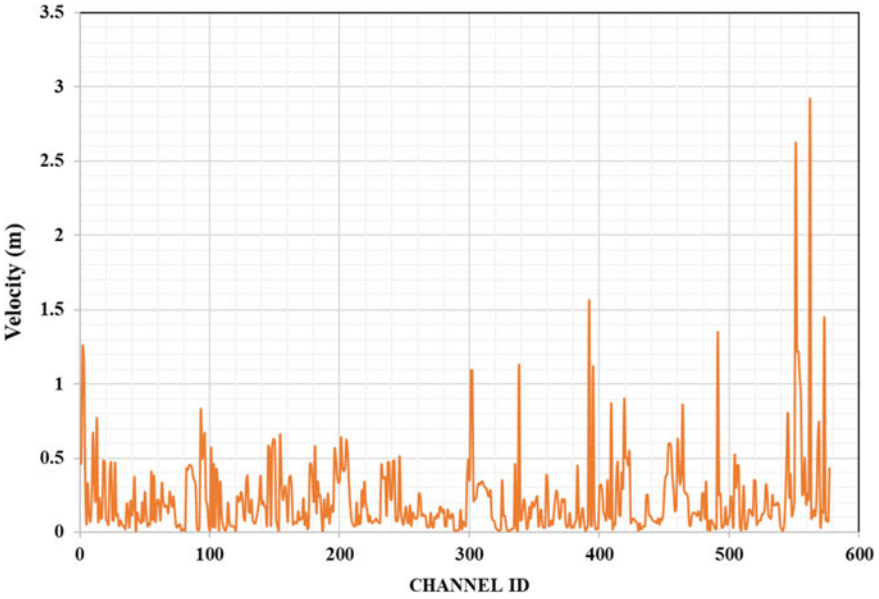

Fig. 5 Velocity profile in each channel depicting few channel velocities less than 0.6 m/s to ensure the stagnancy of water in the region

The hydraulic design of pressure flow can be considered apt if the HGL is above the crown of the stormwater-sewer drains. On the other hand, if the drain's crown is above the HGL, the hydraulic design of open channel flow is apt. Another concern with the operation of stormwater drains under pressure flow conditions is that in the event of HGL rising above the ground surface, inlet surcharging and a probable manhole cover displacement might occur. Careful planning of design based on open channel conditions is also required. An assessment of the likelihood of extreme flood conditions occurring in the event of a storm greater than the design storm may burden the drainage network. As the hydraulic computations are made, the presence of desired flow conditions must be often confirmed. The storm drainage system can often switch from one section to another between pressure and open channel flow conditions.

The detailed methodology used to calculate the HGL through the system starts with the tail water elevation at the system outfall. If the outfall is in a prevailing network, the computations of the HGL should begin from the outlet end of the prevailing network, proceeding to the upstream inlet of the proposed network. Understanding that there is negligible research on this emerging issue, this pilot study may be treated as a reference to the upcoming sewer network project since all the necessary steps are followed for designing a sewer network.

5 Conclusions

The entire study is based on the data collected by surveying ward number four of Rajarhat. A few non-relevant assumptions had been taken while simulating the inputs in SewerGEMS software like temperature, viscosity, etc. It is always a relevant fact that the quality of the outcome depends on the quality and relevant quantum of survey/existing data as available. According to the results obtained from this study, the existing storm and sewer drainage facility in ward 4 at Rajarhat is insufficient to transport the peak discharge during the essential design period at the maximum permissible velocity within the CPHEEO range.

Due to zero discharge but having positive hydraulic grade in several channels, overflowing also occurred, and the area is flooded. The results clearly denote that these issues are primarily owing to drainage clogging from garbage and other materials, unsuitable flow width, construction practices implemented by overlooking obligatory hydrological and hydraulic examination, and inadequate slope of the drains. Due to water logging conditions, the occurrence of various water-borne diseases like cholera, malaria, dengue, etc. affects the community.

From the result, it has been noticed that in some stormwater drains, the velocity is very low. In accordance with the CPHEEO guidelines, the permissible velocity of 0.6 m/s must be established in all drainage channels to prevent deposition within the stormwater drains. Low velocity would hinder free flow within the drainage channels leading to further deposition in turn resulting in complete blockage of the drains. In addition, to managing problems from government authority, the community is also responsible for disposing of their waste into open drains resulting in water clogging. It is also observed that there is an intense lack of awareness of the consequential impact of the disposal of plastic and solid materials on the drainage network.

In order to avoid the problems stated in the study, the following appropriate mitigation measures are recommended:

1. To avoid the problems of flooding in several areas, proper dimensions and slopes of the stormwater drains should be recommended.
2. Intermittent maintenance and cleaning of the drainage network are also suggested for the municipality.
3. The community must take the initiative to create awareness of the concerning effects of disposing of solid materials into drains.

The outcomes of the present case study will help water designers in the future to access the drainage systems of similar types of tropical region areas, especially in West Bengal to manage both stormwater and wastewater in the rainy season.

Acknowledgements The authors sincerely thank Bidhannagar Municipal Corporation, GoWB, for providing some research data. The master's dissertation of Ms. Kuntal Chaudhuri greatly helped to reflect the research.

References

1. Burian SJ, Nix SJ, Pitt RE, Durran SR (2000) Urban waste water management in the United States: past, present, and future. J Urban Technol 7(3):33–62
2. Lloyd SD, Wong THF, Porter B (2002) The planning and construction of an Urban storm water management scheme. Water Sci Technol 45(7):1–10
3. D'Asaro F, Grillone G (2010) Runoff curve number method in silicy: CN determination and analysis of the initial abstraction ratio. In: 2nd joint interagency. Las Vegas, NV, USA
4. Belete AD (2011) Road and urban storm water drainage network integration in Addis Ababa: Addis Ketema sub-city. J Eng Technol 3(7):217–255
5. Needhidasan S, Nallaathel M (2013) Design of storm water drains by rational method and approach to storm water management for environmental protection. Int J Eng Technol 5(4):3203–3214
6. Gajjar HH, Dholakia MB (2014) Storm water network design of Jodhpur tekra area of city of Ahmedabad. Int J Eng Dev Res 2(1):744–747
7. Bhadiyadra JK, Goyani VC, Dobariya TN, Vaghani CR, Gajera DJ (2015) Study of storm water drainage problem of Surat city and its solutions due to flood in River Tapi. Int J Civ Struct Eng Res 3(1):61–89
8. Kumar SP, Santhi T, Srivastav MP, Reddy SVS, Prasad AM, Praveen TV (2015) Storm water drainage design (case study Vijayawada). Int J Earth Sci Eng 8(2):507–511
9. Asfaw B (2016) Assessment of storm water drainage system in Kemise town. ME thesis, School of Graduate Studies Addis Ababa Institute of Technology, Addis Ababa University
10. Kyi MP, Zin WW, Kyi CCT, Maung T (2017) Study on storm water drainage system of Kyee-myaindaing township. Department of Civil Engineering, Yangon Technological University, pp 1–5
11. Raval SK (2018) Storm water drainage solutions for urban area. Int J Innov Res Sci, Eng Technol 7(4):3706–3711
12. Noori AR, Singh SK (2021) Assessment and modeling of sewer network development utilizing Arc GIS and SewerGEMS in Kabul city of Afghanistan. J Eng Res-ICARI Spec Issue 22–31
13. Naresh A, Naik MG, Nagalaxmi G (2019) Analysis of existing stormwater drainage system for Central Zone of Hyderabad city using stormcad. In: Proceedings of the 38th IAHR world congress. Panama, pp 1226–1231
14. Chaudhuri K (2019) Study of storm and sewer drains for Rajarhat (ward no 4) in West Bengal using SewerGEMS Software. Master of Engineering thesis, School of Water Resources Engineering, Jadavpur University, Kolkata, India

Micro-irrigation: An Unsustainable Race to Achieve Higher Irrigation Efficiency

Prasun Mukherjee, Subhasish Das, and Asis Mazumdar

Abstract In the advent of irrigation water scarcity, most scientific and engineering efforts are focusing more on increasing irrigation efficiency while aiming to increase "more crop per drop". Incremental advancements have been seen recently in drip irrigation, sprinkler irrigation and allied technologies. Although in a view of micro-level irrigation management this approach might seem beneficial, from a basin level to a large level viewpoint the economic sacrifices far outweigh the benefits. The study aims at increasing the understanding of the importance of promoting basin-level macro-irrigation for policymakers and stakeholders. The present research was done for the western basins of South 24 Parganas, West Bengal, which is severely challenged by the availability of fresh water for irrigational purposes. The reductions in monsoon periods and the increase in saltwater intrusion have contributed more to the already water-scarce region. Detailed comparative analysis was performed to analyze the aspects of drip irrigation, and sprinkler irrigation which not only fails to increase the basin-level irrigational water availability but also is climatologically devastating in the long run for the basin. While being economically more ineffective, these types of irrigation technology also fail to become sustainable even in the short term. This study also aims to act as a model framework for policymakers and stakeholders to increase their attention more toward sustainable irrigation by a combination of utilizing advanced technologies which are targeted at not only increasing the crop production per unit of water but also at an overall improvement in basin-level water availability.

Keywords Macro irrigation · Micro-irrigation · Irrigation efficiency

P. Mukherjee (✉) · S. Das · A. Mazumdar
School of Water Resources Engineering, Jadavpur University, Kolkata, India
e-mail: mukherjeeprasun3@gmail.com

© The Author(s), under exclusive license to Springer Nature Singapore Pte Ltd. 2023

S. Kumar et al. (eds.), *Sustainable Environmental Engineering and Sciences*,
Lecture Notes in Civil Engineering 323, https://doi.org/10.1007/978-981-99-0823-3_2

1 Introduction

Integrating high irrigable water demand into the finite freshwater resources is still the primary problem of any nation. 70% of the global water withdrawals are for providing irrigation water to crops [1]. Withdrawals from groundwater resources are not only depleting the limited reserves but are also affecting the water quality [2]. Administrative bodies and policymakers are henceforth inclined to promote innovative technologies to improve irrigation efficiency (IE). This delivers private benefits to agriculturists but should be acceptable partially as a significant scientific indication has revealed that an increase in IE seldom delivers the assumed public benefits of increased water availability.

Policymakers typically have not provided enough importance to basin-level large-level water accounting. Water required for irrigation largely account for plant biomass, evapotranspiration (ET) by the crops and water required for the removal of salt to sustain soil production. Irrigation efficiency of a farm is the ratio between the volume of irrigation water utilized, to the volume of irrigation water applied (adjusting for variations in soil water content) [3]. Every year, countries spend a large amount of funds to subsidize innovative irrigation technologies, like sprinkler irrigation or drip irrigation [4]. Their primary aim is to increase the IE, on the belief that this would create the opportunity for them to reallocate the water from irrigation to cities [5], industry and other regions with the scarcity of water, while sustaining or increasing the agricultural yield. But this water which is saved at the farm level usually does not decrease the consumption of water at the watershed level.

It has been seen that the increase of IE for farm crops can rarely be associated with improved water availability on a basin level [6], and increased IE that decreases the need for water extractions might have a low to negligible effect on the water consumption of the region. This paradox that increased IE at the farm level fails to increase the basin-level water availability can be explained by the logic that earlier non-consumed water or "losses" at the farm level (like runoff) are often reclaimed at the watershed level. Advanced irrigation technologies like sprinkler or drip irrigation which increase IE may also increase the water consumption of the farm per hectare [7], and also result in more groundwater extractions [8].

Though the hydrological concepts of IE are well known, it is frequently disregarded. There is also misperception among the policymakers on the effects of increased efficiency (bio-physical or economic output per unit of water) on basin-level availability of water. The manuscript aims at solidifying the scientific evidence so as to assist the policymakers and stakeholders in the process of analyzing a sustainable irrigational and agricultural practice for a region than just focusing on improved irrigation efficiency quotient.

2 Mathematical Calculation

At the farm or basin level, the Water Budget Equation (WBE) states that the volume of inflow (V_i) is equal to the summation of evaporation (E), transpiration (T), groundwater infiltration and interception (G), and the run-off (R), adjusted for change in water storage (ΔS), as in Eq. 1:

$$V_i = E + T + G + R + \Delta S \tag{1}$$

The inflows at basin level are precipitation (P) and inflow from other sources into the basin, as the precipitation can be considered constant for a region; as this study is primarily based on a comparative analysis, it is unnecessary to carry it for the subsequent calculations. At the farm level, inflows are precipitation and irrigation conveyance from surface water sources or groundwater sources. Outflow from the basin includes evapotranspiration, infiltration and surface runoff. At any level, outflow from evapotranspiration is lost to atmospheric moisture. Such outflows add up to the fraction consumed (C) of water. Other than the fraction consumed, outflow gets returned to the region's hydrological cycle in the form of groundwater recharge or runoff. These outflows make the fraction non-consumed (C_n) which can be used downstream. As our emphasis is on IE, we can assume that other outflows which are not connected with irrigation are apprehended in extrinsic factors and are negligible for our analysis. We can also consider the ΔS to be zero as the aim is to emphasize primarily the sustainable irrigation water supply and water usage at the basin level. Under these conditions, Eq. 1 can be modified as fractions to form Eq. 2:

$$V_i = \{r(E) + r(T) + r(G) + r(R)\} \times V_i \tag{2}$$

where r in Eq. 2 is a fraction of inflows distributed among the four outflows which are considered by denoting the outflow within brackets. Therefore, we can get

$$1 = \{r(E) + r(T) + r(G) + r(R)\} \tag{3}$$

Transpiration is a very important element in crop yield. Transpiration helps in the uptake of nutrients in plants. So, transpiration can be considered beneficial for water consumption. Evaporation from soil or foliage on the other hand can be considered non-beneficial in the context of irrigation. In any case, these phenomena happen simultaneously. We can hence write

$$C = \{r(E) + r(T)\} \tag{4}$$

$$C_n = \{r(G) + r(R)\} \tag{5}$$

The importance of G and R can be only decided according to regional conditions. These two types of non-consumed outflows can be reclaimed in downstream

catchments and/or help in improving the environmental conditions, in several cases even acting as an additional drainage system. In certain conditions, these outflows might not be reclaimed, resulting in flowing into the ocean or saline water channels, in which case it will have no direct economic value. We are denoting this non-recoverable fraction of water as (α). Hence, the recoverable fraction of water (β) would be

$$\beta = (1 - \alpha)C_n \tag{6}$$

According to the WBE, any interference resulting in the variation of any one component of the equation would also correspondingly change other fractions to confirm the law of conservation of mass. To understand the consequences of variations in IE, let us first assume that (i) there is no variation in the evaporation associated with the interference of the increase of IE, and (ii) the non-recoverable fraction of water is zero ($\alpha = 0$). In practicality, at least, the evaporation component would vary according to the type of irrigation. The process of irrigation which has a higher IE, like drip irrigation, is bound to have different rates of evaporation in comparison to surface irrigation. If an interference increases the IE and also increases the transpiration, then the β must decrease to confirm the WBE. For instance, let us consider the transpiration rate increases from T_1 to T_2, where transpiration before the interference is T_1 and the transpiration after interference is T_2, then $T_2 > T_1$. So, it can be written as

$$\Delta\beta = \{r(G_2) - r(G_1)\} + \{r(R_2) - r(R_1)\} = \{r(T_2) - r(T_1)\} \tag{7}$$

As in this case, there is no change in evaporation as has been considered, $\Delta E = 0$.

It can be now seen that the change in the recoverable fraction will reduce, due to higher IE, and the evaporation is taken constant; the variation in transpiration will increase so as to suffice the WBE.

Now, if we consider that there will be a change in evaporation, with respect to the interference in the IE, we get

$$\Delta\beta = \{r(G_2) - r(G_1)\} + \{r(R_2) - r(R_1)\} = \{r(T_2) - r(T_1)\} - \{r(E_2) - r(E_1)\} \tag{8}$$

or

$$\Delta\beta + \{r(E_2) - r(E_1)\} = \{r(T_2) - r(T_1)\} \tag{9}$$

It can be now seen that the change in the recoverable fraction and evaporation must get reduced, due to higher IE, while the change in transpiration will increase so as to suffice the WBE.

If we make the $\alpha > 0$ then it might be possible to increase the transpired fraction to be allied to an increased β, but only if the decrease in the evaporated fraction and

non-recoverable fraction both increase in association with the transpiration. This will then result in an increase in the non-recoverable volume of irrigation water, thus providing no value as such.

3 Practical Evaluation

The projected benefits (like high yields and high farm revenues) should be equated to the peripheral costs which will arise from the fall in recoverable return flow (like loss of aquatic ecosystem, groundwater reduction and salt removal from watersheds). The study area for the practical evaluation was monitored in the Magrahat basin of South 24 Parganas, West Bengal, India (Fig. 1).

The area suffers from a scarcity of rainfall during the winter seasons, and the groundwater is getting rapidly affected by saltwater intrusion. Seasonal storms often carry saltwater onto the farmland regions, resulting in salty soil. Moreover, groundwater is also affected by arsenic contamination in several places. The primary source of water during the winter season is the Diamond Harbour Sluice at the east of the catchment area.

The area balances itself on the edge of creating a butterfly effect on the agriculture and livelihood of the people in the region. The presence of an intense network of canals has provided a solace but no solution to the irrigational water requirements of the region. Previous studies had been done on the region to effectively increase the irrigation yield of the region by the introduction of tidal backwater into the region [8–10].

As this is a comparative analogy, it is considered that the effects of precipitation, resulting in the change in water storage to be similar for all cases (surface, drip, sprinkler), henceforth could be considered zero. The current analysis required the evapotranspiration rate (ET_o) of the region. The meteorological and climatological data was hauled from "CLIMWAT 2.0 for CROPWAT" software for the nearest recording station Sagar Island. The data was accounted for in the CROPWAT 8.0 software. The data showed an average ET_o of 3.45 mm/day.

The cultivable command area (CCA) of the basin is 334.89 km^2 [10]. The total rate of ET_o expected would be the product of the rate and the CCA, which would be 1.156×10^6 m^3/day. The average evaporation rate of the region for the canal network is 0.044×10^6 m^3/day [10].

As this is a comparative analogy, it is considered the water required for the plant biomass would be the same for all cases, so the amount of water required other than plant biomass build-up, i.e., the water necessary for evapotranspiration can be considered as the total water required/applied. Now from Eq. 4, we can derive the volume of consumed water:

Canal irrigation: $C_I = 1.2 \times 10^6$ m^3/day;

Drip irrigation: $C_D = 1.156 \times 10^6$ m^3/day (evaporation can be considered negligible); Sprinkler irrigation: $C_S = 1.1733 \times 10^6$ m^3/day (evaporation is considered as 1.5% of applied water [11]).

Fig. 1 Magrahat catchment area

The increase in water use efficiency of drip irrigation and sprinkler irrigation with respect to canal irrigation can be clearly seen as only 3.6 and 2.25% at the basin scale. Even though farm-level irrigation efficiency can be much higher for the drip and sprinkler irrigation systems, it can be effectively seen that the increase in efficiency at the basin level is not justified in accounting for the cost-benefit ratio of the systems.

4 Conclusion

Comprehensive and elaborate records need to be developed from individual farm level to basin level to help in the decision-making process. This would require the estimation and measurement of all influxes, water requirements, recoverable water and non-recoverable water from return flows. Advances in satellite imagery and remote sensing can greatly help in estimating the inflow and outflow much more easily and inexpensively. To confirm that the anticipated results are produced, risk assessments and sustainability analysis are immensely needed when considering shifting toward a system of irrigation with higher IE. Also, while subsidizing a system with higher IE, regression analysis should be performed regarding the costs exceeding the potential benefits, and if adequate return flows are generated for subsequent basins. As farmlands worldwide are in a race to increase the yield so as to satisfy demand, the global water crisis would only worsen. Blindly trying to increase the irrigation efficiency at the farm level will not resolve this problem—it might even

make it worse. Policymakers and stakeholders must approach each problem on a "case to case" basis and not by a generalized means.

References

1. Grafton R, Williams J, Jiang Q (2017) Possible pathways and tensions in the food and water nexus. Earth's Future 5:449–462
2. John B, Roy P, Das S (2020) Analysing the influence of groundwater exploitation on its quality in Kolkata. In: Kumar S, Kalamdhad A, Ghangrekar M (eds) Sustainability in environmental engineering and science, LNCE, vol 93. Springer, Singapore, pp 83–89
3. Burt CM, Clemmens AJ, Strelkoff TS, Solomon KH, Bliesner RD, Hardy LA, Howell TA, Eisenhauer DE (1997) Irrigation performance measures: efficiency and uniformity. J Irrig Drain Eng 123(6):423–442
4. Scheierling SM, Loomis JB, Young RA (2006) Irrigation water demand: a meta-analysis of price elasticities. J Water Resour Res 42:W01411
5. Flörke M, Schneider C, McDonald RI (2018) Water competition between cities and agriculture driven by climate change and urban growth. Nat Sustain 1:51–58
6. Perry CJ, Steduto P (2017) Does improved irrigation technology save water? A review of the evidence. Food and Agriculture Organization of the United Nations, Cairo
7. Pfeiffer L, Lin CYC (2014) Does efficient irrigation technology lead to reduced groundwater extraction? Empirical evidence. J Environ Econ Manag 67(2):189–208
8. Das S, Roy PK, Mazumdar A (2012) A plan for the enhancement of backwater for irrigation for sustainable livelihood of rural communities at Magrahat basin, South 24 Parganas, West Bengal. Reason-A Tech Mag (XI):29–37
9. Mukherjee P, Das S, Mazumdar A (2020) Evaluating volatility in quality indexing of saline water during tidal backwater incursion in Western Canals of South 24-Parganas, West Bengal. J Indian Chem Soc 97(4):577–586
10. Mukherjee P, Das S, Mazumdar A (2021) Introducing winter rice cropping by using non-saline tidal water influx in western basins of South 24 Parganas India. Sci Rep 11(1):553
11. Mila AJ, Chakraborty S, Islam N, Sarkar PK (2010) Evaporation loss during sprinkler irrigation. Bangladesh J Sci Res 23(1):81–90

Prioritization of Groundwater Quality Parameters for Drinking and Irrigation Purposes: A Perspective Analysis

Chinmoy Ranjan Das and Subhasish Das

Abstract Water is probably the utmost prime natural asset after air. Though a large portion of the earth's surface consists of water, just a few portions of it are usable. Apart from drinking purposes, water resources have a crucial role in several segments of the economy. Day-by-day, surface and groundwater quality has deteriorated due to rapid industrialization and urbanization. Considering the environmental and economic aspects, the quality and quantity of water are very important. Since water is used for various purposes, its compatibility must be tested before use. Moreover, sources of water must be monitored on a regular basis and checked whether they are in good condition or not. Water quality assessment is very essential to overcome the adverse condition resulting from the deterioration of water quality. Standard protocol-based guidelines are now set after many years of research on water quality assessment. In this paper, several parameters with standard guidelines provided by different agencies have been discussed with comparison to measure the groundwater class for the use of drinking and irrigation. Groundwater sampling, water quality index, and Piper trilinear diagram are also associated. Finally, a rating analysis of water quality parameters has been done on a priority basis of the perspective assessment of groundwater characteristics for the use of drinking and irrigation.

Keywords Groundwater sampling · WQI · Piper trilinear diagram · Rating analysis

C. R. Das (✉)
Civil Engineering Department, Global Institute of Science and Technology, Purba Medinipur, Haldia, West Bengal 721657, India
e-mail: chinmoycivilengg@gmail.com

S. Das
School of Water Resources Engineering, Jadavpur University, Kolkata 700032, India

© The Author(s), under exclusive license to Springer Nature Singapore Pte Ltd. 2023

S. Kumar et al. (eds.), *Sustainable Environmental Engineering and Sciences*,
Lecture Notes in Civil Engineering 323, https://doi.org/10.1007/978-981-99-0823-3_3

1 Introduction

In many areas of a country, the available sources of water get exhausted and also contaminated due to rapid industrialization and urbanization [1]. Salinization, resulting from seawater intrusion, chemicals used in agricultural, geogenic activities, and irrigation, is the major issue for contamination of groundwater [2]. Water with some chemical hazards is unsuitable for specific use. A severe health problem can occur due to the utilization of unsafe water for drinking and cooking. For drinking purposes, water quality assessment involves the appraisal of chemical composition and identification of probable sources for the contamination of groundwater and also provides the curative measure for fixing the quality of water.

A sufficient amount of water is necessary for the growth of the plant. On the other hand, the quality of irrigation water should be within the permissible limit to avoid adverse effects on the growth of the plant. Characteristics of irrigation water are influenced by the quantity of suspended silt and chemical ingredients present in the water. In addition to surface water bodies and rainwater, another source of water supply is essential to attain continual crop production. Groundwater is considered an alternative source for irrigation farming [3].

In a region, the variation of groundwater quality depends on physical and chemical properties which are highly affected by geological features and humans' interference [4–6]. Groundwater contamination has been issued in many areas caused by normal climatic activities and human interruption in the geo-systems. To realize the method of controlling the hydro-chemical characteristics of groundwater in a particular region, it is necessary to culture the geologic formation of rocks, natural and human activity, melting of rocks and minerals, and weather conditions which affect the hydrochemistry of the region [7]. The water facies with respect to the most influential ions is classified by the Piper trilinear plot [8]. Water quality assessment is the major tool for reliable evolution and also gives conclusive details to manage water resources [2]. Water class evaluation is a method of finding the correct nature of water by calculating the presence of parameters and their range through several experiments. Considering the facts, groundwater quality assessment is necessary to find whether requisite water quality is in accordance with specified standards or not. Evaluating the class of water for proper groundwater sampling is very important for water quality analysis [9]. This paper aims to review the parameters with standards for ascertaining the compatibility of groundwater for drinking and irrigation purposes. Every parameter is important in water quality testing for different uses. But the presence of some of the parameters above the permissible limit has a significant impact on water quality as well as human growth and plant growth. Some parameters such as pH, chloride, calcium, magnesium, and sulfate have a major impact on human health. Parameters such as fluoride and arsenic have a profound effect on human health [10]. For irrigation water, parameters like total dissolved salts, electrical conductivity, and sodium absorption ratio have a significant impact on plant growth [1, 11]. Therefore, before using water for different purposes, parameters should be considered as per

their importance in analyzing water quality. A rating analysis on a priority basis has been done to judge the groundwater class as well.

2 Groundwater Quality Assessment Parameters for Drinking Purpose

Limitations of drinking water quality have been proposed by many organizations such as APHA [12], WHO [10], and Indian standard [13] drinking water specifications. The acceptable limit (AL) and the permissible limit (PL) of water for drinking are given in Table 1 as per Indian standard drinking water specifications.

Generally, **pH** has an indefinite impression on users, but it is the utmost significant parameter to judge the class of water [10, 14, 15]. For drinking purposes, the pH value should be 6.50–8.50 [13].

Chlorine is the most common element that exists in terms of chloride ions in water. The sources of chloride in groundwater are possibly seawater intrusion, weathering, seepage of soil, household effluents, and industrial sewage [2]. Excess chloride imparts salted flavor to water and liquid refreshment. Chloride levels over 250-ppm can create perceptible flavor in water [10]. The high concentration of chloride causes a salty flavor to water and a purgative effect in unaccustomed consumers.

Fluorine is a general component that is broadly spread on the earth's layer and is present in terms of fluorides. The highest allowable range of fluoride in drinkable water is 1.50 ppm. Dental fluorosis is owing to the existence of fluoride in water over the allowable limit and skeletal fluorosis is caused by a much higher level of fluoride present in water [10].

It has been observed that people consuming **arsenic**-contaminated water suffer chronic diseases like skin lesions, skin cancer, bladder and lung cancers, peripheral neuropathy, and peripheral vascular disease. The most commonly viewed symptom is dermal lesions which occur due to at least exposure times of around five years.

Table 1 AL and PL of water for drinking [13]

Parameters	AL	PL
pH	6.50–8.50	No relaxation
Chloride (as Cl) (ppm)	250	1000
Fluoride (as F) (ppm)	1.0	1.5
Arsenic (as As) (ppm)	0.01	0.05
Total dissolved solids (TDS) (ppm)	500	2000
Nitrate (as NO_3) (ppm)	45	No relaxation
Calcium (as Ca) (ppm)	75	200
Magnesium (as Mg) (ppm)	30	100
Total hardness (as $CaCO_3$) (ppm)	200	600
Sulfate (SO_4) (ppm)	200	400

Melanosis, diffuse keratosis, and leuco-melanosis are the major dermatological signs. It has a substantial impact on the circulatory system of kiddies who are ingesting arsenic-contaminated water with a mean concentration of 0.60 ppm for a mean of seven years [10].

TDS indicates mineral ingredients exist in the water in dissolved forms. It is a special significant parameter to evaluate water class in drinkable water [4, 7, 16]. The high level of TDS in groundwater is mostly caused by the existence of calcium, chlorides, sulfates, carbonates, and bicarbonates [2]. Water is considered palatable if the TDS is under 600-ppm and the TDS level (ppm) > 1000 is not good for drinking [10]. Considering TDS concentration, groundwater quality is categorized as fresh (TDS $\leq$ 1000), brackish (1000 $\leq$ TDS $\leq$ 10,000), saline (10,000 $\leq$ TDS $\leq$ 1,000,000), and brine (TDS > 1,000,000) [14]. In potable water, water class with respect to TDS (ppm): below 300 $\rightarrow$ excellent water; 300–600 $\rightarrow$ good; 600–900 $\rightarrow$ fair; 900–1200 $\rightarrow$ poor; over 1200 $\rightarrow$ not acceptable [11].

The possible roots of **nitrate** are found in groundwater due to seepage of nitrogenous fertilizer and manures, disposal of wastewater, septic waste, human and animal excreta, etc. Rarely, nitrate possibly exists in groundwater as a consequence of leaching through normal plants. Changes in nitrate concentration in surface water occurred quickly due to runoff of manure, uptake by algae, and removal of nitrates by bacteria, but on the other hand nitrate concentration in groundwater changes relatively slowly. The allowable limitation of nitrate in drinkable water is 50-ppm [10]. The most common cause of thyroid disease, diabetes, gastric cancer, and methemoglobinemia (blue baby syndrome) is water with high nitrate concentration.

Calcium and Magnesium (**Ca-Mg**) are commonly utilized to identify the compatibility of water. The hardness of water is directly connected to these ions. Ca-Mg ions are the utmost numerous substances in the surface and groundwater and are present in the form of bicarbonates, sulfate, and chloride. A high level of calcium ions in water may create abdominal disease and is unacceptable for households as it is the source of encrustation and scaling. Magnesium is a vital component for human health, as it is essential for the usual bone formation in the body. Hard water is not acceptable for domestic purposes as it carries excessive levels of magnesium or calcium. Ca-Mg is the utmost conventional mineral responsible for the **hardness** of the water. The presence of bicarbonate of Ca-Mg creates the temporary hardness of water and the existence of sulfates, chlorides, and nitrates of Ca-Mg indicates the permanent hardness of the water. This hardness of water indicates the soap destroying the property of water. Public acceptability criteria may differ from one society to another. Excess hardness in water can cause scaling in the distribution system, treatment system, pipes, and water reservoirs in residences. For drinking purposes, water class concerning total hardness as $CaCO_3$ (ppm): below 75 $\rightarrow$ soft; 75–150 $\rightarrow$ moderate; 150–300 $\rightarrow$ hard; and over 300 $\rightarrow$ extremely hard [17, 18].

The existence of **sulfate** in drinking water can make the perceptible flavor, and excessive concentration can cause a purgative effect in unwonted consumers [10]. The sulfate concentration over 400-ppm can probably react with the parts of the human body and creates a purgative effect on the human body with too much magnesium in groundwater.

3 Groundwater Quality Assessment Parameters for Irrigation Purpose

The main benefit of **pH** is a fast appraisal of the expectation of water being standard or not. The range of pH for irrigation water is 6.50–8.40. A pH above 8.20 in irrigation water can increase the potentiality of sodium problems. The high level of pH within groundwater is caused by the concentration of calcium, sodium, bicarbonate, carbonate, and magnesium [2].

All irrigation water carries **dissolved salts** such as NaCl, $CaSO_4$, $MgSO_4$, and $NaHCO_3$, but the levels and constituents of such salts differ concerning the origin of the irrigation water. The standard of water for irrigation is influenced by the number of soluble salts existing within the water. Due to the accumulation of salt at the root zone, crops are unable to withdraw enough water from the salty soil solution and that affects the plant growth as well as yield. Water with total dissolved salts below 450-ppm is regarded as excellent and above 2000-ppm is considered unsuited for irrigation [1]. Irrigation water class concerning the risky effects of total salt in terms of EC (μmhos/cm): below 1500 → low risk; 1500–3000 → moderate risk; 3000–6000 → high risk; and over 6000 → extremely high risk [19].

The entire level of the ionized components in natural water is indicated by **EC**. It is nearly connected to the amount of the cations (or anions) ascertained by the chemical test, and it corresponds well with the amount of soluble salts [20]. For irrigation water, salinity hazard is determined by electrical conductivity [21]. EC depends on the temperature, type, and concentration of various ions [4]. It is extremely meaningful as it raises the temperature and total dissolved salts in water [7]. Plants are unable to absorb enough water for growth from the soil solution (physiological drought) because of the existence of more EC in water. With the increase of EC, utilizable plant water in the soil reduces. EC (μmhos/cm) value in water below 250 is considered excellent and above 750 is regarded as unsuited to irrigation [1, 22–24]. The salinity class of irrigation water by EC (μmhos/cm) is represented as follows: below 250 → low salinity; 251–750 → moderate salinity; 751–2250 → high salinity; and extremely high → 2250–5000 [21].

Sodium percentage is a significant criterion to study sodium hazards. It is the prime factor to decide the class of water for the utilization of agricultural activities [1]. It is effective to distinguish the water, as a low amount is a sign of hard water and a high amount implies soft water. Sodium percentage indicates the sodium hazard, but it is not an efficient criterion as sodium adsorption ratio [2, 21]. Plant growth is reduced due to the application of water with a high percentage of sodium. The addition of gypsum to soil can decrease the outcome of a high level of sodium in irrigation water [1]. Equation 1 is used to compute the sodium percentage [17, 21] with reference to comparative ratios of cations that exist in water. The class of irrigation water regarding Na percentage:

$$\mathrm{Na\%} = \frac{\mathrm{K^+ + Na^+}}{\mathrm{Mg^{2+} + Ca^{2+} + K^+ + Na^+}} \times 100 \tag{1}$$

where Ca^{2+}, Na^{+}, Mg^{2+}, and K^{+} are the ion concentrations of calcium, sodium, magnesium, and potassium expressed in millie-quivalents per litre (m-eq/l). Irrigation water quality based on sodium percentage: below 20 → excellent; 20–40 → good; 40–60 → permissible; 60–80 → doubtful; and over 80 → not suitable [3].

Sodium-Absorption Ratio, **SAR**, is a vital factor to determine the compatibility of groundwater in irrigation works [2]. Soil properties are changed because the use of irrigation water with excess sodium and excess sodium in water also makes the soil impervious [1, 11]. High and extremely high sodium water is considered unsuited for irrigation purposes [2]. If groundwater with a high sodium proportion is used for irrigation purposes, it can demolish the soil structure [4, 11]. Equation 2 is used to compute the SAR [19, 21]:

$$\mathrm{SAR} = \frac{\mathrm{Na}^{+}}{\sqrt{\frac{\mathrm{Ca}^{2+}+\mathrm{Mg}^{2+}}{2}}} \tag{2}$$

where Ca^{2+}, Na^{+}, and Mg^{2+} are the ion concentrations of calcium, sodium, and magnesium expressed in milli-equivalents per litre (m-eq/l). Irrigation water class concerning risky effects of SAR (m-eq/l)1/2: under 10 → less; 10–18 → moderate; 18–26 → high; and over 26 → extremely high [19].

The compatibility of water for irrigation use relies on the concentration of **carbonate and bicarbonate** [1]. For agricultural purposes, the serious outcome of bicarbonate and carbonate on the class of water is checked by Residual-Sodium-Carbonate, **RSC** [2]. In irrigation water, the parameters like pH, EC, and SAR are seriously affected by RSC. The physical properties of soil are seriously influenced by the irrigation water with high RSC. The permeability of soil minimizes due to more RSC in irrigation water [4]. Water is considered safe if the water contains an RSC value below 1.25 m-eq/l, and an RSC value within 1.25–2.50 m-eq/l is regarded as low class. RSC value above 2.50 m-eq/l is unsuited for irrigation [21]. Equation 3 is used to calculate the RSC [19, 21]:

$$\mathrm{RSC} = \left(\mathrm{HCO}_3^{-} + \mathrm{CO}_3^{2-}\right) - \left(\mathrm{Ca}^{2+} + \mathrm{Mg}^{2+}\right) \tag{3}$$

where HCO_3^{-}, Ca^{2+}, CO_3^{2-}, and Mg^{2+} are ion concentrations of bicarbonate, calcium, carbonate, and magnesium expressed in m-eq/l. Irrigation water quality based on RSC (m-eq/l): under 1.5 → small; 1.5–3 → moderate; 3–6 → high; and over 6 → extremely high risk [19].

Though the existence of **boron** within irrigation water is a crucial micronutrient for the development of the plant, overdose can create toxicity symptoms in particular crops. Naturally, boron is present in groundwater because of the seepage through rocks and soils carrying borates and borosilicates. Contamination of water due to boron is probably caused by water-rock interaction, seawater interference, sewage effluents, and fertilizers [2]. Normally, plants do not show any sign of boron deficiency if irrigation is done with water containing boron of at least 0.10 ppm. But in the case of more sensitive crops, damage may exhibit if irrigation is done with

Table 2 Impact on crops concerning the concentration of chloride in irrigation water [25]

Chloride (ppm)	Impact on plants
≤70	Normally every plant is safe
71–140	Low to medium damage can occur in sensitive plants
141–350	Low to substantial damage can occur in moderately tolerant plants
≥351	May create acute problems

water containing boron of more than 1.00 ppm [21]. The rating of the quality of irrigation water concerning the harmful effects of boron (ppm): under 1 → less; 1–2 → moderate; 2–4 → high; and over 4 → extremely high toxicity [19].

The existence of **chloride** in irrigation water is generally in the form of chlorine. Normally, the lack of chloride has not ever been observed as it is spread extensively and can be responsible for salinity issues. In irrigation water, the utmost usual toxic ion is chloride [2, 25]. In natural waters, chloride level is relatively low excluding brackish or saline water. Though chlorides are essential for the growth of the plant, overdose can create toxicity to some kinds of plants [25]. The chloride (ppm) in groundwater below 70 is regarded as harmless and above 350 can cause acute problems for crops [2, 25]. Table 2 shows the effect on crops concerning the level of chloride in irrigation water.

4 Groundwater Sampling

For appropriate evaluation of water quality parameters, accurate sampling is very essential. Even if leading skills with advanced tools are applied, the parameters may provide a false reflection of the original structure due to inaccurate sampling [9]. The samples are collected before and after monsoon periods in a year. Groundwater specimens are collected from bore/hand pumps that must be in active condition. Polyethene bottles of one-litre capacity are used for the collection of groundwater samples. A bottle should be washed properly with distilled water first and then deionized water and labeled before collecting the samples. Groundwater specimens are stored after driving out water for around 10 min to extract stagnant water present in the well. After that, the samples are moved to the laboratory and kept at 40 °C [8]. After that, the samples are examined with the help of a standard method as per guidelines provided by APHA [12].

For accurate sampling, the factors given below should be planned perfectly [9]: (a) method of sampling, (b) volume/size of the sampling, (c) sampling location number, (d) sample number, (e) sample type, and (f) intervals of time. At the time of sampling, the following factors must be considered [9]: (a) selection of an accurate sampling container, (b) contamination should be avoided, and (c) safety.

5 Water Quality Index (WQI)

WQI is one of the most productive and appropriate mechanisms to assess and report the quality of water of a particular water source [26]. It converts a huge amount of water quality data into an isolated digit and describes the class of water in a very simple way. It provides a common structure for comparing a large number of measured data with specified standard limits. Thus, it is easily acceptable to the administration and common people [9]. It was evolved to inspect the condition of groundwater class by including important parameters. There are a lot of water quality indices like the NSFWQI, CCMEWQI, OWQI, and WAWQI. Three steps are executed for determining WQI. At first, the weight (w_i) of every water class parameter is assigned as per its importance for drinkable water. Equation 4 is used to calculate the relative weight (W_i):

$$W_i = \frac{w_i}{\sum_{i=1}^{n} w_i} \tag{4}$$

where n indicates the number of parameters. Then, a rating of quality (q_i) is measured for each parameter. Equation 5 is used to calculate the rating of quality (q_i):

$$q_i = \left(\frac{C_{ic}}{S_{id}}\right) \times 100 \tag{5}$$

where C_{ic} indicates the concentration level of chemical parameters of the sample of water in ppm, and S_{id} represents the standard limit of each parameter of drinkable water in ppm provided by WHO [10]. In the end, the WQI is calculated by Eq. 6:

$$\text{WQI} = \sum_{i=1}^{n} W_i q_i \tag{6}$$

The class of water based on the WQI: under 50 → excellent; 50–100 → good; 100–200 → poor; 200–300 → very poor; and over 300 → not suitable [7] for drinking.

6 Piper Trilinear Diagram

Piper [27] trilinear diagram (Fig. 1) is an efficient graphical method for introducing water chemistry data that assist to understand the origins of the dissolved elements in the water. This model composes of three specified portions with pairs of triangular and a diamond. The positively charged and negatively charged ions are represented on the left and right triangles, respectively. The left triangle consists of major cations like Mg^{2+}, Ca^{2+}, and ($K^+ + Na^+$). The right triangle consists of major anions like $SO_4{}^{2-}$,

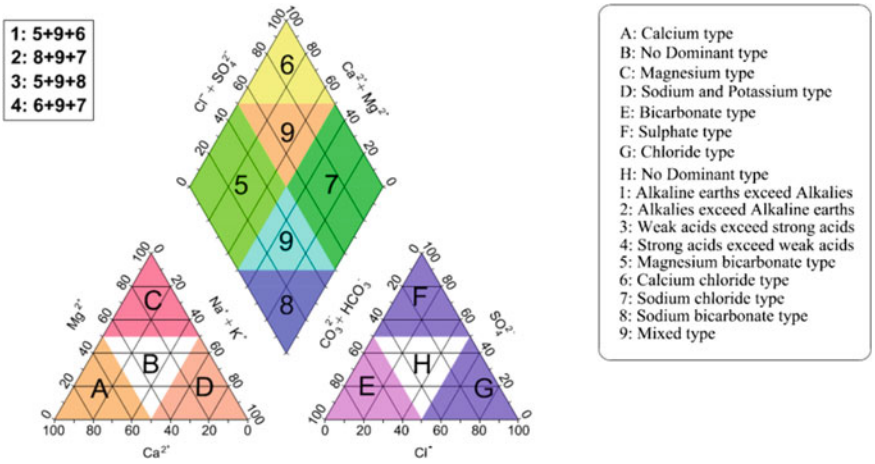

Fig. 1 Piper trilinear diagram describing the groundwater composition with respect to cation and anion

Cl^-, and $(CO_3^{2-} + HCO_3^-)$. The pair of triangular plots are then projected onto a diamond. Here, diamond field is a formation of anions [(sulfates + chlorides)/(total anions)] and cations [(potassium + sodium)/(total cations)] [8, 27].

7 Rating Analysis

Considering the above groundwater quality parameters for drinking, some of the parameters with a concentration above the permissible limit have a great impact on the human body. Depending on the effect of water quality parameters on human fitness, a quantitative rating analysis has been done on a priority basis for the prospective evaluation of groundwater class for drinking. The maximum rating value of 3 is assigned. The parameter with rating value 1 indicates less priority, rating value 2 indicates medium priority, and rating value 3 indicates a high priority to judge the groundwater class for drinking purposes as shown in Table 3.

8 Rating of Groundwater Quality Parameters Concerning Crops Using Irrigation

Considering the above parameters for irrigation, some of the parameters with a concentration above the permissible limit have a great impact on crops. Concerning the impact of parameters on crops, a rating analysis has been done on a priority basis to judge the groundwater quality for irrigation works. The maximum rating value of

Table 3 Rating of groundwater drinking quality parameters

Parameters	Rating value out of 3	Explanation concerning the impact on human health
pH	1	No direct impact on health [10]. The concentration of pH increases due to the intrusion of seawater in coastal areas [28]
Chlorides	1	No guideline value is provided based on human health [10]. Chloride is one of the important parameters in coastal areas [28]
Fluoride	3	The concentration of fluoride is comparatively high in groundwater [10]. Water containing fluoride above permissible limit results in dental fluorosis and skeletal fluorosis [10]. In India, around 12 million tons of fluorides are found out of 850 lakh tons of overall fluoride available on the earth's crust [29]. So, it's alarming as the concentration of fluoride is widely spread over India
Arsenic	3	Arsenic possibly exists in potable water sources, especially in groundwater, at high concentrations [10]. Arsenic is regarded as a high-precedence element for screening in potable water sources [10]. Use of water with excessive levels of arsenic results in skin cancer, bladder, and lung cancers [10]
TDS	2	No guideline value is provided concerning human fitness but a high level of TDS in drinkable water may be rejected by consumers [10]. In the seaside area, the level of TDS is excessive in groundwater due to the intrusion of seawater into the aquifer [28]. The salinity of water enhances due to the surplus TDS in groundwater
Nitrate	2	The concentration of nitrate in groundwater is relatively low, but water with a high concentration of nitrate can cause thyroid disease, diabetes, gastric cancer, and methemoglobinemia [10]. In recent times, groundwater contaminated by nitrates has been found out extremely over the world [2]
Calcium and Magnesium	1	The concentration of Ca and Mg is high in hard water, but it has an insignificant effect on human fitness [10]
Hardness	1	No guideline value is provided based on human health. The degree of hardness can affect the admissibility criteria of the consumers [10]. In the seaside area, water becomes hard because of the interference of seawater in the aquifer [28]

(continued)

Table 3 (continued)

Parameters	Rating value out of 3	Explanation concerning the impact on human health
Sulfate	1	No guideline value is provided based on human health [10]

3 is assigned. The parameter with rating value 1 indicates less priority, rating value 2 indicates medium priority, and rating value 3 indicates a high priority to evaluate the groundwater class for irrigation purposes as represented in Table 4.

Table 4 Rating of irrigation groundwater quality parameters

Parameters	Rating value out of 3	Explanation based on the impact on crops
pH	1	It is an inadmissible standard of water class as the pH of water is absorbed by the soil. And maximum crops can bear a broad range of pH limits [25]
TDS	3	Excessive salt is present in irrigation water responsible for saline soil. The salinity problem is a major issue in crop production. It reduces plant growth and yield [1]. Groundwater salinity will increase because of rare rainfall in hot arid areas. The plants will wilt due to high salt concentration in irrigation water [25]. The salinity of soil enhances due to the surplus dissolved salts in groundwater. The natural characteristics and fruitiness of soil are influenced by the surplus dissolved salts in groundwater
EC	3	EC is the key factor in deciding the appropriateness of groundwater for cultivation works [8]. With the increase of total dissolved solids, EC will also increase. Excess concentration of electrical conductivity in groundwater occurs because of the interference of seawater in the seaside aquifers and sewage water input [28]. It reduces plant growth and yield
Na%	2	It is the key factor to decide the eligibility of groundwater for cultivation works [8]. It has a great impact on soil permeability and as a result, it is difficult to plow and unfit for seed maturation [8]. Sodium accumulation affects the soil structure, infiltration, and aeration, therefore, affects on plant growth [2]. It is not an efficient criterion as SAR for groundwater quality assessment [21]

(continued)

Table 4 (continued)

Parameters	Rating value out of 3	Explanation based on the impact on crops
SAR	3	For sensitive fruits, SAR in irrigation water shouldn't be above 4, and for common crops and herbages, a limit of 8–18 is generally considered appropriate [2]. More SAR concentration results in soil grinding, bad seedling emergence, and bad aeration. It also makes the soil impermeable and demolishes the soil structure [4, 25]. In irrigation water, surplus sodium can collapse the quality of soil and can harm sensitive crops [11]
RSC	2	High levels of calcium and magnesium in groundwater are indicated by a negative value of RSC. More RSC in water can reduce the yield of crops and cause the burning of plant leaves [30]. It makes the soil impervious and affects the parameters like pH, EC, and SAR
Boron content	1	Semi-sensitive, semi-tolerant, and tolerant crops can tolerate boron concentrations of more than 1.25, 2.50, and 3.75, respectively. It has serious effects on sensitive crops if the concentration of boron is above 1 ppm [17, 21]. A level of boron above 1 ppm is regarded as significant intimidation to the utilization of groundwater for cultivation purposes. It is an essential water quality parameter for irrigation, but boron toxicity is a minor issue in maximum fields [25]
Chloride	1	It is necessary for the growth of plants, but high concentration can cause acute problems for some particular plants [21, 25]. Leaf burn may be caused if irrigation is done with water containing high chloride concentrations [2]
pH	1	It is an inadmissible standard of water class as the pH of water is absorbed by the soil. And maximum crops can bear a broad range of pH limits [25]

pH: potential of hydrogen; TDS: total dissolved salts; EC: electrical conductivity; Na%: sodium percentage; SAR: sodium-absorption ratio; RSC: residual-sodium-carbonate

9 Conclusions

Evaluation and monitoring of groundwater standard parameters for drinking and irrigation uses are very essential, particularly in growing nations like India because of rapid industrialization and urbanization. As groundwater is a valuable resource, so, it is required to maintain and save this precious resource by following some measures to prevent contamination. It is mandatory to analyze the groundwater quality for checking the compatibility criteria for the designated use. Various water quality parameters are evaluated and differentiated with their standard values to decide the acceptability of water to be used. In this paper, several parameters with their standards are mentioned in brief in one place, and rating analysis on a priority basis has been done to judge the groundwater class for drinking and irrigation uses. The rating value

3 is assigned for the parameters like fluoride and arsenic, rating value 2 is assigned for the parameters like TDS and nitrate, and rating value 1 is assigned for the parameters like pH, calcium, chloride, hardness, magnesium, and sulfate for the evaluation of groundwater class for drinking. The rating value 3 is assigned for the parameters like total dissolved salts, EC, and SAR, rating value 2 is assigned for the parameters like Na% and RSC, and rating value 1 is assigned for the parameters like pH, chloride, and boron for the evaluation of groundwater class for irrigation. It may be useful for researchers and analysts to get a detailed outline to evaluate the groundwater class for drinking and irrigation purposes.

References

1. Joshi MD, Kumar A, Agrawal N (2009) Assessment of the irrigation water quality of River Ganga in Haridwar district. Rasayan J Chem 2(2):285–292
2. Bhat AM, Wani AS, Singh KV, Sahoo J, Tomar D, Sanswal R (2018) An overview of the assessment of groundwater quality for irrigation. J Agric Sci Food Res 9(1):1000209
3. Annor AA, Bewil NP, Boateng D (2018) Evaluation of groundwater suitability for irrigation in the Lambussie-Karni district of Ghana. Ghana Min J 18(1):9–19
4. Tiwari P (2017) Water quality assessment for drinking and irrigation purpose. Indian J Sci Res 13(2):140–142
5. Maity PK, Das S, Das R (2017) Assessment of groundwater quality and saline water intrusion in the coastal aquifers of Purba Midnapur district. Indian J Environ Prot 37(1):31–40
6. Maity PK, Das S, Das R (2018) A geochemical investigation and control management of saline water intrusion in the coastal aquifer of Purba Midnapur district in West Bengal, India. J Indian Chem Soc 95(3):205–210
7. Wagh MV, Mukate VS, Panaskar BD, Muley AA, Sahu LU (2019) Study of groundwater hydrochemistry and drinking suitability through water quality index (WQI) modelling in Kadava river basin India. SN Appl Sci 1:1251
8. Madhav S, Ahamad A, Kumar A, Kushawaha J, Singh P, Mishra KP (2018) Geochemical assessment of groundwater quality for its suitability for drinking and irrigation purpose in rural areas of Sant Ravidas Nagar (Bhadohi) Uttar Pradesh. Geol Ecol Landsc 2(2):127–136
9. Roy R (2019) An introduction to water quality analysis. Int Res J Eng Technol 6(1):201–205
10. WHO (2011) Guidelines for drinking water quality, 4th edn. World Health Organization
11. Oinam DJ, Ramanathan LA, Sing G (2012) Geochemical and statistical evaluation of groundwater in Imphal and Thoubal district of Manipur India. J Asian Earth Sci 48:136–149
12. APHA (1995) Standard methods for the examination of water and wastewater, 17th edn. APHA, Washington, USA
13. IS 10500 (2012) Indian standard drinking water specification, 2nd revision. Bureau of Indian Standards, New Delhi, India
14. Das S, Nayek M, Das S, Dutta P, Mazumdar A (2014) Impact on water quality in Piyali River, Sundarbans, India due to saline water intrusion. Indian J Environ Prot 34(12):1010–1019
15. Das S, Roy D, Majumder A, Mazumdar A, Rit K (2018) A preliminary investigation on water quality of Jai Hind Jal Prakalpa in Kolkata. Indian J Environ Prot 38(2):148–153
16. Mukherjee P, Das S, Mazumdar A (2020) Evaluating volatility in quality indexing of saline water during tidal backwater incursion in Western Canals of South 24-Parganas, West Bengal. J Indian Chem Soc 97(4):577–586
17. Todd KD, Mays WL (2005) Groundwater hydrology, 3rd edn. Wiley and Sons, USA
18. Sawyer NC, McCarty LP (1967) Chemistry for sanitary engineers, 2nd edn. McGraw-Hill, New York, USA

19. IS 11624 (1986) Indian standard guidelines for the quality of irrigation water. Bureau of Indian Standards, New Delhi, India
20. John B, Das S (2020) Role of electrical conductivity on salinity and mineralization due to groundwater level fluctuations in Kolkata city. IOP Conf Ser Earth Environ Sci 505(1):012021
21. Wilcox VL (1955) Classification and use of irrigation waters. United States Department of Agriculture, Washington D.C., Circular no 969 (1955)
22. Chakraborty S, John B, Maity PK, Das S (2020) Increasing threat on groundwater reserves due to seawater intrusion in Contai Belt of West Bengal. J Indian Chem Soc 97(5):799–817
23. Chakraborty S, Maity PK, John B, Das S (2020) Overexploitation of groundwater causing seawater intrusion in the coastal aquifer of Egra in West Bengal. Indian J Environ Prot 40(4):413–423
24. Chakraborty S, John B, Das S, Maity PK (2020) Examining the extent of seawater intrusion from groundwater quality analysis at Purba Medinipur coast of India. J Indian Chem Soc 97(4):587–594
25. Zaman M, Shahid AS, Heng L (2018) Irrigation water quality. Guid Salin Assess, Mitig Adapt Using Nucl Relat Tech 5:113–131
26. John B, Roy P, Das S (2021) Analysing the influence of groundwater exploitation on its quality in Kolkata. In: Kumar S, Kalamdhad A, Ghangrekar M (eds) Sustainability in environmental engineering and science 2019, LNCS, vol 93. Springer, Singapore, pp 83–89
27. Piper AM (1944) A graphic procedure in the geochemical interpretation of water-analyses. Trans Am Geophys Union 25:914–923
28. Kuttimani R, Raviraj A, Pandian JB, Kar G (2017) Determination of water quality index in coastal area (Nagapattinam) of Tamil Nadu India. Chem Sci Rev Lett 6(24):2208–2221
29. Teotia SP, Teotia M (1994) Endemic fluorosis in India: a challenging national health problem. J Assoc Physicians India 32:347–352
30. Ramesh K, Elango L (2012) Groundwater quality and its suitability for domestic and agricultural use in Tondiar river basin, Tamil Nadu India. Environ Monit Assess 184:3887–3899

Regional Ocean Modeling System (ROMS) Simulations to Identify the Sensitivity of Forcing Conditions on the Thermohaline Features of the Bay of Bengal

Tarumay Ghoshal and Arun Chakraborty

Abstract The Bay of Bengal (BOB) is known for prominent seasonal and annual climatic variability. The bay is locked from three directions, north, east, and west, and open to the Indian Ocean from the southern direction. BOB experiences local and remote effects in its thermohaline features. The BOB always has a higher surface temperature (SST) compared to the Arabian Sea which can be observed from basin average SST values. The semiannual signal in those SST values shows higher than 26 °C. The basin is very much prone to various categories of cyclones which are known to cause prominent upwelling and mixing in the basin. However, most of the times, satellite data cannot track the thermohaline changes within a short period of time due to poor temporal and spatial resolutions and that too only limited to the surface, not below it. Moreover, in situ data are not sufficient or not present at the required locations to provide the data for the particular event. The same situation is also prevalent for remote effects when Indian Ocean Dipole (IOD) and El Nino-Southern Oscillation (ENSO) events create surface-to-subsurface thermohaline variability. Therefore, these problems can be tackled through numerical modeling where a realistic initial condition will provide much more accurate results within a short time gap. To meet this objective, Regional Ocean Modeling System (ROMS) is set up for BOB with a climatological run. In addition, forcing conditions and initial conditions are adopted for specific events like IOD, ENSO, or cyclones. Satellite-derived wind velocity components, stress, precipitation, and chlorophyll data are provided as data input in initial and boundary conditions. The simulation results show high sensitivity to wind and other forcing conditions for specific events which provide better feature extraction compared to climatological runs.

Keywords Bay of Bengal · IOD · ENSO · ROMS

T. Ghoshal (✉)
Center of Excellence in Land, Air and Water (Environmental Sustainability), Department of Civil Engineering, DIT University, Dehradun, Uttarakhand, India
e-mail: tarumay.ghoshal@dituniversity.edu.in

A. Chakraborty
Centre for Ocean, River, Atmosphere and Land Sciences (CORAL), IIT Kharagpur, Kharagpur, India

© The Author(s), under exclusive license to Springer Nature Singapore Pte Ltd. 2023

S. Kumar et al. (eds.), *Sustainable Environmental Engineering and Sciences*,
Lecture Notes in Civil Engineering 323, https://doi.org/10.1007/978-981-99-0823-3_4

1 Introduction

The Bay of Bengal (BOB) basin is limited by land from East, West, and North. The basin is open to the Indian Ocean in the south. In spite of land surrounded from three sides, BOB experiences local and remote forcing conditions due to reversing monsoon winds, freshwater flux coming from some of the major rivers of the Indian subcontinent, and remote effects entering from the Indian Ocean in the form of oscillating ocean waves. The north-east monsoon winds starting from November up to February and south-west winds from July to August are responsible for creating currents and Gyres in BOB in a complex interaction process [1–6]. The Kelvin and associated Rossby waves in BOB enhance circulation and strengthen East India Coastal Current (EICC) which flows near the east-coastal boundary of India. These wind-induced waves cause upwelling and downwelling which attribute to BOB circulation patterns, thermohaline changes, and heat distributions [7–10]. Variability is also observed in BOB's surface temperature (SST) and salinity (SSS). Low values of SST are predominant in northern BOB at the time of winter, and the values are noted ranging 26–27 °C with the lowest observed where the influx of the Ganges river is very prominent. Warm SST is prominent all over the BOB during the summer season, especially during April-June and crosses 30 °C. Including the fact that summer and winter time SSTs show variability, the basin average SST always remains higher than 26 °C [9]. This condition is one of the favorable reasons for creating cyclones in BOB. SSS pattern in BOB shows distinctive variations between northern and southern BOB. This variation is due to the effect of freshwater discharge in northern BOB which lowers salinity values. Here, it is to note whether it is about circulation or thermohaline variability; wind is the most influential factor in BOB [11]. Due to wind-induced forcing, surface-to-subsurface ocean stratification is disturbed and mixing occurs which also creates variability in biogeochemical parameters. Recent studies have also shown that wind pattern over the BOB has a close affinity with El-Nino-Southern Oscillation (ENSO) event. Similar observations also exist for Indian Ocean Dipole (IOD) [12]. Moreover, during cyclones, wind induces heavy storm surge that leads to large inundations in the areas of coastal parts of India and Bangladesh [13–15]. Therefore, it is very much imperative to accept the role of wind forcing behind the BOB's thermodynamic and biogeochemical variability, and one needs to apply proper wind forcing conditions even in numerical model studies to properly delineate intrinsic features [16, 17].

Every year, BOB faces tropical cyclones. These cyclones are created during, before, and after summer monsoons and also in between. The number and intensity of such cyclones are found in increasing trend [18, 19]. Also, the physical, biogeochemical parameters, circulation patterns, and even tropical cyclone intensification in BOB are known to be affected due to remote effects from ENSO and IOD events [20–22]. However, to investigate the effect of such ocean-atmospheric interactions on the complex thermodynamic processes of BOB, observational data are not sufficient. Rather, model simulations can identify such effects when controlled and

forced model runs are performed [23]. Therefore, in this study, a numerical simulation experiment is done for a specific case of a cyclone and ENSO-IOD event to observe the effect of wind forcing on BOB's physical and biogeochemical parameters. In order to do so, Regional Ocean Modeling System (ROMS) is set up along with forcing and initial conditions both at surface and subsurface levels. It is necessary to mention here that while the variability is to be observed at the surface level, then satellite-derived variables play an important role but at subsurface levels satellite data are unavailable and in situ sensors still are not sufficient enough in number to produce high-resolution spatially gridded data for BOB region [24]. Therefore, in this context climatological run becomes important. However, mere climatological runs can't distinguish synoptic features. It needs realistic forcing conditions exclusively to be associated [25]. Therefore, in this study, an effort has been made to detect wind forcing effect on various ocean parameters (e.g. temperature, salinity, and chlorophyll (Chl)) through ROMS simulations and for this purpose, a comparative analysis is performed on simulations that are forced with satellite-derived wind components for 'SIDR' cyclone in BOB. Also, the year 2015 has been considered for observing the effect of El Nino-Positive IOD (ElNino-PIOD) event [26] on BOB's Chl values.

2 Data and Methodology

The high-resolution ROMS (www.myroms.org) model [27] is established for the BOB region. The model is widely used to understand oceanic processes and the influence of atmospheric forcing [24, 28–30]. The basic governing equations (momentum, advective–diffusive, equation of state, hydrostatic, continuity) of ROMS are written in Cartesian coordinates which include z-axis that points upwards vertically and the horizontal plane residing on the surface of water [31] (https://www.myroms.org/wiki/Equations_of_Motion). The BOB region is considered in this study with the geographical boundary: 4°N–24°N and 76°E–100°E. The model has been run with default climatological forcing conditions for achieving stability conditions till the annual cycle is achieved after three years.

The following datasets are used in ROMS simulations:

- Advanced Scatterometer (ASCAT) derived wind components (0.25°) [32]. These wind data are made available from the Centre de Recherche et d'ExploitationSatellitaire (CERSAT), at IFREMER, Plouzané (France).
- Quick Scatterometer (QuikSCAT) wind components (0.25°) [33–35] QuikScat data are generated by Remote Sensing Systems and sponsored by the NASA Ocean Vector Winds Science Team. Data can be obtained from www.remss.com.
- Moderate Resolution Imaging Spectroradiometer (MODIS) Chlorophyll (Chl) [36] https://modis.gsfc.nasa.gov/data/dataprod/chlor_a.php.
- The ocean current data are used from Ocean Surface Currents Analyses Real-time (OSCAR) [37].
- Tropical Rain Measuring Mission Microwave Imager (TRMM TMI) SST [38].

- A Group for High Resolution Sea Surface Temperature (GHRSST) [39, 40].
- The cyclone track information is obtained from Regional Specialized Meteorological Centre for Tropical Cyclone over North Indian Ocean, India Meteorological Department (RSMC-IMD) [41].

Initial ROMS Run has been done with World Ocean Atlas [42] temperature and salinity data. After the model has been stabilized, different forcing conditions are applied to simulate various events. Since cyclone is a synoptic case and the variations of wind components are maximum within a very short period of time, ASCAT and QuikSCAT wind components have been used for cyclone simulation for testing the sensitivity of the model toward wind data, and a comparative study is done. 'SIDR' cyclone has been considered for this analysis. For ElNino-PIOD, only ASCAT wind components have been used. The winter season of the year 2015 is considered for simulations and wind-forcing conditions were applied accordingly.

TMI SST and GHRSST have been used in the validation of model results for cyclone case and ElNino-PIOD simulations, respectively.

3 Results and Discussion

3.1 ROMS Simulation for 'SIDR' Cyclone

The tropical cyclone 'SIDR' was formed on the BOB on November 11, 2007, with depression at 10°N and 92°E and subsequently turned into Extremely Severe Cyclonic Storm (ESCS) on November 13, 2007, and ultimately crossed the Bangladesh coast on 15 November as Very Severe Cyclonic Storm (VSCS).

The cyclone track information is obtained from RSMC-IMD. Figure 1 shows the SST and SSS from ASCAT and QuikSCAT wind-forced ROMS simulation with 'SIDR' cyclone track. The effect of wind is prominent on the parameters as upwelling is very strong to bring the bottom water to the top. This is observed as common for both wind components but ASCAT winds have produced a larger effect on simulations. Another difference is observed that ASCAT wind has produced a larger area under influence but QuikSCAT effect is more gradual and limited to the cyclone center. The star symbol in Fig. 1 represents one of the prominent cyclone centers of strong wind rotation. Figure 2 gives the effect on subsurface temperature and salinity along 89°E. The strong upwelling has caused the upliftment of isothermal and isohaline surfaces in the vicinity of the strong wind rotation. There are some differences observed between the two simulations. QuikSCAT wind shows two distinctive displacements of isotherms and isohalines, while it is completely missing for ASCAT. These variations are attributed to data variations in both wind-forcing components. These show the ROMS model is highly sensitive toward wind data variability. Table 1 provides root mean square error (RMSE) values computed between ROMS SST with TMI SST for data validation. The values are shown for 5 days. The data shows an error is less than 2 °C which is acceptable [43]. However,

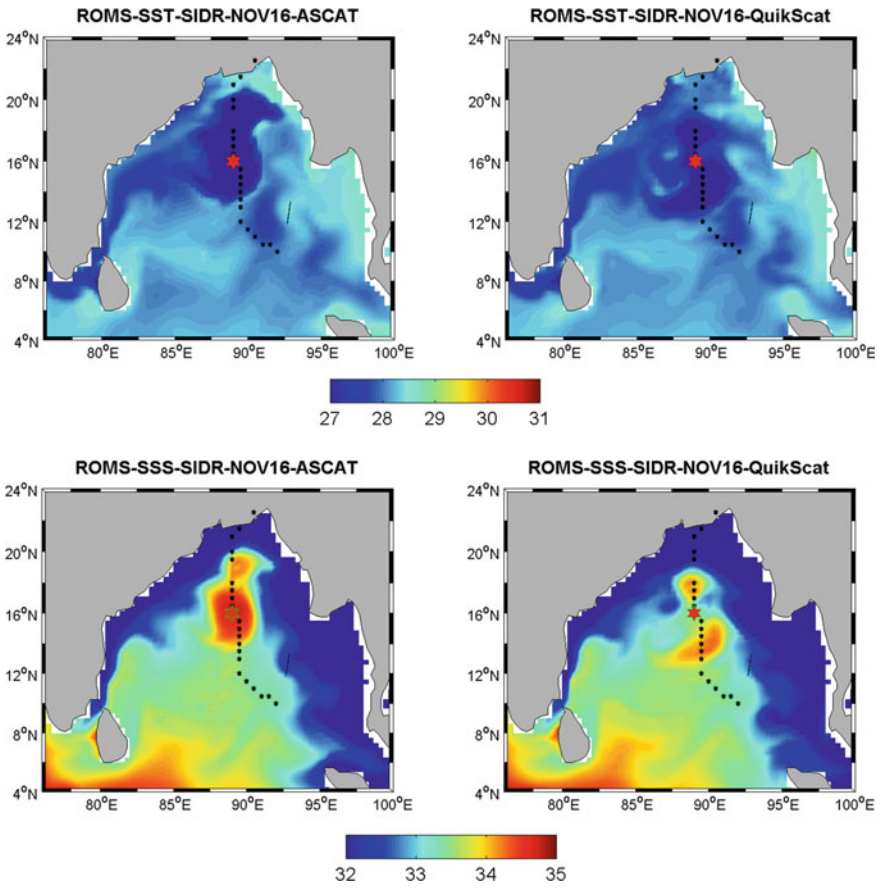

Fig. 1 ROMS simulated SST and SSS with ASCAT and QuikSCAT forcing for 'SIDR' cyclone

ASCAT wind simulation shows a larger deviation compared to QuikSCAT wind simulation as for these 5 days ASCAT SST RMSE values are 15% more on average compared to its counterpart. Figure 3 depicts the ROMS simulated Chl for QuikSCAT forcing. The cyclone-induced upwelling has caused nutrient-rich water to come to surface as well as wind-induced mixing has caused a surge in Chl concentration in post-cyclone period.

3.2 Simulation of Chl for ElNino-PIOD Year

Figure 4 shows the ROMS simulated Chl data for ElNino-PIOD year 2015, December month. The left panel shows the results from ROMS forcing run by ASCAT wind components, satellite-derived SST. The right panel shows the climatological run.

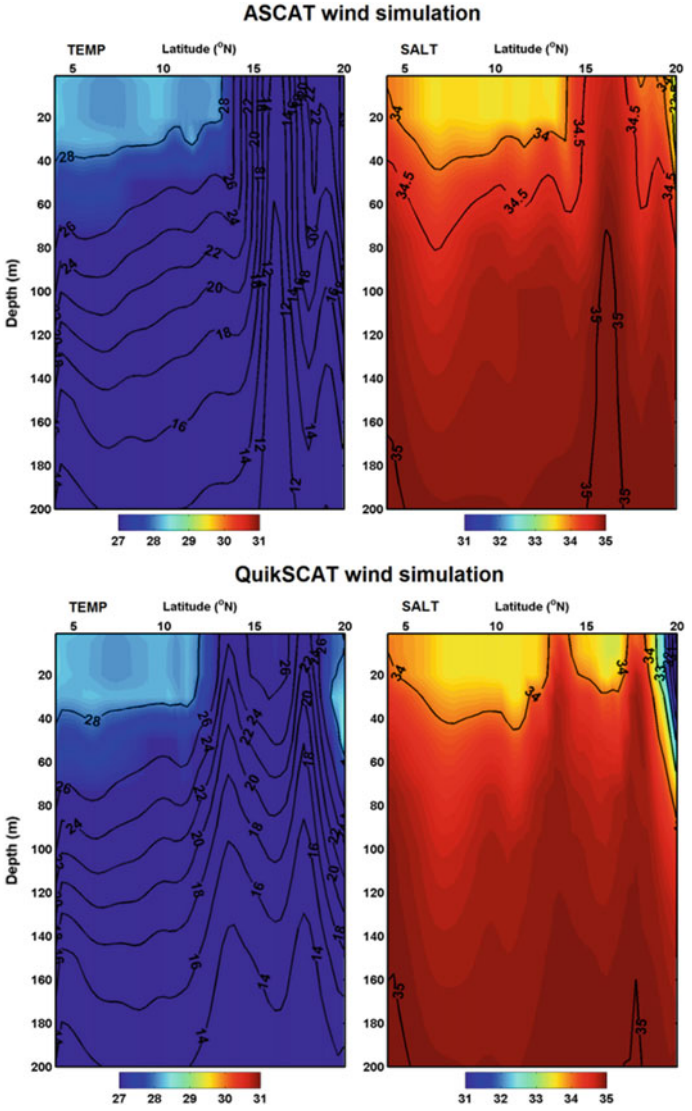

Fig. 2 ROMS simulated temperature and salinity with ASCAT and QuikSCAT forcing for 'SIDR' cyclone

Table 1 RMSE of ROMS simulated SST versus TMI SST

Day index	1	2	3	4	5
ASCAT simulated ROMS SST versus TMI SST	1.0272	0.9632	1.3561	1.4667	1.4559
QuikSCAT simulated ROMS SST versus TMI SST	1.0272	0.9275	1.1744	1.1713	1.1311

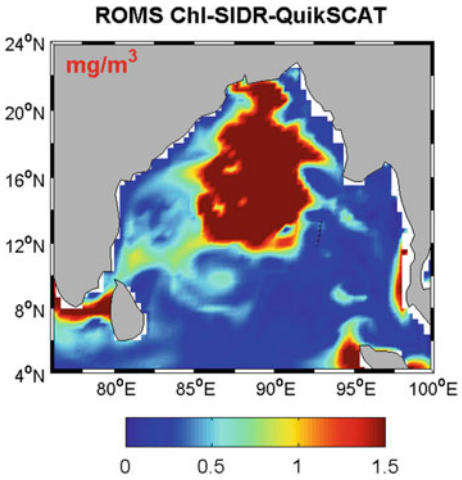

Fig. 3 ROMS simulated Chl for 'SIDR' cyclone

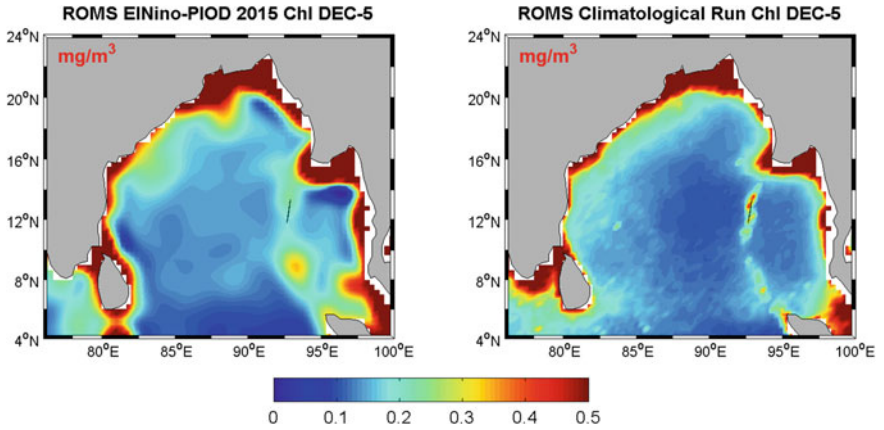

Fig. 4 ROMS Chl: forcing induced run (left panel) and climatological run (right panel)

The high Chl values are observed in the forcing run compared to the climatological run. Moreover, it is observed that Chl values are more concentrated in the east side of the BOB due to wind-forcing conditions. This finding is in correlation with the observational study made by Martin and Shaji [44]. The study also reported a detailed mechanism of shifting the winter-specific Chlorophyll concentration toward the east. This shifting happens in the opposite direction specific to Rossby waves and also average zonal currents. This is observed from November to March.

The validation of model results is compared with MODIS daily Chl values with root mean square error (RMSE) calculations. RMSE calculation is obtained for the entire BOB and a central area denoted by 87–92°E and 8–12°N. The RMSE values are provided in Table 2. The data shows the RMSE values for the entire BOB are

Table 2 Root mean square error (RMSE) with MODIS daily Chlorophyll data

Day index	1	2	3	4	5	6	7	8
Entire BOB	0.4393	0.2351	0.2076	0.2810	0.7301	0.8331	0.7405	0.9958
Central BOB	0.0319	0.0236	0.0312	0.0647	0.0723	0.2034	0.1277	0.0819

Table 3 Root mean square error (RMSE) of ROMS SST with GHRSST (DEC 2015)

Day index	1	2	3	4	5	6	7	8
Entire BOB	0.7537	0.6558	0.7332	0.7902	0.8499	0.8306	0.8523	0.9484

higher however for the central part, values are much smaller. Here, it is to note that MODIS has a lot of data gaps and variations. Also, it shows differences with in situ data [45]. However, notwithstanding this, there may be an overshoot of values near the coastal part in simulation, but the overall trend shows a dominance of Chl values toward coastal zones. The central and lower BOB shows less Chl data due to less circulation and mixing processes. Table 3 estimates RMSE values of ROMS SST compared with GHRSST for December 2015. The values indicate consistent results and are lower than 1. So the deviation is insignificant. Previous studies indicate that there is a value difference of 0.5–1 in RMSE when we compare satellite-derived SSTs with in situ data [44]. Since ROMS model conditions are primarily derived from World Ocean Atlas in situ climatology data, these deviation values are normal in that context.

4 Conclusion

The study has confirmed that ROMS simulation is highly influenced by wind forcing. It is found that variability in the wind dataset induces changes in thermohaline and biological parameters which are clearly evident in model results. It is also concluded from this model study that upwelling and mixing processes due to strong winds are responsible for breaking the existing stratification and shifting of isotherm and isohaline surfaces for the cyclone and post-cyclone periods. The synoptic cyclonic events however are more clearly expressed compared to ENSO-IOD events while here the remote effects coming from the Indian Ocean are stronger near the coastal areas as evident from high Chl concentration in the model simulation. The boundary of the study region chosen here can be an impediment in the ENSO-IOD study. The future study will include simulations in broader regions and a study of wave patterns for specific ENSO-IOD events. The authors will also focus on the role of other atmospheric forcing parameters in simulations for such types of events in future.

Acknowledgements The authors are very much grateful to Science & Engineering Research Board (SERB), Department of Science & Technology, Government of India, for providing financial support through a sponsored research project (FILE NO. EMR/2016/006392, Title: Implication of data

assimilation for identifying short scale variations in various biogeochemical characteristics in the Bay of Bengal through Regional Ocean Model Simulations) to conduct this research.

In addition, the authors express sincere gratitude toward the reviewers of this paper for their valuable suggestions toward improving the manuscript.

References

1. Babu MT, Sarma YVB, Murty VSN, Vethamony P (2003) On the circulation in the Bay of Bengal during northern spring inter-monsoon (March–April 1987). Deep Sea Res Part II 50(5):855–865
2. Schott FA, McCreary JP (2001) The monsoon circulation of the Indian Ocean. Prog Oceanogr 51(1):1–123
3. Eigenheer A, Quadfasel D (2000) Seasonal variability of the Bay of Bengal circulation inferred from TOPEX/Poseidon altimetry. J Geophys Res Ocean (1978–2012)105(C2):3243–3252
4. Varkey MJ, Murty VSN, Suryanarayana A (1996) Physical oceanography of the Bay of Bengal and Andaman Sea. Oceanogr Mar Biol Annu Rev 34:1–70
5. Kumar SP, Unnikrishnan AS (1995) Seasonal cycle of temperature and associated wave phenomena in the upper layers of the Bay of Bengal. J Geophys Res: Ocean (1978–2012)100(C7):13585–13593
6. Potemra JT, Luther ME, O'Brien JJ (1991) The seasonal circulation of the upper ocean in the Bay of Bengal. J Geophys Res Ocean (1978–2012)96 (C7):12667–12683
7. Girishkumar MS, Ravichandran M, Pant V (2012) Observed chlorophyll-a bloom in the southern Bay of Bengal during winter 2006–2007. Int J Remote Sens 33(4):1264–1275
8. Rao RR, Kumar MG, Ravichandran M, Rao AR, Gopalakrishna VV, Thadathil P (2010) Inter-annual variability of Kelvin wave propagation in the wave guides of the equatorial Indian Ocean, the coastal Bay of Bengal and the southeastern Arabian Sea during 1993–2006. Deep-Sea Res Part I Ocean Res Pap 57(1):1–13
9. Vinayachandran PN, Shetye SR, Sengupta D, Gadgil S (1996) Forcing mechanisms of the Bay of Bengal circulation. Curr Sci 753–763
10. Yu L, O'Brien JJ, Yang J (1991) On the remote forcing of the circulation in the, Bay of Bengal. J Geophys Res Ocean (1978–2012)96(C11):20449–20454
11. Natesan U, Subramanian SP (1992) Wind-wave relationship for Bay of Bengal from GEOSAT data. J Indian Soc Remote Sens 20(2):159–164
12. Rashmi R, Polnikov V, Pogarskii F, Gomorev I, Samiksha V, Vethamony P (2016) Long-term variability of the wind field over the Indian Ocean based on ERA-Interim reanalysis. Atmos Ocean 54(5):505–518
13. Bhaskaran PK, Rao AD, Murty T (2020) Tropical cyclone–induced storm surges and wind waves in the Bay of Bengal. Tech Disaster Risk Manag Mitig 237–294
14. Murty PLN, Srinivas KS, Rao EPR, Bhaskaran PK, Shenoi SSC, Padmanabham J (2020) Improved cyclonic wind fields over the Bay of Bengal and their application in storm surge and wave computations. Appl Ocean Res 95(102048)
15. Amarendra P, Bharathi G (2018) Variability of wave energy flux and wind during Phailin cyclone over Bay of Bengal. Int J Appl Eng Res 13(16):12792–12797
16. Remya PG, Kumar R, Basu S (2014) An assessment of wind forcing impact on a spectral wave model for the Indian Ocean. J Earth Syst Sci 123(5):1075–1087
17. Han W, Webster PJ (2002) Forcing mechanisms of sea level interannual variability in the Bay of Bengal. J Phys Oceanogr 32(1):216–239
18. Balaguru K, Taraphdar S, Leung LR, Foltz GR (2014) Increase in the intensity of postmonsoon Bay of Bengal tropical cyclones. Geophys Res Lett 41(10):3594–3601

19. Unnikrishnan AS, Kumar MR, Sindhu B (2011) Tropical cyclones in the Bay of Bengal and extreme sea-level projections along the east coast of India in a future climate scenario. Curr Sci 327–331
20. Mahala BK, Nayak BK, Mohanty PK (2015) Impacts of ENSO and IOD on tropical cyclone activity in the Bay of Bengal. Nat Hazards 75(2):1105–1125
21. Currie JC, Lengaigne M, Vialard J, Kaplan DM, Aumont O, Naqvi SWA, Maury O (2013) Indian Ocean dipole and El Nino/southern oscillation impacts on regional chlorophyll anomalies in the Indian Ocean. Biogeosciences 10(10):6677–6698
22. Aparna SG, McCreary JP, Shankar D, Vinayachandran PN (2012) Signatures of Indian Ocean Dipole and El Niño–Southern Oscillation events in sea level variations in the Bay of Bengal. J Geophys Res Ocean 117(C10)
23. Akhil VP, Lengaigne M, Vialard J, Durand F, Keerthi MG, Chaitanya AVS, Papa F, Gopalakrishna VV, De Boyer Montégut C (2016) A modeling study of processes controlling the Bay of Bengal sea surface salinity interannual variability. J Geophys Res Ocean 121(12):8471–8495
24. Ghoshal T, Chakraborty A (2019) Response of quick scatterometer wind forcing on the ROMS simulation during 'MALA' cyclone. Indian J Geo-Mar Sci 48(5):707–715
25. Chakraborty A, Gangopadhyay A (2015) Development of a high-resolution multiscale modeling and prediction system for Bay of Bengal, part I: climatology-based simulations. Open J Mar Sci 6(1):145–176
26. Avia LQ, Sofiati I (2018) Analysis of El Niño and IOD phenomenon 2015/2016 and their impact on rainfall variability in Indonesia. In: IOP conference series: earth and environmental science, vol 166, no 1. IOP Publishing, pp 012034
27. Vic C, Roullet G, Carton X, Capet X (2014) Mesoscale dynamics in the Arabian Sea and a focus on the Great Whirl life cycle: a numerical investigation using ROMS. J Geophys Res Ocean 119(9):6422–6443
28. Wilkin JL, Arango HG, Haidvogel DB, Lichtenwalner C, Glenn SM, Hedström KS (2005) A regional ocean modeling system for the long-term ecosystem observatory. J Geophys Res Ocean (1978–2012)110(C6)
29. Lermusiaux PFJ, Chiu CS, Robinson AR (2001) Modeling uncertainties in the prediction of the acoustic wavefield in a Shelfbeak environment. In: Theoretical and computational acoustics 2001, Er-Chang Shang, ICTCA2001, 21–25 May 2001. Beijing, China, pp 191–200
30. Haidvogel DB, Arango HG, Hedstrom K, Beckmann A, Malanotte-Rizzoli P, Shchepetkin AF (2000) Model evaluation experiments in the North Atlantic Basin: simulations in nonlinear terrain-following coordinates. Dyn Atmos Ocean 32(3):239–281
31. Song Y, Haidvogel D (1994) A semi-implicit ocean circulation model using a generalized topography-following coordinate system. J Comput Phys 115(1):228–244
32. Bentamy A, Denis CF (2012) Gridded surface wind fields from Metop/ASCAT measurements. Int J Remote Sens 33(6):1729–1754. https://doi.org/10.1080/01431161.2011.600348
33. NASA Quick Scatterometer, QuikSCAT Science Data Product (2000) User's manual, overview & geophysical data products, version 2.0-draft. Jet Propulsion Laboratory, California Institute of Technology, Doc. D-18053
34. Weiss B (2000) Level 2B data software interface specification, QuikSCAT Era, SeaWinds processing and analysis centre. Jet Propulsion Laboratory, California Institute of Technology, Doc. D-16079
35. Bentamy A, Queffeulou P, Quilfen Y, Katsaros K (1999) Ocean surface wind fields estimated from satellite active and passive microwave instruments. IEEE Trans Geosci Remote Sens 37:2469–2486
36. NASA Goddard Space Flight Center (2014) Ocean ecology laboratory, ocean biology processing group: MODIS-aqua ocean color data; NASA goddard space flight center, ocean ecology laboratory Ocean Biol Process Group. http://dx.doi.org/https://doi.org/10.5067/AQUA/MODIS_OC.2014.0. Last Accessed 28 July 2015
37. Bonjean F, Lagerloef GSE (2002) Diagnostic model and analysis of the surface currents in the tropical Pacific Ocean. J Phys Oceanogr 32:2938–2954

38. Wentz FJ, Gentemann C, Hilburn KA (2015) Remote sensing systems TRMM TMI (indicate whether you used daily, 3-day, weekly, or monthly) environmental suite on 0.25 deg grid, version 7.1, (indicate subset if used). Remote sensing systems, Santa Rosa, CA. www.remss.com/missions/tmi. Last Accessed 31 Dec 2021
39. UK Met Office (2005) OSTIA L4 SST Analysis. Ver. 1.0. PO.DAAC, CA, USA. Dataset. https://doi.org/10.5067/GHOST-4FK01. Last Accessed 01 Aug 2021
40. Donlon CJ, Martin M, Stark JD, Jones JR, Fiedler E, Wimmer W (2012) The operational sea surface temperature and sea ice analysis (OSTIA) system. Remote Sens Environ 116:140–158. https://doi.org/10.1016/j.rse.2010.10.017
41. Best Track. Regional specialized meteorological centre for tropical cyclone over North Indian Ocean. https://www.rsmcnewdelhi.imd.gov.in/uploads/besttrack/842f18___Ga1806__Best%20Track_2021%20Final.xls. Last Accessed 15 Aug 2021
42. Sydney L (2013) US DOC/NOAA/NESDIS > National oceanographic data center. NODC standard product: world ocean atlas 2005 (4 disc set) (NCEI accession 0097967) (indicate subset used). NOAA National Centers for Environmental Information (2013). Dataset. https://accession.nodc.noaa.gov/0097967. https://www.ncei.noaa.gov/metadata/geoportal/rest/metadata/item/gov.noaa.nodc%3A0097967/html. Last Accessed 15 Aug 2021
43. Ghoshal T, Sil S, Chakraborty A (2014) An inter-comparison of daily and monthly in situ, satellite derived and reanalyzed sea surface temperature climatology fields over the Bay of Bengal. Mar Geodesy 37(1):65–76
44. Martin MV, Shaji C (2015) On the eastward shift of winter surface chlorophyll-a bloom peak in the Bay of Bengal. J Geophys Res Ocean 120(3):2193–2211
45. Gregg WW, Casey NW (2007) Sampling biases in MODIS and SeaWiFS ocean chlorophyll data. Remote Sens Environ 111(1):25–35

Variation of Clearwater Scouring Geometry at Isolated Structures Obliging in Sediment Shifting

Priyanka Chowdhury, Subhasish Das, Buddhadev Nandi, and Rajib Das

Abstract The technique of using unsubmerged structures with vanes for guiding the flow or shifting the sediments is an effective way to control sediment in any watercourse. Based on this feature, six laboratory-based scouring tests were performed using isolated vertical structures of shapes, square, rhombus, and triangular. Of these six tests, one test had no vane, three tests had one vane, and the remaining two had double vanes. The vanes were attached at a 45° angle with such structures. These tests were performed under clearwater scouring conditions for a fixed approach flow depth on a fixed sandbed with a constant discharge. The aim was to observe the variations in the equilibrium local scouring depth on both sides of the structures, the shifting angle of sandbed material on the left and right sides of the waterway, and the volume of sand deposited on the downstream side. The souring and deposition profiles were monitored, measured, and graphically represented. From these graphs, the shifting angle of sand was found to be the highest in rhombus-shaped structures, although the total scouring area (surface) and scouring volume were found to be significantly increased when using the square structure with a dual vane combination rather than a structure with single vane composition. From the overall analysis, the square structure with a combination of the dual vane was found to be very efficient and economical among these six structures.

Keywords Sediment shifting · Isolated structure · Unsubmerged vane · Scour profile · Shifting angle

1 Introduction

Sediment transport and its management is a very important issue that needs the concern of researchers and scientists around the world. The silting and scouring phenomenon approaches the interrelationship between flowing water and bed sediment materials. The waterway depth significantly reduces due to sediment deposition

P. Chowdhury (✉) · S. Das · B. Nandi · R. Das
School of Water Resources Engineering, Jadavpur University, Kolkata 700032, India
e-mail: pchowdhury284@gmail.com

© The Author(s), under exclusive license to Springer Nature Singapore Pte Ltd. 2023

S. Kumar et al. (eds.), *Sustainable Environmental Engineering and Sciences*,
Lecture Notes in Civil Engineering 323, https://doi.org/10.1007/978-981-99-0823-3_5

at the bed of waterways which has become the most talked about topic for hydraulic engineers. In front of an unsubmerged vane, the vortices exert shear stress upon contact with bed material which has several applications in protection against bank erosion maintaining depth in the navigation waterway and controlling sediment at water intakes.

To date, many laboratory-based clearwater scour experiments were designed to predict scour geometry. Most of the previous studies have focused on lowering scour volume. Due to the complexity of the nature of the scouring action, several formulas and mathematical models were obtained to determine the equilibrium depth of scouring (S_{deq}) in a range of test conditions, such as structure sizes, flow characteristics, scouring duration, and sand material properties. The presence of isolated structures creates a significant increase in local scour around their bases and sides [1]. Under clearwater scouring, the S_{deq} is asymptotically reached with respect to the time and usually takes a few days to achieve a state of equilibrium. The waterway depths may be significantly reduced by sand deposits and a few experiments have been performed on the scouring geometry study of a square structure with vanes by changing its direction, flow depth (h_i), and discharge (Q_i) [2].

Several studies around multiple structures have focused on predicting S_{deq} [3] and the subsequent impact of the intermediate structure gap on S_{deq}. The researchers [4] performed experiments using two structure arrangements positioning flow-wise and described two additional parameters, (a) reinforcement and (b) sheltering effect, on scouring. The researchers have made some estimates around double structure arrangements focusing on scour geometry. Several researchers [5–14] observed variations in scour depth using multiple identical structures. The consequences of the intermediate gap between structures on flow and scour depth characteristics were described by [15]. Some researchers [16] have described how pier-like structures with inline eccentric arrangements can improve sand movement towards a bank of a waterway and downstream of structures.

In most cases, it is uneconomical to remove the sediments and debris by mechanical means from the bed of an alluvial waterway. In the past, various studies have been done to reduce scouring. Excessive scouring can damage a bridge-like structure during high flow. But very few researchers have chosen the insightful prospect of shifting the bed sediment load towards the bank of the waterway by increasing the scouring process. It ultimately helps in dredging out the deposited sediments without the help of the traditional dredge mechanism.

In this study, it was tested whether the sand load could be diverted and transported to a specific side of the pier-like structure aimed at maximizing non-symmetrical scouring and shifting more sand downstream of the structures. This technique may help to dredge out the materials from the bed or the bank of the waterway to deepen or extend waterways for navigation or to obtain fill materials for land development. Therefore, if sand can be diverted and moved to the side of the watercourse, it will help to ultimately stabilize the depth of that watercourse. In the present study, the focus was to investigate the scour features around differently shaped single structures with or without vanes. The main function of an unsubmerged vane is to create a turbulent

wake vortex in scouring action to lift up any sand mobilized by the horseshoe vortex towards flow to divert and move sands.

2 Experimental Equipment and Setup

Six tests have been carried out using square, rhombus and triangular structures attached with or without rectangular vane to observe the nature of the scour, its amount and the sand shifting towards channel bank. Out of these, one test consisted of a rhombus (R) shaped structure having no vane attached, and three tests consisted of a single vane (V) attached at a 45° angle with a single side of the square (S) or triangular (T) structure in different orientations, and the rest of the two tests consisted with two vanes attached at a 45° angle at opposite sides of the single square (S) or triangular (T) structure (Fig. 1 and Table 1). Earlier researchers used rectangular vanes [17, 18]. The triangular shape was used by Fouli and Elsebaie [19]. For all six tests, one side of the structure was facing the flow perpendicularly. In all tests, pier-like structures were considered to have a fixed side width (b) of 0.070 m. In Table 1, test number 4T1V indicates the fourth test using the formation of a triangular (T) structure and one (1) vane (V). The thickness of the vanes was 0.5 cm, the length of the vanes was taken 7 cm, and the vane angles at which the vane was attached were 45° when the side of the corresponding structure was extended approximately.

Each test was started with a flattened bed. The geometric standard deviation of experimental sand was set at 1.8. The grade of the prepared sandbed was fixed at 0.00042 in all six tests. The threshold level was set fixed at 68.2% following [20, 21]. In six tests, the inlet flow depth (h_i) was set constant at 0.125 m by the operating tailgate, and the discharge of the approaching flow (Q_i) was set constant at 25 lps. The value of h_i/b was set equal to 1.8 to obtain restricted flow in the rectangular waterway. After closing the exit valves, the water was very gradually filled in flumes without disturbing the sand until it reaches the desired h_i. Then the inlet valve adjustment was performed to get the desired discharge for tests and at the same time, the exit valve was opened slightly. During all six investigations, the maximum magnitude of the scouring depths was found at the upstream end of each structure. The temporal rate of scour was at its peak in the period of the first three hours and then the temporal scour rate was less. Knowing that S_d changes rapidly at the commencement of tests and slows down towards the end, the S_d measurements were noted more customarily at the commencement. To observe the nature of the developing scour depth around structures, the time variation of scouring was taken into account.

The duration of the test varied from 29 to 42 h. After testing, the pump was allowed to stop draining out the water from the working section without interfering with the scour topography. Thereafter, testing sandbed was allowed for drying, and a photo was taken to scrape the surrounding area of the structures and also observed armouring of the bed material. Then undulated bed levels were randomly gauged

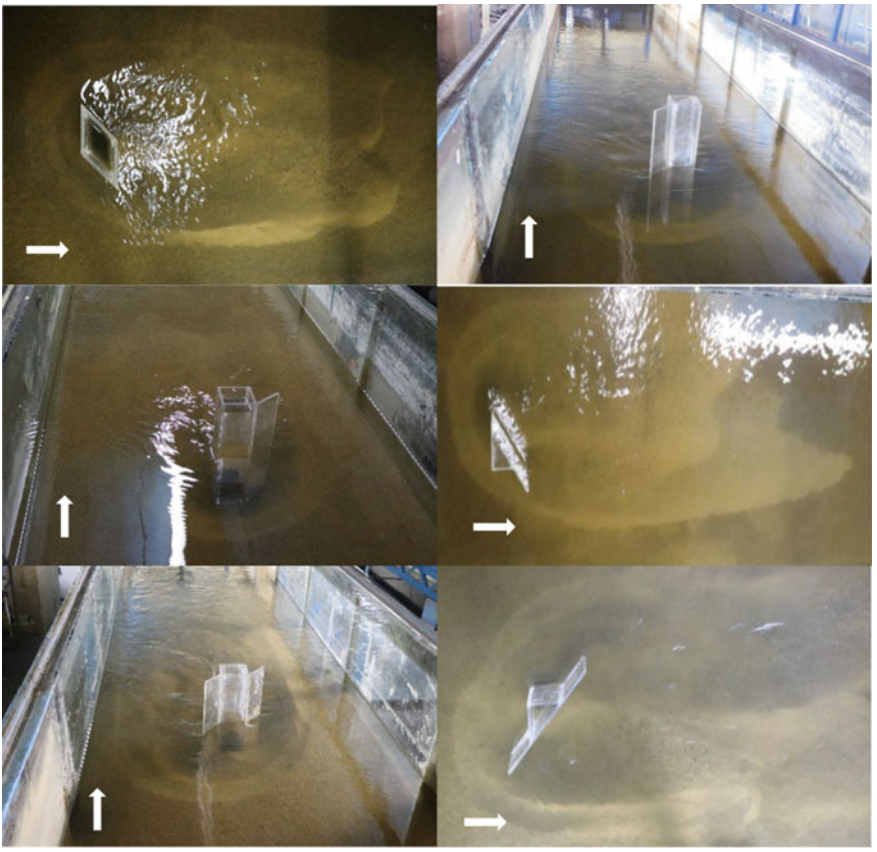

Fig. 1 Pictorial view of six structural arrangements (Row 1: 1R, 2S1V; Row 2: 3S1V, 4T1V; and Row 3: 5S2V, 6T2V) (arrows show flow directions)

Table 1 Testing considerations

Test number	Structure shape	Discharge (Q_i) (lps)	Flow depth (h_i) (cm)	Structure width (b) (cm)	Number of vanes	Vane angle (degree)	Run duration (hr)
1R	Rhombus	25	12.5	7	No vane	–	29
2S1V	Square	25	12.5	7	Single	45°	36
3S1V	Square	25	12.5	7	Single	45°	42
4T1V	Triangular	25	12.5	7	Single	45°	35
5S2V	Square	25	12.5	7	Double	45°	30
6T2V	Triangular	25	12.5	7	Double	45°	35

using electronic laser-type gauges attached to a moving trolley that was used simultaneously to check the sandbed levelling. The laser type gauges were used to record the scouring depths.

The scour is symmetric or non-symmetric due to the addition of a vane at the side of the structure to find out by the formation of the dune. If it is non-symmetric, then it has to be found on which side of the structure the scour is high. Comparison of the different scour parameters (equilibrium depth, length of scouring, max-width of scouring, total scour area, total scour volume and both side volume, angle of shift) is to be carried out with the vane angle of 45°.

3 Result and Discussion

Research on local scouring around pier/piers was carried out in clearwater conditions using different types of structures of shapes, triangular, square, and rhombus, with or without vane positioning in different orientations. After performing six scour hole tests, several geometrical parameters such as equilibrium scour depth S_d, distance traversed by the extracted sand towards downstream, max-width of scouring and deposition, surface area of scouring hole, total volume of scouring hole, volume of deposited sand, scour volume on both left side (LES) and right side (RIS) of the centre line of the waterway, and shifting angle of the sand on the LES and RIS were analyzed.

Previous studies have mainly focused on the scour development around single or eccentric circular structures. But in the present study, the morphometric consequences of scouring around above-mentioned structural arrangements of different shapes have been investigated. Scouring, shifting, and deposition patterns were studied simultaneously. The coordination of vane direction is also varied to assess the scour morphology.

Figure 2 shows a morphometric view after the third test run. A symmetry line, shown by dashed lines in Fig. 2, perpendicular to the face of the square structure is illustrated. It separates the left (LES) and right zones (RIS). According to Fig. 2, the LES zone is above the symmetry line, and the LES with respect to the flow direction as well. Similarly, the RIS zone is below the symmetry line and the RIS zone with respect to the flow direction. The symmetry line also separates the shifting angle towards the RIS and LES respecting flow direction.

Figures 3, 4 and 5 refer to contours in the locations of scouring, shifting, and depositions of sand. Here, the negative contours indicate scouring surface area, and positive contours indicate dune formation (sand deposition). To compare contours, only three contour plots of the same structure, i.e. square are shown. When the vane was attached to one side of the square structure, the scour was non-symmetric. From the beginning to the end of the six tests, scouring patterns and shifting of sand were observed for each arrangement. The total surface area and volume for sand scouring differed significantly for identical test conditions in different vane profile arrangements.

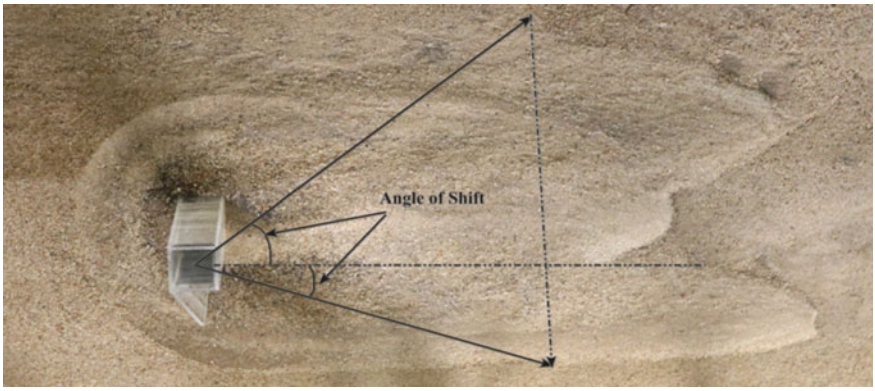

Fig. 2 Zones affected by scouring around square structure with vane for 3S1V test

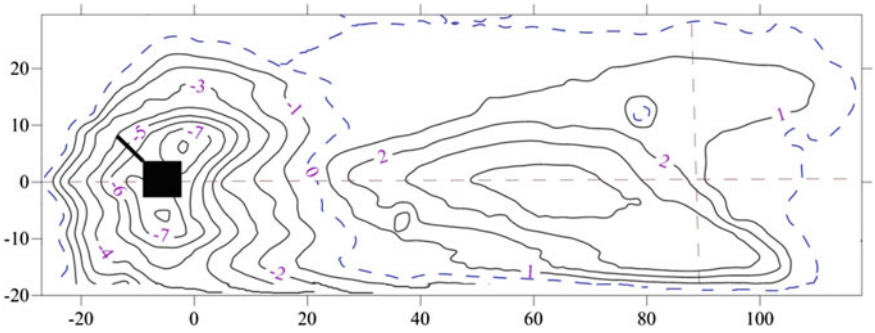

Fig. 3 Contour profile showing scouring and deposition for 2S1V test (all units: cm)

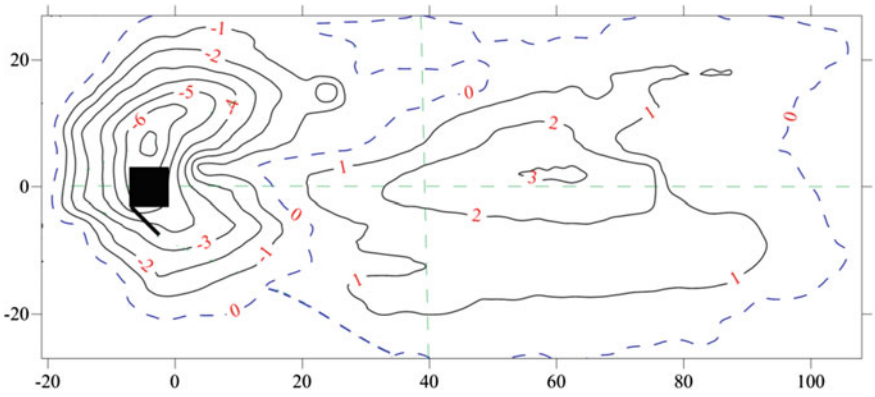

Fig. 4 Contour profile showing scouring and deposition for 3S1V test (all units: cm)

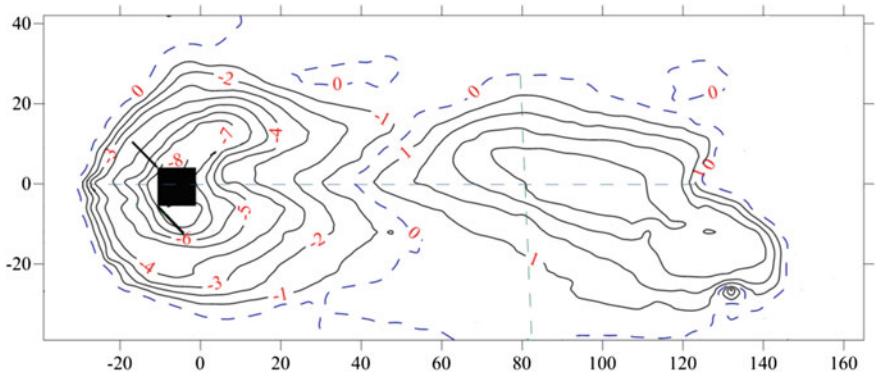

Fig. 5 Contour profile showing scouring and deposition for 5S2V test (all units: cm)

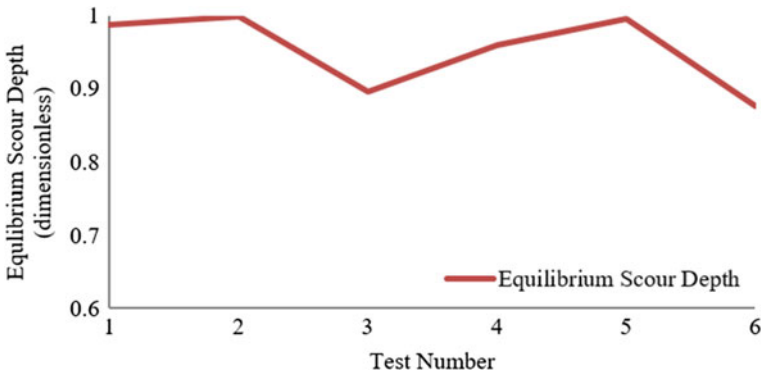

Fig. 6 Experiment-wise equilibrium scouring depth changes

Figures 6 and 7 show variations of equilibrium scour depth, maximum scour length, and width obtained in the six tests. These three different parameters are non-dimensionalized by dividing them by their maximum values to fit a 0–1 scale. Maximum observed scour depths S_d were obtained in test 2S1V in which the vane was attached to the upstream face of the structure relative to the flow attacks. That is due to the vortices created around the back face of structures, as well as the flow accelerated owing to contraction created by the adjacent vane. Thus, a higher sand transport induced by the attached vane hence contributes substantially to increasing the scour depth. One of the most significant observations in the single rhombus structure test 1R was that the scour width was much larger compared to other tests. As a result, the shifting angle was also found to be more on both sides compared to other tests. But the sand shifting was slightly higher on the RIS facing flow direction of the single rhombus structure, and as a result, the scour planner area was more on the right side also.

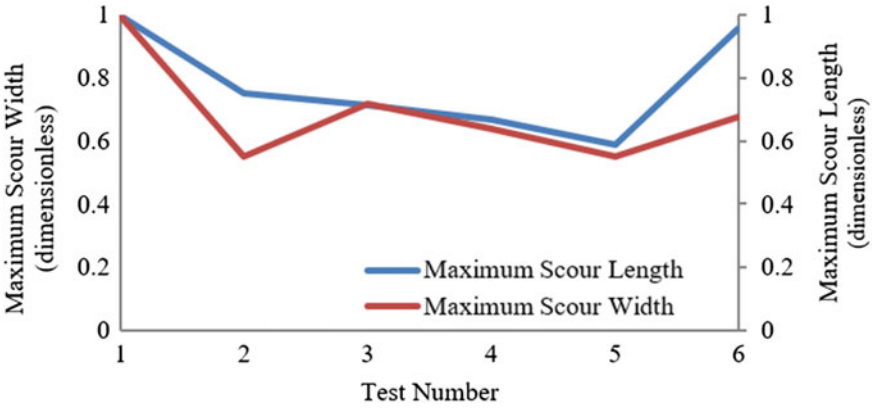

Fig. 7 Experiment-wise maximum scouring length and width changes

Figures 8, 9 and 10 show the changes in total scour area (surface) and volume for different tests. Here again, the parameters are non-dimensionalized by dividing them by their maximum values to fit a 0–1 scale. From the two tests 4T1V and 6T2V of triangular structure with a vane/vanes on one side and both sides, we can decide if the sand shifting is more on the vane side. For example, in the 4T1V test, the vane side scouring volume was more compared to the without vane side scour volume. And the shifting angle of the sands on the vane side was higher, as can be seen from the dune formation downstream of the structure. In the case of the 6T2V test, where the vane was attached on both sides of the structure, it was found that the scour was more on the side that has its vane directed towards the downstream. The shifting angle of the sand was also more on the side where the vane was in the same flow direction (left when facing the flow direction). Hence, we conclude with the first two tests 1R and 2S1V that the scour and also sand shifting were more on the side where the vane was attached with an angle directed towards the downstream.

From the graphical representations, it is observed that the sand scouring around the single structure was significantly increased by a single structure with a dual vane arrangement. Additionally, in the dual vane profile, the scour hole volume was found to be increased by 20% more than in the single vane case. To understand further scouring hole characteristics surrounding the structures, volumes of sand scour and depositions were calculated from the data observed. In the 5S2V test, the scour volume, scour surface area, and scour planer area were found to be significantly increased due to the dual vane arrangements.

The observed scouring depths around single structure cases were found close to the observations of [2]. Larger scouring hole volume and scouring surface area were anticipated due to different vane orientations. From the experimental results furnished above, the morphology of the scour was found non-symmetric at the LES and RIS end of the structure considering from the upstream end in both the cases when the vane was attached at single and both sides of the structure.

Fig. 8 Experiment-wise total scouring volume and surface area changes

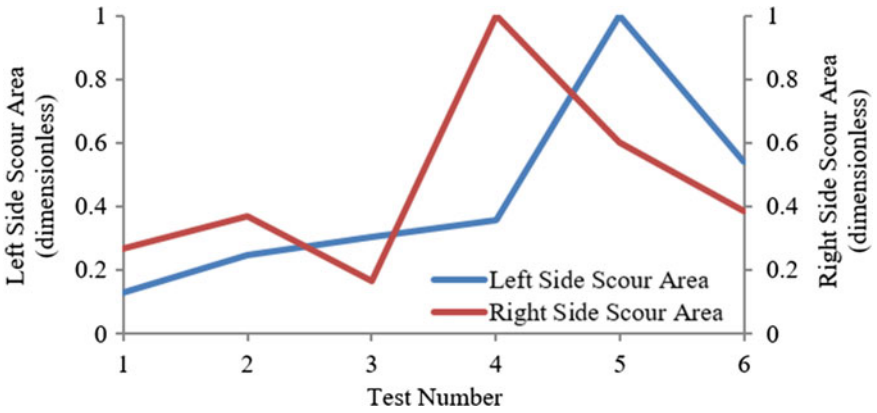

Fig. 9 Experiment-wise scouring area changes at LES and RIS of symmetry line

The determined results clearly show more scouring in the dual vane structure than that for a single structure. In addition, the sand was found to be removed from the waterway bed from all around the structures and was deposited in the waterway downstream. The sediment (sand) was found to be deposited more on one side of the waterway, i.e. the dune formed downstream of the structures was not symmetrical. The shifting angle for scouring and dune was more on the vane side. This is significant as it ensures that loads of sand transported on the waterway can be judiciously diverted towards the side bank using a suitable structure with a combination of the vane. Figure 11 represents the angle of shifting of sands towards the LES and RIS banks. For the 1R test, the shifting angle was the highest. Test 3S1V and test 5S2V were found in the second and third positions respecting the 1R test to shift sand.

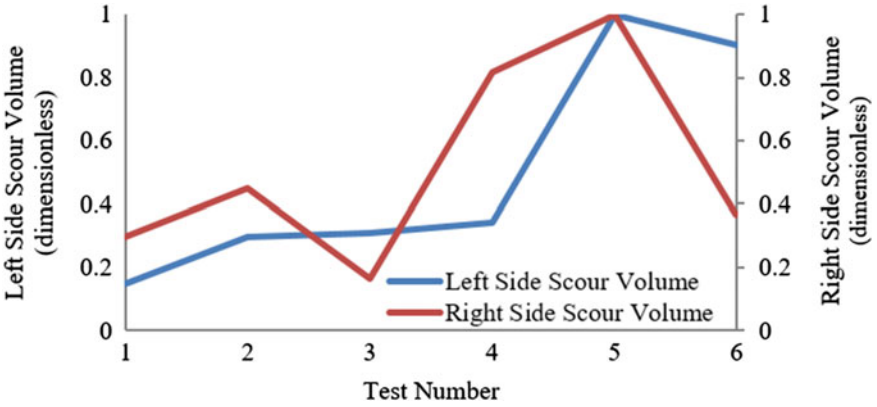

Fig. 10 Experiment-wise scouring volume changes at LES and RES of symmetry line

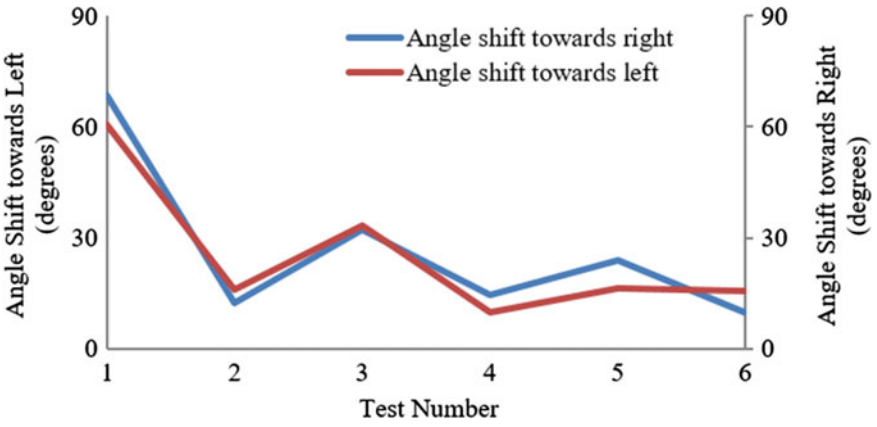

Fig. 11 Experiment-wise angle of shift changes at LES and RIS of symmetry line

4 Conclusion

In the present study, scour hole characteristics in the clearwater scour tests have been performed using isolated vertical structures of shapes, square, rhombus, and triangular, with a vane fixed in different positions of it keeping inflow depth and discharge constant. Six tests were conducted using uniformly graded sand material on a tilting flume. The scour depths around such structures were gauged and monitored. The contours of scouring, depositions and quantum of the sand movement were analysed. From the current experimental study, the following conclusions are reached:

(i) In a single rhombus structure, the shifting angle on both sides was observed significantly larger from other cases. But the maximum depth of scouring was achieved in the case where the vane at the upstream side faces the flow.
(ii) Although the shifting angle of scouring and the dune was found more on a single side vane structure, the dual vane was significant as it attests to a large amount of sand carried off the water.
(iii) Volume of the shifted sand was estimated higher on the vane side and also the shifting angle was detected more compared to the no-vane side.
(iv) The structure with dual vane was found to be more efficient thus creating an additional capacity for sand shifting on the waterway bed. In the case of the dual vane structure, the scour volume was found to be increased by 20% more than that of the single vane structure.
(v) In addition, the volume of sand extracted from the bed is deposited on both sides of the waterway.
(vi) Overall, the test using the square structure with two vanes showed the most effective performance among these observations.

These outcomes are important as they provide an idea to extract the deposited sand on the waterway bed and simultaneously shift them towards the bank of the waterway. These kinds of models with a suitable structure vane arrangement may be very beneficial for self-dredging. This research can also be expanded into a number of scenarios apart from the geometry of the structures with different layouts with different sizes of the vane which can be useful in comparing real field problems.

References

1. Chang WY, Constantinescu G, Lien HC, Tsai WF, Lai JS, Loh CH (2013) Flow structure around bridge piers of varying geometrical complexity. J Hydraul Eng 139(8):812–826
2. Das S, Das R, Mukherjee R, Mazumdar A (2017) Enhancement of sediment transportation by increasing scour around a square pier with vane attached on one side. In: Proceedings of the 37th IAHR world congress. Kuala Lumpur, Malaysia
3. Ashtiani BA, Ghorghi ZB, Beheshti AA (2010) Experimental investigation of clear-water local scour of compound piers. J Hydraul Eng 136(6):343–351
4. Sheppard DM, Zhao G, Copps TH (1995) Local scour near multiple pile piers in steady currents. In: Proceedings of ASCE, international conference on water resources engineering. San Antonio, USA
5. Das S, Mazumdar A (2015) Comparison of Kinematics of Horseshoe Vortex at a Flat Plate and Different Shaped Piers. Int J Fluid Mech Res 42(5):418–448
6. Das S, Mazumdar A (2015) Turbulence flow field around two eccentric circular piers in scour hole. Int J River Basin Manag 13(3):343–361
7. Das S, Mazumdar A (2018) Evaluation of hydrodynamic consequences for horseshoe vortex system developing around two eccentrically arranged identical piers of diverse shapes. KSCE J Civ Eng 22(7):2300–2314
8. Das S, Das R, Mazumdar A (2014) Variations of clear water scour geometry at piers of different effective widths. Turk J Eng Environ Sci 38(1):97–111
9. Das S, Das R, Mazumdar A (2016) Comparison of local scour characteristics around two eccentric piers of different shapes. Arab J Sci Eng 41(4):1199–1213

10. Das R, Das S, Jaman H, Mazumdar A (2018) Impact of upstream bridge pier on the scouring around adjacent downstream bridge pier. Arab J Sci Eng 44(5):4359–4372
11. Jaman H, Das S, Das R, Mazumdar A (2017) Hydrodynamics of flow obstructed by inline and eccentrically-arranged circular piers on a horizontal bed surface. J Inst Eng (India): Ser A 98(1–2):77–83
12. Jaman H, Das S, Kuila A, Mazumdar A (2017) Hydrodynamic flow patterns around three inline eccentrically arranged circular piers. Arab J Sci Eng 42(9):3973–3990
13. Kuila A, Jaman H, Das S, Mazumdar A (2020) Computing equilibrium flow structures at three interfering square piers causing relative scour. In: Mandal JK (eds) Topics in intelligent computing and industry design (ICID), vol 1, pp 20–24
14. Narayana PL, Timbadiya PV, Patel PL (2020) Bed level variations around submerged tandem bridge piers in sand beds. J Hydraul Eng. https://doi.org/10.1080/09715010.2020.1723138
15. Michael SA, Mohamed GM, Mohamed SBAM (1991) Wake vortex scour at bridge piers. J Hydraul Eng 117(7):891–904
16. Das R, Khwairakpam P, Das S, Mazumdar A (2014) Clear-water local scour around eccentric multiple piers to shift the line of sediment deposition. Asian J Water Environ Pollut 11(3):47–54
17. Ouyang HT, Lin CP (2016) Characteristics of interactions among a row of submerged vanes in various shapes. J Hydro-Environ Res 13:14–25
18. Roy P, Das S, Dey A, Das R (2022) Analytical study of scour mechanism around immersed rectangular vane structures. In: Rao CM, Patra KC, Jhajharia D, Kumari S (eds) Advanced modelling and innovations in water resources engineering 2021, LNCE, vol 176. Springer, Singapore, pp 703–717
19. Fouli H, Elsebaie IH (2016) Reducing local scour at bridge piers using an upstream subsidiary triangular pillar. Arab J Geosci 9:598
20. Das S, Das R, Mazumdar A (2013) Circulation characteristics of horseshoe vortex in the scour region around circular piers. Water Sci Eng 6(1):59–77
21. Das S, Midya R, Das R, Mazumdar A (2013) A study of wake vortex in the scour region around a circular pier. Int J Fluid Mech Res 40(1):42–59

Flow Kinematics Around Two Submerged Inline Eccentric Rectangular Vanes Under Clearwater Scouring

Priyanka Roy, Subhasish Das, Rajib Das, and Chakit Samanta

Abstract Submerged vanes are vortex-generating devices that are capable of controlling stream bed progression in the course of natural waterways. For an intended angle of attack, these vanes act as baffles of low height, re-directing the streamflow and thereby generating secondary currents in the mainstream. In the present study, an equilibrium scour experiment was carried out with the two identical shaped vanes aligned horizontally at a 15-degree angle to flow direction with a constant discharge and depth of water of 25 l/sec and 10.5 cm, respectively for the measurement of 3D velocity components, above, within and around the scour cavities according to the Cartesian co-ordinate system, with the help of velocity meter. The time-averaged absolute velocity profiles and the flow velocity contours (flow-wise, crosswise, vertical) along with the velocity vectors have been plotted. The consequent flow patterns are analyzed and compared at four different horizontal cross-sections (for the depths of 6, 4, 3, and 0 cm) as well as a vertical cross-section. The experimental study majorly focuses on understanding the flow kinematics around the submerged vanes useful for active sediment channelization toward the banks improving the channel navigability.

Keywords Scouring mechanism · Inundated rectangular vane · Scour pattern · Sediment channeling

1 Introduction

Sediment control in an alluvial channel is significant for, facilitating proficient channel volume, maintaining a definite optimum stream profundity, enhancement of non-regimen channels, anticipation of bed and bank disintegration, or for redirection of stream starting with one channel to another or to a water inlet. A submerged vane acts as an effective measure for sediment management by modifying the flow pattern downstream resulting in shear stress moderation and sediment redistribution.

P. Roy (✉) · S. Das · R. Das · C. Samanta
School of Water Resources Engineering, Jadavpur University, Kolkata 700032, India
e-mail: roypriyanka2604@gmail.com

© The Author(s), under exclusive license to Springer Nature Singapore Pte Ltd. 2023

S. Kumar et al. (eds.), *Sustainable Environmental Engineering and Sciences*,
Lecture Notes in Civil Engineering 323, https://doi.org/10.1007/978-981-99-0823-3_6

It is a low-height baffle which is installed on stream bed with a definite angle of attack deterring the course of movement, in turn generating secondary undercurrents within the stream. These results in an amendment in direction and intensity of the bed shear stresses and thus the sediments are restructured along the cross-segment of the stream. Thereafter, vanes are used in many applications, including the protection of curved stream banks; securing numerous bridge piers and abutments by reducing undesirable scour; and the elimination of sediment deposition in irrigation canals to increase water availability in channels, thereby improving general stream navigability and irrigation potential of the channel [1].

Controlling the sediment deposit in alluvial streams is a severely problematic issue for hydraulic engineers. A submerged vane can act as a very effective and practical approach toward governing sediment control in such streams. Introducing a variety of vanes, positioned at fixed angles on the stream bed, the flow configuration at the downstream side of the vanes is modified, along with the redistribution of bed shear stress. The proper spatial arrangement of the vanes at a specific area of the stream bed that is controlled by the vanes may then be changed into any desired profile for stream management.

The design and dimension of immersed vanes are additionally imperative for their compelling use. Commonly the vanes used for practical purposes are rectangular assemblies, majorly owing to their ease of fabrication and development. The confined scouring surrounding the structures is the foremost source of obliteration of numerous manmade structures within the stream. An approximation of the concentrated conceivable scour around any manmade structure is obligatory for adequate design. In the case of free surface flow surrounding the bridge pier, the occurrence of the horseshoe vortex is commonly observed, and the choppiness intensifies at severe positions of the front, around, and behind the piers.

Additionally, the scouring phenomenon is distinctively observed on the wobbly stream bed near the bridge pier. Investigational and analytical research studies have concluded that the streaming tide and the resulting deposit transport process, both are profoundly intricate during the scour hole advancement. Another aspect of scouring formation, around the structures is that the sediments are transported downstream.

Sediment channelizing studies have been carried out with predicting flow characteristics around structures and based on that several researchers have originated numerous equations. Assessments on a few imperative experimental works were carried out by [2–15]. A wide scope of equations was accessible, and no undeniable similitude in either their appearance or their expectations. The evident struggles emerged from before contemplates, various of which showed live-bed scour surpassing clear-water scour and others of which showed the converse [16]. The impact of such drenched vanes was contemplated as a counter-system on a nearby scale on the cylindrical construction. It was attempted to check the possible shifting of the silt particles aside from the appended vane structure, for four different vane arrangements of 0 (with no vane), 15, 30, and 45° [17, 18]. A few research and tests were managed without and with inundated vane structures. A solitary submerged

vane stationary with projection upstream front was observed to be powerful in lessening, changing, and securing disintegration [19]. An endeavor was made to assess and affirm the discoveries on drenched vanes utilizing CFD [20].

In our present set of experiments, a set of vanes are taken and are positioned within a flume on a sand bed under constant depth and flow conditions and analyzed the velocity profiles. At some horizontal cross-sections and a vertical cross-section (passing through the center line of the vanes), the contour patterns of the flowwise, lateral, vertical, time-averaged absolute velocities were measured for the two vanes arrangement. This enables us to comprehend the reason for shifting of the bed materials from the upstream side and depositing toward the downstream. This phenomenon gives us a distinct idea of the scour mechanism and enables us to recognize as well as diminish the problems of non-navigability of stream in the practical scenario.

2 Materials and Methodology

The investigative assessment conveyed here is established on the basis of experiments executed in a re-circling flume having 1100 cm extent, 81 cm breadth (internally), and 60 cm depth. The functioning segment of the re-circling flume is crammed with sand in order to achieve a consistent thickness of 20 cm. The sand-bed dimensions are 700 cm length × 81 cm breadth and it was arranged at 290 cm upstream fromthe re-circlingflume inlet. The functioning segment of the re-circling flume was comprised of a metallic base. Both sides of the flume along its length were enclosed with Plexiglass sidewalls to enable visual interpretations during the work. Two centrifugal pumps located upstream end of the flume served alternatively the re-circulating flow system. Two identical rectangular vane structures are used and they are of the same dimensions. The dimension of the vane is 15.75 cm (length) × 8.4 cm (height above the sand bed) and the thickness of the vanes is 0.5 cm. The vanes are employed on the sand bed at an angle of 15° with the flow direction. While conducting the experiments, the width of the regulating flume is strictly maintained to be eight times greater than that of the vane width, for avoiding wall friction factor.

An acoustic Doppler type down-looking velocity meter with Vectrino + probe produced by Nortek-AS was utilized in measuring the prompt 3D velocity components. The velocity meter provides instantaneous velocities at 100–200 Hz sampling rate, 0.6 cm diameter cylindroid sampling volume, 1 cm sampling height, and 1 cm smallest horizontal resolution [13, 21]. For maintaining the fixed investigation procedure, the sampling intervals were varied from the 60 to 120 s to accomplish a methodically time-independent average velocity. The investigation period was longer compared to [14, 22] where a smaller time period of 120 s was adopted. By measuring the velocity, based on fluvial turbulent boundary layers, researchers [14, 23] determined the standard error for turbulence statistics and verified that the optimum record length (i.e. minimal sampling effort to accomplish the lowest standard errors) may

restrict between 60 and 90 s. The run duration for the experiment was 24 h. Subsequently, the pump was stopped to permit slow drainage of water in the flume, keeping the scour contour profile intact and allowing the flume bed to dry gradually.

With the subsequent completion of the experimental run, it was evident that the maximum number of equilibrium scouring depths were detected on the upstream side of selectedsubmerged vanes. Using Vernier point gauges, appended with a mobile trolley, the utmost scour depth was affectively measured and recorded. The velocity meter was attached to the same trolley for measuring flow-field velocity encircling the vane scour area. The contour line data recorded, was plotted by using the Golden software Surfer10 version and the velocity vector, and velocity's contour lines surrounding such selected submerged vanes were plotted using Origin-Pro software.

3 Experimental Results and Discussion

3.1 Flow-Fields at Selected Horizontal Cross-Sections

Flow-wise velocities

The flow-wise velocity contours (u) are shown in Fig. 1. The contour pattern for $h = 4$ cm was similar to that of $h = 6$ cm. It is noted for this case, that the velocities distant from the vane (in transversal directions) are larger than the velocities closer to the concerned vane for four selected horizontal cross-sections. Because the flow is impeded at such vane, the flow-wise part of velocity i.e., u drops drastically. It is found that as water depth decreases, the corresponding velocity decreases. The values of flow-wise velocities in the intermediate cross-sections were lowered by 10–50 percentages relative to the top cross-section, whereas the bottom cross-section was reduced. It is because the viscous effect is more predominant here than the turbulence effect. There is also minimal variance in velocities away from such vanes in four selected cross-sections since there is no significant impediment. At the right bank of the first vane flow-wise velocities decrease slowly from $h = 6$ cm to $h = 0$ cm.

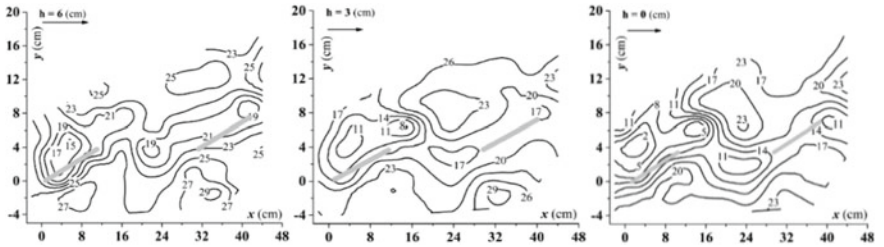

Fig. 1 Flow-wise velocity contours for selectedcross-sections $h = 6$, 3, and 0 cm, respectively

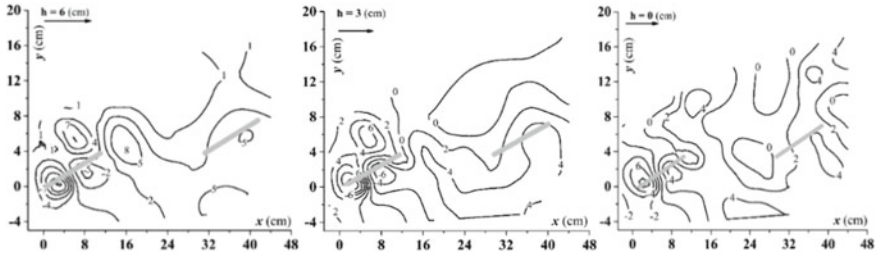

Fig. 2 Transversal flow velocity contours for selectedcross-sections $h = 6$, 3, and 0 cm, respectively

Transversal flow velocities

The transversal velocity diagram in Fig. 2, shows that whenever the flow is blocked by the vanes it gets alienated. It is also observed that on either side of the vanes the magnitude of the velocity is opposite. Transversal velocity at the left-hand side of such selected **submerged** vane is positive and is negative on the right-hand side. At $h = 0$ cm flow separation is more compared to $h = 6$ cm.

Vertical velocities

Vertical velocity i.e., w is observed as positive in the upward direction in this case. As can be seen from its plotted contour maps in different selected cross-sections (Fig. 3), the vertical velocity in the scouring affected region is in the downward direction, whereas it is in the upward direction in the dune area. Though it is clear because a horseshoe vortex forms in the contact section of each vane, velocity is in the downward direction, which helps in scouring concerned bed particles, and dunes form on downstream side of submerged vanes, termed wake vortices, for up-flow. It is perceived that downward flow is more at $h = 0$ cm. So, near the scour area (at $h = 0$ cm) the downward velocity is more as compared to $h = 6$ cm.

Absolute velocities

From contour plots illustrated in Fig. 4, it is detected that for time-averaged absolute velocity contours, the velocities distant from the submerged vane in cross-wise directions are higher than the region closest to such vane for three selected horizontal

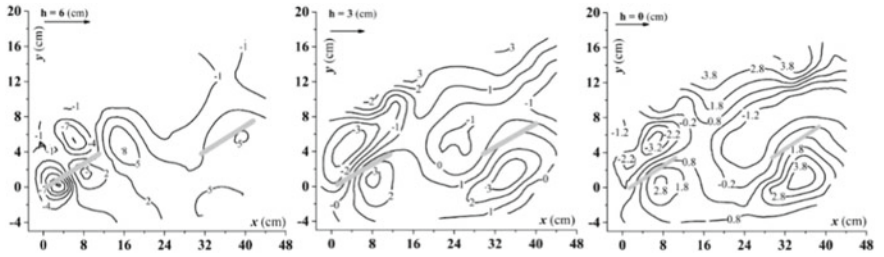

Fig. 3 Vertical flow velocity contours for selectedcross-sections $h = 6$, 3, and 0 cm, respectively

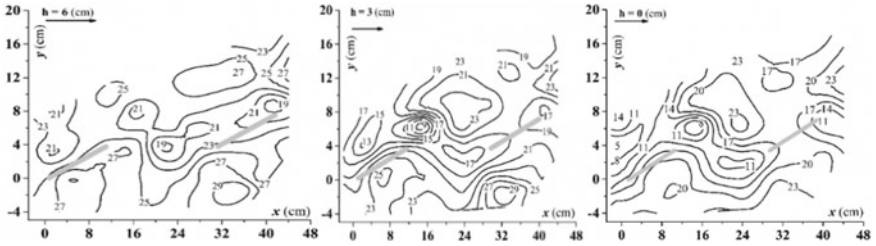

Fig. 4 Absolute flow velocity contours for selectedcross-sections $h = 6$, 3, and 0 cm, respectively

cross-sections. The flow-wise u component is relatively low at the vane because the flow is impeded there. As a result, the outcome is likewise reduced. It is found that as the water depth decreases, the corresponding absolute velocity decreases. The values of absolute velocities in the intermediate cross-sections are lowered by 5–20% compared to the top cross-section, while the bottom cross-section is reduced by 25–50% and in some places by more than 70%. It is because of the shear effect of the adjacent layer which is higher for the bottom cross-section. Time averaged absolute velocity is more at $h = 6$ cm compared to $h = 0$ cm because flow-wise velocity is more at $h = 6$ cm than $h = 0$ cm.

Vectors of velocity

In comparison to the other three cross-sections, the velocity pattern around the vanes deviates significantly in the bottom cross-section. It clearly indicates the direction toward which the flow of water is shifting across the horizontal cross-section (Fig. 5).

3.2 Flow-Fields at Central Vertical Cross-Section

Flow-wise velocities

The flow-wise flow velocities are observed to be lower where it meets the vane and no appreciable variation in the middle space where there is no vane. Velocity is much lower close to the bed as the viscous effect is predominant here.

Transversal flow velocities

As the considered cross-section passes through the downstream edge of the upstream vane, it is observed that lateral flow velocity is positive on the left side of the contour map which follows the thumb rule of the flow. In the middle part of the contour map where there is no vane, lateral velocity tends to zero so it is concluded, that the velocity is more or less in the flow-wise direction.

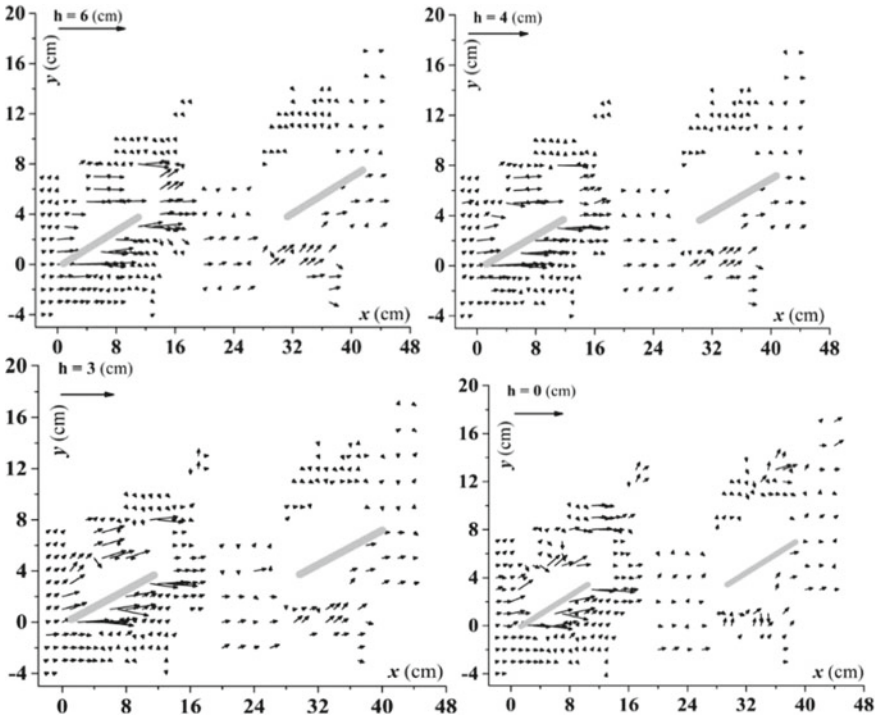

Fig. 5 Vectorsresultant velocity contours for selected four cross-sections $h = 6$, 4, 3, and 0 cm, respectively

Vertical flow velocities

In the left portion of the vertical velocity contour where flow just meets the vane velocity is negative as the horseshoe vortex is formed in that zone. In the middle where there is no vane, vertical velocity tends to zero. It is also observed that in this region, vertical component v also tends to zero, so it can be said that only flow-wise velocity is predominant here. Though it is obvious as there is no obstruction (Fig. 6).

Absolute velocity contour

From two contour plots in Fig. 7, it is noted that vane structures obstruct the velocity and hence time average velocity value is lower, adjacent to the vane but in the middle region where there is no vane, the value of time average velocity is more or less undisturbed.

Vectors of velocity

In the case of vector velocity diagrams, it is seen that the velocity outline pattern surrounding the vanes deviates more in the bottommost cross-section compared to the other cross-sections. As a result, the direction of the fluid particles along the horizontal cross-section is clearly indicated.

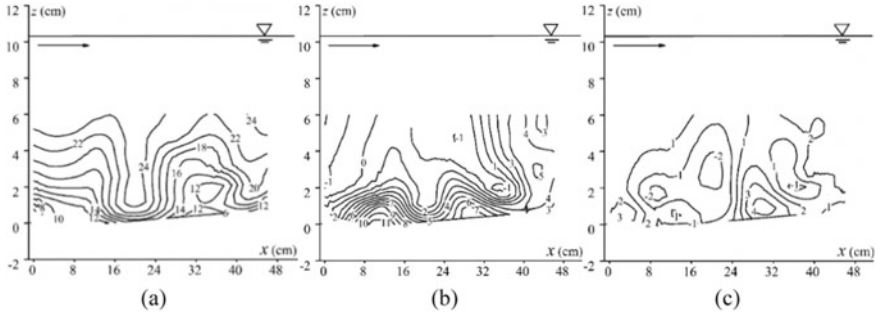

Fig. 6 **a** Flow-wise flow velocity, **b** transversal flow velocity, **c** vertical flow velocity for central vertical cross-section

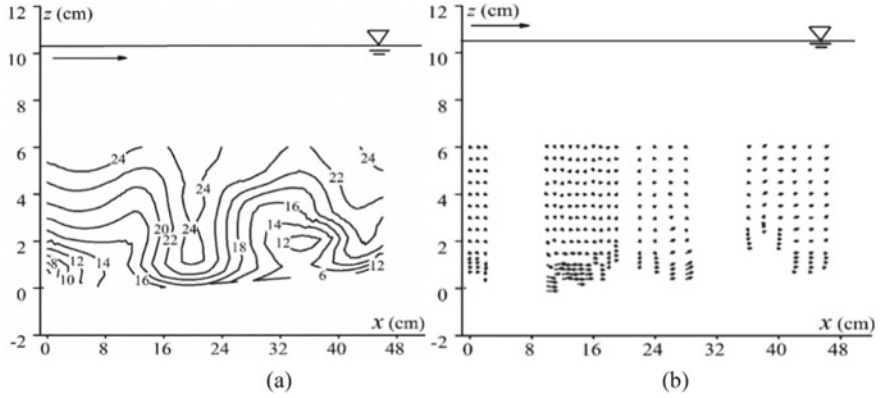

Fig. 7 **a** Time-averaged absolute velocities contour and **b** Vector velocity diagram for central vertical cross-section

4 Conclusion

From the flow fields measured around two eccentrically arranged tandem rectangular submerged vanes of identical shapes at clear-water equilibrium scour conditions; the following conclusions are drawn:

i. Different directional velocities, i.e., flow-wise, transversal and vertical have varied magnitudes as well as directions about the vanes, thus providing a clear picture of the flow patterns around such a configuration of vanes.
ii. It is observed that the downward velocity component (w) at just the upstream point of the selected submerged vane which is located downstream is higher than the upstream vane because the effect of scouring is increasing for the obstruction.
iii. The amplitude of the transverse velocity component (v) is greater at the adjacent locations of the vanes, resulting in greater velocity separation in the transverse direction.

iv. Away from the vanes, flow-wise flow velocity (u) is largely unaffected. As a result, the vane has no discernible influence on the flow.

The velocity profiles give the idea at which direction flow is moving, where the direction is reversed, and where the magnitude is more. It was observed that the formation of scour and dune was prominent on the eccentric side of the upstream vane. From the magnitude of the vertical part of velocity in vortex zones, it can be therefore established that both horseshoe and wake vortices are much stronger around the downstream vane than the upstream vane.

References

1. Mukherjee P, Das S, Mazumdar A (2021) Introducing winter rice cropping by using non-saline tidal water influx in western basins of South 24 Parganas, India. Sci Rep 11(1):553
2. Odgaard AJ, Spoljaric A (1986) Sediment control by submerged vanes. J Hydraul Eng 112(12):1164–1180
3. Laursen EM, Toch A (1956) Scour around bridge piers and abutments, vol 4. Iowa Highway Research Board. Ames, Iowa
4. Melville BW (1992) Local scour at bridge abutments. J Hydraul Eng 118(4):615–631
5. Liu HK, Chang FM, Skinner MM (1961) Effect of bridge constriction on scour and backwater. Report No. CER60HKL22, Civil Engineering Section, Colorado State Univ. Fort Collins, Colo
6. Ahmed F, Rajaratnam N (1998) Flow around bridge piers. J Hydraul Eng 124(3):288–300
7. Barbhuiya AK, Dey S (2004) Local scour at abutments: a review. Sadhana 29(5):449–476
8. Coleman SE (2005) Clearwater local scour at complex piers. J Hydraul Eng 131(4):330–334
9. Das R, Khwairakpam P, Das S, Mazumdar A (2014) Clear-water local scour around eccentric multiple piers to shift the line of sediment deposition. Asian J Water Environ Pollut 11(3):47–54
10. Das S, Ghosh S, Mazumdar A (2014) Kinematics of horseshoe vortex in a scour hole around two eccentric triangular piers. Int J Fluid Mech Res 41(4):296–317
11. Das S, Das R, Mazumdar A (2014) Variations of clear water scour geometry at piers of different effective widths. Turk J Eng Environ Sci 38(1):97–111
12. Lede AD, Barman J, Kumar B (2021) High-order moments of velocity fluctuations around a cylinder in a dredged channel. ICE—Water Manage 1–9. https://doi.org/10.1680/jwama.20.00070
13. Jaman H, Das S, Kuila A, Mazumdar A (2017) Hydrodynamic flow patterns around three inline eccentrically arranged circular piers. Arab J Sci Eng 42(9):3973–3990
14. Das S, Mazumdar A (2015) Turbulence flow field around two eccentric circular piers in scour hole. Int J River Basin Manage 13(3):343–361
15. Das S, Mazumdar A (2018) Evaluation of hydrodynamic consequences for horseshoe vortex system developing around two eccentrically arranged identical piers of diverse shapes. KSCE J Civ Eng 22(7):2300–2314
16. Breusers HNC, Nicollet G, Shen HW (1977) Local scour around cylindrical piers. J Hydraul Res 15(3):211–252
17. Das S, Das R, Mukherjee R, Mazumdar A (2017) Enhancement of sediment transportation by increasing scour around a square pier with vane attached on one side. In Proceedings of the 37th IAHR world congress, Kuala Lumpur, Malaysia
18. Roy P, Das S, Dey A, Das R (2022) Analytical study of scour mechanism around immersed rectangular vane structures. In: Rao CM, Patra KC, Jhajharia D, Kumari S (eds) Advanced modelling and innovations in water resources engineering 2021, LNCE, vol 176. Springer, Singapore, pp 703–717

19. Bejestan MS, Khademi K, Kozeymehnezhad H (2015) Submerged vane-attached to the abutment as scour Counter measure. Ain Shams Eng J 6(3):775–783
20. Sharma H, Jain B, Ahmad Z (2016) Optimization of submerged vane parameters. Sadhana 41(3):327–336
21. Das S, Das R, Mazumdar A (2015) Velocity profile measurement technique for scour using ADV. In Proceedings of the 2015 international conference on testing and measurement: techniques and applications, TMTA 2015, Phuket Island—Chan (ed.), Taylor & Francis Group, London, pp 249–252
22. Das S, Das R, Mazumdar A (2014) Vorticity and circulation of horseshoe vortex in equilibrium scour holes at different piers. J Inst Eng (India): Series A 95(2):109–115
23. Buffin-Bélanger T, Roy AG (2005) 1 min in the life of a river: selecting the optimal record length for the measurement of turbulence in fluvial boundary layers. Geomorphology 68:77–94

Electrical Conductivity as an Indicator of Sea Water Intrusion in South 24 Parganas, West Bengal, India

Souvik Chakraborty, Baibaswata Das, Souradeep Roy, Sourav Kumar Singha, and Anindya Mukherjee

Abstract Electrical conductivity is the number of ions present in water. In fresh water value of electrical conductivity should be remain within 400μs/cm as per WHO guideline. But it is enhanced if the existence of number of ions is increased. In sea water free state of ions are plenty available. If sea water is mixed with fresh water aquifer than number of ions present in ground water aquifer is enhanced resulting in high value of electrical conductivity. So from the electrical conductivity data if that exceeds the standard specification laid down by world health organisation WHO then the groundwater is unfit for drinking. On the investigation it can also be concluded that saline water from Bay of Bengal is intruding into South 24 Parganas which is the study area. So electrical conductivity is also an indicator of salty water encroachment in fresh water aquifer in South 24 Parganas. It has been observed that all the seventeen sample points in South 24 Pargana possess high value of electrical conductivity which indicates that South 24 Parganas is highly affected by sea water intrusion. As remedial measure rain water harvesting can be adopted.

Keywords Electrical conductivity · Drinking water specification · Saline water intrusion · Rainfall · Population

1 Introduction

Water is a chemical compounds which is made up of many chemical parameters. Electrical conductivity is one of the properties of water which can be measured by conductivity meter or conductivity probe. From the point of view of properties of water parameters of water like pH, chloride, electrical conductivity, magnesium, iron, sodium chloride, manganese etc. must have value within acceptable limit laid down by WHOfor drinking water standard, so that water can be safely utilized by drinking water. Electrical conductivity represents number of ions present in water. Although

S. Chakraborty (✉) · B. Das · S. Roy · S. K. Singha · A. Mukherjee
CE Department, Dr. Sudhir Chandra Sur Institute of Technology and Sports Complex, Kolkata 700054, India
e-mail: schakraborty@dsec.ac.in

© The Author(s), under exclusive license to Springer Nature Singapore Pte Ltd. 2023

S. Kumar et al. (eds.), *Sustainable Environmental Engineering and Sciences*,
Lecture Notes in Civil Engineering 323, https://doi.org/10.1007/978-981-99-0823-3_7

there is nonlinear relationship exists between number of ions and electrical conductivity as because enhancement of number of ions impedes electrical conductivity. According to World Health Organization standard the permissible limit of EC for drinking water purpose is 400 μs/cm. If the value of Electrical conductivity (EC) is exceeded from the permissible limit as per WHO guideline which means number of ions present in water is higher and for that reason it is unfit for drinking water purpose. India has large coastal belt. It has around 7530 km length of coastline. In the west of India from Tamilnadu to Gujrat coastal belt of India has a width of ten to twenty five Km. In the Eastern portion of Indian coastal belt the length and width are much greater than western coastal belt, because of existence of Bay of Bengal, Krishna, Cauvery, Mahanadi river. Moreover, the soil profile of eastern India is made up of alluvium soil which possesses more horizontal hydraulic conductivity than vertical conductivity. For that reason saline water is intruded in the fresh water in the eastern portion more than the western counterpart. Moreover out of eight Union territories in India seven Union territories are having coastal region. The eastern India lithological character and overdraft of groundwater than the permissible limit and less amount of rainfall are such that saline water is intruded into fresh water aquifer. It is inevitable as because according to Ghyben Herzberg principle for one unit decrease of groundwater table forty unit of sea water is intruded into the mainland. Due to the prolonged inadequate amount of rainfall and salty surface water people are inclined to use groundwater. Due to which overexploitation of groundwater is taking place as groundwater table declines as a result of which sea water is intermingled with fresh water aquifer. Pure water is non electrolyte. But in sea water plenty of anion and cation are present in free state. When saline water is mixed with the fresh water aquifer quantity of ions are enhanced in it. As a result of which EC value is also enhanced. For that reason, if EC value is obtained then it will indicate whether the study area is affected by sea water intrusion or not. The study area chosen is South 24 Parganas, West Bengal, India. The northing and easting of South 24 Parganas are 22.14° N and 88.41° E. South 24 Parganas is very close to Bay of Bengal. Population density of South 24 Parganas is higher than that of West Bengal. Rainfall over here is also very low. So water used for domestic work, industrial work and irrigation work is obtained from groundwater. The stress in groundwater makes the water table decline. According to the principle stated above sea water invasion is taking place over here. From the spatial distribution of electrical conductivity values and judging with standard reference we can come into conclusion if South 24 Parganas is saline prone.

Malmberg [1] has experimented the increase of value of electric conductivity value due increase of pressure and temperature in salty water. Moore et al. [2] has discussed the details about of electrical conductivity from the point of view of chemistry and also illustrated it is as an indicator of hydrological process. Golnabi et al. [3] has investigated the existence of electric conductivity in pure drinking water, industrial water and water required for irrigation. Yacoob et al. has invented the new method of determination of electrical conductivity byelectrical physical property. It is determined by the help of electrodes made up of silver. Salahuddin [4] has collected large samples of groundwater from Dildarnagar

village. He has obtained electrical conductivity value by electrolysis method. He has done validation also by comparing graphical data with actual data. He has concluded that electrical conductivity depended on area as well as month. Pal et al. [5] has monitored the water quality parameter on spatial and temporal basis in Rudra Sagar Lake in West Tripura. He has done analysis on relationship between electric conductivity (EC) and total dissolved solids (TDS). They have found that there was linear relationship existed between EC and TDS in their study area. Mengran et al. [6] have determined the electrical conductivity value in mine bursting liquid in their study area. Sakuma and Ichiki [7] has discussed the evolution of electrical conductivity in NaCl-H_2O fluid as a result temperature rise, increase of pressure and chemical reactions. The result is obtained by Molecular Dynamic Simulations. Shrestha et al. [8] have determined different values of electrical conductivity in different sources in Nepal. They have also determined variation of electrical conductivity value due to presence of electrolytic solution NaCl. Corwin and Yemoto [9] has illustrated that electrical conductivity, total solids are indicator of salinity. Chakraborty et al. [10] has simulated the groundwater level in various locations of Purba Medinipur from the year 2019 to 2023. The results were also validated with the existing data. Chakraborty et al. [11] has identified the saline water affected area of Egra, Purba Medinipur as a result of overexploitation of groundwater. Chakraborty et al. [12] has examined the saline water affected area of coastal region of Purba Medinipur. John et al. [13] have investigated that if groundwater table is declined then electrical conductivity is increased. The study has been taken place in Kolkata city. They also recommended mineralisation has also an effect on electrical conductivity.

2 Material and Method

2.1 Study Area

The study area chosen for this research paper is South 24 Parganas, West Bengal, India. The latitude and longitude of South 24 Parganas are 22.14° N and 88.41° E respectively. To its north North 24 Pargana is located. In the North-East direction Kolkata is located. In the Western portion Haora is situated. In the South-West portion Medinipur is located. In the South portion of South 24 Parganas Bay of Bengal is located. In the eastern portion of study area Bangladesh is situated. Pictorially the study area is represented in Fig. 1.

From twenty nine locations of South 24 Parganas groundwater samples were collected. It is tested in lab. From the test electrical conductivity values were determined. After obtaining EC values spatial distribution of electrical conductivity was obtained. Contour map of electrical conductivity over entire South 24 Parganas is drawn by Arc GIS. From this map pathline of sea water into the fresh water aquifer can be predicted. The details of spatial distribution of Electrical conductivity values over South 24 Parganas are shown in Table 1.

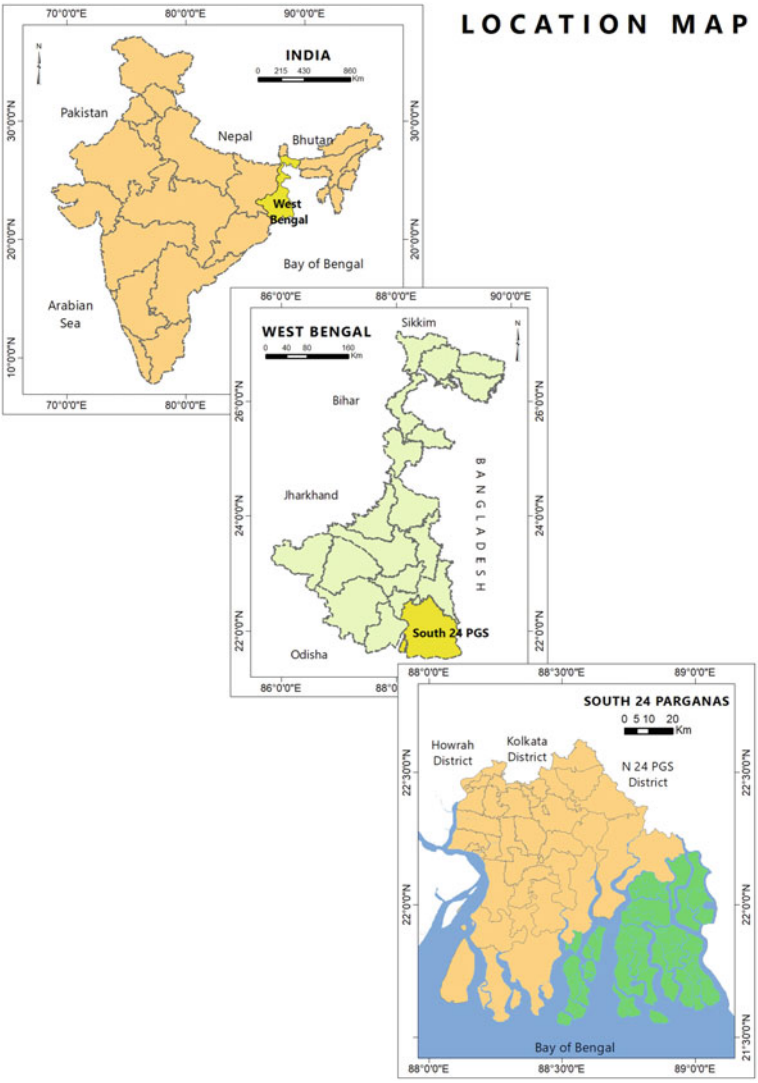

Fig. 1 Location map of Gosaba, South 24 parganas

2.2 Rainfall Distribution of Study Area

Rainfall distribution in South 24 Parganas is moderate. From IMD Kolkata Rainfall distribution in South 24 Parganas and average rainfall in West Bengal are collected for the tenure of one decade i.e., from 2010 to 2020. The decadal rainfall in South 24 Parganas is ranged from 1503 to 1887 mm. The variation of rainfall is not much. The variation is only 2% per year. From the comparison of decadal rainfall distribution

Table 1 Electrical conductivity values in South 24 Parganas

Sl no	Location	EC µs/cm
1	Dholerhat	1820
2	Hatuganj	1930
3	Namkhana	1320
4	Baruipur	879
5	Raidighi	1520
6	Budge budge	1110
7	Falta Dw	1550
8	Jaynagar	1380
9	Ramdhari	3230
10	Dhosa	1340
11	Ambikanagar (Kellar hat)	1300
12	Dakshin Barasat	1360
13	Usti	1660
14	Langalberia	918
15	Athaarobanki	4560
16	Nalmuri	664
17	Bhojerhat	1440

in South 24 Parganas and average decadal precipitation of West Bengal it is seen that precipitation values in South 24 Parganas over the year in running decade is almost below than that of South 24 Parganas except in the year 2015, 2017 and 2019. From here it can be concluded that rainfall in South 24 Parganas is not at par with its state. Since rainfall is less in South 24 Parganas, so surface water is not fulfilled by rainfall. So people do not get an adequate amount of water from surface sources and by which they are more inclined to withdraw groundwater resulting saline water to be intermingled with aquifer water (Fig. 2).

2.3 Population in South 24 Parganas

From the census india.gov.in website the population in South 24 Parganas over the last seven decades has been obtained. It has been found that the increase of population in South 24 Parganas is almost 7% per year which is very high. Since the population density in South 24 Parganas is much more than that of West Bengal so much stress in groundwater has fallen which causes sea water intrusion. The increase of population in South 24 Parganas is shown graphically in Fig. 3.

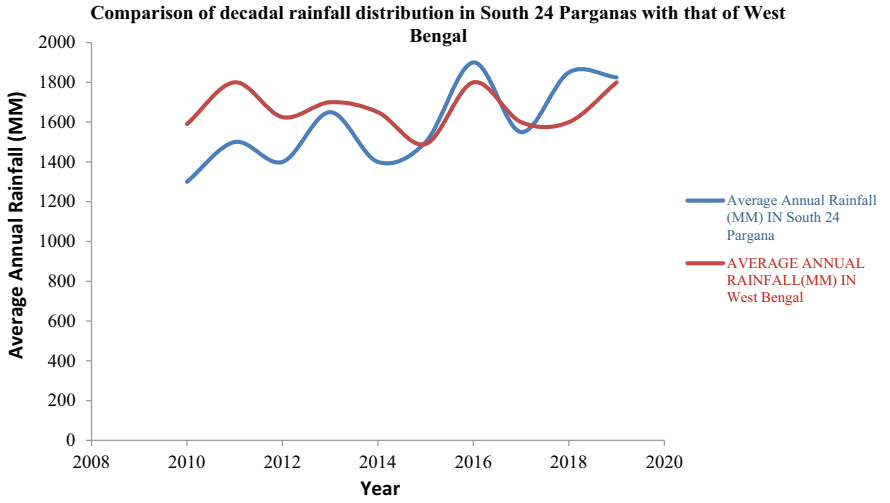

Fig. 2 Comparison of decadal rainfall distribution in South 24 Parganas with that of West Bengal

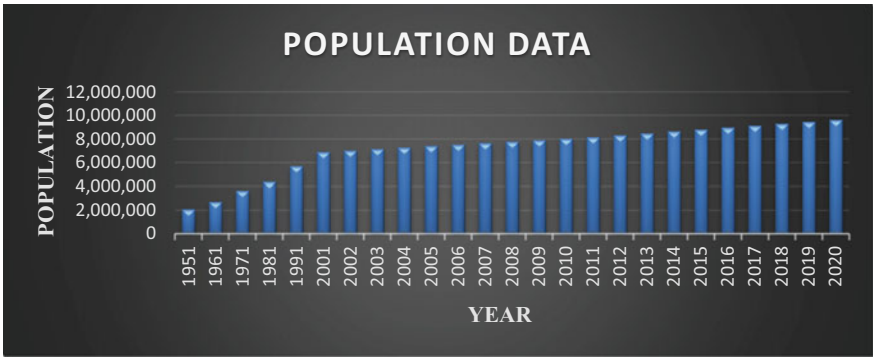

Fig. 3 Population data of South 24 Parganas over the years

3 Results and Discussions

Electrical conductivity values in seventeen locations of South 24 Parganas were obtained from South 24 Parganas water quality information booklet. It is given in table number 1. It is also mapped by ArcGIS. It is shown below.

From Table 1 it is observed that all the sample locations of South 24 Parganas possess EC value beyond safe limit according to WHO guideline. So 100% of the sample locations possess EC value beyond acceptable limit for drinking water according to WHO guideline according to which the safe limit of EC for drinking water is 400 μs/cm. From Fig. 4 it is also confirmed that north portion of South 24 Parganas like Goragacha, Rajpur, Baruipurhave EC value comparatively less than

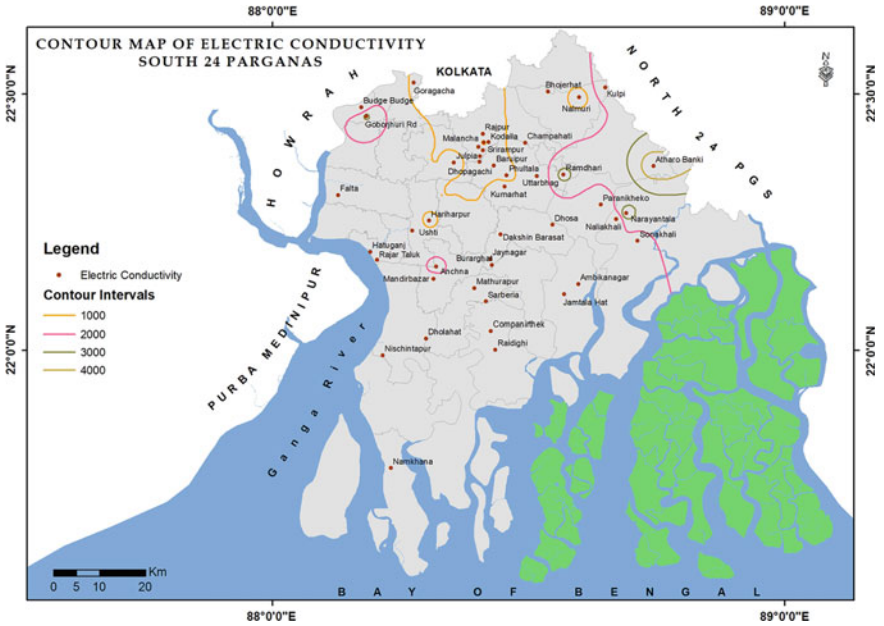

Fig. 4 Contour map of electrical conductivity in South 24 Parganas

other locations. Western portion of South 24 Parganas like Paranikheko, Sonakhali possess EC value 2000 μs/cm which is beyond the safe limit from the standard of drinking water specification and indicates saline water affected zone. In the west portion of South 24 Parganas few locations likeNarayantala are indicating same as it possesses EC value about 3000 μs/cm. In the West portion also place like AtharoBanki possesses high value of EC indicating saline water intrusion in Western South 24 Parganas. From this analysis it is observed that the west portion of South 24 Parganas is highly affected by sea water intrusion and northern portion of South 24 Parganas are less affected by sea water invasion.

3.1 Preventive Measure

1. A high ridge between Bay of Bengal and mainland of South 24 Parganas can be established.
2. Surface water must be maintained at higher level than that of Bay of Bengal.
3. Water harvesting must be done at South 24 Parganas to reduce dependency on groundwater.

3.2 *Probable Pathline of Sea Water*

From the analysis above it can be inferred that sea water is entering into the east portion of Bay of Bengal first as it is in close proximity to the Bay of Bengal. After that it is intruding into the central portion and northern portion of South 24 Parganas. From the central portion of South 24 Parganas it is moving toward eastern South 24 Parganas (Fig. 5).

4 Conclusion

Electrical conductivity is the number of ions present in the water. Pure water is non electrolyte. But with the increase of ions in water Electrical conductivity increases. Cation and anion are present in sea water in free state. South 24 Parganas is very close to the Bay of Bengal. Due to high population density and lack of fresh surface water people are withdrawing groundwater at a high rate resulting sea water intrusion in the fresh aquifer of South 24 Parganas. As a result of which ions in the fresh water increase. For this reason spatial distribution of electrical conductivity also increases. So electrical conductivity is an indicator of saline water intrusion in the study area. From the obtained result of electrical conductivity from South 24 Parganas groundwater information booklet it is observed that 17 locations out of 17 locations in South 24 Parganas possess EC values which are beyond the acceptable limit of drinking water specifications according to WHO. So it is an indication that almost entire locations of South 24 Parganas are saline water affected. From the analysis

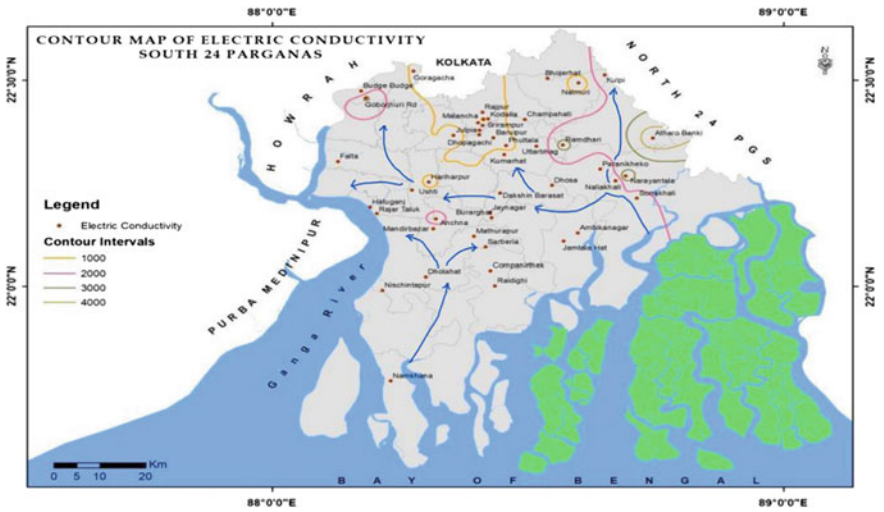

Fig. 5 Probable pathline of sea water intrusion in South 24 Parganas

it can be also predicted the pathline of sea water ingression into the mainland of South 24 Parganas. It is most likely that sea water is entering into the west South 24 Parganas first and after that it is moving toward central and northern portion of South 24 Parganas. Western South 24 Parganas is most affected by sea water intrusion. Since fresh water is scarce in South 24 Parganas, so alternative arrangement has to be made to protect the groundwater which in turn is a factor of sea water intrusion in South 24 Parganas. South 24 Parganas is heavily affected by saline water encroachment. In the present study it is found that electrical conductivity values in groundwater in all the locations in South 24 Parganas are beyond acceptable limit as per WHO guideline. It is also an indicator of sea water intrusion. To remediate it rain water harvesting can be the alternate method by which need for drinking water, industrial water, irrigation water can be provided in sufficient amount in entire South 24 Parganas.

Acknowledgements We are very much thankful to the State Government. From the information of groundwater booklet in South 24 Parganas this paper has been made.

References

1. Malmberg CG (1965) Electrical conductivity of dilute solutions of "Sea Water" from 5 to 120 °C. J Res National Bureau of Standards-A. Phys Chem 69A(1)
2. Moore RD, Richards G, Story A (2008) Electrical conductivity as an indicator of water chemistry and hydrologic process. Watershed Manage Bull 11(2)
3. Golnabi H, Sharifian M, Bahar M (2009) Investigation of electrical conductivity of different water liquids and electrolyte solutions. Iran Phys J 3–2, 24–28
4. Salahuddin (2015) Analysis of electrical conductivity of ground water at different locations of Dildar Nagar of U.P, India. Adv Appl Sci Res 6(7):137–140
5. Pal M, Roy PK, Sasmal NR, Roy MB (2015) Electrical conductivity of lake water as environmental monitoring—a case study of Rudra Sagar Lake. https://www.researchgate.net/publication/275353467
6. Mengran Z, Chenyang H, Dong L, Xiaoyun W (2016) Research of electrical conductivity measurement system for mine bursting water based on dual frequency method. MATEC Web Conf 68:12007. https://doi.org/10.1051/matecconf/20166812007
7. Sakuma H, Ichiki M (2016) Electrical conductivity of NaCl-H_2O fluid in the crust. AGU Publication. https://doi.org/10.1002/2015JB012219
8. Shrestha AK, Basnet N, Bohora CK, Khadka P (2017) Variation of electrical conductivity of the different sources of water with temperature and concentration of electrolyte solution NaCl. Int J Recent Res Rev X(3)
9. Corwin D, Yemoto K (2017) Salinity: electrical conductivity and total dissolved solids. https://www.researchgate.net/publication/320456153
10. Chakraborty S, Maity PK, John B, Das S (2020) Examining the extent of seawater intrusion from groundwater quality analysis at Purba Medinipur coast of India. J Indian Chem Soc Special Issue 97:1–8
11. Chakraborty S, Maity PK, John B, Das S (2020) Overexploitation of groundwater and as a result sea water intrusion into the coastal aquifer of Egra, purbamedinipur. Ind J Environ Protection 40(4):413–423
12. Chakraborty S, Maity PK, Das S (2020) Investigation, simulation, identification, and prediction of groundwater levels in coastal areas of Purba Medinipur, India using MODFLOW. Ind J Environ Protection 40(4):413–423

13. John B, Das S (2020) Role of electrical conductivity on salinity and mineralization due to groundwater level fluctuations in Kolkata City, IOP Conf Series: Earth Environ Sci 505:012021. https://doi.org/10.1088/1755-1315/505/1/012021

Evaluation of River Health Status Based on Water Quality Index and Multiple Linear Regression Analysis

Suyog Gupta and Sunil Kumar Gupta

Abstract The present study was abstracted to investigate the health status of the river Damodar, India, for drinking purpose using water quality index (WQI) method. Eleven water quality parameters, i.e., pH, DO, BOD, TDS, Cl^-, $NO_3{}^-$, $SO_4{}^{2-}$, TC, F^-, Fe, and Pb were analyzed from ten monitoring sites designated on the river stretch. The multiple linear regression (MLR) model was also anticipated as an efficient methodology for the prediction of WQI. The accuracy of the MLR model was assessed by using the coefficient of determination (R^2), root mean square error (RMSE), and mean absolute error (MAE). The results obtained from the WQI method revealed that the river health diverse between good (26–50) and unfit (>100) categories, whereas it was not found excellent for drinking purpose in any monitoring site. The values of WQI were primarily affected by the high concentration of BOD (>2 mg/L), TC (>50 MPN/100 ml), and Fe (>0.5 mg/L) in the river water. Moreover, the study disclosed that MLR models performed well ($R^2 = 0.999$, RMSE = 0.110 and MAE = 0.085) for the estimation of WQI. Therefore, the established MLR model can be applied for affordable, quick, and effective evaluation of river health for efficient river management practices.

Keywords River health · Water quality index · Multiple linear regression

1 Introduction

Rivers are the important natural resource of fresh water in planet earth. Fresh water is essential for the aquatic ecosystem and human consumption. It must be free from any detrimental physical, chemical, and biological impurities [8, 12, 16]. With rapid growth and development, surface water as rivers has been polluted with an extensive range of pollutants from various sources [8, 17, 23]. It is important to be trying to evaluate and protect the river health. Many components decide the chemical, physical,

S. Gupta (✉) · S. K. Gupta
Department of Environmental Science and Engineering (Indian School of Mines), Indian Institute of Technology, Dhanbad, Jharkhand 826004, India
e-mail: suyog.iitdh@gmail.com; suyog.17dr000525@ese.ism.ac.in

© The Author(s), under exclusive license to Springer Nature Singapore Pte Ltd. 2023

S. Kumar et al. (eds.), *Sustainable Environmental Engineering and Sciences*,
Lecture Notes in Civil Engineering 323, https://doi.org/10.1007/978-981-99-0823-3_8

and organic arrangements of surface water, both natural (precipitation, the topography of the watershed, climate, and geography) and anthropogenic (mechanical exercises, homegrown and agricultural run-off) [8, 14, 18]. Growing surface water pollution causes decay of water quality and undermines human wellbeing, and upsets the equilibrium of the sea-going biological system, financial progression, and social achievement [7, 18]. Rivers are indispensable for the food and thriving of society, yet during late many years, these are constantly being undermined around the world [5, 15, 19].

2 Literature Review

To assess the river health, many researchers [8, 11, 13, 17, 20, 23] calculated only the different indices using the traditional and laborious methodologies without exploring the recent modeling techniques. Yadav et al. [22] applied Carlson's index, eutrophication index, and organic pollution index for ascertaining the water quality of the river Chambal for public consumption. Wu et al. [21] screened out the permanganate index for assessing the WQ of the Lake Taihu Basin. Tian et al. [17] calculated the WQI to ensure the WQ of the Luanhe river during spring, summer, and autumn periods. Abba et al. [1] applied the MLR method to predict the DO concentration at downstream of Agra city. Abyaneh [2] used the MLR method to determine the BOD and COD. Kadam et al. [9] evaluated the MLR model's performance for the prediction of WQI. However, the present study combined the MLR method for the prediction of WQI to determine river health efficiently.

3 Objectives

The objectives of the paper are (i) to apply WQI for determining the river health, and (ii) to study the applicability of MLR model for the prediction of WQI efficiently.

4 Methodology

4.1 Study Area

The study was steered on Damodar River, India (see Fig. 1). It drains into two states of India, i.e., Jharkhand and West Bengal with 541 km of length and approximately 22,000 Km^2 of drainage area. It is most important river for drinking and aquaculture in the region. This river rises in the southeast corner in the hills of the Chhotanagpur plateau and joins the river Hugli. This river basin experiences scorching summer (up

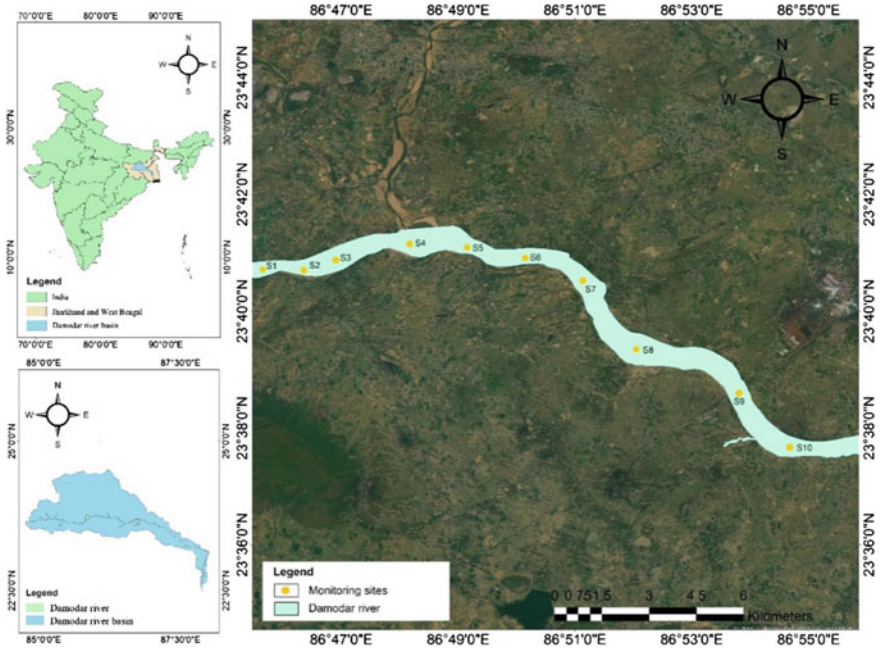

Fig. 1 Study area map with monitoring sites

to 48 °C) and freezing winter (~2 °C). The annual rainfall varies between 765 and 1850 mm, with a mean value around 1300 mm [20].

4.2 River Water Sampling and Analytical Procedures

The sampling was performed from 2018 to 2019 during pre-monsoon and post-monsoon periods at ten monitoring sites. Three samples were accumulated properly from each monitoring site, and their means were reported. Furthermore, eleven RWQPs were analyzed as per the standard procedures [3] given in Table 1.

4.3 Water Quality Index (WQI)

The weighted arithmetic WQI was employed for figuring out the river health. It pursued the three essential steps, parameter selection, weight assignment, and aggregation [4, 6, 8, 10, 13]. The WQI method was described in Eq. (1).

Table 1 Standard procedures for determination of RWQPs

Parameters[a]	Methods of determination
pH	Electrometric method
DO	Iodometric method
BOD	5-Day BOD Test
TDS	Gravimetric method
Cl−	Argentometric method
NO3−	Ultraviolet spectrophotometry
SO42−	Turbidimetric method
TC	Multiple-tube fermentation technique
F-	SPADNS method
Fe	Atomic absorption spectroscopy
Pb	Atomic absorption spectroscopy

[a]Unit of parameters is mg/L except TC (MPN/100 ml)

$$WQI = \sum_{i=1}^{m} Q_i W_i / \sum_{i=1}^{m} W_i \tag{1}$$

where Q_j: quality rating, and W_j: relative weight for ith (1, 2, 3……, m) water quality parameter of Damodar River. In addition, WQI was used to classify river health as excellent (0–25), good (26–50), fair (51–75), poor (76–100), and unfit (>100) categories [8].

4.4 Multiple Linear Regression (MLR)

MLR, a linear modeling technique was used for establishing the relationship between independent and dependent variables [8, 9]. It is described as Eq. (2).

$$y = \delta_0 + \delta_1 x_1 + \delta_2 x_2 + \ldots \delta_m x_m + \varepsilon \tag{2}$$

where y: dependent variable, δ_o: constant, δ_1-δ_m: coefficients, x_1-x_m: independent variables, m: number of independent variables, and ε: error. The least-squares fitting approach was used to establish this relationship.

4.5 Accuracy Assessment

The statistical parameters, i.e., R^2, RMSE, and MAE were applied to evaluate the accuracy of the developed model [8].

5 Results and Discussion

5.1 Physicochemical Characteristics of the River

A critical observation of the physicochemical characteristics of Damodar River revealed that river water was slightly acidic to alkaline. The variation in pH (7.392 ± 0.691) was due to effluents regularly disposed of in various industries situated on the bank of the river. DO (6.995 ± 0.716 mg/L) concentration level was sufficient for several physiological activities due to the geological conditions. The higher BOD (3.45 ± 1.664 mg/L) revealed the existence of massive quantity of organic matter due to effluent expulsion at some locations at the Damodar River. Except for some monitoring stations, TDS (329.05 ± 244.095) was found within the desirable limit. It increased due to the direct discharge from thermal power plants. The main causes of Cl^- concentration (21.53 ± 7.925 mg/L) were sewage waste and different anthropogenic activities in the river [11]. The level of NO_3^- (10.347 ± 6.908 mg/L) fluctuated due to aquatic plant growth/decay, municipal wastewater, and industrial wastewater [8, 20].

Additionally, water consumption with high nitrate concentration causes methemoglobinemia disease in infants, abnormal pain, and diabetes. The prime contributors of SO_4^{2-} were sewage, agricultural runoff, and industrial discharges. Higher coliform counts (156.025 ± 101.436 mg/L) indicated inadequate sanitation facilities at that monitoring station along the river stretch. Due to the health risk, proper treatment as water disinfection was strictly suggested to reduce the higher MPN values [20]. A high level of F^- (0.871 ± 0.062 mg/L) was due to the geographical conditions of the river basin. The heavy metals in natural surface water may be associated with either natural or anthropogenic processes [8]. The concentrations of Fe (0.579 ± 0.197 mg/L) and Pb (0.018 ± 0.019 mg/L) were found above detection limits. These metals become toxic pollutants and affect human health where they cross the permissible levels (Singh et al. 2020) [20].

5.2 Status of River Health Based on WQI

In this study, WQI was applied to evaluate the Damodar River health. Eleven water quality parameters were taken into account to calculate WQI for each monitoring site. The analysis results belonging to all 10 monitoring sites were used for river health evaluation. Furthermore, the standard limits of the WQPs described by the Bureau of Indian Standards were employed for calculations.

To calculate WQI at each monitoring site, the weight values were estimated for the WQPs conferring to their relative importance. The computed WQI values were between 27.698 and 121.899. In addition, Damodar River health was categorized between good to unfit for drinking purpose due to the input of municipal and industrial

Fig. 2 Status of Damodar River health based on WQI

wastes and agricultural discharge in the river stretch. The status of the Damodar River health was described in Fig. 2.

5.3 Assessment of MLR Model

A program code was written in the R language for the development of MLR model. Then, MLR model was validated using a test dataset and evaluated employing the performance statistics. In this model, WQI acted as a response variable, and the river water quality parameters represented the predictors. The regression coefficients associated with the predictors computed the changes in the response variable. The standard error (SE) was used to estimate the firmness of regression coefficients. The t-test and f-test were also used for assessing the significance of means and variance, respectively. The p-value (Pr) associated with the t-test defined the probability of observing the values equal or more significant than the t-value. The cutoff p-value was taken 0.05 for significance in this study. The degree of freedom (DoF) is the number of independent pieces of information used to calculate an estimate. The R^2 and adjusted R^2 were used to assess the vigorous MLR model, which was interpreted similarly except that the adjusted R^2 took into reflection the DoF. The statistical summary of the MLR model is described in Table 2.

Table 2 represented that SE was 0.002 on 20 DoF, with R^2 and adjusted R^2 as unity. It was equated through f-value, which was 1.102E + 05 on 7 and 20 DoF, with a p-value < 2.2E-16. The p-value < 0.05, interpreted that developed model was significant. The MLR model was validated using the testing dataset. According to the performance statistics ($R^2 = 0.999$, RMSE = 0.110, MAE = 0.085), MLR model was helpful in determining the connotation between independent and dependent variables (Fig. 3).

Table 2 Statistical summary of MLR model

Parameters	Estimate	SE	t-value	Pr(>|t|)
Intercept	−0.081	0.001	−55.781	<2e-16***
pH	0.006	0.001	5.152	4.85e-05***
BOD_5	0.112	0.002	59.029	<2e-16***
NO_3^-	0.005	0.001	3.780	0.00117**
TC	0.010	0.002	5.811	1.10e-05***
F^-	0.006	0.002	4.223	0.00041***
Fe	0.532	0.002	352.204	<2e-16***
Pb	0.507	0.002	325.815	<2e-16***

Asterisks mark aside p values defines significance of values, lower the value have high significance. Significance codes: 0 '***' 0.001 '**' 0.01 '*' 0.05 '.' 0.1 ' ' 1

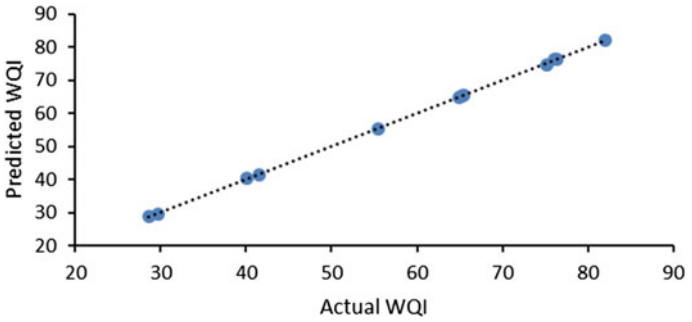

Fig. 3 Performance of MLR model

6 Conclusion

In this study, Damodar River health was appraised using the WQI method for its suitability as drinking water. This method determined that the river health was varied from good to unfit at the different locations for drinking purposes. This method can be used as one of the critical tools for efficient river health monitoring and management. The suitability of the MLR model was also investigated for simplifying the complex calculation associated with the WQI method. The performance of the developed MLR model showed that it could be implanted as a module for estimating the WQI values. Further investigations are desired to test the other models than the MLR with more WQPs to assess the WQI for monitoring the river health.

References

1. Abba SI, Hadi SJ, Abdullahi J (2017) River water modelling prediction using multi-linear regression, artificial neural network, and adaptive neuro-fuzzy inference system techniques. Procedia Comput Sci 120:75–82
2. Abyaneh HZ (2014) Evaluation of multivariate linear regression and artificial neural networks in prediction of water quality parameters. J Environ Health Sci Eng 12(1):1–8
3. APHA, AWWA, WEF (2017) Standard methods for the examination of water and wastewater, 22nd edition, American Public Health Association, Washington D.C, USA
4. Chabuk A, Al-Madhlom Q, Al-Maliki A, Al-Ansari N, Hussain HM, Laue J (2020) Water quality assessment along Tigris River (Iraq) using water quality index (WQI) and GIS software. Arab J Geosci 13(14):1–23
5. Das S, Sarkar R (2021) Monitoring and evaluating the spatiotemporal variations of the water quality of a stretch of the Bhagirathi-Hugli River, West Bengal, India, using geospatial technology and integrated statistical methods. Environ Sci Pollut Res 28(13):15853–15869
6. Fathi E, Zamani-Ahmadmahmoodi R, Zare-Bidaki R (2018) Water quality evaluation using water quality index and multivariate methods, Beheshtabad River, Iran. Appl Water Sci 8(7):210
7. Garcia CAB, Silva IS, Mendonça MCS, Garcia HL (2018) Evaluation of water quality indices: use, evolution and future perspectives
8. Gupta S, Gupta SK (2021) Development and evaluation of an innovative enhanced river pollution Index model for holistic monitoring and management of river water quality. Environ Sci Pollut Res 28(21):27033–27046
9. Kadam AK, Wagh VM, Muley AA, Umrikar BN, Sankhua RN (2019) Prediction of water quality index using artificial neural network and multiple linear regression modelling approach in Shivganga River basin, India. Model Earth Syst Environ 5(3):951–962
10. Matta G, Nayak A, Kumar A, Kumar P (2020) Water quality assessment using NSFWQI, OIP and multivariate techniques of Ganga River system, Uttarakhand, India. Appl Water Sci 10(9):1–12
11. Mukherjee D, Dora SL, Tiwary RK (2012) Evaluation of water quality index for drinking purposes in the case of Damodar River, Jharkhand and West Bengal Region, India. J Bioremediation Biodegrad 3(9)
12. Nayak JG, Patil LG, Patki VK (2020) Development of water quality index for Godavari River (India) based on fuzzy inference system. Groundw Sustain Dev 10:100350
13. Olasoji SO, Oyewole NO, Abiola B, Edokpayi JN (2019) Water quality assessment of surface and groundwater sources using a water quality index method: a case study of a peri-urban town in Southwest, Nigeria. Environments 6(2):23
14. Sadat MA, Guan Y, Zhang D, Shao G, Cheng X, Yang Y (2020) The associations between river health and water resources management lead to the assessment of river state. Ecol Ind 109:105814
15. Singh RK, Chaturvedi A, Kumari K (2019) Water-quality assessment of Damodar River and its tributaries and subtributaries in Dhanbad Coal mining areas of India based on WQI. Sustain Water Resour Manage 5(2):381–386
16. Singh R, Tiwari AK, Singh GS (2021) Managing riparian zones for river health improvement: an integrated approach. Landsc Ecol Eng 1–29
17. Tian Y, Jiang Y, Liu Q, Dong M, Xu D, Liu Y, Xu X (2019) Using a water quality index to assess the water quality of the upper and middle streams of the Luanhe River, northern China. Sci Total Environ 667:142–151
18. Tripathi M, Singal SK (2019) Use of Principal Component Analysis for parameter selection for development of a novel water quality index: a case study of river Ganga India. Ecol Ind 96:430–436
19. Ustaoğlu F, Tepe Y, Taş B (2020) Assessment of stream quality and health risk in a subtropical Turkey river system: a combined approach using statistical analysis and water quality index. Ecol Ind 113:105815

20. Verma RK, Murthy S, Tiwary RK, Verma S (2019) Development of simplified WQIs for assessment of spatial and temporal variations of surface water quality in upper Damodar river basin, Eastern India. Appl Water Sci 9(21):27–40
21. Wu Z, Wang X, Chen Y, Cai Y, Deng J (2018) Assessing river water quality using water quality index in Lake Taihu Basin, China. Sci Total Environ 612:914–922
22. Yadav NS, Kumar A, Mishra S, Singhal S (2018) Assessment of water quality using pollution-index in the study stretch of river Chambal, India. Integr Res Adv 5(1):20–25
23. Zhang Q, Yu R, Jin Y, Zhang Z, Liu X, Xue H, Hao Y, Wang L (2019) Temporal and spatial variation trends in water quality based on the WPI index in the shallow lake of an arid area: a case study of lake Ulansuhai, China. Water 11(7):1410

Assessment of Air Quality with Respect to Particulate Matter (PM_{10}, $PM_{2.5}$) in Mining Industrial Areas of Keonjhar District, Odisha, and Its Public Health Implications

Soumyak Palei, Sreetama Das, Rajasree Sarkar, Amrita Chaudhuri, Subhankar Dutta, and Sumanta Nayek

Abstract The incidence of air pollution in industrial and mining areas is a common observed phenomenon worldwide. The detrimental effect of atmospheric pollution specifically PM_{10}, $PM_{2.5}$ on the health of native population is a major concerning area required to be assessed under serious notion. In this context, this research study has aimed to carry out an assessment of air quality and simultaneously, the resulting impacts on public health of the interviewed local residents from 10 selected sites within the Joda-Barbil mining industrial areas of the Keonjhor district, Odisha, India. The air quality measurement and field study had conducted during 2018–19. The large scale of excavation due to mining operations has led to a substantial volume of particulate matter (PM_{10}, $PM_{2.5}$) discharge in the atmosphere, which ultimately leads to a decline in air quality and causing health problems among local residents. As per the obtained results, the air quality is within the recommended standard in monsoon, however, it exceeds the recommended standards during the pre-monsoon and post-monsoon seasons respectively. The study also reveals that large number of interviewed people had suffered from various diseases including Asthma, Tuberculosis Bacillus, Pneumoconiosis, etc. mainly because of air pollution. Therefore, appropriate implementation of air pollution curbing policies, usage of modern environment-friendly technologies, may prove to be effective to mitigate the problem in the region.

S. Palei · R. Sarkar · S. Nayek (✉)
Department of Environmental Science, AIES, Amity University Kolkata, Kolkata, West Bengal, India
e-mail: sumanta.nayek@gmail.com

S. Das
Department of Geography, AISS, Amity University Kolkata, Kolkata, West Bengal, India

A. Chaudhuri
Department of Geography, Hiralal Mazumder Memorial College for Women, Dakshineswar, Kolkata, West Bengal, India

S. Dutta
Amity Research Center, Amity University Kolkata, Kolkata, West Bengal, India

© The Author(s), under exclusive license to Springer Nature Singapore Pte Ltd. 2023

S. Kumar et al. (eds.), *Sustainable Environmental Engineering and Sciences*,
Lecture Notes in Civil Engineering 323, https://doi.org/10.1007/978-981-99-0823-3_9

Keywords Air quality · Particulate matter (PM10 · PM2.5) · Seasonal variation · Mining industrial activity · Health risk

1 Introduction

The occurrence of air pollution due to industrial and mining activities is a growing concern worldwide, especially in developing countries. The impact of open-cast mining activities has actually possessed long term and serious consequence as it leads to negative impacts on air quality, which badly affect the local ecological conditions and at the same time threaten the sustainability of local livelihood structures [1]. The major contributors of air pollution, which is found in ongoing mining areas, are excavation, drilling, blasting, fire, exposed materials, transportation, exhaustion from earthmoving equipment etc. All such factors have caused decline in air quality, and subsequently creating health problems among local people not only within the mining regions but also in the surrounding locations [2, 3].

This research study is focusing on the assessment of air quality, and its impacts on the public health due to industrial and mining operations. The study area is located at the Joda-Barbil mining industrial areas of the Keonjhor district, Odisha (Keonjhar), India. (Fig. 1). For the purpose of carrying out research work, 10 sites such as Soyabali, Thakurani, Barbil, Bhadrasahi, Serenda, Joda, Banspani, Khuntpani, Khandbandh, and Kasia were selected for the data collection. In this study, collection of data has been done for the suspended and respirable particulate matter i.e., PM_{10} and $PM_{2.5}$. The study reveals the seasonal variation for the locations selected. Three seasons were taken into consideration for the variation study including pre-monsoon, monsoon, and post-monsoon.

In terms of geographic features, Keonjhar district is situated in the northern part of Odisha. Being considered a small and landlocked district, Keonjhar has recorded an area of 8303 km^2. It lies between 21° 1′ N to 22° 10′ N latitude and 85° 11′ E to 86° 22′ E longitude. Furthermore, Keonjhar district is surrounded by several localities such as Singhbhum district of Jharkhand in the North, Mayurbhanj and Bhadrak in the East, Jajpur in the South, and Dhenkanal and Sundargarh in the West [4].

From the viewpoint of mineral availability, Keonjhar district has an abundant quantity of manganese and chromite deposits. Moreover, Keonjhar contributes approximately over 80% of the total manganese production in Odisha. The manganese mines are located at Banspani, Barbil, and Barjamda while the chromite mines are situated at Baula, Nuasahi, and Phulinjhorhuli. In this study, two areas Joda and Barbil are located at planned industrial cities and municipalities in the Keonjhar district. As the Joda area is having large-scale enriched iron and manganese ore deposits, therefore, it is considered a prime revenue zone. Barbil and its surrounding regions are recognized as the world's largest deposits of iron and manganese ore, which contributes to significant revenue generation for both central and state government. Besides excavation at mining sites, the process of land clearing, removal

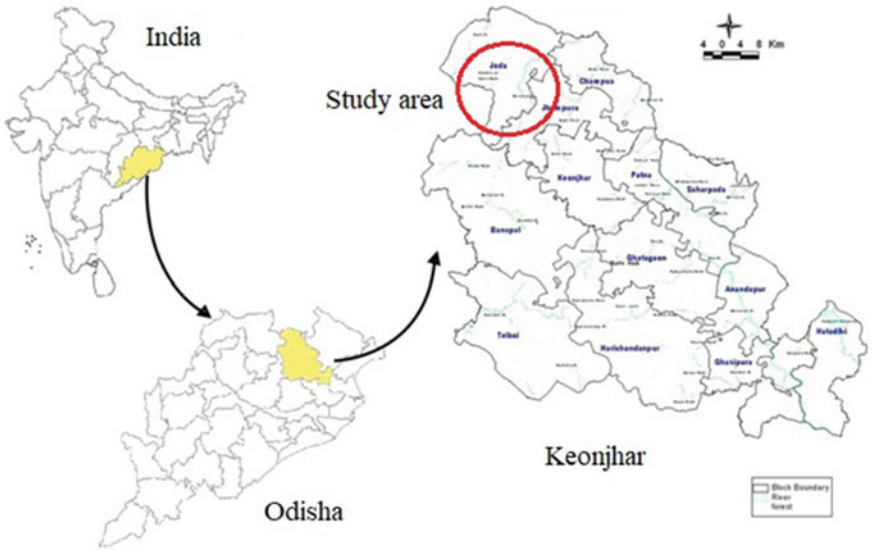

Fig. 1 Geographical set-up of study location

of overburden, and bulk transportation are the major contributors of atmospheric particulate matter (PM_{10}, $PM_{2.5}$) in the region [5].

As a result of mining operations and establishment of industries in the region, a significant proportion of air pollution has been generating over the years. The coarse particles (PM_{10}) near mining areas are majorly originated due to crushing, grinding and abrasion of surfaces, re–suspension of dust [6]. Subsequently, higher abundance of coarse particles was found in the mining area. Besides, fine ($PM_{2.5}$) and ultra-fine particles (PM1.0) are originated through chemical reactions such as nucleation, condensation, evaporation of fog, and cloud droplets. Combustion of coal and active mine fires are considered to be the prime sources for ultrafine and fine particles [7]. In this study, the air quality measurement and field study had conducted during 2018–19. The considerable amount of excavation because of mining operations has led to a large volume of PM_{10}, $PM_{2.5}$ discharges, which eventually leads to diminish in air quality and causing health problems among local people. Finally, the study aims to highlight the air quality evaluation particularly with respect to PM_{10}, $PM_{2.5}$ concentrations in the Joda-Barbil mining industrial areas of the Keonjhor district, seasonal variability of PM_{10}, $PM_{2.5}$ in various sampling sites within the study area, and impact of mining related diseases (mainly air pollution centric) on local people with possible health hazards.

2 Objectives

The present study is aiming to focus on (i) air quality evaluation with respect to PM_{10}, $PM_{2.5}$ concentrations in the Joda-Barbil mining industrial areas of the Keonjhor district, (ii) seasonal variability of PM_{10}, $PM_{2.5}$ in various sampling sites within the study area, and (iii) impact of mining-related diseases (mainly air pollution centric) on local residents with potential health hazards.

3 Methodology

For the purpose of air quality assessment, 10 different sampling sites were strategically selected which represents the characteristics of the entire study region. The concentrations of PM_{10}, $PM_{2.5}$ in the air were measured in a High volume sampler (HVAS: TSP) using glass fiber ambient (GF = A) filter paper during 2018–19 throughout the annual cycle covering all three seasons. The sample collection and analysis were performed as per the Indian standard method for measuring air pollution (IS 5182) [8]. The implication of air pollution on existing population was analyzed by conducting a field survey. The collected field dataset was statistically standardized, and mean values (along with standard deviations) were represented in tabular form (Table 1). The conventional graphical method was also used to represent the analyzed results (Fig. 2). From public health-related primary survey, the field data was collected by interviewing 100 local residents selected randomly (irrespective of age, gender, education, economic background) from 10 different sampling sites (Table 2).

4 Result and Discussion

4.1 Air Quality Assessment with Respect to PM_{10} and $PM_{2.5}$ Concentrations in the Study Area

The measured values of PM_{10} and $PM_{2.5}$ showed notable seasonal variations. In pre-monsoon season, mean values of PM_{10} were in the range of 102.12–61.69 μm; and the results for $PM_{2.5}$ ranges from 47.74 μm to 28.15 μm, indicating the higher level of particulate matter in the study area. Sampling site Kandbandh was registered the highest concentrations for PM_{10} (105.78–98.77 μm) among the sampling sites selected for the study; while the maximum values for $PM_{2.5}$ were recorded at Bhadrasahi (55.89–40.64 μm, exceeding the permissible limit as per the NAAQ standards (Table 1). Among the sampling station, Saranda execute the maximum deviation (SD = 26.98 μm) in PM_{10} concentration during pre-monsoon season. While maximum standard deviations in $PM_{2.5}$ concentration (8.20 μm) is recorded

Table 1 Measured values for PM_{10} and $PM_{2.5}$ at various sampling stations in the study area

Sampling sites	Pre monsoon		Monsoon		Post monsoon	
	PM_{10}	$PM_{2.5}$	PM_{10}	$PM_{2.5}$	PM_{10}	$PM_{2.5}$
Soyabali	98.00 ± 3.46	36.26 ± 8.20	42.07 ± 2.87	37.38 ± 9.84	84.12 ± 18.81	37.95 ± 7.41
Thakurani	56.70 ± 4.92	38.42 ± 7.15	55.79 ± 3.61	40.35 ± 8.94	82.13 ± 15.96	41.32 ± 6.48
Barbil	82.73 ± 19.79	42.13 ± 2.15	45.33 ± 6.30	42.42 ± 2.97	85.95 ± 16.23	42.57 ± 5.87
Bhadrasahi	81.90 ± 16.56	46.00 ± 6.19	51.21 ± 2.89	47.51 ± 7.74	68.40 ± 29.82	48.27 ± 6.09
Serenda	87.69 ± 26.98	31.90 ± 2.74	39.22 ± 3.75	32.03 ± 3.02	58.44 ± 28.54	32.09 ± 1.79
Joda	75.20 ± 13.22	43.75 ± 5.28	55.82 ± 3.53	44.23 ± 5.24	94.02 ± 13.18	44.47 ± 2.49
Banspani	93.91 ± 6.62	41.59 ± 7.09	47.19 ± 1.50	42.23 ± 8.70	101.89 ± 1.80	42.55 ± 3.79
Khuntpani	73.88 ± 7.56	41.52 ± 5.86	40.50 ± 3.09	42.33 ± 7.87	77.24 ± 5.04	42.74 ± 1.03
Khandbandh	102.17 ± 3.02	32.96 ± 4.96	50.08 ± 1.44	33.34 ± 6.22	100.06 ± 3.01	33.53 ± 4.84
Kasia	61.69 ± 18.23	43.45 ± 7.89	41.05 ± 2.52	43.95 ± 9.10	69.01 ± 13.69	44.20 ± 7.94

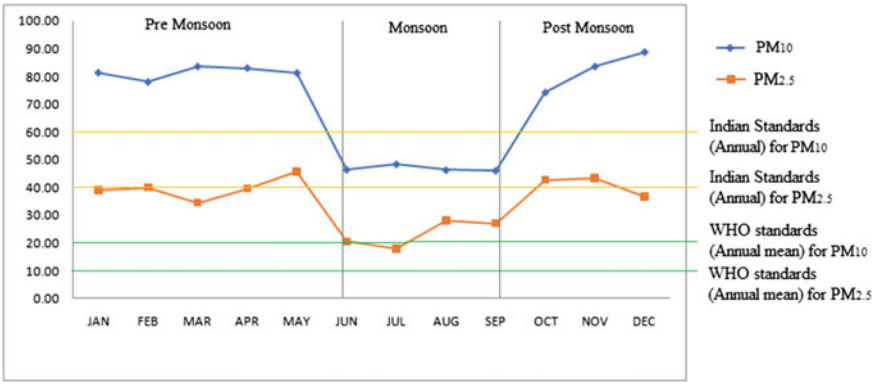

Fig. 2 Variations in PM10 and $PM_{2.5}$ level throughout the season and its comparison with recommended Indian standard (NAAQS) and WHO standards [10]

Table 2 Survey results based on selected socio-economic and public health-related variables of existing population in the study area

Selected variables	Category	% of 100
Gender Male: 52 Female: 48	Male versus female	04
Age	<40 years 40–59 years >60 years	50 41 09
Education	Primary Secondary High school Graduate Postgraduate Literate Illiterate	05 13 29 28 16 91 09
Household income per month	<5000 5000–10,000 >10.000	30 35 34
Occupation	Directly related to mining activity Transport service Farmer Others	70 14 09 07
Treatment facility available	Private hospital and related other facilities Government hospital Primary health center	64 26 10

(continued)

Table 2 (continued)

Died in mining hazards	Yes versus no	−62
Young generation willing to migrate or not	Yes versus no	−60
Suffering from mining related diseases	Asthma Tuberculosis bacillus Pneumoconiosis Hearing loss Silicosis Cancer No	21 15 13 09 04 04 34
Awareness about bad effects of industries, mining, and diseases	Yes versus no	44

for Soyabali. The pre-monsoon period (i.e., January–May) is considered as the dry months with sharp increase in temperature during April–May, which may act as the provoking factor for increase in the level of particulate matter (Fig. 2). This observation is very much consistent with the earlier investigation [1].

The monsoon data which includes results of June to September reveal a distinctive decline in the concentration of PM_{10} and $PM_{2.5}$ in all the sampling stations (Table 1). The highest recorded values for PM_{10} and $PM_{2.5}$ were noted at Thakurani and Khandbandh respectively. The obtained results in the monsoon season are very close to the prescribed standard for $PM_{2.5}$. The similar type of observation was also reported by Jayamurugan et al. [9]. The decline in the concentration of particulate matter can be attributed to atmospheric precipitation, which results settling of suspended particulate matter.

The post-monsoon season, which includes September to December, naturally records low-temperature range. The results (Table 1) exhibit that sampling site Banspari was having the highest level of PM_{10} (103.69 μm), while the maximum concentration for $PM_{2.5}$ was recorded at Barbil (59.37 μm). The maximum standard deviation found for $PM_{2.5}$ was 13.55 for Bhadrasahi. The observation of post-monsoon data suggests that during September i.e., immediately after the monsoon the level of particulate matter is comparatively low. While from October onwards the concentrations of particulate matter (both PM_{10} and $PM_{2.5}$) exhibit an increasing trend, which reached to the pick level during the winter season (November–December). This situation can be explained due to the variation in the meteorological conditions such as low temperature, high wind velocity, and higher humidity [10]. The results and findings of the present study are significantly relevant to all the findings for different seasons with the National Ambient Air Quality Standard (NAAQS) for India [11] with respect to the annual average Air Quality Standards of any other industrial zone.

The mean concentration of particulate matter (specifically PM10) is noticeably higher than the air quality standards for India [11] and WHO recommended standards [12] (except monsoon season). This will not only deteriorate the air quality of the

region, but also the dispersion of pollutants may cause chronic health problems on existing and surrounding population exposed directly or indirectly to the polluted conditions.

4.2 Impact of Mining and Industries (Specifically Air Pollution Centric) on Existing Population and Related Public Health Hazards

Mining and industrial activities are considered to have a strong influence on the economic wealth of the area and on social life [13]. In this research study, the targeted population comprises of all those people who experience the negative impact of mining activities. In this context, 10 sampling stations were strategically selected for carrying out the survey, and total 100 individuals were interviewed of the local population within the study area. Some important variables have selected to measure the impact of mining-related diseases (mainly air pollution centric) on public health, and these are reflected in the table (Table 2). From the observed responses related to the first variable 'Gender', it has been found that the study area has more concentration to the male contingent compared to their female counterpart as the percentage difference between male and female types of gender is recorded as 4. The second variable 'Age' highlights that 91% of surveyed people are aged below 60 years, which means that the study area has comprised of a large section of working-class population. The next variable 'Education' reveals that 91% of the interviewed population is literate. Among them, 29% people have cleared the high school standard and 28% people have passed as graduate. Also, 16% people are post graduate. It reflects that education level is more than satisfactory in the region and the educated people may have a high chance of probability to concern with the environmental crises prevailing in the area. The responses under the 'Household income per month' variable show that 69% of surveyed people have earned at least INR 5000 to more than INR 10,000 per month, signifying that the study area is consisted of low to middle-income group population. In terms of 'Occupation' variable, 70% people have directly associated with mining activity and 14% population has related to transport service activities. Apart from 9% agricultural workers and 7% other type of occupational jobs, most of the working people are engaged in the mining industry for their livelihood. The following variable 'Treatment facility available' shows that 64% people can afford private hospital and related other facilities, while 26% people depend on government hospital, and rest 10% people rely on primary health center for their respective medical treatments. Such result signifies that most of the surveyed people have access to accomplish the better healthcare facilities. The next variable depicts that the mortality rate is moderate due to mining hazards. In the survey response, 62% people's family member did not face death because of mining hazards. The following variable 'Young generation willing to migrate or not' highlights that 60% of the

surveyed working population do not favor to migrate to other places for employment opportunities, that means they are satisfied with their existing job facilities and believing the chance of getting promoted in future within the study area. After that, the variable 'Suffering from mining related diseases' reveals that a large section of the working population, i.e., 66% people in the mining area has been suffering from various diseases including Asthma (21%), Tuberculosis Bacillus (15%), Pneumoconiosis (13%), Hearing loss (9%), Silicosis (4%), and Cancer (4%). Such result projects that the mining workers are highly prone to life-threatening diseases and in many cases, they succumb to death because of the severe nature of the diseases. Finally, the variable 'Awareness about bad effects of industries, mining and diseases' discloses that 44% respondents in the study area are aware of all dreadful effects related to socio-economic and environmental perspectives. Hence, in a nutshell, the overall observation of the socio-economic status of the monitored areas highlights that most of the people are educated and they are aware of the prevailing environmental problems in the region. Moreover, the mining workers are more vulnerable to experience multifarious deadly diseases and subsequently, the mortality rate is moderate among them.

5 Conclusion

In this research study, the excavation of mining activities was considered as one of the prime factors for air pollution. Subsequently, harmful particulate matter emissions from industrial operations had led to a significant rise of air pollution in the study locations. While carrying out the assessment of air quality in 10 selected sampling stations, it had been observed that the air pollution level was recorded significantly high compared to the recommended standard limit for PM_{10} and $PM_{2.5}$ throughout the observation period, except monsoon season. Contrastingly, during monsoon season, the air pollution was registered under the permissible standard in all 10 selected study locations. As the average quality of air was recorded higher than the standard level in the study regions, the air pollution had badly impacted on the public health of the local people. Consequently, a large number of the population had suffered from various diseases such as Asthma, Pneumoconiosis, etc. Despite suffering from such deadly ailments, most of the young working people were unwilling to migrate from the study regions. Apart from that, a large section of people had possessed deep awareness about the bad effects of living in the industrial areas, incidence of air pollution due to mining activities, and subsequent health diseases of the same. In the backdrop of such research findings, the proper use of advanced mining technology and implementation of effective measures to reduce the discharge of particulate matter can improve the level of air quality as well as a public health condition in the study areas. Therefore, appropriate execution of air pollution curbing policies, usage of modern environment-friendly technologies in industrial and mining operations and taking up necessary precautions from getting ill due to mining-related diseases may consider the requisite steps for future.

Acknowledgements The authors wish to thank Amity University Kolkata for its support through infrastructures to conduct this research work.

References

1. Mishra N, Das N (2017) Coal mining and local environment: a study in Talcher coalfield of India. Air, Soil Water Res 10:1–12
2. Ghose MK, Majee SR (2000) Assessment of the impact on the air environment due to opencast coal mining—an Indian case study. Atmos Environ 34:2791–2796
3. Pandey B, Agrawal M, Singh S (2014) Assessment of air pollution around coal mining area: emphasizing on spatial distributions, seasonal variations and heavy metals, using cluster and principal component analysis. Atmos Pollut Res 5:79–86
4. Senapati N, Sahu NK (1966) Orissa District Gazetteers: Kendujhar. Gazetteer of India. Superintendent, Orissa Government Press, p 2
5. Dash SK, Dash AK (2015) Determination of Air Quality Index status near Bileipada, Joda area of Keonjhar, Odisha, India. Indian J Sci Technol 8(35):1–7
6. Cole CF, Zapert JG (1995) Air quality dispersion model validation at three stone quarries. National Stone Association, Washington, D.C., p 14884
7 Wilson WE, Suh HH (1997) Fine particles and coarse particles: concentration relationships relevant to epidemiologic studies. J Air Waste Manag Assoc 47:1238–1249
8. IS: 5182 (2006) Indian standards: method of measurement of air pollution: Guidelines for planning the sampling for atmosphere
9. Jayamurugan R, Kumaravel B, Palanivelraja S, Chockalingam MP (2013) Influence of temperature, relative humidity and seasonal variability on ambient air quality in a coastal urban area. Int J Atmos Sci 1–7
10. Ahmed A, Taani A, Howari FM, Nazzal Y, Yousef A (2018) Seasonal impact to air qualities in industrial areas of the Arabian Gulf Region. Environ Eng Res 23(2):143–149
11. National Ambient Air Quality Standards, Central Pollution Control Board Notification (2009) http://www.cpcb.nic.in/upload/Latest/Latest_48_FINAL_AIR_STANDARD.pdf in the Gazette of India, Extraordinary, New Delhi
12. WHO (2006) Air Quality Guidelines for particulate matter, ozone, nitrogen dioxide and sulfur dioxide. Global update 2005. Summary of risk assessment. World Health Organization
13. Zobrist J, Sima M, Dogaru D, Senila M, Yang H, Popescu C, Roman C, Bela A, Frei L, Dold B, Balteanu D (2009) Environmental and socioeconomic assessment of impacts by mining activities—a case study in the Certej River catchment, Western Carpathians, Romania. Environ Sci Pollut Res 16:14–26

Development of Nutrient Stocks and Soil Properties of Restored Solid Waste Dump After 5 Years of Afforestation with Guava Fruit Orchard

Sneha Bandyopadhyay and Subodh Kumar Maiti

Abstract The disposal of industrial solid wastes damages the terrestrial ecosystem due to the complete removal of vegetation cover, deterioration in soil quality and loss of soil nutrients. Therefore, the restoration of waste dumps is mandatory with forestry development especially with fruit orchard to make it self-sustainable. The present study assessed chronological variation in soil properties and nutrient stock from two profile depths (0–10 and 10–20 cm) in restored waste dump (RWD) of an integrated sponge iron unit, Chhattisgarh, India. With reclamation age, soil characteristics such as organic carbon (SOC), moisture content, nutrient content, organic matter, bulk density, soil fraction (<2 mm) improved with afforestation age. The total stock ranged between 4.32–19.5 Mg C ha^{-1}, 1.11–2.29 Mg N ha^{-1} and 0.0005–0.0015 Mg P ha^{-1} in 0–20 cm profile depth and was significantly varied amongst the reclaimed chronosequence and natural forest sites. The surface layer (0–10 cm) showed more than half of the nutrient stocks among different profile sampling. Magnitude of variations in soil characteristics may be attributed to the development of guava orchard. After 5 years of afforestation with fruit orchard, SOC and nutrient stocks recovered by 80% compared to natural forest site which may help to endure nutrient cycle and serve as an indicator of the re-establishment of a self-sustainable ecosystem. The present study suggested the use of guava fruit orchard as a reclamation strategy for sponge iron waste dump with significant recovery of SOC and nutrient stock.

Keywords Solid waste dump · Restoration · Chronosequence · Nutrient stock · Guava fruit orchard

S. Bandyopadhyay (✉) · S. K. Maiti
Ecological Restoration Laboratory, Department of Environmental Science and Engineering, Indian Institute of Technology (Indian School of Mines), Dhanbad, Jharkhand 826004, India
e-mail: sneharupayan@rediffmail.com

© The Author(s), under exclusive license to Springer Nature Singapore Pte Ltd. 2023

S. Kumar et al. (eds.), *Sustainable Environmental Engineering and Sciences*,
Lecture Notes in Civil Engineering 323, https://doi.org/10.1007/978-981-99-0823-3_10

1 Introduction

Globally, degradation of natural ecosystems due to the human-induced land-use change and destruction of terrestrial habitat has become significant environmental issue resulting in loss of biodiversity, deterioration of nutrient stock and land degradation. With rapid civilization, generation of industrial solid wastes is increasing exponentially as one of the eminent by-products of urbanisation. Terrestrial ecosystems are extensively damaged with the disposal of industrial solid waste resulting in deterioration in soil health, soil nutrient stock and aesthetic value of landscape. The suitable management practices of waste dumps are not only an ethical requirement to improve environmental quality, but also important for ecosystem stability. Therefore, reclamation of wastelands with vegetation succession has gained global importance to make it self-sustainable ecosystem. Due to the unfavourable properties of solid wastes, natural recovery of waste dumps is slow. Nevertheless, effective restoration practices such as forestry or selective plantation with fruit orchard that sequesters atmospheric CO_2 and improves nutrient stocks, could be one of the viable options to some extent [10].

Forestry is known to be one of the cost-effective and eco-friendly reclamation approaches to reestablish soil health and nutrient cycle, to ameliorate climatic condition and to support ecosystem succession [22]. Though, different tree species has its unique growth characteristics that regulate its nutrient enriching and stabilising capacity, fruit orchard may also be an alternative that can provide permanent vegetation cover on waste dump sites with little or no aftercare. In present study, *Psidium gujava* (guava) orchard was selected due to its (i) capability to grow in both silty or sandy soil texture, (ii) tolerance of alkaline pH, (iii) draught resistance properties, and (iv) ability to survive in adverse circumstances [1].

In forest ecosystem, the equilibrium between soil organic carbon (SOC) and nutrient cycling is represented by their stocks. For the development of restored ecosystem, the prime prerequisites are the availability of nutrients and SOC content. Though in waste land, the inflow of soil nutrients (N, P, K) and SOC are very less compared to agricultural or natural forest land. The majority of previous studies have focused on the changes in SOC and nutrient dynamics under agriculture, forest, grassland, and reclaimed mine soil and its role in global climate crisis [12, 19, 20, 25].

India has emerged as the world's leading producer of DRI (Direct Reduced Iron or sponge iron) since 2003, accounting for more than 27 million metric tonnes at the end of the year 2019. The hazardous solid wastes such as dolochar, slag, flyash generated from coal-based sponge iron industry are generally alkaline in nature and rich in toxic metals. In present study, restoration of 40–60 m high solid waste dump of sponge iron industry with steep slope is a challenging task in consideration to the recovery of pedospheric environment. Due to scarcity of space (space between dump edge and nearby forest reserve was hardly kept 5–7 m), sequence of restoration strategies was undertaken without benching of slope before the establishment of vegetation cover. The strategies included (i) labelling and regrading of dump, (ii) blanketing with good quality topsoil excavated from the forest area (substratum for vegetation growth),

(iii) blanketing the dump slope with coir-mat (surface stabilization), (iv) seeding of grass-legume mixture on slope (conditioning for revegetation), (v) construction of drainage, (vi) arrangements of watering during dry season, (vii) plantation of guava fruit orchard, and (vii) maintenance of the site.

2 Literature Review

Previous studies of reclamation of integrated sponge iron solid waste dumps often involved vegetation succession, mycorrhizal diversity, impact of revegetation in a chronosequence manner [13, 14]. Several researchers have reported the practice of fruit tree species such as *Artocarpus heterophyllus* (jackfruit), *Mangifera indica* (Mango), *Phyllanthus emblica* (amla), *Anacardium occidentale* (cashew), *Olea europaea* (olive) during reclamation of waste dumps to make it self-sustainable [18, 24]. But there are no such studies have reported the development and recovery of soil carbon and nutrient stocks of chronologically restored industrial solid waste dumps.

3 Objective

This present study is based upon the hypothesis that recovery of soil quality, carbon, and nutrient stock in a restored solid waste dump (RWD) depend on nature of substrate, afforestation age, types of vegetation species used for reclamation. The aims of present study were to (i) evaluate the variations and vertical distribution of soil characteristics chronosequence restored waste dump sites, (ii) estimate SOC and nutrient (N, P) stock of restored sites, and (iii) determine the recovery of SOC and nutrient stock in RWD compared to reference forest sites.

4 Methodology

4.1 Study Area

Solid waste dump of an integrated sponge iron unit (Chhattishgarh, India) was selected for the present study which lies between 22°00′–22°02′ N and 83°22′–83°23′ E, and covers an area of approximately 7 ha (Fig. 1). The restoration of the same site initiated in the year 2012, and the topsoil (used as blanketing material from undisturbed nearby forest) characteristics was monitored in 2012 by one of the authors [16]. The study site comprised of dry tropical climate with three distinctive

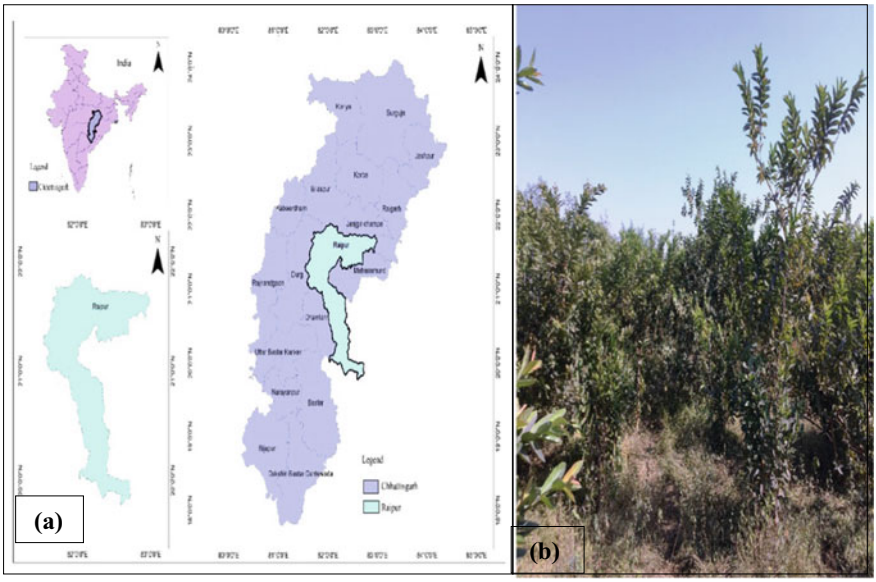

Fig. 1 **a** Location map of study area (Industrial solid waste dump, Chhattisgarh, India); **b** Restored waste dump after 5- years of afforestation with guava fruit orchard

seasons i.e. winter (December–February), summer (April–June), and monsoon (July–September). The temperature variation in summer and winter is within 30–49 °C and 8–25 °C respectively.

4.2 Soil Sampling

During winter season (December, 2017), soil samples were collected through the given sampling design: Ten 10 × 10 m quadrates were placed in restored waste dump. From each quadrate 5 composite soil samples (four from corners and one from centre) were collected by coning quartering method [17] from a vertical distribution of profile depth of 0–10 cm and 10–20 cm near rhizosphere of guava tree. The collected samples, sealed in plastic zipper bag, were brought to the laboratory. A total 100 soil samples (10 quadrate × 5 composite samples from restored waste dump and forest site as control [CS]) were collected.

Table 1 Standard protocol for physicochemical analysis of soil samples

Soil characteristics	Analytical procedure	Apparatus	References
Fine earth fraction	Sieving method	2 mm sieve	Maiti [17]
Moisture content	Gravimetric method	Hot air oven	Dakshinamurthi and Gupta [7]
Water holding capacity	–	Keen box	Maiti [17]
pH_{H2O} (1:2.5 w/v)	Soil: water suspension	pH metre	Thomas [27]
Soil organic matter	Loss on ignition method	Muffle furnace	Maiti [17]
Bulk density	Sieving method	2 mm sieve	Maiti [17]
Organic carbon	Rapid dichromate oxidation method	–	Walkley and Black [28]
Available nitrogen	Alkaline potassium permanganate method	Kjeldahl assembly	Subbiah and Asija [26]
Total nitrogen	Kjeldahl method	Kjeldahl assembly	Jackson [11]
Available phosphorus	Acidic soils—Bray's method and Neutral and alkaline soils—Olsen's method	UV–Visible spectrophotometer	Bray and Kurtz [5], Watanabe and Olsen (1965)
Cation exchange capacity	Na saturation method	Flame photometer	Jackson [11]

4.3 Soil Analysis

All soil samples were air-dried at laboratory room temperature (20–25 °C), then gently crushed by using a porcelain made mortar and pestle (500 cc capacity), and sieved (<2 mm; mesh size 8) for the determination of soil physicochemical properties. The physicochemical properties of soil samples were analysed as per standard protocols mentioned in Table 1.

4.4 Determination of SOC and Nutrient Stock

The temporal changes in SOC and nutrient (N, P) stocks were evaluated by estimating SOC and nutrient concentration along revegetation age. SOC, nutrient concentrations, corrected bulk density (BD_c), and soil profile thickness (T) were used to assess the soil stock [6]. The quantification of BD_c was necessary because the occurrence of a high coarse fraction in mine soils interferes with stock measurements. The latter is determined in the following manner:

$$\begin{aligned} &\mathrm{BDc}\left(\mathrm{Mgm}^{-3}\right) \\ &= \left[\text{Weight of soil sample(Mg)} \times \text{fine earth fraction(\%)}\right] / \left[\text{Volume of soil corer}\left(\mathrm{m}^3\right) \times 100\right] \end{aligned} \tag{1}$$

The SOC and nutrient stocks of the chronosequence restored waste dump sites were determined as follows from the respective SOC and nutrient concentrations, corrected bulk density, soil fraction and soil profile thickness:

$$\text{SOC stock}\left(\text{Mg ha}^{-1}\right) = \left[\text{SOC}(\%) \times \text{BDc} \times \text{T(m)} \times 10^4\left(\text{m}^2\text{ha}^{-1}\right)\right]/100 \quad (2)$$

$$\text{TN stock}\left(\text{Mg ha}^{-1}\right) = \left[\text{TN}(\%) \times \text{BDc} \times \text{T(m)} \times 10^4\left(\text{m}^2\text{ha}^{-1}\right)\right]/100 \quad (3)$$

$$\text{P stock}\left(\text{Mg ha}^{-1}\right) = \left[\text{P}(\%) \times \text{BDc} \times \text{T(m)} \times 10^4\left(\text{m}^2\text{ha}^{-1}\right)\right]/100 \quad (4)$$

4.5 Statistical Analysis

Multivariate statistical analysis (mean, range, standard deviation) was carried out for physicochemical properties of soil. Homoscedasticity and normality of datasets were checked with the help of Levene's test and Shapiro–Wilk test respectively. Significant difference between mean values of normally distributed data was calculated using ANOVA with Duncan's Multiple Range Test (DMRT) as a part of post-hoc study at the $p < 0.05$. All the statistical analysis was done by using SPSS 21.0 (IBM SPSS Inc., Chicago, USA).

5 Result and Discussion

5.1 Recuperation of Soil Properties

The vertical distribution of soil properties of chronosequence restored waste dump (RWD) and reference forest was shown in Table 2 and Fig. 2. Afforestation of solid waste dump with fruit orchard (*Psidium guajava*) enhanced the soil properties since it improved the soil fraction, WHC, SOC, and nutrient stocks. Amelioration of soil properties with the revegetation age (1–5 years) acts as an indicator of ecosystem recovery. After 5 years of afforestation, the 14% increase in the soil fraction could be due to vegetation development and weathering of rock fragments. The soil fraction (<2 mm) in the RWD (0–10 cm) increased from 68 to 78% along the chronosequence age and was highest at the reference forest site (82%). The changes in soil pH could be due to the presence of base cation, nature of rocks and plant growth [2, 15]. The significant improvement in the WHC_{max} (32–40%) could also attributed to the root growth in topsoil that also further regulated by SOM content and soil texture. Moisture content is an oscillating parameter driven by sampling time, height of dump, texture, organic carbon, stone content and thickness of litter layers on the

dump surface. Increased moisture at 5-year-old RWD may be the result of reduced stone content, increased OM, and soil structure [3]. Bulk density of the RWD varied from 1.16 to 1.74 Mg m^{-3} in surface soil layer (0–10 cm) and was of 0.75 Mg m^{-3} at the control site (undisturbed reference forest).

SOC percentage of RWD ranged from 0.4 to 1.74% along the chronosequence in the surface soil layer (0–10 cm) and 1.56% at the control site. During the early stages of waste dump restoration, SOC content rapidly increased and was maximum at 0–20 cm depth. In present study, SOC improved with revegetation age and was highest in RWD-5 (5-year-old reclaimed site) could be attributable to the aggregation of leaf litter biomass and its decomposition to humus. Plant available N concentration in surface layer (0–10 cm) increased from 50 to 134 mg kg^{-1} after 5 years of reclamation with fruit orchard and was 154 mg kg^{-1} at the control site. Lower concentration of available N in the WD- 2012 (initial age of restoration; RWD - 1) suggests that N is limiting initially due to the presence of very little organic matter. Plant available P concentration ranged from 0.40 to 0.93 mg kg^{-1} along the five years of forestry reclamation and found highest (4.30 mg kg^{-1}) in the control site. [17] This findings proposed that the variation in P content mainly depends on plant species, plantation age, spoil characteristics. The vertical distribution of soil physicochemical characteristics significantly varied ($p < 0.05$) between the two studied profile depths (0–10 cm, 10–20 cm). The surface layer (0–10 cm) showed more than 60% of the total nutrient stock at RWD.

5.2 SOC and Nutrient Stock

Soils consist of significant percentage of the nutrient stocks of terrestrial ecosystems. Due to the disposal of solid waste, nutrient stocks were drastically decreased, resulting in ecological destruction. As a result, soil preservation is critical in order to maintain nutrient cycling. Along the studied chronosequence, the SOC stock in RWD increased from 2.70 to 13.54 Mg ha^{-1} in the 0–10 cm depth and from 4.32 to 19.5 Mg ha^{-1} in the 0–20 cm depth. The current study estimates temporal variations in the SOC stock and found a 4.5-fold rise in the 0–20 cm depth from 4.32 to 19.5 Mg C ha^{-1} in 5 years, i.e. an increase of 3.89 Mg C ha^{-1} y^{-1}. At the reference forest site, the SOC stock was 12.83 Mg ha^{-1} in the 0–10 cm and 22.13 Mg ha^{-1} in the 0–20 cm of soil profile depth. Along the chronosequence in RWD, the surface layer (0–10 cm) showed 62–69% of the total SOC stock. The variations of nutrient stock between reclaimed sites of various ages may be due to plant growth and SOM material [9] (Table 3).

After 5 years of reclamation, the vertical distribution of the SOC stock showed that topsoil (0–10 cm) accounted for 62.5% of the total SOC stocks. This could be attributable to the presence of maximum root density and related microbial activity in the surface layer. The surface layer (0–10 cm) had a higher N stock (58%) than the deeper layers, suggesting that biomass accumulation and mineralization initiated primarily in topsoil [8]. After five years of afforestation, the total N stock in the

Table 2 Physical properties of soil samples (n = 10)

Parameter	Type of soil					
	RWD-1		RWD-5		Reference forest	
	0–10 cm	10–20 cm	0–10 cm	10–20 cm	0–10 cm	10–20 cm
pH (1:2.5H_2O)	5.17 ± 0.08b	4.96 ± 0.27c	6.10 ± 0.24a	5.91 ± 0.20a	5.97 ± 0.14a	5.64 ± 0.13b
MC	3.23 ± 0.43c	4.52 ± 0.89c	9.75 ± 0.16b	11.75 ± 0.48b	11.28 ± 0.83a	13.68 ± 0.54a
WHC_{max}	32.94 ± 2.32b	32.07 ± 3.07c	40 ± 2.54a	38.35 ± 2.25b	41.74 ± 3.38a	43.72 ± 4.45a
SOM	1.26 ± 0.07c	0.858 ± 0.10c	1.97 ± 0.18b	1.56 ± 0.11b	3.98 ± 0.15a	3.70 ± 0.30a
BD	1.74 ± 0.10a	2.193 ± 0.18a	1.16 ± 0.12b	1.48 ± 0.30b	0.75 ± 0.16c	1.17 ± 0.14c
FEF	68.42 ± 4.64b	60.88 ± 3.43c	78.17 ± 7.5a	72.19 ± 4.48b	82.21 ± 5.8a	80.67 ± 3.92a

Different alphabets in a row represents significant differences between a soil parameter of RWD-1, RWD-5 and Reference forest at $p < 0.05$

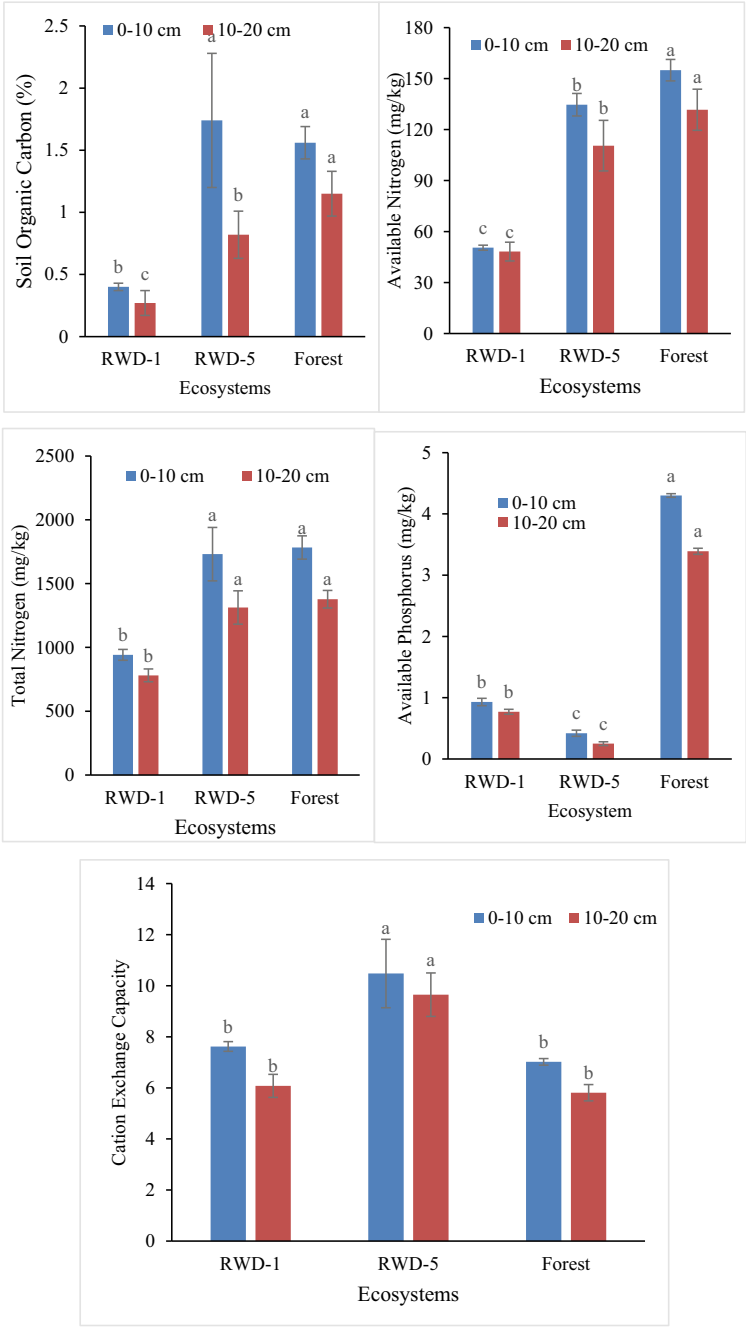

Fig. 2 Chemical properties of soil samples (n = 10)

Table 3 SOC and nutrient stock under reclaimed chronosequence and reference forest site

Stocks	RWD-1		RWD-5		Reference forest	
	0–10 cm	10–20 cm	0–10 cm	10–20 cm	0–10 cm	10–20 cm
SOC stock	2.70 ± 0.29	1.62 ± 0.65	13.54 ± 4.48	5.94 ± 1.66	12.83 ± 1.40	9.3 ± 1.61
TN stock	0.64 ± 0.06	0.47 ± 0.04	1.34 ± 0.12	0.95 ± 0.13	1.46 ± 0.12	1.11 ± 0.06
P stock	0.001 ± 0.00005	0.0005 ± 0.00004	0.0003 ± 0.0001	0.0002 ± 0.00003	0.004 ± 0.0003	0.003 ± 0.0001

RWD increased from 0.64 to 1.34 Mg ha^{-1} in the 0–10 cm depth and from 1.11 to 2.29 Mg ha^{-1} in the 0–20 cm profile depth. In the reference forest soil, the total N stock in 0–10 cm depth was 1.46 Mg ha^{-1}, and in the 0–20 cm depth, it was 2.57 Mg ha^{-1}. Along the chronosequence, the available P stock decreased from 0.001 to 0.0003 Mg ha^{-1} at 0–10 cm depth, and from 0.002 to 0.0005 Mg ha^{-1} at 0–20 cm depth. The available P stock in the 0–20 cm depth of the control soil was 0.007 Mg P ha^{-1}. The surface layer (0–10 cm) of the chronosequence sites stored 60–66% of the available P stock, which declined with soil profile depth.

5.3 SOC and Nutrient Stock Recovery

The recovery of nutrient and SOC stock in restored waste dump was assessed through nutrient stock comparison of the studied chronosequence with reference forest site. After five years of forestry reclamation with fruit orchard, SOC, N stocks recovered by 86.8%, 89% respectively. At initial stage of reclamation, recovery of nitrogen stock was higher (43%) than the SOC stock (19.5%). Recovery of available P stock was very slow reaching up to 7% after five years of reclamation in comparison to reference forest site. The estimation of soil nutrients and SOC as well as their recovery over time, can be used to evaluate reclamation success [4]. SOC and nutrients stocks recovery is significant in the degraded ecosystem since, it improves the soil fertility and encourages the species establishment. Furthermore, an increase in woody biomass and the SOM accumulation improves wasteland soil quality, allowing nutrient stocks to gradually recover [23]. The ability of *Psidium guajava* L. to reestablish nutrient cycling and increase nutrient stocks suggested that it is suitable for the reclamation of solid waste dump sites. Soil conditions, climate and species composition have a significant impact on C stock accretion in the RWD. Likewise, the accretion rate of SOC stock for a specific site corresponds to the site characteristics like soil fraction, texture, WHC, SOM, soil fertility, bulk density and types of vegetation species. The SOC stock increase accounted for yearly increase of 3.89 Mg C ha^{-1} y^{-1} in present study. According to the present study, it can be predicted that the SOC stock in the RWD could take up to 6 years to reach levels that comparable to the control site.

6 Conclusion

Hazardous solid waste produced by DRI plant must be cleaned up in a way that preserves environmental quality, reduces the risk of pollution, and allows the land to be economically viable after use. The study recommends afforestation using fruit orchard as a means of land reclamation to make it self-sustaining and to improve the local community by financial return. *Psidium guajava* (L.) acts a pivotal role in recovering soil fertility (SOC, N, P) as well as the soil physicochemical characteristics

through chronosequence reclamation. After 5 years of afforestation with guava fruit orchard, the nutrient stock recovery was of 89% for nitrogen, 86.8% for SOC and 7% for available P in comparison to control soil. In restored waste dump, the surface layer (0–10 cm) exhibits more than 60% of the total nutrient stock. Furthermore, in present study, the improvements of soil properties with reclamation age indicates the ecosystem recovery in waste dump. Therefore, it can be concluded that guava fruit orchard could be a sustainable alternative land-use approach towards waste dump restoration.

References

1. Adrian JAL, Arancon NQ, Mathews BW, Carpenter JR (2015) Mineral composition and soil-plant relationships for common guava (Psidium guajava L.) and yellow strawberry guava (Psidium cattleianum var. lucidum) Tree Parts and Fruits. Commun Soil Sci Plant Anal 46(15):1960–1979. https://doi.org/10.1080/00103624.2015.1069310
2. Bandyopadhyay S, Novo LA, Pietrzykowski M, Maiti SK (2020) Assessment of forest ecosystem development in coal mine degraded land by using integrated mine soil quality index (IMSQI): the evidence from India. Forests 11(12):1310. https://doi.org/10.3390/f11121310
3. Bandyopadhyay S, Rana V, Maiti SK (2018) Chronological variation of metals in reclaimed coal mine soil and tissues of eucalyptus hybrid tree after 25 years of reclamation, Jharia coal field (India). Bull Environ Contam Toxicol 101(5):604–610. https://doi.org/10.1007/s00128-018-2466-6
4. Banning NC, Grant CD, Jones DL, Murphy DV (2008) Recovery of soil organic matter, organic matter turnover and nitrogen cycling in a post-mining forest rehabilitation chronosequence. Soil Biol Biochem 40(8):2021–2031. https://doi.org/10.1016/j.soilbio.2008.04.010
5. Bray R, Kurtz LT (1966) Determination of total, organic and available forms of phosphorus in soil. Soil Sci 59:39–45
6. Chatterjee A, Lal R, Shrestha RK, Ussiri DAN (2009) Soil carbon pools of reclaimed minesoils under grass and forest landuses. Land Degrad Dev 20(3):300–307. https://doi.org/10.1002/ldr.916
7. Dakshinamurthi C, Gupta RP (1968) Practicals in soil physics. IARI, New Delhi
8. Ganjegunte GK, Wick AF, Stahl PD, Vance GF (2009) Accumulation and composition of total organic carbon in reclaimed coal mine lands. Land Degrad Dev 20(2):156–175. https://doi.org/10.1002/ldr.889
9. Grüneberg E, Ziche D, Wellbrock N (2014) Organic carbon stocks and sequestration rates of forest soils in Germany. Glob Change Biol 20(8):2644–2662. https://doi.org/10.1111/gcb.12558
10. IPCC, 2000. Intergovernmental Panel on Climate Change (2000) Land Use. Land Use Change and Forestry. Special report Cambridge Univ. Press, Cambridge, U.K.
11. Jackson ML (1973) Soil chemical analysis. Prentice Hall Pvt. Ltd., New Delhi
12. Kirsten M, Kaaya A, Klinger T, Feger KH (2016) Stocks of soil organic carbon in forest ecosystems of the Eastern Usambara Mountains, Tanzania. CATENA 137:651–659. https://doi.org/10.1016/j.catena.2014.12.027
13. Krishna RS, Mishra J, Meher S, Das SK, Mustakim SM, Singh SK (2020) Industrial solid waste management through sustainable green technology: case study insights from steel and mining industry in Keonjhar, India. Materials Today: Proc 33:5243–5249. https://doi.org/10.1016/j.matpr.2020.02.949
14. Kullu B, Behera N (2012) Status and diversity of vesicular arbuscular mycorrhiza in different age series sponge iron solid waste dumps with respect to reclamation. The Bioscan 7(3):539–542

15. Macdonald SE, Landhäusser SM, Skousen J, Franklin J, Frouz J, Hall S, Jacobs DF, Quideau S (2015) Forest restoration following surface mining disturbance: challenges and solutions. New For 46(5):703–732. https://doi.org/10.1007/s11056-015-9506-4
16. Maiti SK, Maiti D (2015) Ecological restoration of waste dumps by topsoil blanketing, coir-matting and seeding with grass–legume mixture. Ecol Eng 77:74–84. https://doi.org/10.1016/j.ecoleng.2015.01.003
17. Maiti SK (2013) Ecorestoration of the coal mine degraded lands. Springer, New York
18. Maiti SK, Kumar A, Ahirwal J (2016) Bioaccumulation of metals in timber and edible fruit trees growing on reclaimed coal mine overburden dumps. Int J Min Reclam Environ 30(3):231–244. https://doi.org/10.1080/17480930.2015.1038864
19. Mukhopadhyay S, Maiti SK (2014) Soil CO_2 flux in grassland, afforested land and reclaimed coalmine overburden dumps: a case study. Land Degrad Dev 25(3):216–227. https://doi.org/10.1002/ldr.1161
20. Mukhopadhyay S, Masto RE, Cerdà A, Ram LC (2016) Rhizosphere soil indicators for carbon sequestration in a reclaimed coal mine spoil. CATENA 141:100–108. https://doi.org/10.1016/j.catena.2016.02.023
21. Olsen SR, Sommers LE (1982) Phosphorus. In: Page AL et al (eds) Methods of soil analysis, Part 2, 2nd ed. ASA and SSSA, Madison, WI, pp 403–430
22. Patra DK, Pradhan C, Patra HK (2020) Toxic metal decontamination by phytoremediation approach: concept, challenges, opportunities and future perspectives. Environ Technol Innov 18:100672. https://doi.org/10.1016/j.eti.2020.100672
23. Paz CP, Goosem M, Bird M, Preece N, Goosem S, Fensham R, Laurance S (2016) Soil types influence predictions of soil carbon stock recovery in tropical secondary forests. For Ecol Manage 376:74–83. https://doi.org/10.1016/j.foreco.2016.06.007
24. Shaheen N, Irfan NM, Khan IN, Islam S, Islam MS, Ahmed MK (2016) Presence of heavy metals in fruits and vegetables: health risk implications in Bangladesh. Chemosphere 152:431–438. https://doi.org/10.1016/j.chemosphere.2016.02.060
25. Shrestha RK, Lal R (2010) Carbon and nitrogen pools in reclaimed land under forest and pasture ecosystems in Ohio, USA. Geoderma 157:196–205. https://doi.org/10.1016/j.geoderma.2010.04.013
26. Subbiah BV, Asija GL (1956) A rapid procedure for the estimation of available nitrogen in soils. Curr Sci 25(8):259–260
27. Thomas GW (1996) Soil pH and soil acidity. In: Sparks DL et al (eds) Methodsof soil analysis, Part 3. Chemical methods, SSSA Book Series No. 5. SSSA–ASA,Madison, WI, pp 475–490
28. Walkley A, Black IA (1934) An examination of the Degtjareff method for determining soil organic matter, and a proposed modification of the chromic acid titration method. Soil Sci 37(1):29–38. https://doi.org/10.1097/00010694-193401000-00003

Measurement of Noise Levels Inside and Outside Environment of Roadside Schools in Urban Area: A Case Study of Surat, India

Ramesh B. Ranpise and B. N. Tandel

Abstract Urban roads play a significant part in advancement of a particular city. The urban roads help to connect each part of the city very smoothly, but the noise from such urban roads create annoyance to the people in this area. The objective of this research work was to monitor and evaluate the noise levels prevailing in schools located near urban traffic streams. For this purpose, inside and outside campus noise measurements were done in 4 schools. In all measurements taken both outside and inside the campus of schools, the noise level was higher than the prescribed maximum noise levels by CPCB. Noise levels recorded outside the school premises were relatively high compared to inside the schoolyard. Results show that the school environment was noisy, and noise levels in these roadside schools were severe, exceeding the CPCB's noise levels. The schools located near the urban traffic flow are particularly exposed to noise coming from urban traffic and hence require urgent local and institutional policy intervention in the form of noise mitigation measures.

Keywords Noise levels · Silence zone · School · Urban road traffic noise

1 Introduction

Noise pollution may affect physiological health. It can cause sleep disturbances, hypertension, tinnitus, high stress levels, hearing loss, etc. [1]. Vulnerability to noise is a potential component of individuals' well-being and affects life quality [2]. In Surat city, several hospitals, schools, and colleges faces the main stream of traffic which are actually notified as silence zones. Also, the noise level in this area exceeds the permissible limit given by CPCB [3]. Road transportation is a major part in the development of traffic noise [4, 5].

R. B. Ranpise (✉) · B. N. Tandel
Department of Civil Engineering, S. V. National Institute of Technology, Surat, India
e-mail: d18ce017@ced.svnit.ac.in

B. N. Tandel
e-mail: bnt@ced.svnit.ac.in

© The Author(s), under exclusive license to Springer Nature Singapore Pte Ltd. 2023

S. Kumar et al. (eds.), *Sustainable Environmental Engineering and Sciences*,
Lecture Notes in Civil Engineering 323, https://doi.org/10.1007/978-981-99-0823-3_11

Santika et al. considered environmental noise, which influence the quality of life, generally it is a combined source due to highway traffic and industrial activity. Roadway traffic is the main reason for noise generation in urban regions [6]. It may affect upon speech intelligibility cognitive learning of school students. According to the author, the Leq level of noise in private schools was 72–87 dBA. This is due to noise coming from the roadway produce impact, rather than the others that make a local impact [7].

Daytime urban noise quality assessment of educational, recreational, residential, along with silence zone was done for Kolhapur city, India. They noticed the maximum Leq of 72.25 dBA in industrial-cum-residential area subsequently 64.47 dBA in commercial-cum-residential zone, 63.71 dBA in the silence area [8].

Shukla et al. assessed the current condition of noise levels and its impacts due to further expansion of the Lucknow city in India. They studied noise levels at various locations such as silence zone, residential and commercial zones, and heavy traffic. Finally, they deduced that noise levels were higher (75–90 dB) than the acceptable norms at all locations [9].

This research work explored the noise levels of schools at both locations, inside and outside the school premises, and discusses the effects of urban traffic noise on students and the urban school environment.

2 Methodology

Road traffic noise monitoring was done in the urban area of Surat city. Four secondary schools were selected near urban roads for this study. The schools have same capacity of students (1500–2000), structural characteristics, and layout such as dimension, elevation, and orientation of the buildings. All four schools were located alongside the arterial roads of the city (Table 1 and Fig. 1).

Table 1 List of monitoring points (school)

Sr. No.	Name of schools	Type of building	Type of road	Class of road
1	S D Jain School, Vesu, Surat	Institutional building	Bituminous road	Arterial road
2	London house, Lancer Army School, Dumas road, Surat	Institutional building	Bituminous road	Arterial road
3	SVP Secondary School Surat	Institutional building	Bituminous road	Sub arterial road
4	Shardayatan School, Piplod, Surat	Institutional building	Bituminous road	Arterial road

(a)Noise monitoring at the front of SVP School

(b)Sound Level meter

(c)Radar gun

Fig. 1 Photograph of noise monitoring at the front of SVP School (**a**), Instrument used for noise measurement (**b**), and vehicle speed measurement gun (**c**)

Measurement of noise has been done at four schools located at the roadside of urban area from morning 9.00 am to evening 9.00 pm for continuous 12-h to get the most extensive data set for analysis. Noise monitoring and measurement were done inside and outside the premises of school buildings. Noise monitoring was done using KIMO DB 300 Sound Level Meter, and a SONY Handy cam was used to record the vehicles count. The speed of the vehicles was measured by Falcon HR radar gun.

3 Results

The noise monitoring was done as per the protocol given by the Central Pollution Control Board. According to CPCB India guidelines the sound level in silence zones should not go beyond 50 dB at the day and 40 dB at night. But, decibel levels in these locations assorted from 50 to 78 dB for the daytime as well as 50–72 dB during night time.

Table 2 shows traffic composition and the noise levels at inside and outside the premises of the S D Jain school the school buildings (Fig. 2).

At S D Jain School, inside and outside noise levels were the same from the afternoon onwards, till 9.00 pm. The noise level was higher in the morning period, and it was 77.9 dBA; the reason could be the high traffic and the morning peak period of office hours as this road passed away from various commercial areas (Table 2).

Figure 3 shows the diversity between inside and outside noise levels at the school building premises, and it shows a difference of almost 8–10 dBA. The traffic count is also nearly the same over the entire period. However, in morning period, noise level increases along with an increase in traffic count and the traffic count is more in the morning peak hour than in the evening (Table 3 and Fig. 3).

Table 2 Traffic composition and noise levels at S D Jain School Surat (school no. 1)

Time	Leq in (dBA)		Traffic volume (Nos.)				Speed of vehicles (Kmph)				Avg. building height (m)	Road width (m)
	Outside campus	Inside campus	2-w	3-w	4-w	H.V	2-w	3-w	4-w	H.V		
9.00 AM–10.00 AM	77.9	64	1650	134	680	30	42	32	46	30	30	18
10.00 AM–11.00 AM	78	64.9	1801	144	767	31	47	33	50	22	30	18
11.00 AM–12.00 PM	77.6	68	1900	164	748	48	48	36	48	18	30	18
12.00 PM–1.00 PM	71.4	66.5	1009	147	802	43	50	27	48	32	30	18
1.00 PM–2.00 PM	66.9	64.1	958	132	650	38	44	30	51	26	30	18
2.00 PM–3.00 PM	58	63.2	1080	131	649	34	42	35	46	30	30	18
3.00 PM–4.00 PM	61.6	64	977	120	625	30	39	32	52	29	30	18
4.00 PM–5.00 PM	61.4	63.9	899	111	709	36	38	36	48	28	30	18
5.00 PM–6.00 PM	64	63.2	1370	134	777	30	42	34	49	25	30	18
6.00 PM–7.00 PM	63	62.3	1802	165	780	48	41	30	46	28	30	18
7.00 PM–8.00 PM	64	60.9	1788	166	670	28	44	29	43	26	30	18
8.00 PM–9.00 PM	63.4	60.3	1561	147	722	31	39	32	44	24	30	18

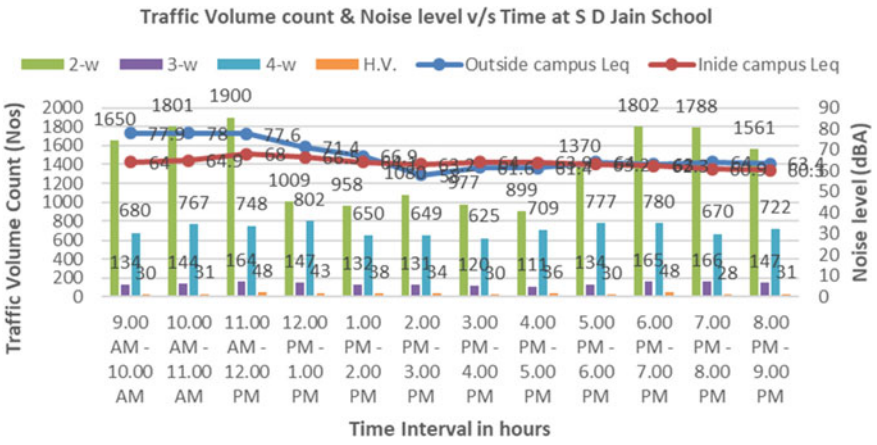

Fig. 2 Traffic count, noise levels and time at S D Jain School

At SVP school noise level was 78.4 and 66.9 dB (A) outside and inside the premises, respectively. The above figure shows an increase in noise level at morning period 9.00 am to 1.00 pm inside the premises of the school building; the main reason could be the building is just away from the traffic stream and entering the vehicles of staff inside the gate as well as the movement staff and students (Table 4 and Fig. 4).

At, Shardayatan school there is a difference in the noise level of 2–4 dBA. The school building was situated alongside the road, and there was a compound wall around the premises still there was 63.2 Leq level was observed (Fig. 5). Also, it was observed that the number of four-wheelers was almost the same during morning 9.00 am to afternoon 2.00 pm. The minimum noise level was 58.0 dBA observed from 8.00 pm to 9.00 pm (Table 5).

Figure 6 gives the idea about equivalent noise levels, maximum noise level, and minimum noise levels for four-school buildings; the maximum equivalent noise level at SD Jain School was 78.4 and 66.9 dBA at outside and inside the campus, respectively (Table 6). On the other hand, in school no. 4, the outside and inside noise levels are almost the same, 63.2 and 62.6 dBA, respectively. Also, there is a slight difference in the equivalent noise level of schools no. 2 and 4.

4 Conclusion

As per the data collected from this study, it is noticed that the minimum equivalent noise level (Leq) was 61.4 dBA outside the campus at school no. 3 out of four school and maximum corresponding noise level was 78.4 dBA outside the campus of the school. The maximum Leq at outside and inside the campus of the school no.1 was 78.4 dBA and 66.9 dBA respectively.

Table 3 Traffic composition and noise levels at Lancer Army School, Surat (school no.2)

Time	Leq in (dBA)		Traffic volume (Nos.)				Speed of vehicles (Kmph)				Avg. building height (m)	Road width (m)
	Outside campus	Inside campus	2-w	3-w	4-w	H.V	2-w	3-w	4-w	H.V		
9.00 AM–10.00 AM	73.4	64	1489	311	702	20	43	31	45	28	30	18
10.00 AM–11.00 AM	74	63.2	1547	333	789	22	44	33	48	24	30	18
11.00 AM–12.00 PM	72.9	62.9	1910	298	777	24	46	34	46	20	30	18
12.00 PM–1.00 PM	73.2	62	1600	299	810	40	49	28	48	32	30	18
1.00 PM–2.00 PM	72.8	61.2	1444	305	766	47	41	31	50	28	30	18
2.00 PM–3.00 PM	71.6	60.4	1532	278	847	65	42	34	45	32	30	18
3.00 PM–4.00 PM	72.6	60	1578	290	835	68	38	35	50	30	30	18
4.00 PM–5.00 PM	71	60	1423	310	785	60	36	34	49	29	30	18
5.00 PM–6.00 PM	73.9	62	1501	245	880	23	43	36	48	26	30	18
6.00 PM–7.00 PM	73.4	64	1843	288	1111	18	40	30	47	28	30	18
7.00 PM–8.00 PM	74.1	60.2	1780	321	1090	24	43	30	44	28	30	18
8.00 PM–9.00 PM	73.2	58.9	1589	254	899	22	40	32	42	25	30	18

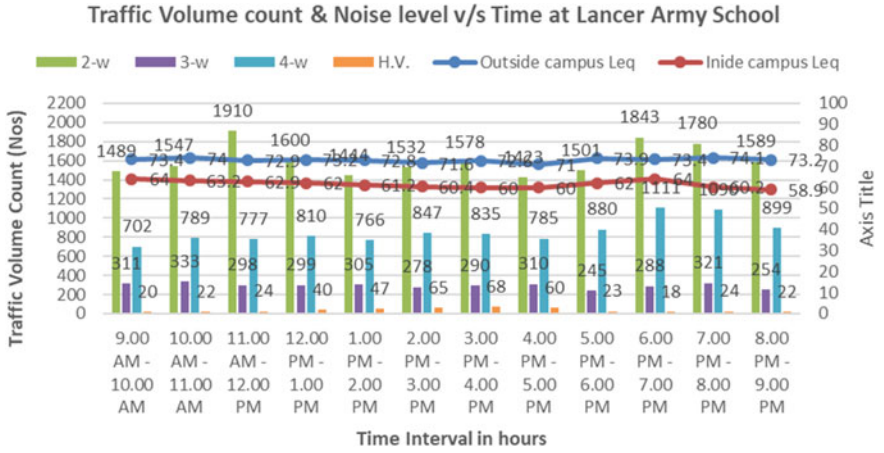

Fig. 3 Traffic count, noise levels and time at Lancer Army School

The noise levels inside the school were 66.9 dBA, 62.3 dBA, 62.5 dBA, and 62.6 dBA in schools No. 1, 2, 3, and 4, respectively. The noise levels exceeded the limits of CPCB standards of silence zone at all locations. In general, there is a need for improvement in acoustics to reduce noise from urban road traffic.

The value obtained from onsite measurements give a clear idea about the current scenario of noise pollution in the school environment of Surat City. Traffic density has a direct correlation with the measure of noise generation and its intensity. Higher the number of vehicles, the higher the traffic noise. Likewise, various vehicles produce various amount of noise. Heavy vehicles generate the large amount of noise as compared to light weight vehicles. The condition of vehicles, speed of vehicles, road width, and height of building affects the conglomerated noise generation. Lower the road width, higher the hindrance while commuting, which leads to a higher generation of noise. Results show that the school premises' environment was noisy, and noise levels in these roadside schools were severe, exceeding the CPCB's noise levels.

5 Suggestions for Noise Mitigation and Reduction

With an exponential growth of vehicular population in developing countries like India and also a typical phenomenon of mixed land use pattern, there is an urgent need for traffic noise abatement measures in silence zones. Results obtained in this research have validated this hypothesis.

Table 4 Traffic composition and noise levels at SVP, Surat (School No.3)

Time	Leq in (dBA)		Traffic volume (Nos.)				Speed of vehicles (Kmph)				Avg. building height (m)	Road width (m)
	Outside campus	Inside campus	2-w	3-w	4-w	H.V	2-w	3-w	4-w	H.V		
9.00 AM–10.00 AM	61.4	63.9	959	155	471	22	26	18	24	18	18	9
10.00 AM–11.00 AM	63.1	64.8	1002	201	467	24	24	17	22	17	18	9
11.00 AM–12.00 PM	61.9	66.3	987	198	512	21	29	15	24	18	18	9
12.00 PM–1.00 PM	62.2	64.6	1015	170	463	26	28	15	22	16	18	9
1.00 PM–2.00 PM	60.7	65.1	940	161	409	20	27	20	23	18	18	9
2.00 PM–3.00 PM	59.0	62.7	932	172	431	15	30	18	26	18	18	9
3.00 PM–4.00 PM	59.1	59.6	886	145	398	18	29	19	25	20	18	9
4.00 PM–5.00 PM	61.8	60.7	890	192	373	22	26	19	26	17	18	9
5.00 PM–6.00 PM	61.7	60.7	971	188	490	16	24	18	24	17	18	9
6.00 PM–7.00 PM	61.5	58.7	1029	177	520	15	27	20	24	18	18	9
7.00 PM–8.00 PM	61.5	58.4	1041	167	505	17	26	20	22	16	18	9
8.00 PM–9.00 PM	61.3	57.4	953	142	455	16	25	18	24	16	18	9

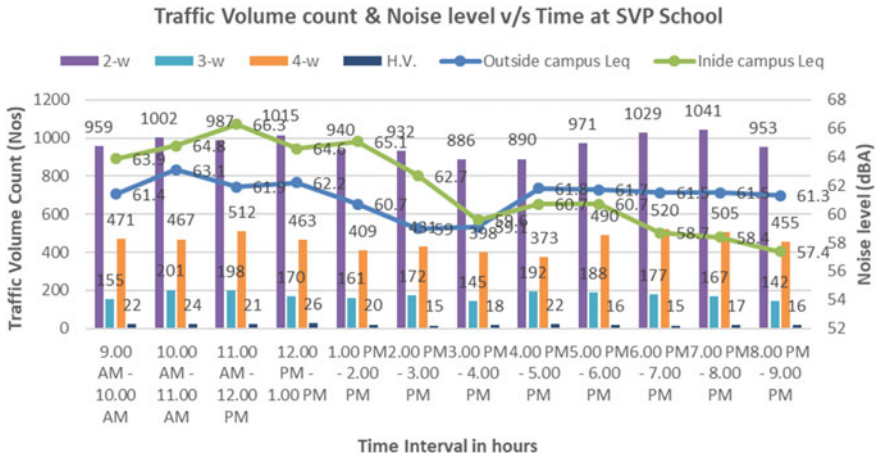

Fig. 4 Traffic count, noise levels and time at SVP School

Looking into this significance of the traffic noise pollution problem in silence zones of India, the following generic steps to reduce them are proposed.

(1) Signboards and hoardings will go far in mass awareness about problems related to noise and new schemes related to noise pollution.
(2) Banning the entry of heavy vehicles within the silence zone during peak hours of morning and evening can lead to a reduction of 3–5 dBA noise levels [10].
(3) Scrupulous implementation of the ban and levying heavy fines on air pressure horns in motor riders and cars and also prohibiting honking of horns in silence zones, will go a long way in curbing this ubiquitous and omnipresent menace of traffic noise pollution.

Table 5 Traffic composition and noise levels at Shardayatan School Surat (school no.4)

Time	Leq in (dBA)		Traffic volume (Nos.)				Speed of vehicles (Kmph)				Avg. building height (m)	Road width (m)
	Outside campus	Inside campus	2-w	3-w	4-w	H.V	2-w	3-w	4-w	H.V		
9.00 AM–10.00 AM	65.2	62.4	1020	158	488	23	26	18	24	18	18	9
10.00 AM–11.00 AM	65	63.8	1109	206	490	26	24	17	22	17	18	9
11.00 AM–12.00 PM	66.1	64.4	919	204	510	22	29	15	24	18	18	9
12.00 PM–1.00 PM	64.2	61.2	1045	188	460	24	28	15	22	16	18	9
1.00 PM–2.00 PM	62.4	62	991	172	410	22	27	20	23	18	18	9
2.00 PM–3.00 PM	61.1	60.6	955	184	440	16	30	18	26	18	18	9
3.00 PM–4.00 PM	63.2	58.9	995	166	392	20	29	19	25	20	18	9
4.00 PM–5.00 PM	65	59.8	1066	210	388	20	26	19	26	17	18	9
5.00 PM–6.00 PM	63.4	60.4	990	190	510	17	24	18	24	17	18	9
6.00 PM–7.00 PM	62.8	59.2	1066	182	540	14	27	20	24	18	18	9
7.00 PM–8.00 PM	63.4	60	1081	178	510	18	26	20	22	16	18	9
8.00 PM–9.00 PM	64.5	58	978	146	466	14	25	18	24	16	18	9

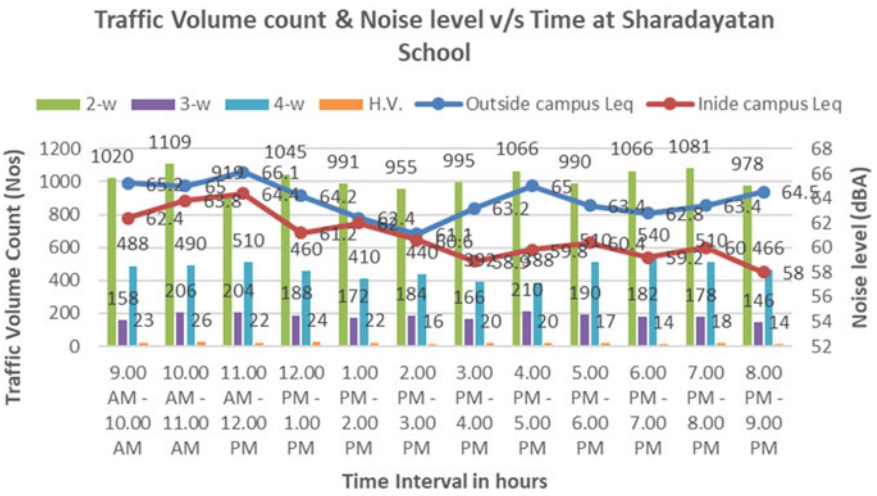

Fig. 5 Traffic count, noise levels and time at Shardayatan School

Table 6 Leq levels at inside and outside the four schools

Monitoring point	Time period	Equivalent noise levels in (dBA)		Lmin (dBA)	
		Outside campus Leq	Inside campus Leq	Outside campus Leq	Inside campus Leq
School no. 1	9.00 AM–9.00 PM	78.4	66.9	48.6	52.2
School no. 2	9.00 AM–9.00 PM	72.9	62.3	57.4	48.7
School no. 3	9.00 AM–9.00 PM	61.4	62.5	45.2	48.6
School no. 4	9.00 AM–9.00 PM	63.2	62.6	49.2	46.2

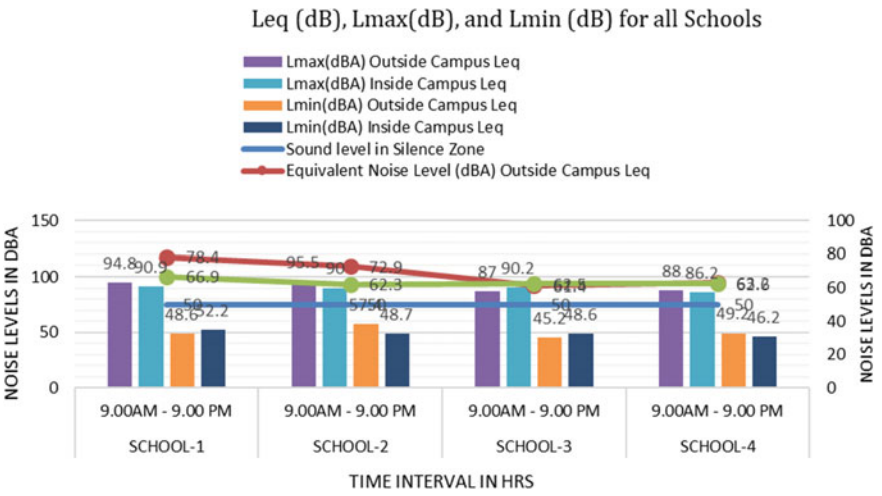

Fig. 6 Leq (dB), Lmax (dB), and Lmin (dB) for all schools

References

1. Mishra RK, Parida M, Rangnekar S (2010) Evaluation and analysis of traffic noise along bus rapid transit system corridor. Int J Environ Sci Technol 7:737–750. https://doi.org/10.1007/BF03326183
2. Freitas EF, Martins FF, Oliveira A, Segundo IR, Torres H (2018) Traffic noise and pavement distresses: modelling and assessment of input parameters influence through data mining techniques. Appl Acoust 138:147–155. https://doi.org/10.1016/j.apacoust.2018.03.019
3. Ministry of Environment and forest: the Noise Pollution (Regulation and Control) Rules (2000) 12311:1088–1569
4. Ranpise RB, Tandel BN, Darjee C Assessment and MLR modeling of traffic noise at major urban roads of residential and commercial areas of Surat city
5. Licitra G, Teti L, Cerchiai M, Bianco F (2017) The influence of tyres on the use of the CPX method for evaluating the effectiveness of a noise mitigation action based on low-noise road surfaces. Transp Res Part D: Transp Environ 55:217–226. https://doi.org/10.1016/j.trd.2017.07.002
6. Ranpise RB, Tandel BN, Singh VA (2021) Development of traffic noise prediction model for major arterial roads of tier-II city of India (Surat) using artificial neural network. Noise Mapp 8:172–184. https://doi.org/10.1515/noise-2021-0013
7. Santika BB, Indrawati S, Suyatno BB, Yahya E (2017) Noise Evaluation of traffic flows and its effect to concentration capability of the students in one of private school in Surabaya. Procedia Eng 170:274–279. https://doi.org/10.1016/j.proeng.2017.03.026
8. Hunashal RB, Patil YB (2012) Assessment of noise pollution indices in the City of Kolhapur, India. Procedia Soc Behav Sci 37:448–457. https://doi.org/10.1016/j.sbspro.2012.03.310
9. Shukla AK, Jain SS, Parida M, Srivastava JB (2009) Performance of FHWA model for predicting traffic noise: a case study of metropolitan city, Lucknow (India). Transport 24:234–240. https://doi.org/10.3846/1648-4142.2009.24.234-240
10. Sonaviya DR, Tandel BN (2020) Integrated road traffic noise mapping in urban Indian context. Noise Mapp 7:99–113. https://doi.org/10.1515/noise-2020-0009

Quality Assessment of Various Curd Samples Based on Their Microbiological and Biochemical Properties

Argha Dutta, Sushmit Bauldas, Arpan Roy, Chandrani Dutta, and Fatema Calcuttawala

Abstract Curd is one of the most widely consumed traditional fermented milk products which has a high nutritional value. The present study was conducted in order to assess and compare the quality of various curd samples. These samples consisted of home-made curd, local sweet shop curd, probiotic curd and commercially available curd samples such as Amul Masti and Mother Dairy Classic. Both microbiological and biochemical parameters were used in order to monitor the quality of the curd samples. Pure cultures were obtained from all the curd samples by subjecting them to the spread plate and streak plate methods respectively. After determining the total viable cell count the Gram character was ascertained by staining. Catalase test and methylene blue reduction tests were performed. A comparison of the results obtained gave us an insight into which curd sample is best for regular consumption. As Good Manufacturing Practices and strict hygienic conditions are followed for the production of commercial curd, it generally exhibits a better quality than the one obtained from local sources.

Keywords Curd · Microbiological · Biochemical · Good manufacturing practices

1 Introduction

Milk is a highly nourishing and beneficial food product for consumption by human beings. However, in the present era where rapid commercialization is taking place, the food habits of people are changing too. People are becoming more health conscious and there is a growing demand for milk converted to various products such as probiotic curd. In general, curd has a therapeutic potential especially for people suffering from gastrointestinal disorders [2]. Lactic acid bacteria (LAB) which are found in these processed dairy products are responsible for many positive health effects [1, 3]. Besides, fermented products are also recommended for lactose intolerant individuals [7]. As they reduce the cholesterol level, they are ideal for consumption by patients

A. Dutta · S. Bauldas · A. Roy · C. Dutta · F. Calcuttawala (✉)
Department of Microbiology, Sister Nivedita University, Newtown, West Bengal, India
e-mail: fatema.c@snuniv.ac.in

© The Author(s), under exclusive license to Springer Nature Singapore Pte Ltd. 2023

S. Kumar et al. (eds.), *Sustainable Environmental Engineering and Sciences*,
Lecture Notes in Civil Engineering 323, https://doi.org/10.1007/978-981-99-0823-3_12

suffering from atherosclerosis [9, 11]. Our study deals with a comparison of the quality of curd samples most commonly consumed by people of Eastern India. Our results help us to uphold good quality products. The Food and Agriculture sector is in dire need of this approach to ensure that the best quality products reach the consumer thereby ensuring a cleaner, greener and healthier future for the citizens of the country [8]. Our nation has been progressing rapidly in various sectors of industrialization in recent years. The dairy industry is one of the major directions where this development has been spearheaded. But, the supply of milk products is divided into two broad categories. On one hand we have the corporate and reputed dairy industries where strict hygiene standards and the newest techniques of Industrial microbiology are implied. On the other hand, there are small local shops scattered in most localities of Eastern India. These shops locally procure their raw materials and process the items under the same roof as they are often locally owned. They employ cheap labour. Understandably the standards of cleanliness are not up to par in many instances. The main philosophy of our project was to compare the microbial load of these curd samples from various sources and study its impact on the biochemical properties of the sample. This study would be a public service as a considerable part of the population in our country procures their dairy products from these local sources.

2 Literature Review

Curd is a traditional fermented milk product whose positive health effects have been widely explored. Research has been conducted from time to time in various parts of the country for the purpose of comparing the microbiological profiles of dairy food items which are locally consumed by the people in that region [4, 10]. Attempts have also been made to compare the curd produced from the milk of cow, buffalo and goat [6]. We followed a holistic approach by taking into account the local curd samples consumed by people in the rural areas as well as the commercial probiotic curd widely consumed by the urban population in the country. Our study was performed keeping in mind the goal of improving national health. To our knowledge, this is the first report highlighting an elaborate microbiological and biochemical comparison of fermented milk products widely consumed by the people of Eastern India.

3 Objective

Through this paper we have tried to understand how commercialisation has benefitted the dairy industry by studying one of the most widely used dairy product in the country, curd. A qualitative analysis of several curd samples, namely, home-made curd, local sweet shop curd, curd made from pasteurized toned milk, and probiotic curd was done based on their microbiological and biochemical properties.

Table 1 Results of spread plating the various curd samples

Sample type	Dilution of curd sample	Observation (mean of 3 plates)
Local sweet shop curd	10^{-4}	One large single colony
Mother dairy classic curd	10^{-4}	21 colonies (colonies of varied sizes and shapes were obtained, mostly large and small)
Amul masti curd	10^{-3}	14 colonies (colonies of varied sizes and shapes were obtained, mostly large and small)
Probiotic curd	10^{-4}	18 colonies (colonies of varied sizes and shapes were obtained, mostly large and small)
Home-made curd	10^{-4}	28 colonies (colonies of varied sizes and shapes were obtained, mostly large and small)

4 Methodology

4.1 Media Preparation and Bacterial Isolation from Curd Samples

The media that was used consisted of 0.5% peptone (by weight), 0.3% yeast extract (by weight), 0.5% NaCl (by weight) and 1.5% agar (by weight). Isolation of the culture from the curd samples was done by the spread plate technique, using the serial dilution method. The curd samples were serially diluted ten-fold up to 10^{-6} dilution. This process was done for all the curd samples. Following serial dilution, 100 µl of each sample was thoroughly spread on the nutrient agar plate using a glass spreader under proper sterile conditions to avoid any contamination and to get pure isolated colonies required for the qualitative study. After the spread plate was done for all the samples, the plates were incubated for 48 h at 37 °C (Table 1).

4.2 Isolation of Pure Colonies by Streak Plate Method

The curd samples were subjected to the quadrant streak plate method, on nutrient agar media in order to obtain pure well-isolated single colonies. The plates were incubated overnight at 37 °C. After incubation, the plates were taken and observed and single colonies were subjected to Gram-staining.

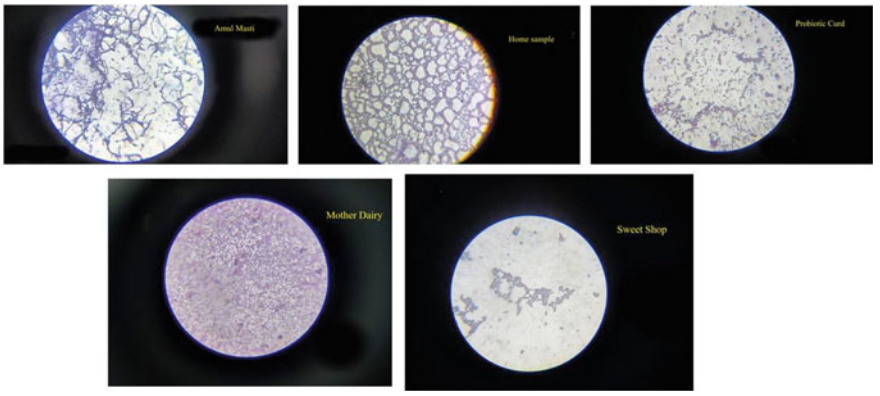

Fig. 1 Some observations through the compound microscope after gram-staining of representative colonies from all the curd samples

4.3 Gram-Staining of Single Colonies

The single colonies obtained on the various plates were subjected to Gram-staining and observed under the microscope. Majority of them appeared as long violet-coloured rods and were Gram-positive in nature. Some samples also showed the presence of short rod-shaped Gram-positive bacteria (Fig. 1).

4.4 Catalase Enzyme Detection Test

This procedure was performed to distinguish bacteria on the basis of catalase enzyme activity [5]. Microorganisms like obligate aerobes and facultative anaerobes produce reactive oxygen species like hydrogen peroxide during metabolism. These toxic substances are cleared by the catalase enzyme which dissociates hydrogen peroxide into oxygen and water. Bacteria which synthesize catalase enzymes show a positive result for this test. This test was performed from two representative colonies of sweet shop curd sample and Mother Dairy curd sample as they exhibited a difference in morphology (Table 2). A small amount of inoculum was smeared on a smudge free glass slide. Upon the addition of hydrogen peroxide (3%), liberation of oxygen bubbles was considered to be positive, and in the absence of catalase, no oxygen bubbles were produced. Samples A2, B2, C, D showed catalase negative results. Samples A1, B1, E showed catalase positive results (Fig. 2).

Table 2 Sample designation for catalase test

Source of curd	Sample denomination
Sweet shop	A1, A2
Mother dairy	B1, B2
Probiotic	C
Amul masti	D
Homemade	E

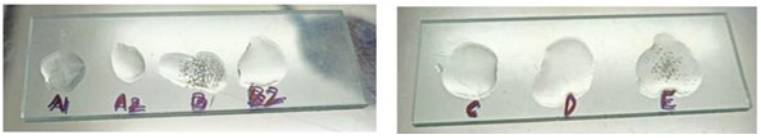

Fig. 2 Results of catalase test

4.5 Methylene Blue Dye Reduction Test

The methylene blue dye reduction test is performed so as to assess the magnitude of bacterial contamination within a sample of dairy product. This test when performed in the laboratory visually indicates the concentration of bacteria by inducing a colour change in the prepared sample of dairy product. Methylene blue is an oxidation–reduction indicator that loses its colour in the absence of oxygen. Normally it is in an oxidized state, but after accepting H^+ ions it is reduced. Bacteria in curd samples ferment the lactose, so oxygen gets used up. Certain enzymes present in bacteria known as oxido-reductases which can oxidize substrates by removing the hydrogen present. The methylene blue dye accepts the hydrogen and gets reduced to a colourless leuco-compound. The speed of decolourization remains inversely proportional to microbial population in milk. In our experiment, we prepared a solution from each of the curd samples and added the methylene dye to them. Then we recorded the observation after every one hour for six hours and tabulated the result (Table 3). This test helped us understand the quality of curds obtained from different sources with greater clarity. The local sweet shop curd showed the most rapid decolourization (Fig. 3).

5 Conclusion

A comparison of the results obtained gave us an insight into which curd sample is best for regular consumption. As Good Manufacturing Practices and strict hygienic conditions are followed for the production of commercial curd, it generally exhibits a better quality than the one obtained from local sources. These hygienic practices must be propagated towards the local manufacturers and the consumers can be educated

Table 3 Observations for methylene blue reduction test

Time (h)	Sweet shop (A)			Mother dairy (B)			Probiotic (C)			Amul Masti (D)			Homemade (E)		
	A_1	A_2	A_3	B_1	B_2	B_3	C_1	C_2	C_3	D_1	D_2	D_3	E_1	E_2	E_3
0	++++	++++	++++	++++	++++	++++	++++	++++	++++	++++	++++	++++	++++	++++	++++
1	+++	+++	+++	++++	++++	++++	++++	++++	++++	++++	++++	++++	++++	++++	++++
2	–	–	–	++++	++++	++++	+++	+++	+++	+++	+++	+++	++++	++++	++++
3	–	–	–	++++	++++	++++	+++	+++	+++	+++	+++	+++	++++	++++	++++
4	–	–	–	++++	++++	++++	+++	+++	+++	+++	+++	+++	++++	++++	++++
5	–	–	–	++++	++++	++++	+++	+++	+++	+++	+++	+++	++++	++++	++++
6	–	–	–	++++	++++	++++	+++	+++	+++	+++	+++	+++	++++	++++	++++

++++ No colour change
+++ Slight decolourization
++ Partial decolourization
+ Fairly decolourization
– Complete decolonization

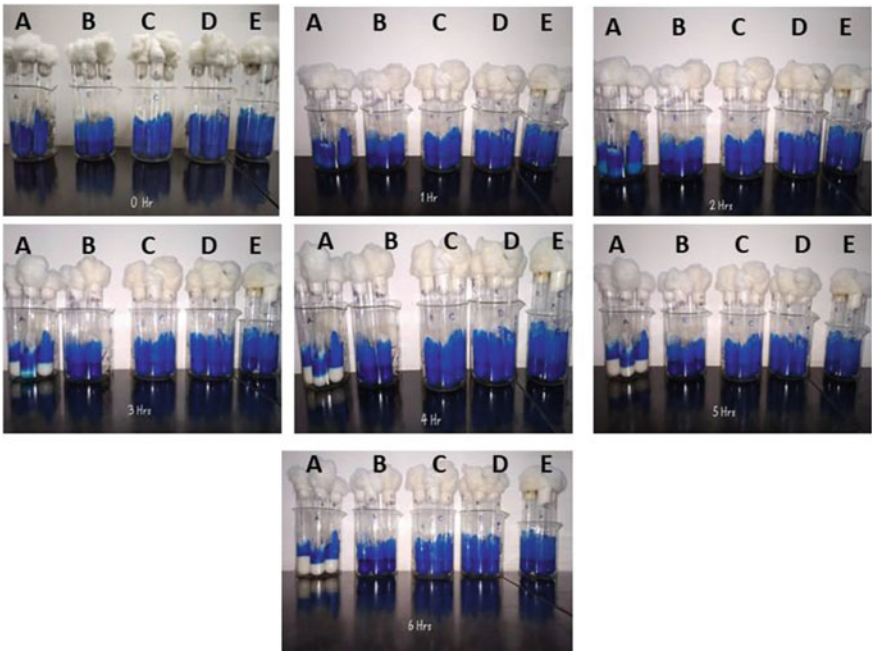

Fig. 3 Results of the methylene blue reduction test of milk samples (all sets were in triplicate)

about brands which maintain better quality control. This shows how commercialization has given us products of higher quality. As for future work, one can routinely conduct these kinds of independent comparative studies to ensure that the curd being used generally for consumption is of optimum quality. The inference of this result will help us to determine the importance of funding and resources required in the various sections of research and development in dairy industries. In the local dairy segments which include home-made products, topographical or small industries, local sweet shops, the lack of proper research and development wing leads to the compromise in quality of the dairy products which affects the choice of masses in an era of growing development and commercialization of food products. Thus, a proper study and data regarding the quality assessment of the dairy products in this case, curd, can help in the betterment of product choices ranging from a small to a wide area of commercialization. The data we acquired from our experimentation included different curd samples which varied in the area from which they were obtained, texture and nutritive property. In most parts of India, a significant percentage of the population procures their dairy products from the aforementioned small, locally owned businesses so the assessment and maintenance of these industries is not only important for our country's economy but also to keep its population safe and healthy for a cleaner, greener and sustainable future.

References

1. Bostan K, Unver Alcay A, Yalçin S (2017) Identification and characterization of lactic acid bacteria isolated from traditional cone yoghurt. Food Sci Biotechnol 26:1625–1632
2. Hajela N, Nair GB, Ganguly N (2010) K: Are probiotics a feasible intervention for prevention of diarrhoea in the developing world? Gut pathogens 2(1):10
3. Heller KJ (2001) Probiotic bacteria in fermented foods: product characteristics and starter organisms. Am J Clin Nutr 73(2Suppl):374S–379S
4. Kakati S, Talukdar A, Hazarika RA, Raquib M, Laskar SK, Saikia GK, Hussein Z (2021) Bacteriological quality of raw milk marketed in and around Guwahati city, Assam, India. Vety World 14(3):656–66
5. Nageswararao G, Derbyshire J, Berman DT (1969) Sources and mechanism of catalase activity in the catalase test for abnormal milk. J Milk Food Technol 32(7):261–264
6. Nahar A, Al-Amin M, Alam SMK, Wadud A, Islam MN (2007) A comparative study on the quality of Dahi (Yoghurt) prepared from cow, goat and buffalo milk. Int J Dairy Sci 2:260–267
7. Oak SJ, Jha R (2019) The effects of probiotics in lactose intolerance: a systematic review. Crital Rev Food Sci Nutr 59(11):1675–1683
8. Pozhidaeva E (2021) Quality rating and shelf-life prediction of curd products with biocorrective action. Biosci Biotechnol Res Commun 14:806–810
9. Shiby VK, Mishra HN (2013) Fermented milks and milk products as functional foods—a review. Crit Rev Food Sci Nutr 53(5):482–496
10. Sivakumar N, Kalaiarasu S (2010) Microbiological approach of curd samples collected from different locations of Tamil Nadu India. Int J Curr Res 10:027–030
11. Solomons NW (2002) Fermentation, fermented foods and lactose intolerance. Eur J Clin Nutr 56(Suppl 4):S50–S55

Role of Fly Ash as an Alternative Filler Material in Asphalt Concrete Road

Krishnendu Kundu, Sudipta Adhikary, Sanglappaul Chowdhury, and Sahana Ray

Abstract In this study, the true role of fly ash has been explored, the various test results have considered the ash as a very good substitute of common filler material in asphalt concrete road, which significantly reduces the air borne waste content from the environment is investigated. For this research, Trials were carried with various bitumen content i.e., 3.5–6.5% with the addition of 2% of slacked lime (SL) in the mix and also wavering the percentages of fly ash i.e., 2–8% as a substitute filler material of these reformed mixes. Through Marshall Mix design method, percentages of optimum bitumen content (OBC) for all the reformed mixes were determined. The results showed that in spite of lower percentages of optimum bitumen content (OBC) there were higher stability values when it was mixed with 4% fly ash as an optimum percentage of filler content in comparison with the conventional mix along with the standard specification. So, the fly ash, which is a very cheap waste material as well as possesses very easy availability, can be used as a substitute of hydraulic lime in asphalt concrete road as a filler material.

Keywords Optimum bitumen content · Fly ash · Filler · Reformed mix · Slacked lime

Abbreviations

SSA	Sewage sludge ash
SL	Slacked lime
FA	Fly ash
ASTM	American society for testing and materials
OBC	Optimum bitumen content
VMA	Void filled my mineral aggregate
VFB	Void filled my bitumen

K. Kundu (✉) · S. Adhikary · S. Chowdhury · S. Ray
Dr. Sudhir Chandra Sur Institute of Technology and Sports Complex, Kolkata 700054, India
e-mail: krishnendu.kundu@dsec.ac.in

© The Author(s), under exclusive license to Springer Nature Singapore Pte Ltd. 2023

S. Kumar et al. (eds.), *Sustainable Environmental Engineering and Sciences*,
Lecture Notes in Civil Engineering 323, https://doi.org/10.1007/978-981-99-0823-3_13

Marshall Quotient The highest Marshall Quotient indicates that the asphalt mixture has the highest stability and the lowest flow

1 Introduction

In the era of globalisation, transportation system, especially on roads, have been increased significantly and to cope up the space large amount of road construction and proper maintenance is a parts and parcel of the daily life of the engineer those mainly deals with roads. The space of progression enhances the daily requirement of good quality materials. As a result of these, heavy axle traffic naturally demands for best quality material for an application as a paving material. These needs of communities can be meet up by the remarkable progress along with proper practice of reformed asphalt mix. The asphalt modification process can be traced primarily by the methods of polymer modification; however, this method demands raw polymer, skilled labour and special equipment, which turns it to a very expensive at all. On the contrary, asphalt modification can also be practised by substituting traditional filler material (i.e., lime, cement or stone dust); by fine grain substances that typically pass by the 0.075 mm India Standard sieve [1], with additional required materials. In recent times, because of the severe threats from environmental and economic perspective, researchers are extensively searching for recycled materials as a substitute of common traditional material [2, 3]. Global Sustainability can also be ensured through the process of recycling. A mineral by-product, i.e., 'fly ash' generated through the ignition process of coal in thermal power plant and stored nearby land which proves as a great source of air pollution directly affecting human health as well as other living bodies. Basically, in India, a huge amount of fly ash accumulated every year. The innovative approach to use waste material has been become a prior national interest. In research work, basically in connection with concrete, the fly ash was successfully using since last few years, but it seems very limited application on asphalt pavement road. The study was carried out to access the true impact of fly ash and its appropriate percentage has been explored from Marshall Test values for the DBM (Dense Bituminous Macadam). Fly ash is such a material that usually meets up the specific requirements for mineral filler for sorting, organic waste and plastic. Apart from this, fly ash also has a very good hydrophobic property to reduce the dissolution into the asphalt; the presence of Slacked lime in some classes of fly ash can also be very much effective to reduce erosion. From our experiment result, it has clearly shown the applicability of the fly ash as a filler material in asphalt pavement satisfactorily.

2 Materials and Methods

2.1 Materials

Aggregate

Coarse and Fine aggregates around our close proximity have been collected, the Specific gravity of the aggregates are 2.89 and 2.73. The gradation of these aggregates belongs to DBM Gr-2 set by MORT & H.

Bitumen

Paving bitumen of 'VG 30' from haldia petrochemicals has been collected and used in the study to make hot mix asphalt according to the IS: 73:2002 [3].

Filler

Waste material Fly ash (FA) has been used as a filler material which was collected from kolaghat thermal power station placed in kolaghat, West Bengal and Slacked lime (SL), collected from the local market. The chemical and physical properties of filler materials were explored and presented in Table 1. The SEM image and physical appearance of the used fly ash are also shown in Fig. 1.

Table 1 Chemical and physical properties of slacked lime and fly ash

Fillers	Chemical compositions								Physical properties	
	SiO_2	CaO	Al_2O_3	Fe_2O_3	MgO	K_2O	SO_3	LOI*	SSA** (m^2/Kg)	Specific gravity
SL	3.2	72.4	0.41	0.3	0.4	0.10	1.21	21.7	431.2	2.16
FA	49.60	12.30	25.31	4.8	1.41	2.4	0.9	3.05	309.41	2.32

LOI*- Loss of ignition
SSA**- Specific surface area

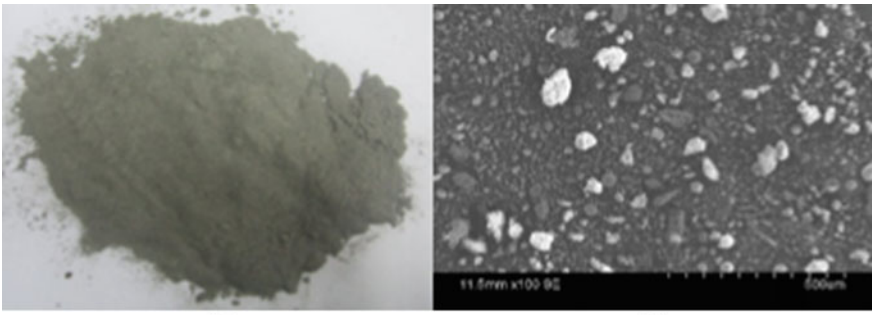

(a) (b)

Fig. 1 **a** Initial appearance **b** Scanning through electronic micro cope (SEM) image

2.2 Methods

Design of DBM mix

Marshall mix design method has been used to design HMA mix. By applying 75 blows on each layer, the standard Marshall specimens were prepared according to ASTM: D6926 [4, 5], Seven different bitumen samples were prepared between 3.5 to 6.5% by total weight of aggregate at 0.5% increment for control mix (i.e., the mix that contain 2% HL as filler) and also the mix containing Fly ash as a filler material of 2, 4, 6 and 8%.

Marshall quotient tests, Marshall stability, and flow test

To detect optimum bitumen content (OBC) for various mix proportions, Marshall mix design method has been selected. So, it was required to execute flow test and Marshall stability test for every distinctive trial under a rate of loading 50.5 mm/min at 60 °C according to ASTM: D6927 [5, 6]. A pseudo stiffness, which is designated as 'Marshall Quotient', can also be explored as the ratio of stability to flow.

3 Results and Discussion

The optimum bitumen content (OBC) is calculated from the data, which is attached herewith in Fig. 2 and also selected the percentage of air voids as 4%. Apart from this, various other Marshall properties as voids filled by mineral aggregate (VMA), voids filled by bitumen (VFB), flow, stability and Marshall quotient (MQ) were evaluated within the MORTH specified limits at that specific percentage of bitumen.

In Table 2, various properties of Marshall mixes have been illustrated, these properties helped to obtain optimum bitumen content values at also helped to study the filler content percentage for regulator mix and for modified amalgamation with the

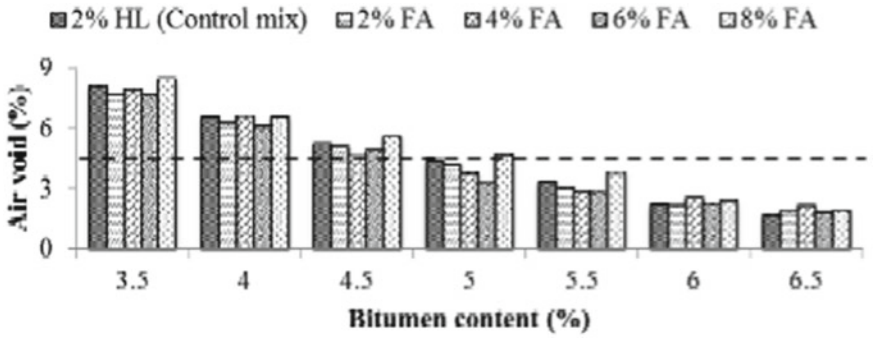

Fig. 2 The graph shows the variation of Bitumen content (%) with different percentages of air voids along with the different percentages of filler content

Table 2 Marshall properties for the mixes corresponding to OBC at various filler content

Filler type	Percentage filler	OBC (%)	VMA (%)	VFB (%)	Stability (KN)	Flow (mm)	MQ (Kn/mm)
HL	2	5.21	16.08	74.57	16.08	3.82	3.53
FA	2	5.07	15.58	73.58	13.98	3.09	4.54
	4	4.9	15.11	74.33	15.44	3.77	4.11
	6	4.8	14.78	73.62	19.48	3.35	5.23
	8	5.4	16.16	74.87	17.52	3.79	5.34

ash as well. The optimum bitumen content for the control mix is 5.21% is shown in Table 2. In addition, with that the various percentages of fly ash (FA) as 2, 4, 6 and 8% are mixed as filler material and observed optimum bitumen content (OBC) are 5.05%, 4.86%, and 4.79% respectively. The obtain results are shown that the value of optimum bitumen content reductions with the rise of the percentages of fly ash (FA) raised to 6%, but additional increase of the percentages of filler content shown the increment of optimum bitumen content (OBC). Furthermore, we have also received values through Marshall stability test, which is attached in Table 2 of the control mix as 12.98 KN. On contrary the mix containing filler material (FA) at various percentages as 2, 4, and 6%, reflects the Marshall stability (MS) values as 13.98, 15.39, 18.98 and 17.38 KN correspondingly. The results of flow values for all mixes with respect to optimum bitumen content remained in between the range of 1.5–3.5 mm (Ref: Table 2). In addition, the obtained result for the values of Marshall Quotient is also shown significant improvement along with the increase of the percentages of fly ash (filler content) and afterwards 4% of the fly ash (filler material), the values are also remaining the same go beyond the extreme permissible specified value of 5 (Ref. Fig. 3). As a source of these used materials, gradation of aggregates, all are also remaining the same for the various proportions, as an outcome of the study reflects, that the changes in the percentages of optimum bitumen content (OBC) which is observed are accredited due to the type of filler material i.e., fly ash and their content only.

4 Conclusion

Through Marshall mix design method, it has been exploitability tested that the probable practice of FA as a filler material in hot mix asphalt road. Through the data which were received from the experiment, the following conclusions are being made.

According to the obtained Marshall parameters through experiments, the inclusion of fly ash up to 4% in DBM mix, as a substitute of conventional filler material like HL or SL, ensure economic advantages of bitumen in resulting mix.

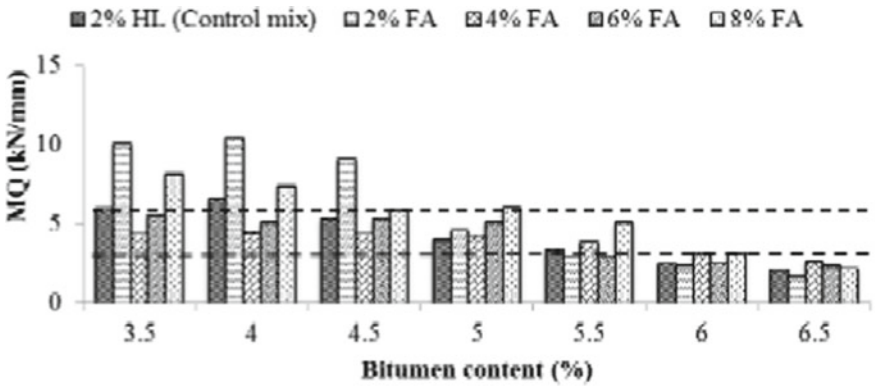

Fig. 3 Variation of MQ values versus bitumen content at a different filler content

Obtained results are also reflects that the addition of filler material i.e., fly ash (FA) provides much better strength with lesser deformation in connection with the conventional mix.

FA is a byproduct of coal combustion process, which is very cheap and easily available. Globally it is considered as soil ameliorator, so the disposal of FA in the land caused many undesirable changes of the soil. In addition, due to its micro grains, it can spread air pollution drastically and causes some severe disease, mainly pulmonary disorders. So, through our study we are trying to focus on some alternative uses of this FA and as per our study is concerned it (FA) has shown great efficacy as a filler material for asphalt concrete road. This filler material is also responsible to reduce the cost of the entire project which is also a great outcome in the various developing countries like India.

Acknowledgements The authors are very much thankful to 'Dr. Raja Mistry', 'Dr. Tapas Roy' of the Department of Civil Engineering, IIEST, Shibpur. Further, the authors like to express their sincere gratitude to all the members of the department of Civil Engineering, 'Dr. Sudhir Chandra Sur Degree Engineering College'.

References

1. Ministry of Road Transport, and Highways (MORT&H) (2013) Specifications for road and bridge works, fifth revision, Indian Roads Congress, New Delhi, India
2. Choudhary R (2006) Evaluation of bituminous concrete mixes with industrial wastes as filler. Ph.D. dissertation, Department of Civil Engineering, Indian Institute of Technology, Roorkee, India
3. Kuity A, Jayaprakasan S, Das A (2014) Laboratory investigation on volume proportioning scheme of mineral fillers in asphalt mixture. Constr Build Mater 68:637–643
4. IRC SP: 53 (2002) Guidelines on the use of polymer and rubber modified bitumen in road construction. Specifications of Indian Roads Congress, India

5. ASTM D6926-10 (2010) Standard Practice for Preparation of Bituminous Specimens Using Marshall Apparatus. Annual book of ASTM standards, West Conshohocken, Pa
6. ASTM D6927-10 (2010) Standard Practice for Marshall Stability and Flow of Asphalt Mixture. Annual book of ASTM standards, West Conshohocken, Pa

Consequences of Flow Fields and Vortices Around Crossway Cylinder with Flow Obstructing Downstream Plate

Asim Kuila, Subhasish Das, and Biprodip Mukherjee

Abstract Often vibration of flow-induced vortices is used on oceans, rivers, large channels, and even in shallow channels to harness energy. The shedding vortex depends on the type of structure, flow, and position of the submerged crossway cylindrical structure relative to the bed surface and water surface. In the case of shallow channels, it becomes more difficult to produce such vibration because due to a lack of depth sufficient to form an induced vortex. To overcome this situation, downstream of such cylinders a flow obstructing vertical plate, as a combined structure, is being used in very recent days. The present research aims to understand the flow kinematics around such a combined structure along with its shedding vortex and flow intensity effects which are related to the induced vibration of vortices. In the laboratory, a rectangular re-circulating sloping channel was used to conduct two experiments to analyze the performance of the flow fields and to analyze the induced vortex generated behind such a combined structure. The parameters derived from the velocity fluctuations component are compared for the different cylinder distances from the obstructing plate. It was found that the cylinder-plate gap plays a significant role compared to other parameters in developing a stronger induced vortex at the upstream of the crossway cylinder. The experimental observation and analysis confirm that the second experimental structure is more effective in producing higher kinetic energy despite its smaller cylinder diameter, lower upstream depth, and lower discharge.

Keywords Submerged cylinder · Wake vortex · Absolute velocity · Turbulence intensity · Kinetic energy

A. Kuila (✉) · S. Das · B. Mukherjee
School of Water Resources Engineering, Jadavpur, University, Kolkata 700032, India
e-mail: asimkuila@gmail.com

© The Author(s), under exclusive license to Springer Nature Singapore Pte Ltd. 2023

S. Kumar et al. (eds.), *Sustainable Environmental Engineering and Sciences*,
Lecture Notes in Civil Engineering 323, https://doi.org/10.1007/978-981-99-0823-3_14

1 Introduction

The interaction between fluid structure occurs in various fields which is an interesting topic in engineering subjects. The flow-induced vibration (FIV) in fluid structures is a frequent phenomenon that is observed in offshore structures and cable-supported bridges. A non-linear phenomenon is observed in FIV and vortex shedding in the structure helps to start vibration. FIV is induced on the underwater pipeline and causes weariness on the structure due to vibration which is observed experientially. The FIV is extensively studied to measure the response of amplitude of a spring-damping cylinder structure [1, 2].

The flow-induced vibration becomes destructive in nature when the structure frequency and the flow-induced frequency are in a resonance state and the state is called synchronization. The flow-induced vibration at the resonance state can tear down the structure so previous researches are conducted to restrain the flow-induced vibration. The control of flow is essential for hydraulic structures in a channel [3]. The controlled flow-induced vibration holds a huge amount of energy that can be judiciously used for generating electrical energy [4–9]. Oscillation is generated by the submerged cylinder when the submerged cylinder experiences the flow-induced vibration. The oscillation can sustain over a wide range of Reynolds numbers keeping constant the Strouhal number. A complex flow regime is developed surrounding the cylinder that should be analyzed to understand the flow-induced vibration. The flow becomes more complex when the structure is nearer the boundary because the flow observed three shear layers which develop on both sides of the structure and the surface boundary layer. Such a combination of structure and surface boundary is shown in the underwater pipeline and underwater cables.

The vortex shedding behind the structure is reliant on the gap ratio G/D, where G represents the gap between the bed surface and lower point of horizontal cylinder curvature and D represents crossway cylinder diameter [10–12]. The flow pattern can extensively depend on G/D which can be categorized as the flow characteristic of the single-cylinder, the vortex shedding generated from the upper boundary layer of the crossway cylinder is influenced by the surface of the bed and the vortex shedding frequency is restrained by the smaller gap. The oscillation aspect of the crossway cylinder is impacted by the boundary layer with a gap of less than $1D$ [13]. The vortex formation in the occurrence of bed surface categorizes the wake flow pattern based on the gap ratio [14]. The flow fields and profiles are gauged by the ADV (Acoustic Doppler Velocimeter) around the submerged cylinder. The flow separation at the over-layer of the cylinder and the turbulence are significant terms in fluid–structure interaction. The horseshoe vortex is crucial in scouring phenomena for a vertical or horizontal cylinder and the same was studied on different shapes of pier structures at different depths of water. The contours of the time mean velocities, turbulence intensities, and the turbulence kinetic energy were emphasized to envisage the vortex formation [15, 16].

Although several studies have been done among them, scanty work is applicable for shallow channels that too at low discharges. In the case of shallow channels, it

becomes more difficult to produce vibration by induced vortices due to a lack of depth sufficient to form induced vortices. To overcome this situation, downstream of such cylinders a flow obstructing vertical plate is being used in very recent days. For using this impediment plate successfully, the shedding vortex further depends on the gap between the crossway horizontal cylinder and obstructing plate. There was very little analysis done by the previous researchers on the flow kinematics around such combined structures (including cylinder and plate). Based on this aspect, the present research aims to understand the flow kinematics around such a combined structure along with its shedding vortex and flow intensity effects which are related to the FIV.

2 Experimental Arrangement

In the laboratory, a rectangular re-circulating sloping channel was used to conduct two experiments to analyze the performance of the flow fields and to analyze the induced vortex generated behind the crossway cylinder. The flow around the crossway cylinder is measured by keeping the cylinder stationary at different depths from the flume bed surface and the schema of the composite structure is shown in Fig. 1.

The composite structure is placed at 7.0 m from the flume inlet. The crossway cylinder of the smooth surface is connected with two thin metal rods at its end sides. Using metal rod *G* can be adjusted. Although the cylindrical structure fluctuated to generate energy but to measure the velocity—the position of the horizontal cylinder location was kept adjusted to 4 cm above the bed level. The three-dimensional velocity elements were entirely measured in a Cartesian coordinate system with help of a Nortek-made Vectrino plus probe which operates on the concept of the Doppler effect. This instrument measured the data 5 cm away from the probe tip creating an adjustment sampling volume of 2–5 mm in height and a diameter of

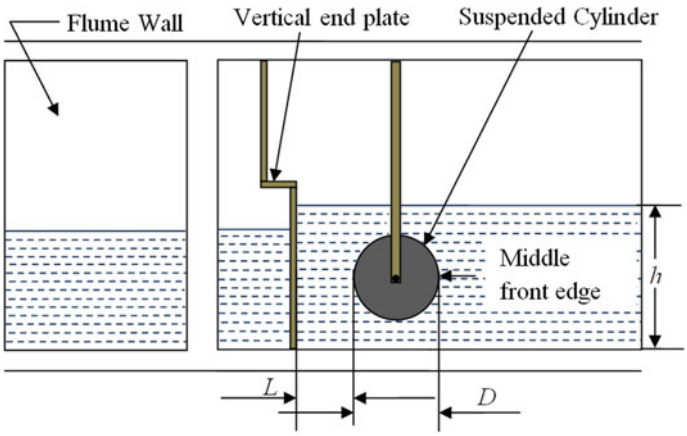

Fig. 1 Schematic diagram highlighting the composite structure

Table 1 Comparative details of two experimental conditions

Experiment number	E1	E2
Diameter of crossway cylinder = D (cm)	5	4 ↓
Width of the obstructing plate (cm)	5	5
Cylinder bottom to bed gap (cm) = G (cm)	$4 = 0.8D$	$4 = 1D$
Obstructing plate and crossway cylinder gap	5.5	9.0 ↑
Flow depth at the upstream of crossway cylinder (cm)	20	17 ↓
Discharge (lps)	52	35 ↓

6 mm. The data were recorded at the sampling rate of 100 Hz [17]. The comparative details of two experimental conditions are provided below (Table 1).

The three-dimensional velocities (u,v,w) and fluctuations (u', v, w') are prepared in the contour frame to observe and analyze the flow arrangement at two operative zones of turbulence (i) in between the obstructing plate and the crossway cylinder, and (ii) at the upstream of the crossway cylinder. The contour is framed in the x–z plane. Here x-direction implies the positive u direction and the z-direction implies the positive w direction. The OriginLab software is used to visualize the contour frame of the time-averaged (t-avg) longitudinal velocity, i.e. $u_{\text{t-avg}}$, t-avg crossway velocity, i.e. $v_{\text{t-avg}}$, and t-avg vertical velocity, i.e. $w_{\text{t-avg}}$. The t-avg absolute velocity, i.e. $V_{\text{t-avg}}$, turbulence intensities (u^+, v^+, w^+), and kinetic energy (TKE) are derived from the $u_{\text{t-avg}}$, $v_{\text{t-avg}}$, and $w_{\text{t-avg}}$ along with its fluctuation and are also plotted using the same software to visualize and analyze the science behind the fluid–structure interaction.

3 Results and Discussions

3.1 Flow Vector

The magnitude $\left[= \sqrt{\left(u^2 + w^2\right)}\right]$ and direction $\left[= \tan^{-1}(w/u)\right]$ of the flow vector are determined from the velocity component and shown in Fig. 2. The flow becomes zero at the stagnation point of the leading edge of the crossway cylinder with the highest static pressure according to Bernoulli's pressure flow equation and the flow separates into upper and lower streamline of flow from the stagnation point as pressure decrease at either side of the crossway cylinder edge. The stagnation point is observed near the center edge with an angle of 0° of crossway cylinder curvature and the stagnation point of the crossway cylinder may move on either side of the cylinder depending on the gap between the cylinder and bed. The fluid passes after the stagnation point through the thin boundary layer where the velocity decreases rapidly due to the resistance of viscous force. The adverse pressure gradient is developed near the boundary layer and the particles reverse their direction due to the exchanged

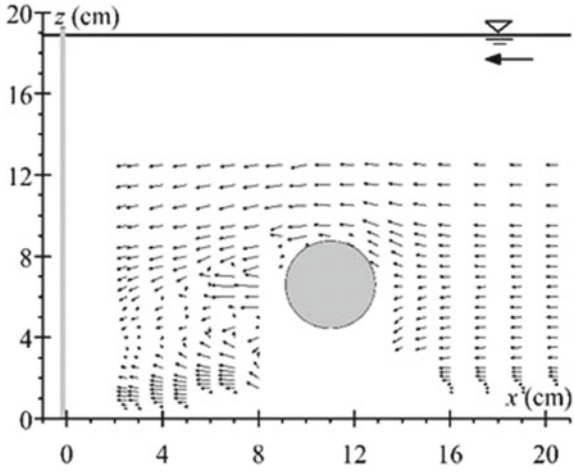

Fig. 2 2D contour of the velocity vector

momentum of flow and subsequently, the flow separation occurs. The angle of the flow separation took place at an angle of 84.5° on upper edge and 86.4° lower edge from the center of the crossway cylinder edge. The separation point may shift due to the uneven flow distribution around the crossway cylinder. The flow separation helps in the formation of the vortices and in the shedding of the vortices at the wake zone of the cylinder.

3.2 Time-Averaged Velocities

The flow passage characteristics over the cylinder are observed by the $u_{\text{t-avg}}$ in cm/s which is shown in Fig. 3a. The magnitude of the $u_{\text{t-avg}}$ increases when it passes over the cylinder curvature after the separation from the stagnation point. But the core of the $u_{\text{t-avg}}$ which is formed at 9.8 cm from the obstructing downstream plate toward the crossway cylinder and 11.7 cm from the bed surface that is observed above the cylinder is 1.41 times more than the core of $u_{\text{t-avg}}$ which develop at 3.6 cm from the obstructing downstream plate and 6.8 cm from the bed that is observed as near bed surface or below the crossway cylinder. This variation of the $u_{\text{t-avg}}$ is due to the more viscous resistance acts between the crossway cylinder and bed surface than the free flow surface region and the presence of obstructing plate. A core of $u_{\text{t-avg}}$ is developed near the bed between the crossway cylinder and obstructing downstream plate is higher in the case of the E1 experiment compared to the E2 experiment.

A negative core of $u_{\text{t-avg}}$ which is located at the lee zone of the crossway cylinder of 7.8 cm from obstructing plate toward the crossway cylinder and 6.4 cm from bed surface is 0.97 times the velocity of the free-stream (U_{fr}). The negative indicates the opposite flow from the U_{fr}. The negative core of $u_{\text{t-avg}}$ for the 5 cm cylinder is 0.125 times the U_{fr} (i.e. 72 cm/s) which is much lower than the core developed in the 4 cm

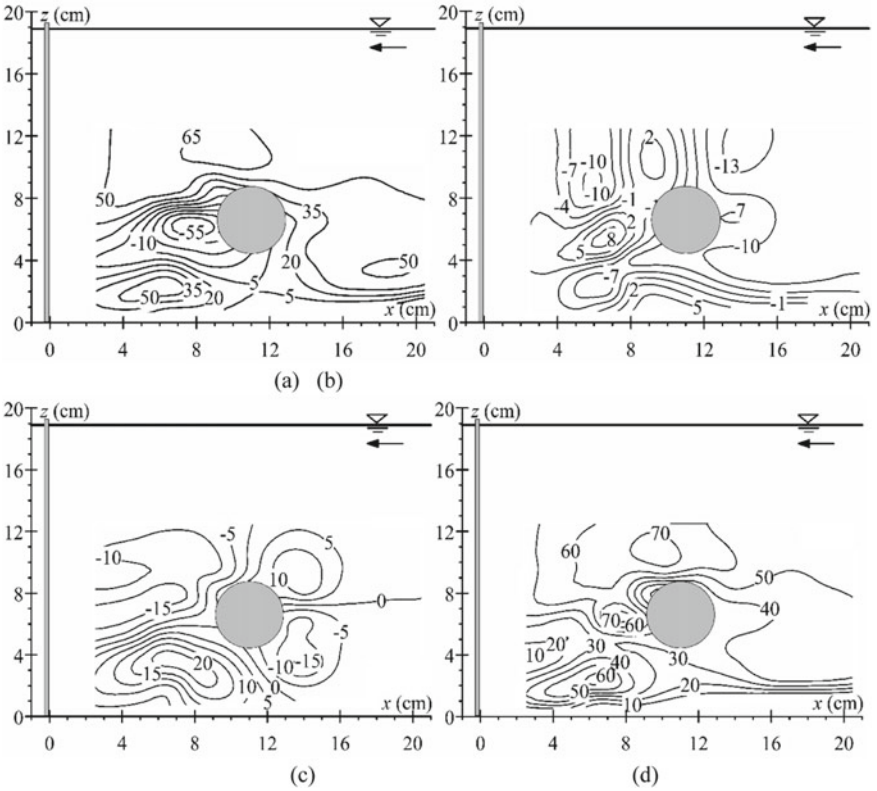

Fig. 3 2D contour representation of **a** $u_{\text{t-avg}}$, **b** $v_{\text{t-avg}}$, **c** $w_{\text{t-avg,}}$ and **d** $V_{\text{t-avg}}$

cylinder. The higher negative core of the $u_{\text{t-avg}}$ at the lee zone for the 4 cm cylinder is due to the greater length between the obstructing downstream plate and crossway cylinder causing a greater adverse pressure gradient with higher backflow toward the rear side of the crossway cylinder. The excessive loss in the adverse pressure gradient at the wake zone of the crossway cylinder causes negative flow in that region.

The $v_{\text{t-avg}}$ in cm/s and shown in Fig. 3b. The $v_{\text{t-avg}}$ lies between 10 cm/s to − 12 cm/s which indicates the lower value of $v_{\text{t-avg}}$ to the U_{fr}. With such a low mean velocity, the $v_{\text{t-avg}}$ does not construct a corresponding effect on the crossway cylinder. But the interaction between water and the crossway cylinder creates high turbulence in that zone which indicates the presence of the $v_{\text{t-avg}}$. Similarly, the $v_{\text{t-avg}}$ is lower than the U_{fr} in the 5 cm crossway cylinder.

The importance of the $w_{\text{t-avg}}$ with the assistance of obstructing downstream plates on the crossway cylinder is shown in Fig. 3c. The positive and negative value is considered to be upward and downward $w_{\text{t-avg,}}$ respectively. The zero $u_{\text{t-avg}}$ is found at the stagnation point and separated into positive and negative directions which are clearly apparent in the $w_{\text{t-avg}}$ frame. The downward $w_{\text{t-avg}}$ is lower than the upward

$w_{\text{t-avg}}$. The downward $w_{\text{t-avg}}$ is 0.9 times lower than the upward $w_{\text{t-avg}}$. The positive $w_{\text{t-avg}}$ is 0.39 times the mean U_{fr}. The $w_{\text{t-avg}}$ after separation from the stagnation point depends on the space between the crossway cylinder and the surface bed. If the ratio between the breach of the crossway cylinder curvature and bed surface to the cylinder diameter is less than one the downward $w_{\text{t-avg}}$ is lower than the upward $w_{\text{t-avg}}$ and if the ratio is greater than 1 the downward velocity is higher than the upward $w_{\text{t-avg}}$. The upward $w_{\text{t-avg}}$ is higher than the downward $w_{\text{t-avg}}$ in a 5 cm cylinder due to the lower gap between the crossway cylinder and obstructing downstream plate causing higher obstruction of flow near bed surface.

The positive $w_{\text{t-avg}}$ takes a tangential path after separation from the stagnation point and then becomes downward which is observed from a negative core of 22 cm/s at the 7.4 cm from the surface bed and 4.1 cm from obstructing downstream plate in the contour of the $w_{\text{t-avg}}$ at the lee zone of crossway cylinder due to decrease in the adverse pressure gradient. Similarly, the negative $w_{\text{t-avg}}$ from the stagnation point takes the tangential path of the crossway cylinder curvature and then becomes upward at the lee zone of the crossway cylinder which is observed from a positive core of 24 cm/s at the 2.9 cm from the obstructing downstream plate and the 7.8 cm over bed surface in the contour of the $w_{\text{t-avg}}$ due to same reason as discussed above. There is a mutual conversion between the $u_{\text{t-avg}}$ and $w_{\text{t-avg}}$ observed from the contour diagram of $u_{\text{t-avg}}$ and $w_{\text{t-avg}}$. The $u_{\text{t-avg}}$ transforms to $w_{\text{t-avg}}$ at the stagnation point and after a quarter it becomes $u_{\text{t-avg}}$ and at the lee side of the crossway cylinder, the flow becomes downward where the pressure gradient is low. The adverse pressure gradient decreases with an increase in the distance from the crossway cylinder at the lee side of the crossway cylinder and downward and upward $w_{\text{t-avg}}$ converges and gradually becomes $u_{\text{t-avg}}$.

The negative core of the $w_{\text{t-avg}}$ is more intense near the vertical plate in the 5 cm cylinder. This is because the flow after separation gets little space to converge with a positive core of $w_{\text{t-avg}}$ causes high w near the vertical plate.

The resultant velocity intensity is observed from $V_{\text{t-avg}}\left[=\sqrt{u_i^2}\right]$ contour which is shown in Fig. 3d. The $V_{\text{t-avg}}$ is a scalar quantity. Higher the core value of the $V_{\text{t-avg}}$ indicates the significant strength of velocity area. The magnitude of the $v_{\text{t-avg}}$ is negligible in the $V_{\text{t-avg}}$ whereas the $u_{\text{t-avg}}$ and $w_{\text{t-avg}}$ have a major consequence on the $V_{\text{t-avg}}$. The $V_{\text{t-avg}}$ measures the magnitude of the flow so there is four cores of $V_{\text{t-avg}}$ are found. A core of the $V_{\text{t-avg}}$ of the magnitude of 72 cm/s is developed at 7.8 cm from the vertically obstructing plate and 6.57 cm over the bed surface and the core of $V_{\text{t-avg}}$ is developed by the reverse direction of flow. A core of $V_{\text{t-avg}}$ is developed above the cylinder and near bed surface due to the high magnitude of $u_{\text{t-avg}}$. There is another core of $V_{\text{t-avg}}$ that is developed near obstructing downstream plate due to the downward flow having a high magnitude.

3.3 Turbulence Intensities

The turbulence intensity contours are framed by the equation of $\sqrt{u'u'}$, $\sqrt{v'v'}$, and $\sqrt{w'w'}$ for longitudinal (u^+), crossway (v^+), and vertical (w^+) turbulence intensities, respectively, in the Cartesian Coordinates system. Here u' indicates the fluctuation of the $u_{\text{t-avg}}$, v' indicates the fluctuation of the $v_{\text{t-avg}}$, and w' indicates the fluctuation of $w_{\text{t-avg}}$. Turbulence intensity is higher where the fluctuation is high which is defined by the equation of the turbulence intensity. The fluctuation may be high in the conflict zone of the fluid structure and also depends on the Reynolds number. The frequency of the vortex shedding depends on the fluctuation of the $u_{\text{t-avg}}$ and also depends on the Strouhul number. The vortex shedding increases as the fluctuation of the $u_{\text{t-avg}}$ increases.

The turbulence intensity of the $u_{\text{t-avg}}$, $v_{\text{t-avg}}$, and $w_{\text{t-avg}}$ is observed between the crossway cylinder and obstructing downstream plate and shown in Fig. 4a–c. The u^+ turbulent intensity is higher compared to crossway and vertical turbulence intensities. The core of longitudinal turbulent intensity is observed at a distance of 7.1 cm from obstructing downstream plate toward the crossway cylinder and 5.4 cm above the bed. The estimated magnitude of longitudinal turbulent intensity is 2.14 times the U_{fr}. The vertical plate causes the mixing of the downward and upward flow after separation from the crossway cylinder creating an extreme adverse pressure gradient. The high longitudinal turbulent intensity indicates the strong vortex shedding in this region. The core of longitudinal turbulent intensity is 1.25 times the U_{fr} and is located at the proximity of the crossway cylinder. The longitudinal turbulent intensity is lesser in 5 cm cylinder as compared to 4 cm cylinder and also lesser strength of vortex shedding.

In the previous section, it is seen that the $v_{\text{t-avg}}$ is low with respect to U_{fr} but the crossway turbulent intensity is quite high. This is because the turbulent intensity measures the energy dissipation and is taken as the square root. The core of the crossway turbulent intensity which is 1.49 times the U_{fr} is measured at 7.8 cm from the obstructing downstream plate toward the crossway cylinder and 5.9 cm above the bed. The core of the w^+ intensity which is 0.69 times the U_{fr} is measured at 4.9 cm from the obstructing downstream plate toward the crossway cylinder and 5.2 am above the bed. The core of the u^+ intensity, v^+ intensity, and w^+ intensity is measured almost in the same region which indicates the higher energy dissipation that is shown in the TKE contour.

3.4 TKE

The TKE $\left[= 0.5 \sum u_i' u_i'\right]$ contour is shown in Fig. 5 and is measured to unit volume to water density in the x–z plane. TKE is a function of three-dimension velocity fluctuations. TKE which is related to eddies measures the severity of the longitudinal, crossway, and vertical fluctuations. The core of TKE is observed at 7.2 cm from the

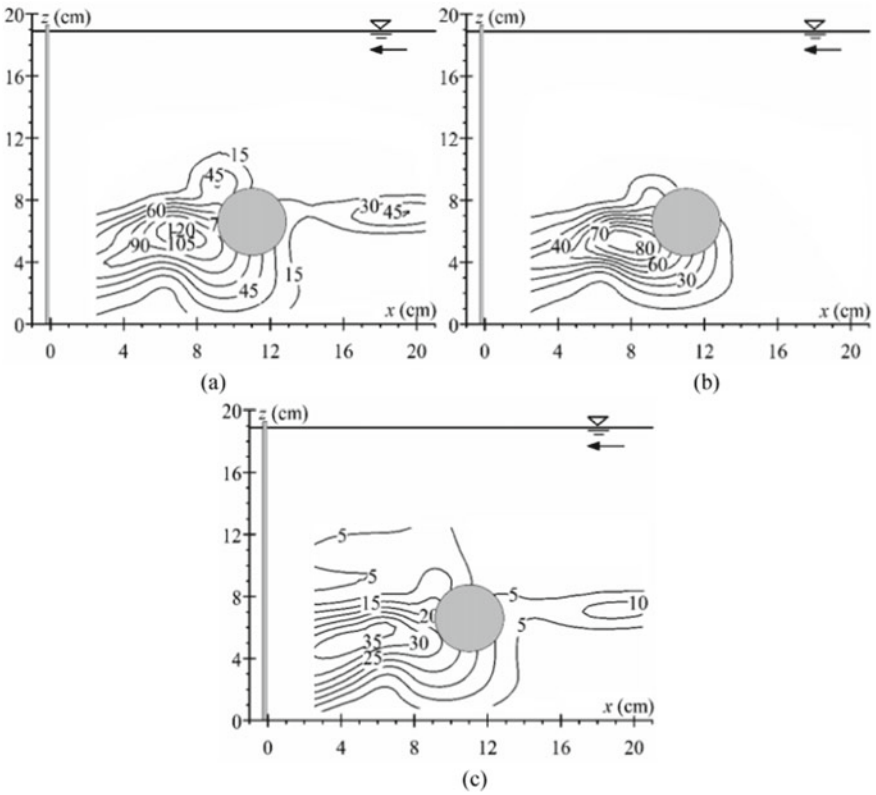

Fig. 4 2D contour representation of **a** u^+ intensity, **b** v^+ intensity, and **c** w^+ intensity

obstructing downstream plate toward the crossway cylinder and 6.1 cm above the bed. Interestingly the turbulent intensity also intensifies in that region which indicates the high rate of energy conversion. The region of high TKE is also specifying the strong vortex shedding. The magnitude of TKE is lower in 5 cm cylinder as compared to 4 cm cylinder. The contour of TKE is found on the curvature of the crossway cylinder rather than in wake of the crossway cylinder.

4 Conclusions

The key aspect of this article is to analyze the kinematics of the composite flow around the proximity of a submerged crossway cylinder with the presence of a vertically obstructing downstream plate respecting to crossway cylinder. The cylinder vertical plate combination is used to yield energy from a low-depth water channel.

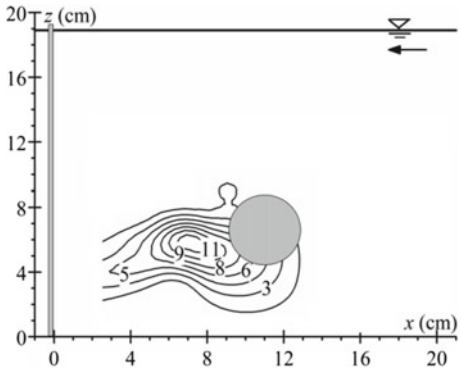

Fig. 5 2D contour representation of TKE (× 1000)

The contours of $u_{\text{t-avg}}$, $v_{\text{t-avg}}$, and $w_{\text{t-avg}}$ illustrated that the characteristics of the flow separation and the vortices are matching despite the different sizes of the structure. The characteristics of the horseshoe vortex differ with different spaces between the crossway cylinder and the downstream obstructing vertical plate. The core of the horseshoe vortex is shifted downward with an increase in the space between the crossway cylinder and obstructing the downstream plate. This is quite important for the vortex vibration phenomena. The flow separation phenomenon can be envisaged upstream of the suspended crossway cylinder. The horseshoe vortex formed before the obstructing plate merges with the vortex shedding behind the crossway cylinder. The stagnation point is dependent on the flow attacking angle with respect to the reference surface. The freestream velocity becomes zero at the location of the upper stagnation point on the cylinder. The stagnation point is developed nearly at the center for the 4 cm cylinder as the gap ratio is one but the stagnation point is developed slightly below the center point at upstream cylinder curvature with an angle of 5° as the gap ratio is 4/5. An opposite flow is developed for the deployment of the obstructing downstream plate and the magnitude of the reverse flow depends on the plate width and the gap between the crossway cylinder and channel bed. The vector diagram of the velocity illustrates the movement of the flow when it crosses through the cylinder and strikes the vertical plate. The core of the time mean longitudinal, crossway, vertical intensities, and TKE is developed near the proximity of the crossway cylinder for the 5 cm cylinder whereas the core of the time mean longitudinal, crossway, and vertical turbulence intensity is developed in the center region of crossway cylinder and downstream obstructing plate. The adverse pressure gradient is increased with the increase in cylinder diameter and the flow separates earlier than the lesser diameter of the cylinder. As a result, the core of the velocity is developed near the cylinder surface for the higher diameter of the cylinder as compared to the lesser cylinder diameter. The TKE has a significant magnitude upstream of the cylinder for the 5 cm cylinder but for the 4 cm cylinder, the core of the TKE is developed in the center region of the crossway cylinder and vertically obstructing plate that indicates the effectiveness of the turbulence kinetic energy is required more a sufficient space for large eddies. The oscillation depends on the alternating nature

of the induced vortex and the effectiveness of the alternating induced vortex depends on the shape and size of the cylinder and plate in shallow water channels. Therefore, by using this second type of structure, kinetic energy can be significantly enhanced to maintain the feature of amplifying the induced vortex in shallow water channels.

References

1. Sarpkaya T (1979) Vortex-induced oscillations: a selective review. J Appl Mech 46(2):241–258
2. Sumer BM, Fredsøe J (1997) Hydrodynamics around cylindrical structures. World Scientific, Singapore
3. Mukherjee P, Das S, Mazumdar A (2021) Introducing winter rice cropping by using non-saline tidal water influx in western basins of South 24 Parganas, India. Sci Rep 11:553
4. Bernitsas MM, Raghavan K, Simon YB, Garcia EMH (2006) VIVACE (Vortex Induced Vibration Aquatic Clean Energy): A new concept in generation of clean and renewable energy from fluid flow. J Offshore Mech Arct Eng 130(4):041101
5. Mukherjee B, Das S, Mazumdar A (2016) Electrical energy generation by enhancing flow induced vibration. In: Proceeding of 2016 2nd international conference on control, instrumentation, energy and communication (CIEC). IEEE, Kolkata, India, pp 368–371
6. Mukherjee B, Das S, Mazumdar A (2016) Sustainable electrical energy generation technique in shallow water channels. In: Proceeding 2016 IEEE students' technology symposium (TechSym). IEEE, Kharagpur, India, pp 47–151
7. Mukherjee B, Das S, Mazumdar A (2017) Complex flow phenomena of horizontally placed underwater cylinder above water bed. Water Energy Int 60(8):57–64
8. Kuila A, Mukherjee B, Das S (2021) Comparison of vortex induced velocity kinematics around underwater horizontal cylinder with vertical end plate. IOP Conf Ser: Mater Sci Eng 1080(1):012048
9. Kuila A, Das S, Mazumdar A (2021) Turbulence spectrum around a suspended cylinder with vertical endplate effects to enhance VIVACE strength. J Waterw Port Coast Ocean Eng 147(5):04021024
10. Bearman PW, Zdravkovich MM (1978) Flow around a circular cylinder near a plane boundary. J Fluid Mech 89(1):33–47
11. Muraoka K, Tashiro S (1985) The effect of the wake from circular cylinder on boundary-layer transition: the effect of gap between the cylinder and surface. Jpn Soc Mech Eng 28(242):1667–1673
12. Lin WJ, Lin C, Hsieh SC, Dey S (2009) Flow characteristics around a circular cylinder placed horizontally above a plane boundary. J Eng Mech 135(7):697–716
13. Fredso/e J, Sumer BM, Andersen J, Hansen EA (1987) Transverse vibrations of a cylinder very close to a plane wall. J Offshore Mech Arct Eng 109(1):52–60
14. He GS, Pan C, Wang JJ (2013) Dynamics of vortical structures in cylinder/wall interaction with moderate gap ratio. J Fluids Struct 43:100–109
15. Das S, Das R, Mazumdar A (2016) Comparison of local scour characteristics around two eccentric piers of different shapes. Arab J Sci Eng 41(4):1199–1213
16. Jaman H, Das S, Kuila A, Mazumdar A (2017) Hydrodynamic flow patterns around three inline eccentrically arranged circular piers. Arab J Sci Eng 42(9):3973–3990
17. Das S, Das R, Mazumdar A (2015) Velocity profile measurement technique for scour using ADV. In: Chan K (ed) Proceedings of the 2015 international conference on testing and measurement: techniques and applications, TMTA 2015, Phuket Island—. Taylor and Francis Group, London, pp 249–252

Assessment of Mitigation Plan for Arsenic and Fluoride in Groundwater by Artificial Recharge of Rainwater

Prasun Mukherjee and Priyanka Roy

Abstract Arsenic and fluoride contamination issues in groundwater are a noteworthy concern. Despite these two parameters being entirely different from one other, the basic circumstances and carcinogenic nature are common to both the parameters. A typical circumstance like Baruipur in the South 24 Parganas of West Bengal, arsenic and fluoride contamination at the same time. This article assesses the potential for dilution of arsenic and fluoride concentration in groundwater dilution, by utilizing rainwater in the campus buildings of Swami Vivekananda Group of institutes in Dakshin Gobindapur, situated in the South 24 Parganas district of West Bengal, India. The total rooftop area of all the surfaces from where rainwater could be endowed is 5180 m^2. Utilizing normal precipitation information, and groundwater data collected from CGWB, the calculations for rainwater harvesting potential along with the groundwater recharge design were made. The volume of water that could be collected and effectively used for groundwater recharge in one year was figured to be 3,951,395.22 L. Appropriate filtration for the removal of suspended particles and reducing the turbidity has also been proposed. This manuscript assesses an alternative solution for the arsenic and fluoride contamination issue in the aquifer of the region by injection of rainwater into the groundwater reserve of the underlying aquifer, raising the water table.

Keywords Rainwater harvesting · Groundwater recharge · Aquifer · Arsenic · Fluoride

1 Introduction

The arsenic contamination of groundwater in this part of West Bengal, India is a major geological issue. The shallow subsurface sediments in the basin are very rich in arsenic and the shallow groundwater demonstrates arsenic contamination in several patches [1]. There are zones in the shallow aquifer that are safe from the

P. Mukherjee (✉) · P. Roy
School of Water Resources Engineering, Jadavpur University, Kolkata 700032, India
e-mail: mukherjeeprasun3@gmail.com

© The Author(s), under exclusive license to Springer Nature Singapore Pte Ltd. 2023

S. Kumar et al. (eds.), *Sustainable Environmental Engineering and Sciences*,
Lecture Notes in Civil Engineering 323, https://doi.org/10.1007/978-981-99-0823-3_15

arsenic contamination. These safe zones display a pattern of a thick clayey top where arsenic pollutants are distinguished to be iron-rich classical grains and authigenic iron-rich carbonates or siderite [2]. The arrival of arsenic from these contaminations into groundwater is incidental and conceivably identified with microbial debasement of natural issues. Since the microorganisms enact more at the aerated conditions, the sediments with higher porosity in the shallow regions of the sedimentary segment will be the perfect locales for their multiplication. It will in the long-run discharge arsenic speedier than the sedimentary segment beginning with an impervious layer [3]. This would be the reason behind the groundwater underneath a thick clayey top is safe. Extreme withdrawal of groundwater will result in the gradual lowering of the water table, which then exposes a larger sediment surface for the microbial reduction. This impact results in the arrival of more arsenic into the groundwater which exponentially increases the issue of arsenic contamination. This could majorly be combated by either reducing the quantity of water withdrawn from the groundwater aquifer to maintain its water table or another process could be by artificial injection of harvested rainwater into the aquifer to not only rapidly rise the water table within the aquifer but also as an effort to dilute the arsenic concentrations in the groundwater currently within the aquifer.

Rainwater harvesting is a basic technique of gathering and holding rainwater where it falls. Possibly, one can store it in tanks or can utilize it to recharge the groundwater aquifer contingent on the circumstances. The framework is monetarily less expensive in development contrasted with different sources. The framework helps in using the primary source of freshwater and further prevents runoff from going into sewer or storm channels. Structures could be explored for harvesting this water, but it is important to determine several parameters to design any hydraulic structure [4]. Rainwater Harvesting frameworks utilized in housing schemes can provide the water for potable and non-potable uses however the type of rainwater harvesting proposed diverts the rainwater into groundwater aquifers which help in enhancing the quality of the existing groundwater in the area through effective dilution. In this type of system, the rainwater needs to be collected, then filtered for basic impurities before recharging into the groundwater aquifer, unless certain heavy metals or other toxic chemicals are present in the water then specific filtration methods needs to be adopted before recharging into the underlaying aquifers. Inadequate filtration of the rainwater before recharge might overturn the objective and would further contaminate the aquifer itself.

The rainwater harvesting system includes segments for collection of the rainwater, transportation of the collected water through pipes, channels, drains, filtration, tanks for storage of gathered water, and borewells for the actual recharge. The basic parts of the rainwater harvesting framework are the catchment surface, conveyance framework, storage tanks, filtration, and borewells.

2 Components and Materials

The catchment area of a rainwater harvesting unit is the surface that receives the precipitation directly and channels the water to the unit. Any roofing material is worthy of gathering water. However, water to be utilized for drinking must not be gathered from thatched rooftops or rooftops secured with asphalt. Likewise lead should not be utilized in these frameworks. Galvanized ridged iron sheets, layered plastic, and tiles make great rooftop catchment surfaces. Concrete or felt-secured rooftops can likewise be utilized given they are clean. It is considered best to avoid asbestos concrete sheets as might have a negative impact on the water quality in terms of asbestos contamination, which is carcinogenic in nature. The type and selection of the catchment area largely dominated the runoff coefficient of the system. Runoff coefficient is a dimensionless coefficient that influences the quantity of water harvested. It is the proportion of the volume of runoff water to the volume of precipitation that the surface receives. The runoff is greater on smooth and impenetrable surfaces. Distinctive catchment materials have different runoff coefficients. An undamaged concrete roof has a runoff coefficient of 0.9, galvanized iron sheets have greater than 0.9 while other types of materials have relatively lower runoff potential [5]. The catchment area in this scenario which was chosen had concrete roofing, corrugated galvanized iron roofing, and corrugated asbestos-cement roofing of which runoff from the asbestos roofing was not considered for the purpose of groundwater recharge.

For effective operation of the rainwater collecting framework, effectively designed, planned, and precisely built plumbing network is essential on the grounds that plumbing is frequently the weakest link in a rainwater harvesting framework. The unit will definitely fail if the drains and the downpipe plumbing networks are not properly fitted or maintained. The most commonly used material for drains and downpipes is polyvinyl chloride (PVC). Cement or metal-based items may likewise be utilized but prior check must be done for any kind of contamination from the plumbing. The choice of PVC pipes was made for the primary plumbing for the ease of handling and maintenance, and the bore pipes of considered galvanized iron were chosen for the durability of the material. It should also be accounted for that vortex formation is not happening as vortex vibration might affect the structure negatively [6].

The water storage tank for the most part represents the greatest capital investment component in a rainwater harvesting system. It, hence for the most part, requires careful design to provide maximum storage capacity along with structural integrity, while keeping the expenses low. Storage tanks might be on the surface or subsurface. Concrete, LLDPE, and brick and mortar tanks are widely used. A relatively new concept, which has been considered for the design is Ferrocement tanks, which are relatively low cost and are easy to build compared to the other materials.

Filtration must be provided for collected rainwater before it enters the borewells to ensure safe and clean water is introduced into the groundwater aquifers. The size and shape of the filter can vary in many ways depending upon the type of filter, the

intensity of rainfall, the groundwater recharge rate, and the filtration rate. The water quality analysis of the rainfall is also an important parameter to determine the type of filter that could be selected.

3 Design Calculation

Primarily for the design of the rainwater harvesting unit the catchment area from where the precipitate would be collected for the recharge was defined. The institutional building of Shree Ramkrishna Institute of Science and Technology (SRIST), administrative building of Swami Vivekananda Institute (SVIST), Mechanical departmental building of SVIST, Civil Departmental Building of SVIST, all have an undamaged concrete roof, an associated storage on the roof of SRIST with corrugated galvanized iron sheets, and a canteen kitchen beside the institutional building in SRIST and SVIST with corrugated asbestos concrete roofing (Fig. 1 and Table 1). The runoff from the canteen kitchen roof is not to be collected for groundwater recharge purposes to avoid the risk of asbestos contamination in the aquifer.

Now the rainfall or precipitate water quality analysis needed to be performed to understand the quantity of rainwater that would be required to be diverted from the initial downpour and also to determine the type of filter that would be required to be designed later. The rainwater was collected after 30 min of continuous rainfall in the monsoon season for a period of 4 months (June–August, 2018) in the vicinity of 8 rainfall events and the average values of the noted parameters were noted for the design considerations. The rainwater was analyzed for the following parameters—pH, TDS, EC, Turbidity, Total Hardness, Alkalinity, Iron, Chloride, Nitrate, and E-coli, the results along with the methods used are mentioned in Table 2.

Fig. 1 Map identifying location of the buildings chosen for rainwater harvesting

Table 1 Coefficient of different types of catchment cover

Sl. No.	Type of building	Total roof area (m^2)	Runoff coefficient
1	Undamaged concrete roof of institutional building at SRIST	2109	Runoff coefficient = 0.9
2	Corrugated sloped Galvanized Iron roof of storage room at SRIST	18	Runoff coefficient = 1
3	Undamaged concrete roof of administrative building at SVIST	1945	Runoff coefficient = 0.9
4	Undamaged concrete roof of Mechanical departmental building at SVIST	261	Runoff coefficient = 0.9
5	Undamaged concrete roof of Civil departmental building at SVIST	847	Runoff coefficient = 0.9
	Total roof area	5180	

Table 2 Tested values for different parameters of the rainfall in the area

Sl. No.	Parameter	Methods used	Average value
1	pH	Membrane electrode	6.53
2	Total dissolved solids (TDS)	Digital meter	11
3	Electrical conductivity (EC)	Digital meter	23
4	Turbidity	Spectrophotometer	<1.00
5	Total hardness	EDTA	<10
6	Alkalinity	Titration (Mohr)	52
7	Iron	Colorimeter	0.12
8	Chloride	Titration (Mohr)	6.51
9	Nitrate	Cd reduction	0.42
10	E-coli	H_2S strip test	Not present in 100 ml sample

Major chemical contrasts between the injectate water and the accepting aquifer may create more risk of contamination when arsenic and radionuclides in the geological network interact with the injectate having relatively high oxidation or reduction potential which is dependent on the pH. Microbial contamination of the rainwater collected indication by E. coli is quite normal, especially in tests gathered soon after precipitation. High microbial concentrations are for the most part found in the primary downpour of water, and the contamination levels lessen as the rain proceeds. A noteworthy decrease in microbial concentration can be found in monsoon seasons when catchments are regularly washed with rainwater.

The data analysis of the rainwater and for keeping provisions for cleaning of a rooftop by initial downpour of rainwater the required initial dirty-water diversion for the system can be allowed as 40%. Hence, the rooftop rainwater to be harvested is 60% of the total rainfall.

Table 3 Distribution of rainfall in the catchment area

Season	Percentage of annual rainfall (%)	Amount of rainfall (mm)
Winter	40	20.5
Pre-monsoon	8	231.7
Monsoon	73	1731.8
Post monsoon	2	42.7

The annual average rainfall in the Baruipur catchment is 17651 mm or 1.7651 m [7]. The annual rainfall in the region distributed annually is described in Table 3 as obtained from Central Groundwater Control Board. The total percentage of rainfall that can be expected in the whole of monsoon season would be 83%.

Now, to determine the rainwater harvesting potential or the quantity of water that could be harvested in one year from the given catchment area would be;

$$\text{Rainwater Harvesting potential} = (\text{C} \times \text{Rc}) \times \text{P} \times \text{Rm} \times \text{Rh} \tag{1}$$

where; C = Catchment area; Rc = Runoff Coefficient; P = Annual average Rainfall; Rm = % of rainfall during monsoon; Rh = % of rainwater to be harvested

Hence;

Annual Rainwater harvesting potential = $[\{(2109 \times 0.9) + (18 \times 1) + (1945 \times 0.9) + (261 \times 0.9) + (847 \times 0.9)\} \times 1.7651 \times 0.8 \times 0.6]\ \text{m}^3 = 3951.39522\ \text{m}^3 = 3{,}951{,}395.22$ L.

This rainfall precipitate collected is to be stored in collection tanks which are to be then filtered before recharging through borewell into the underlying aquifer.

The average recharge depth for the underlying aquifer is 140 mbgl and the available sand layer for the aquifer can be found at 40 mbgl according to the groundwater information booklet South 24 Parganas district, West Bengal. The water is to be passed through a strainer which is to be attached to the borewell pipe.

The length of the Strainer (L) is proposed to be 15 m. The diameter of the pipe (D) is proposed to be 100 mm or 0.01 m. The rate of filtration (vs) of the gravel filter unit proposed has been seen to have a range of 1000 L/h/m^2 to 6000 L/h/m^2. The average rate of filtration (Vs) can hence be assumed to be 2520 L/h/m^2 or 2.520 m^3/h/m^2 for the design considerations. The clogging coefficient (C) is assumed to be 50%. And, the opening area of strainer (P) is considered 60%. Assuming, Rainfall to be collected as 50 mm/h. The Recharging rate (Rr) can be calculated using the formulae;

$$\text{Rr} = (\text{Vs} \times \text{C} \times \pi \times \text{d} \times L \times \text{P}) \tag{2}$$

where; Rr = Recharging rate; Vs = Rate of filtration; C = Clogging coefficient;

L = Length of Strainer; d = Diameter of pipe; P = Opening area of strainer.

Hence;

Recharging rate (Rr) = $(2.520 \times 0.5 \text{ x } \pi \times 0.1 \times 15 \times 0.6) = 3.5625\ \text{m}^3$/h.

As the two Institutes from where the rainwater is to be collected and harvested is nearly 300 m apart within the campus. It is proposed to have separate collection tanks, borewell, and separate plumbing systems. It will not only reduce the cost of unnecessary plumbing but will also reduce the number of points of failure for the overall system.

Design of borewell and collection tanks for a catchment area of the SRIST institute:

For the calculated rate of recharging the maximum rainfall intensity should be (R mm/h. rainfall)

We know;

$$\mathrm{Rr} = 0.6 \times (\text{total area} \times \mathrm{r}/100) \tag{3}$$

$$\text{or, } 3.5625 = 0.6(2127 \times \mathrm{R}/1000)$$

$$\text{or, } \mathrm{R} = 2.7914\,\mathrm{mmh}$$

Since, rainfall intensity is going to be much greater than 2.7903 mm/h, on several occasions, and also as the recharging rate is not more than 3.5625 m^3/h for one borewell surplus water from the storage tank needs to be drained out in the stormwater drainage channel by means of overflow pipe to be provided in the storage tank.

The proposed number of borewells = 17.

Depth of the borewell pipes = 140 m

Length of the borewell pipes = 15 m

Diameter of the borewell pipes = 100 mm = 0.1 m

Now, the estimated total recharging rate = 17 × 3.5625 = 60.5625 m^3/h

The above amount of recharging will have to match for = 17 × 2.7903 = 47.4351 mm/h.

Assuming the rainfall is to be collected at 50 mm/h.

The amount of rainwater to be collected = 2127 × 0.6 × (50/1000) = 63.81 m^3/h.

Hence,

Amount of excess water in received by the system = (63.81 − 60.5625) = 3.2475 m^3/h.

The system design has been made with an allowance for 6 h of excess stormwater.

Hence, quantity of water storage proposed = 3.2475 × 6 = 19.485 m^3 = 19,485 L.

Now, the area of the buildings in the SVIST campus = (1945 + 261 + 847) = 3053 m^2

For the calculated rate of recharging the maximum rainfall intensity should be (R mm/h rainfall).

Hence, rainfall intensity for the SVIST campus buildings can be calculated as;

$$3.5625 = 0.6(3053 \times \mathrm{R}/1000) \tag{4}$$

$$\text{or, } R = 1.9448\,\text{mmh}$$

Since, the rainfall intensity is going to be much more than 1.9448 mm/h, on several occasions, now as recharging rate is not more than 3.5625 m^3/h for one borewell surplus water from storage tank needs to be drained out in stormwater drainage channel. The proposed number of borewells is 25, depth of borewell pipes = 140 m, length of the borewell pipes = 15 m, diameter of the borewell pipes = 100 mm = 0.1 m.

Now, the estimated total recharging rate = 25 × 3.5625 = 89.0625 m^3/h.

The above amount of recharging will have to match for = 25 × 1.9448 = 48.6202 mm/h.

Assuming the rainfall is to be collected at 50 mm/h.

Amount of rainwater to be collected = 3053 × 0.6 × (50/1000) = 91.59 m^3/h.

Hence, amount of excess water received by system = (91.59–89.0625) = 2.5275 m^3/h.

The system design has been made with an allowance for 6 h of excess stormwater.

Hence, quantity of water storage proposed = (2.5275 × 6) = 15.165 m^3 = 15,165 L.

4 Design and Filtration Unit

In spite of being one of the cleanest sources of water, rainwater collected on rooftops might contain a variety of parameters alien to the groundwater source. The introduction of untreated water into the aquifer might cause more adversities than benefits. So, it is recommended to pass the collected water through a pre-filtration system to decrease further chances of aquifer contamination. A sand filtration unit has been proposed for this unit in lieu of the tested parameters for the rainwater that has been collected from the region. In urban or industrial areas other varieties of filtration might be used according to the rainwater quality of the catchment. The plumbing system is designed so as to connect each recharge pit to the sand gravel filter. The recharge rate of the proposed filter is 3.5625 m^3/h. Assuming the rate of filtration as 200 L/h/m^2, the area of the filter unit turns out to be 17.8125 m^2 (by process of dividing the recharge rate of the proposed filter by the rate of filtration). The filter unit proposed is cylindrical in shape. Hence the diameter of the filter can be defined as;

$$\pi/4 \times d^2 = 17.8125 \tag{5}$$

$$\text{or, } d = 4.7623\,\text{m}$$

Thus, Diameter of the filtration unit = 4.7623 m = 4762.3 mm.

Assuming sand thickness = 750 mm, Bottom gravel thickness = 500 mm.

5 Results

The above design was done on the basis of data delineated by the usage of ArcGIS and verifying the same with field recorded data. The rainwater parameters show that there was no severe contamination of any sort in the vicinity. This is possible mostly due to the suburban positioning of the catchment area. The total catchment area selected for the design was 5180 m^2. This provided an opportunity for rainwater harvesting of 3,951,395.22 L of water every year.

6 Conclusion

The reclamation of groundwater by artificial recharge of rainwater is a gradual process requiring large-scale mass awareness and effective execution. It is also widely debatable if the dilution of arsenic and fluoride concentrations is feasible by utilizing the rainwater as injectate. In this region where the proposed design is based on, the groundwater is not continuous and singular in nature but exists in several small patches. The recovery of such pockets can feasibly be attained by artificial recharge. The acidic nature of the rainwater can be reduced by lining the storage tanks with cement and also by the addition of lime or similar low-cost procedures. This added step will undoubtedly help to mitigate the concentration of arsenic and fluoride within the groundwater aquifer. Rainwater is among the most beneficial strategies for utilizing freshwater in a sustainable way. Rain is a natural gift. This method should be used in densely populated places with a water issue and appropriate rainfall. Thus, pressure on groundwater levels might be avoided, and natural recharge could also be accomplished via this approach. Harvested water that is regularly maintained may be acceptable for everyday drinking. Water scarcity will be the most concerning issue in the future all over the world. As a result, municipal planners should reconsider the possibilities, outcomes, and advantages of a rainwater collecting system and develop rules to implement the system. However, water consumption should be evaluated cautiously in light of natural resource availability, safety, and sustainability. Energy conservation is an important aspect of sustainability. Reduced usage of traditional potable water decreases energy consumption, which reduces carbon dioxide emissions. An integrated water management method that includes rainwater collecting, greywater reuse, and reclaimed water reuse might decrease climate change contributions while conserving scarce water and energy resources.

References

1. Halder A, Ray SK (2014) Arsenic and fluoride problems of groundwater in West Bengal and available technologies for remediation. Int J Innov Res Sci Eng Technol 3(6):135–141
2. Pal T, Mukherjee PK, Sengupta S (2002) Nature of arsenic pollutants in groundwater of Bengal basin—a case study from Baruipur area, West Bengal, India. Curr Sci 82(10)
3. Vasudevan P, Tandon M (2008) Microbial quality of rainwater from roof surfaces. J Sci Ind Res 67(6):432–435
4. Nandi B, Das S, Mazumdar A (2020) Experimental analysis and numerical simulation of hydraulic jump. IOP Conf Ser Earth Environ Sci 505(1):012024
5. Kavarana G, Sengupta S (2013) Catch water where it falls—toolkit on urban rainwater harvesting. Center for Science and Environment, New Delhi, India
6. Kuila A, Mukherjee B, Das S (2021) Comparison of vortex induced velocity kinematicsaround underwater horizontal cylinder with vertical end plate. IOP Conf Ser: Mater Sci Eng 1080:012048
7. Kaur S, Purohit MK (2015) Rainfall statistics of India. Hydromet division, Indian Meteorological Department

Spatio-temporal Diversity Exploration of Closed Surface Water Bodies in Borough 1 of Kolkata Using Satellite Images

Bernadette John, Subhasish Das, and Rajib Das

Abstract The increasing rate of urbanization is putting the natural resources at stake. The land being a fixed entity is pressurized by the growing population for meeting the needs of shelter, food, etc., and the ultimate solution being to encroach upon the existing resources. The present work is mainly studying such impacts on the water bodies of Borough I of Kolkata Municipal Corporation. Borough I forms the northern extent of KMC, since it is a developed part of the city no such expansion is seen there, it is expected to see the above impact prominently there, the population density is quite high in the region due to which the open spaces and water bodies have been impacted, the population density is quite high in the region due to which the open spaces and water bodies have been encroached upon. This study mainly concentrates on analyzing the trend of the surface area of such water bodies present in an urban area. The Google imageries were used for demarcating the area of the closed surface water bodies. Historical images from the same were used to find the trend of the above-mentioned feature, which was correlated with Kolkata's rainfall data. The residential areas are increasing in the city due to which the water bodies are shrinking in size and also in number. With the gradual rise in the city's temperature, the rate of evaporation is also increasing which in turn is affecting the water bodies. The surface water bodies are also facing the ill effects of garbage dumping, which is polluting the water bodies. Thus, proper measures are required for its conservation.

Keywords Surface waterbody · Urban · Rainfall · Population density · Satellite imageries · GIS

1 Introduction

Terrestrial surface water bodies are important resources for different types of primary activities and also for the ecosystem. The water bodies not only provide a sense of aesthetic satisfaction but also reduce water stress [1]. Water bodies are so very

B. John (✉) · S. Das · R. Das
School of Water Resource Engineering, Jadavpur University, Kolkata 700032, India
e-mail: bernadettejohn1@gmail.com

© The Author(s), under exclusive license to Springer Nature Singapore Pte Ltd. 2023

S. Kumar et al. (eds.), *Sustainable Environmental Engineering and Sciences*,
Lecture Notes in Civil Engineering 323, https://doi.org/10.1007/978-981-99-0823-3_16

important even in an urban area. Water bodies, flora, and wetlands tend to reduce pollution and maintain the ecology to a greater extent [2].

The assessment of the area of these water bodies is very important to understand their deterioration. Major settlement takes place around the water bodies as they are a source of water for drinking, irrigation, and other industrial purposes [3]. Precipitation and temperature dominantly affect the changes in a surface water body area [4]. The population of Kolkata is increasing which is engulfing the vegetation and water bodies of the area. The lack of awareness and knowledge among the people can be noted evidently as trees are being cut down and the water bodies are being encroached upon to provide shelter to the ever-increasing population of the region [5].

Work done in [6] elucidates the increasing temperature in the core of the city. The residential area of Kolkata, Dum Dum, and Kalyani all show an increasing trend in temperature whereas the temperature around Budge Budge, Sonarpur shows a lower temperature compared to its populated counterparts. In 2008 the mean temperature in the core of the city was 33.5 °C which rose to 35 °C in 2017 whereas in the outskirts the minimum temperature was found to be 10 °C and 14.37 °C in 2017, respectively. The lowering in the number of trees and water bodies will further lead to an increase in temperature.

The major part of the city gets water from the Hooghly River after treatment. A study conducted by Asian Development Bank (ADB) in 2007 found that only 74% of households are connected with pipelines [7]. The inadequacy of the water supply makes people tap the groundwater or depend on the surface water bodies like lakes and ponds for their daily activities. Too much dependence on these water bodies also leads to the problem of sanitation [7]. The water bodies are being used as a dumping ground which is also leading to their siltation.

North Kolkata's land use pattern mainly reflects the domination of the Residential Land use pattern. The city has grown in an unplanned manner [8]. Wards 7, 8, and 9 of Borough 1 are more close to CBD (Central Business District) area and hence the demand for these areas is more. In North Kolkata, the old dilapidated buildings are found together with modern buildings. The narrow lanes and inadequate space cause bottlenecks in the region [9]. According to a recent report published by the Times of India in April 2022, there has been the illegal filling of ponds in KMC-added areas like Garden Reach, Behala, Tollygunge, Jadavpur, and also in Dum Dum, Cossipore, Naktala, and others. Tanks which were recorded in KMC, on enquiry were found that there was no trace of water there and it's been long that it has been filled up. Thus, there is a tendency for ponds and lakes to be filled up. Borough 1 is taken as a study area to see whether still, changes are taking place or not since there is not much development taking place as such in comparison to its southern counterparts.

According to a report published in Down to Earth, the surface water bodies including the river Hooghly is polluted because of which people tend to tap the groundwater reserve and in turn deplete it [10]. The declining groundwater level has been observed as the withdrawal is higher than recharge [11–14].

The information on the water bodies is very important for the management of the resources. The inter-annual variation in surface area is because of the variation in

rainfall and mainly because of its huge exploitation by the masses. The changing climatic conditions such as temperature and precipitation influence the area of the surface water bodies. The main objective of the present study is to examine the areal change in the urban water body in Borough 1 of Kolkata metropolitan. Several works have been done on the depleting water resources that the number of water resources is dwindling which are also expected in a developing region but this study has adopted a smaller area to study the change in the area of the water bodies present in the borough and identify whether or not any change is taking place in these water bodies being affected with rising temperature, change in rainfall pattern and the increasing population.

2 Study Area

The Kolkata Municipal Corporation extends from 22.4667˚ N to 22.625° N and 88.2917° E to 88.4167° E covering nearly 187.3 sq.km.area. Consisting of 144 wards and is divided into 16 Boroughs. For the present study, Borough 1 was taken into consideration which consists of Wards 1–9 (Fig. 1), covering an approximate area of 10.4 sq. km. Thus, covering around 5.5% of the total area of the city. Borough 1 marks the northernmost extension of Kolkata including places like Sinthi, Bagbazar, Shyambazaar, Sovabazar, Sealdah, Rajabazar, etc., also known as the Old/North Calcutta as these places had seen the early development during the British Era. Over the years the city expanded toward the southern part but much has not changed in the northern part of the city. Around 65 numbers of closed surface water bodies have been identified in the said part of the city with many having a decreasing surface area. The population in different wards of Borough 1 is shown in Fig. 2.

There has been variation in the population in different wards, the maximum variation is observed in ward 6 and the least in ward 3. For the census year 2011, a decreasing trend is noticed in wards 4 to 9 but an increase is observed in wards 1 to 3. Looking into the overall population of the borough. It is seen that the population has decreased since 1991 as seen in Fig. 3.

3 Methodology

The present work is mainly based on the analysis done from Google Earth Imageries spanning a period of two decades. Imageries were taken from 2002 to 2019 for nine years depending on the availability and clarity of the Images. The water bodies located in Borough 1 of the Kolkata City were identified and polygons were drawn to find the area of the closed surface water features over different years. The area of each polygon was extracted from GIS software and further analysis was done. The rainfall data for the Kolkata city was obtained from India Meteorological Department, Alipur.

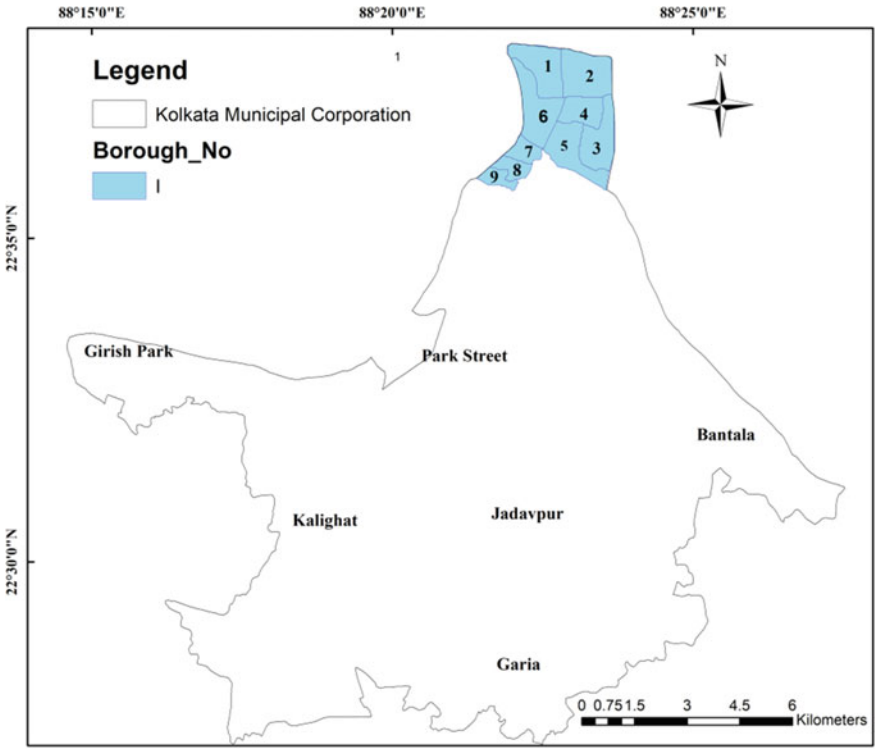

Fig. 1 Borough 1 of KMC

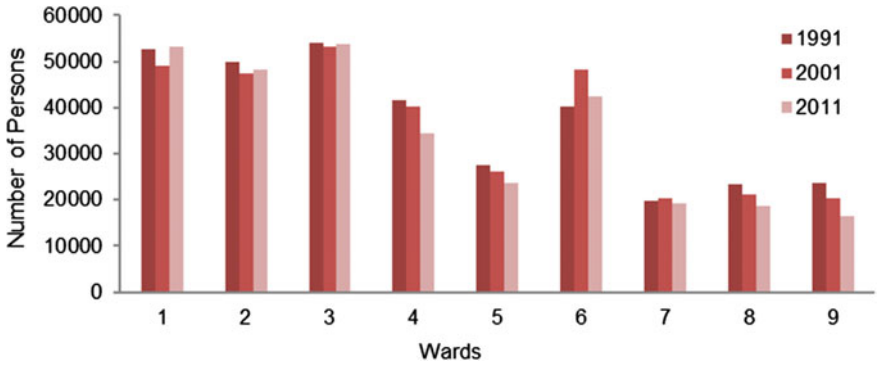

Fig. 2 Population variation in different censuses in nine wards of Borough 1

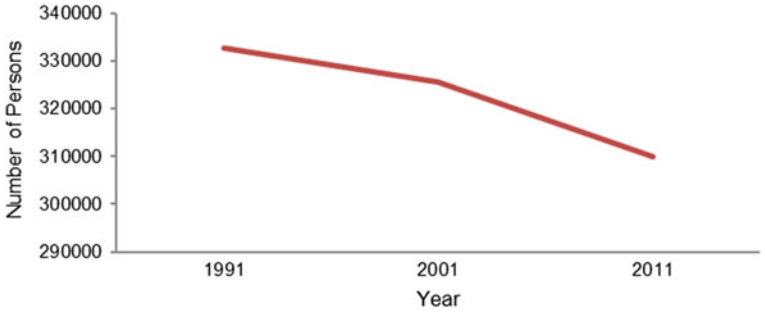

Fig. 3 The declining trend in the absolute population of Borough 1

4 Results and Discussion

From the Google Earth Imageries, the area of the surface water bodies was detected for the years 2002, 2004, 2008, 2011, 2013, 2015, 2016, 2018, and 2019 depending on the availability of the historical images. It was found that there are about 65 closed surface water features in Borough 1 of KMC (Kolkata Municipal Corporation) as seen in Fig. 4. The majority of the water bodies are situated in the northern and eastern parts of the map. It is seen that toward the southern part of the borough there is an absence of any water body which might be due to its proximity to the CBD due to which the demand for land in these areas is high. Figure 5 shows the compound bar graph for the area of water features over different years in Borough 1, KMC. The data on the area of the closed surface water bodies were collected for the years 2002, 2004, 2008, 2011, 2013, 2015, 2016, 2018, and 2019. The different colors in each bar indicate a different time frame. The area of the water bodies is as high as 2.47 ha to as low as 0.1 ha as well. Thus, a huge variation in the surface area is seen. Maximum water bodies are smaller ones with exceptions being a few.

If we compare the surface area of the four largest water bodies, located at Chitpur, Talah Jheel, Dum Dum, and Belgachia, respectively, we see that all the four water bodies show a falling trend, even though the decline is small but the slope is negative (Fig. 6).

Maximum fall is noticed in Belgachia and least in Chitpur, among the four water bodies selected. Thus there is a falling trend noticed in two of the water bodies and a slight positive variation in the other two.

The total surface area of the entire Borough if considered, the trend line shows a negative slope as seen in Fig. 7.

This proves that there is a declining trend in the surface area of the water bodies. The trend line shows a major fall in the year 2011 whereas a rise in the year 2013. This is related to the amount of rainfall in the region. Comparing it with the amount of rainfall the surface area was low due to low rainfall and vice versa. The figure below shows the surplus or deficit in the amount of rainfall. The annual normal rainfall for the city is 161 cm. Thus, a variation in the amount of rainfall is seen in Fig. 8.

Fig. 4 Image surrounded by white border showing the concentration of water bodies in Borough 1

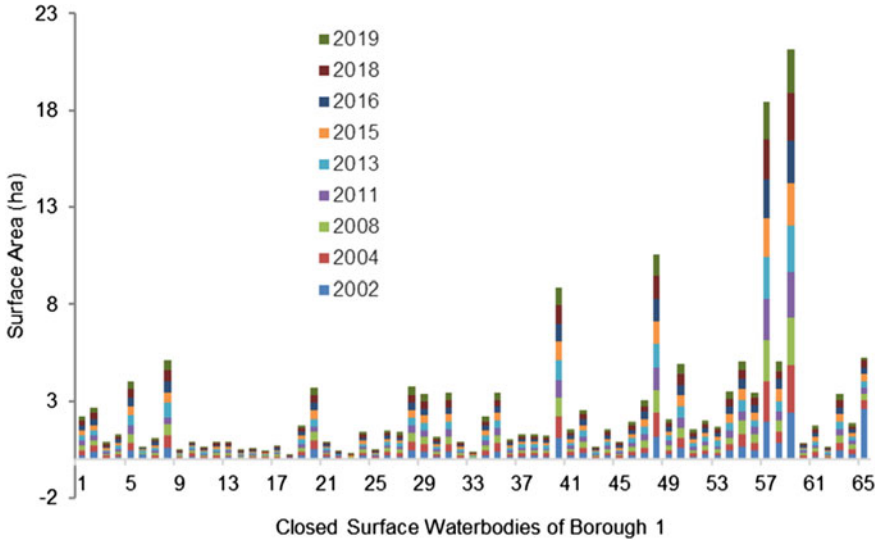

Fig. 5 Compound bar graph showing the temporal variations in the area of closed surface water bodies in Borough 1

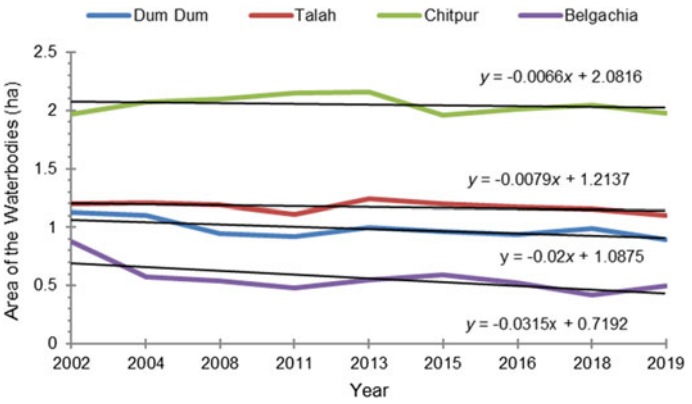

Fig. 6 Graph showing the areal trend line for large water bodies of Dum Dum, Talah, Chitpur, and Belgachia

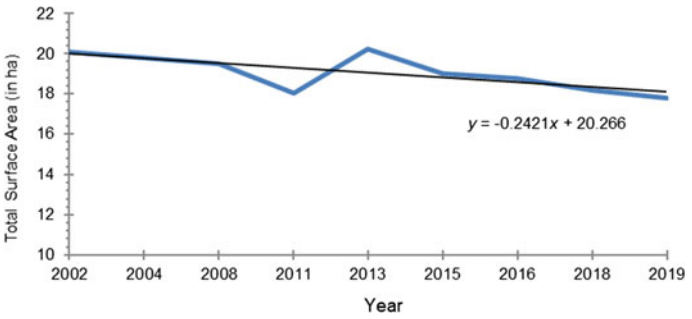

Fig. 7 Graph showing the trend line for all the closed surface water taken into account for the present study

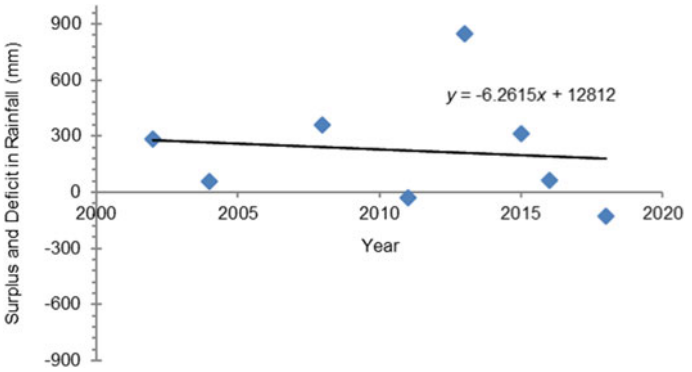

Fig. 8 Graph showing the surplus and deficit in rainfall since 2000 for the city of Kolkata

For the years 2002, 2004, 2008, 2013, 2015, and 2016 there had been rainfall more than the annual normal. Only in the years 2011 and 2018, there was a deficit in rainfall, which affected the surface area of the water bodies. In 2013, the increase in rainfall was about 46%. This also highlights the erratic nature of monsoon rainfall.

5 Conclusions

The water bodies are considered to be the lifeline of any economy. The study done for Borough 1, KMC highlights that the area of the water bodies shows a declining trend but it closely follows the rainfall pattern. The surface area increases with higher rainfall and vice versa. Since North Kolkata had seen an early start in the development process, major development has taken a toll on the open spaces and water bodies present in the area. Considering the work done in [13], it is observed that since 1987 there has been a decline in the percentage of area under the water bodies. The fully urbanized area is not seeing any major development at the present stage and thus, the existing water bodies are being filled up. On the contrary, if the surface area of the southern part of Kolkata is compared, there would have been many vanishing ponds or jheels because of the over-expanding population in the area. The northern part of Kolkata is also properly fed by surface water. Thus, too much dependence on these water bodies is less. Thus, the water bodies which are already there should be protected from further encroachment since many are being just illegally filled up [15].

References

1. Zou Z, Xiao X, Dong J, Qin Y, Doughty RB, Menarguez MA, Zhang G, Wang J (2018) Divergent trends of open-surface water body area in the contiguous United States from 1984 to 2016. Proc Natl Acad Sci 115(15):3810–3815
2. Guha S (2016) Recent decline in water bodies in Kolkata and surroundings. Int J Sci, Environ Technol 5(3):1083–1091
3. Kumar MS, Raju MV, Babu SR, Kumar MSJ (2017) Interpretation and correlative study of water simulation in surface water bodies. Int J Civil Eng Technol 8(5):1206–1211
4. Tao S, Fang J, Zhao X, Zhao S, Shen H, Hu H, Tang Z, Guo Q (2015) Rapid loss of lakes on the Mongolian Plateau. Proc Natl Acad Sci USA 112(7):2281–2286
5. Mukherjee P, Das S, Mazumdar A (2021) Introducing winter rice cropping by using non-saline tidal water influx in western basins of South 24 Parganas, India. Sci Rep 11(1):553
6. Gazi AA, Mondal I (2018) Urban heat island and its effect on dweller of Kolkata metropolitan area using geospatial techniques. Int J Comput Sci Eng 6(10):741–753
7. Singh RB, Haque S, Grover A (2015) Drinking water, sanitation and health in Kolkata metropolitan city: contribution towards urban sustainability. Geogr, Environ, Sustain 4(08):64–81
8. Haque I, Mehta S, Kumar A (2019) Towards sustainable and inclusive cities: the case of Kolkata. ORF Special Report No. 83, Observer Research Foundation
9. Mukherjee M (2012) Urban growth and spatial transformation of Kolkata metropolis: a continuation of colonial legacy. ARPN J Sci Technol 2:365–380

10. Srinivasan RK (2004) Down to Earth magazine. The Centre for Science and Environment, New Delhi, India
11. John B, Das S (2020) Identification of risk zone area of declining piezometric level in the urbanized regions around the city of Kolkata based on ground investigation and GIS techniques. Groundw Sustain Dev 11:100354
12. John B, Das S (2020) Role of electrical conductivity on salinity and mineralization due to groundwater level fluctuations in Kolkata city. IOP Conf Ser: Earth Environ Sci 505(1):012021
13. John B, Das S, Das R (2020) Effect of changing land use scenario in Kolkata Metropolitan on the variation in volume of runoff using multi-temporal satellite images. J Indian Chem Soc 97(4):555–562
14. John B, Roy P, Das S (2021) Analysing the influence of groundwater exploitation on its quality in Kolkata. In: Kumar S, Kalamdhad A, Ghangrekar M (eds) Sustainability in environmental engineering and science 2019, LNCE, vol 93. Springer, Singapore, pp 83–90
15. https://timesofindia.indiatimes.com/city/kolkata/survey-ponds-send-lists-to-kmc-mayor/articleshow/90886580.cms

An Overview of Energy Efficient Optimization and Green Networking

Rinku Supakar, Madhusmita Mishra, Md. Shafi Hussain, and Parthasarathi Satvaya

Abstract Global warming will affect not only the present generation but also future generations. The carbon footprint created by traditional energy sources highlights the need to reduce energy consumption in all possible areas, including the grid. Along with the rapid progress of information and communication technology (ICT), the ability to access the World Wide Web is also on the rise. New networks and servers are introduced regularly, but many of these busy networks are underutilized in terms of time and space. Green grids come to the rescue through more efficient implementation of energy-efficient grid technologies or the use of energy-efficient equipment. The main aim of Green Networking is to provide an energy-optimized model for data centers. There are four lines of research on different interpretations of the causes of energy loss: Interface Proxy, Green Grid from Energy-aware applications, Energy-aware Infrastructure, and Adaptive Link Rate. In this paper, we have summarized the results of some studies on green IT.

Keywords Green networking · Energy-aware applications · Information and computing technology · Energy-aware infrastructure · Interface proxying · Adaptive link rate

1 Introduction

Advances in technology and significant manufacturing have increased the use and availability of inexpensive and readily available products. Meanwhile, the widespread use of technology has increased energy demand. From 1990 to the present, global

R. Supakar (✉) · M. Mishra · Md. S. Hussain
Dr. Sudhir Chandra Sur Institute of Technology and Sports Complex, Dumdum, West Bengal, India
e-mail: rinku.supakar@dsec.ac.in

M. Mishra
e-mail: madhusmita.mishra@dsec.ac.in

P. Satvaya
Jadavpur University, Kolkata, West Bengal, India

© The Author(s), under exclusive license to Springer Nature Singapore Pte Ltd. 2023

S. Kumar et al. (eds.), *Sustainable Environmental Engineering and Sciences*,
Lecture Notes in Civil Engineering 323, https://doi.org/10.1007/978-981-99-0823-3_17

electricity consumption has doubled from 10,000 TWh to 20,000 TWh [1]. The European Commission has stated that enhancing energy efficiency will be the most suitable cost-effective way to minimize greenhouse gas emissions and achieve other long-term climate goals [2]. Although ICT is the best way to achieve this goal, it is also considered one of the major consumers of energy [3, 4]. This became an important issue on the European digital agenda in 2010 [5]. Currently, major data centers occupy between 300 and 4500 square meters and may have multiple servers [6]. A 500-square-meter data center typically consumes around 27,048 kWh every day, which is reported to be significantly higher than the energy consumption of 2,500 households in Europe [1, 6, 7].

The green grid is an example of reducing carbon dioxide emissions from a variety of technologies without compromising performance. This is useful for both general and industrial consumers. In the first case, electricity costs are reduced, and in the second case, operating costs are significantly reduced [8]. Achieving energy savings without sacrificing data center performance requires wise use of existing technologies, such as replacing them with smarter methods or putting devices to sleep or low-power states when not in use. Hibernate, proxies, power off/on resources, and other well-known methods to dynamically adjust the voltage frequency of the server.

Determining the energy-saving state of resources in traffic data is a time-consuming optimization task because of the complexity and volume of the data. Therefore, it is required to focus on heuristics or soft computing techniques to resolve this problem. It is required to build a mathematical model to determine various parameters for the implementation of an energy-efficient network. Other areas of green networking include virtualization and cloud architecture.

The rest of the document is structured as follows: Sect. 2 covers general terms and classifications related to green networks. Section 3 consists of possible solutions that balance environmental thinking with the financial aspects of this industry without compromising productivity. Section 4 lists technologies that are still in the prototype stage but have shown significant promise. Section 5 focuses on the challenges and obstacles to be overcome to carry out future research, and Sect. 6 gives final thoughts on them.

2 Incentives and General Terminology

2.1 Necessity of Energy Conservation

In recent years, worldwide awareness of the harm caused by greenhouse gases (GHG) has increased significantly. As per the report published by the European Union (EU), reducing carbon emissions by 15–20% by 2020 should keep the global temperature rise below 2 degrees Celsius [9].

Greenhouse gas emissions not only affect the environment, but also negatively impact the economy. Industry and government are working together to give green

energy a boost. Reducing energy consumption should cover a variety of industries, including the ICT sector. According to a study, the ICT sector alone accounted for 2% of the total artificial carbon dioxide production in 2007 [10]. This figure is much higher, around 10% in developed countries such as the UK [11]. However, estimating these figures is time-consuming and less accurate. At the same time, these studies confirm that ICT is one of the main origin of greenhouse gas emissions and energy consumption. This makes it possible to make networks and network devices energy-aware to make efficient and green decisions.

2.2 A General Overview of Green Networking

From the environmental point of view, green networking is committed to minimizing greenhouse gas emissions. There are two different initial steps. One is to ensure the use of renewable energy in ICT, and the other is to develop low-energy components without sacrificing performance levels. Other possible solutions include redevelop the network architecture by moving the network equipment to some strategic location. This is cost-effective for two reasons, reducing the distance between the place of production and the object of consumption, thereby reducing energy loss. The second is the cooling of the electronics. The Canadian Network for Advanced Research and Innovation (CANARIE) [12] has made notable advances in the study of cold climates and their subsequent effects on cooling.

Famous ICT companies such as Google have moved their server farms beside the Columbia River to get the benefit of the energy provided by nearby hydroelectric power plants. Water from the river is also used to cool the system. However, an increase in water temperature can affect the river ecosystem by increasing the density of algae [13]. Apart from their direct environmental impact, from an engineering perspective, the green grid can be seen as a more efficient way to reduce energy demand.

2.3 Energy Efficiency

It is difficult to accurately define the energy efficiency of ICT as ICT is a multi-faceted system that includes multiple components from various research fields such as computing, networking, control, etc. [14]. A review by Kim et al. [15] describes an energy model using static and dynamic standby power consumption, and Avelar et al. [16] measure energy dissipation by calculating the difference in energy consumed by ICT and ancillary equipment.

Energy Efficiency includes wasting energy and stopping wasting energy. Energy waste refers to the energy that is supplied to a system but not used for its primary function, including energy used by auxiliary subsystems such as cooling units in a data center. Energy loss, on the other hand, refers to the energy which is being

used by the system to work without useful output [17]. There are four main ways to improve energy efficiency.

i. Reducing energy wastage requires the introduction of more efficient components to reduce the percentage of energy introduced into the system.
ii. Efforts should be made to minimize the maintenance costs of supporting subsystems as much as possible.
iii. During downtime, the energy consumption of the system should be kept to a minimum to avoid wasting energy.
iv. Optimized algorithms should be implemented to avoid wasting energy by minimizing redundant operations.

2.4 Cloud Computing

Due to its dynamism, high bandwidth, computational power, and data storage, cloud computing has become an integral part of the green network field [18]. Utilize cloud data centers using virtualization technology to create reliable and adaptable computing environments. The ubiquitous, service-oriented, and scalable nature of cloud computing has reduced hardware and software costs. Thus, he aroused the interest of various organizations [19]. A shared pool of configurable computes resources, for example CPU, memory, etc.

The main objective of green computing is to reduce the carbon footprint that cloud providers can achieve in two ways: by using clean energy or by improving cloud energy efficiency. Cloud users can replace high-power devices with low-power devices to increase energy efficiency. Energy consumption can be reduced by providing power management to servers in the cloud, or by using simple methods for example switching them on and off or by putting them to sleep [20, 21]. Sophisticated technologies, such as auto-scaling of infrastructure, can be utilized to make a greener computing landscape [22], or virtualization technologies can be used to better manage resources [23–25].

3 Green strategies—A Discussion on Possible Schemes

Some design principles of traditional network systems, such as over-provisioning and redundancy, directly contradict the goals of a green network. Over-provisioning is common because of the deficiency of quality of service (QoS) support in Internet architectures. Networks are designed to withstand peak times, inefficiently wasting resources during downtime. Redundancy is introduced to provide fault tolerance to existing networks. These goals fundamentally conflict with the goals of environmental protection, making Green Networks an interesting and challenging area of research. Described below are four possible directions of research and we can focus on one or more of them:

i. Resource Consolidation—Traffic on this network follows a well-known daily pattern. The consolidation of resources makes it possible to provide the required skill level by using only the amount of resources required for traffic at a specific time [26].
ii. Selective connectivity—consists of a distributed mechanism that allows some devices to remain idle for a period of time in the background without interfering with the functioning of others [27, 28]. When devices are shared on the network, selective connections shut down unused resources, such as shutting down nodes to avoid receiving unnecessary broadcasts.
iii. Virtualization—Improves hardware performance by allowing multiple services to run on a single device. High-load equipment consumes less energy as compared to many high-load equipment and therefore consumes less energy. Virtualization typically involves partitioning servers that can lower the cost of hardware, improves energy management, that minimizes the cost of power and cooling. All of this together leads to a reduction in the organization's carbon footprint. US Postal Service has already virtualized 791 of 895 physical servers [29]. Virtualization is not yet designed to minimize network power consumption.
iv. Proportional Computing—This was introduced by Barosso et al. [30] and can be applied to network protocols, to a system, to some components, or to individual devices. Energy agnostic devices are the ones that consume the maximum possible energy when in the on state and in the off state the energy consumption is null. Both these excesses are undesirable as they hurt the environment as well as the finance. On the other hand, energy-aware devices are the ones in which the energy usage is proportional to the level of consumption. Some of the intermediate states between these two extremes are the single step and multistep devices where energy consumption crudely acclimates to their load. In single step devices there are two operation modes while in multistep devices there are several such thresholds.

4 Emerging Techniques

Though green networking is a new field of research there had been some standard developments and prototype results. Some of the recent works are discussed below in order of their maturity.

4.1 Adaptive Link Rate

The power consumption of Ethernet channels has been shown to be independent of usage [31–33]. Traffic signals are transmitted even when there is no data transmission. So power consumption will depend on the bandwidth of the channel and not on the actual network traffic at any given time. Various researchers have suggested that

the data rate can be throttled by blocking the communication line during periods of inactivity or by lowering the data rate during periods of low utilization. These solutions have already been approved by the IEEE Standards Committee [34]. Future work requires a careful comparison of the different strategies proposed as comprehensive views at regional and global levels do not yet exist. You should also consider the impact of QoS and server resiliency.

4.2 Interface Proxying

This is an approach in which low-power middleware performs multiple network tasks, increasing the downtime of power-hungry devices. Recent studies have shown that this low-power object can be located directly on the main device's network card for a single client, or it can be a standalone device when servicing multiple clients. The complexity range of this method includes mere filtering of unnecessary traffic such as ARP, ICMP, etc., before handling non-interactive traffic for example background FTP or P2P file sharing. Research and standardization in this area continue, and various prototypes have already been implemented [35–37].

4.3 Energy-Aware Infrastructure

Solutions in this area include redesigning the entire network architecture or integrating energy awareness into currently implemented systems. Less progress has been made than before in this area of research due to the inherent difficulties of deploying entirely new architectures or updating existing ones. Many solutions had been proposed to minimize the number of active devices at the operating level. The main focus has been on reducing energy consumption in the network without paying special attention to the reliability of the solution. Dealing with these trade-offs requires careful study. Notable research has been done to find the optimal solution without focusing on practical solutions.

4.4 Energy-Aware Application

Energy consciousness is integrated at the program level. At different levels, attempts had been made to minimize the power consumption of software. At the lowest level, the solutions are related to general aspects of computing architecture, for example operating systems having Tickless kernel cores or networking solutions such as modifying the operating system's network stack. Greening the network stack enables sleep states to optimize both current applications and design protocols.

5 Challenges and Future Directions

The ultimate goal of environmental research is to minimize energy loss and manage energy consumption so that future generations can benefit from this initiative. The development of software that can address energy efficiency and resource management challenges is essential to ensure a green network. This requires a dynamic topology. This means that the system should be able to automatically add or remove resources as needed. Some of the issues that still need to be addressed are:

i. Resources should be allocated dynamically.
ii. Optimizing the cost of execution.
iii. Reduction in consumption of energy.

A virtual machine allocation could minimize the expenses and energy consumption. This technique could be enhanced by reallocating the workload in between the machines in geographically distributed data centers. The workloads may be concentrated in green cloud data centers as well [38]. The unsolved issues in this area are:

i. Complementing the workload to the energy-efficient data centers, particularly those that depend upon renewable energy.
ii. Decreasing the number of servers with an increase in their processing powers.
iii. Increasing the size of the virtual machine while keeping the energy consumption to the minimum.

The problem of heated cloud centers must be addressed using thermal signal management techniques. Addressing this issue requires improving thermal recirculation and planning workloads with thermal considerations in mind [39].

Non-technical issues to be addressed include standards, international environmental regulations, and organizational policies. The main issues to be addressed in this regard are international regulations on the security and environmental protection of cloud computing. Currently, there are significant differences in the application of environmental protection standards from country to country. Some have introduced strict rules, while others are very lenient in this regard. Another important aspect is associated with the cost of adopting green cloud computing. As value is transferred via the service provider to the customer, the price of the service rises. Another major concern for cloud service providers is the disruption of renewable energy, which hinders conservative planning. Several cloud providers have already built data centers in some geographic locations where renewable energy is accessible or may become operationally available.

6 Conclusions

According to the authors, the main direction of future work in the field of green networks should be to achieve early consensus on standards or initial methodologies and metrics. In this regard, we need a common framework that allows us to combine different tasks to find more ambitious solutions. More time should be devoted to studying power modeling in order to create useful and reliable data databases that reflect the real world.

Energy modeling of the Internet is another less explored area of research. Understanding where your major energy costs are coming from is important to pinpoint where the biggest energy savings can be achieved, so you know where your important research should be headed. A lot still remains to be achieved as far as reducing the carbon footprint of the current technologies.

However, the main objective of networking is that the end users should get good without compromising the quality. While energy efficiency is an important issue and a much-debated topic of discussion, it must not be obtained at the cost of loss in network performance. The initial research works in the field of green technology focused primarily on the aspect of energy gain, without taking into consideration the satisfaction of the customers. According to the author, a more methodical evaluation of networking performance from the customer‘s perspective should be carried out. The technologies associated with the Green Grid has thus far been studied individually. Further studies should consider the cumulative effects of different technologies. It should also be borne in mind that sharing the above methods can compromise QoS and cause problems for end users. More time and resources must be invested in collaborative and overlapping areas of research to reach clear conclusions.

References

1. Enerdata (2011) Average electricity consumption per electrified household. http://www.wec-indicators.enerdata.eu/household-electricity-use.html
2. EU (2011) Energy Efficiency Plan 2011. Technical Report. European Commission, European Communities
3. EU (2008) Addressing the Challenge of Energy Efficiency through Information and Communication Technologies. Technical Report. European Commission, European Communities
4. Advisory Group (2008) ICT for Energy Efficiency. Technical Report. DG-Information Society and Media, European Commission. http://ec.europa.eu/information_society/activities/sustainable_growth/docs/consultations/advisory_group_reports/adhoc_advisory_group_report.pdf
5. EU (2010) A digital agenda for Europe. Technical Report. European Commission, European Communities. http://eur-lex.europa.eu/LexUriServ/LexUriServ.do?uri=com:2010:0245:fin:en:pdf
6. Emerson (2008) Data Center Users Group Special Report: Inside the Data Center 2008 and Beyond. Technical Report. Data Center Users' Group, Emerson Electric Co., Emerson Network Power, Ohio
7. Emerson. (2009) Energy Logic: Reducing Data Center Energy Consumption by Creating Savings That Cascade across Systems. Emerson Network Power, Emerson Electric Co., Emerson Network Power, Ohio, Technical Report

8. Mahadevan P, Banerjee S, Sharma P (2010) Energy proportionality of an enterprise network. In: Proceedings of the first ACM SIGCOMM workshop on Green networking (Green Networking '10). ACM, New York, NY, USA
9. Pamlin D, Szomol´anyi K (2007) Saving the Climate @ the Speed of Light–First Roadmap for Reduced CO_2 Emissions in the EU and Beyond. World Wildlife Fund and European Telecommunications Network Operators' Association
10. Global Action Plan (2007) An Inefficient Truth. Global Action Plan Report. http://globalactionplan.org.uk
11. Webb M (2008) SMART 2020: enabling the low carbon economy in the information age. The Climate Group, London
12. Canada's Advanced Research and Innovation Network (CANARIE). http://canarie.ca/
13. Katz RH (2009) Tech titans building boom. IEEE Spectrum, vol 46
14. Fanara A (2007) Report to Congress on Server and Data Center Energy Efficiency. Technical Report. U.S. Environmental Protection Agency, ENERGY STAR Program
15. Kim KH, Beloglazov A, Buyya R (2011) Power-aware provisioning of virtual machines for real-time cloud services. Concurrent Computing: Practical Experiments 23
16. Avelar V, Azevedo D, French A (2012) PUE (TM): a comprehensive examination of the metric. http://www.thegreengrid.org/
17. Mastelic T, Oleksiak A, Claussen H, Brandic I, Pierson JM, et al (2015) Cloud computing: survey on energy efficiency. ACM Computing Surveys, Association for Computing Machinery, vol 47, no 2
18. Rasheed H (2014) Data and infrastructure security auditing in cloud computing environments. Int J Inf Manag
19. Heininger R (2012) IT service management in a cloud environment: a literature review. In: Proceedings of the 9th workshop on information systems and services sciences. München, Germany
20. Wadhwa B, Verma A (2014) Energy and carbon efficient VM placement and migration technique for green cloud datacenters. In: Proceedings of the seventh international conference on contemporary computing (IC3), Noida, India, 7–9 August 2014; IEEE, New York, NY, USA
21. Wadhwa B, Verma A (2014) Energy saving approaches for green cloud computing: a review. In: Proceedings of the recent advances in engineering and computational sciences (RAECS), Chandigarh, India, 6–8 March 2014; IEEE, New York, NY, USA
22. Dougherty B, White J, Schnlidt DC (2012) Model-driven auto-scaling of green cloud computing infrastructure. Future Gener Comput Syst
23. Huang J, Wu K, Moh M (2014) Dynamic virtual machine migration algorithms using enhanced energy consumption model for green cloud data centers. In: Proceedings of the international conference on high performance computing & simulation. Bologna, Italy, 21–25 July 2014; IEEE, New York, NY, USA
24. Lin X, Liu Z, Guo W (2015) Energy-efficient VM placement algorithms for cloud data center. In: Qiang W, Zheng X, Hsu CH (eds) Lecture Notes inComputer Science, Proceedings of the International Conference on Cloud Computing and Big Data in Asia, Fuzhou,China, 16–19 December 2013, Springer: Cham, Switzerland
25. Li J, Li B, Wo T, Hu C, Huai J, Liu L, Lam KP (2012) CyberGuarder: a virtualization security assurance architecture for green cloud computing. Future Gener Comput Syst
26. Qureshi A, Weber R, Balakrishnan H, Guttag J, Maggs B (2009) Cutting the electric bill for internet-scale systems. In: Proceedings of the ACM conference on applications, technologies, architectures, and protocols for computer communications (SIGCOMM 2009), Barcelona, Spain
27. Christensen K, Gunaratne C, Nordman B, George AD (2004) The next frontier for communications networks: power management. Computer Communications, vol 27
28. Allman M, Christensen K, Nordman B, Paxson V (2007) Enabling an energy-efficient future internet through selectively connected end systems. In: Proceedings of the sixth ACM workshop on hot topics in networks (HotNets-VI), Atlanta, Georgia, USA

29. U.S. Environmental Protection Agency—Energy Star Program (2007) "Report to Congress on Server and Data Center Energy Efficiency Public Law 109–431," Tech. Rep. EPA, U.S. Environmental Protection Agency
30. Barroso LA, H¨olzle U (2007) The case for energy-proportional computing. IEEE Comput 40:33–37
31. Chabarek J, Sommers J, Barford P, Estan C, Tsiang D, Wright S (2008) Power awareness in network design and routing. In: Proceedings of the 27th IEEE annual conference on computer communications (INFOCOM 2008), Phoenix, AZ, USA
32. Hlavacs H, Da Costa G, Pierson J-M (2009) Energy consumption of residential and professional switches. In: Proceedings of the IEEE international conference on computational science and engineering (CSE 2009), vol 1, Vancouver, Canada
33. Mahadevan P, Sharma P, Banerjee S, Ranganathan P (2009) A power benchmarking framework for network devices. In: Proceedings of IFI networking 2009, Aachen, Germany
34. IEEE P802.3az Energy Efficient Ethernet Task Force, http://www.ieee802.org/3/az/index.html
35. Ecma TC38-TG4—Proxying support for sleep modes, http://www.ecma-international.org/memento/TC38-TG4.htm
36. ECMA-393 Standard, "ProxZzzy for sleeping hosts". http://www.ecma-international.org/publications/standards/Ecma-393.htm
37. Patel N, Patel H (2020) Energy efficient strategy for placement of virtual machines selected from underloaded servers in compute Cloud. J King Saud Univ—Comput Inform Sci 32(6):700–708
38. Moges FF, Adebe S (2019) Energy-aware VM placement algorithms for the OpenStack Neat consolidation framework. J Cloud Comp 8(1):1–14
39. Usmani Z, Singh S (2016) A survey of virtual machine placement techniques in a cloud data center. Procedia Comput Sci 78(1):491–498

Development of Wireless Communication-Based Intelligent Outdoor Lighting System Using Light Emitting Diodes

Parthasarathi Satvaya, Indraneel Mondal, and Saswati Mazumdar

Abstract At this time, the amount of electricity generated around the world is insufficient to meet global demand. Lighting consumes almost a quarter of the total power generated by power utilities. Reducing lighting power consumption will help save a significant amount of energy, which can then be put to better use in other areas. With the introduction of solid-state lights, i.e. Light Emitting Diodes (LED) in recent years, a hopeful future has been gained toward achieving that goal. Adding further functionality to an LED outdoor light by integrating it with an integrated system and a communication module. Not only would it conserve energy, yet it will also give information about the surrounding environment. This extra feature offers a number of benefits, including remote monitoring of luminaire health, cost savings, improved visual performance, reduced maintenance, automatic pedestrian recognition, and intelligent citizen service. A detailed development of an surrounding environment-sensitive intelligent outdoor lighting system is explained in this paper. A few characteristics of the Internet of Things (IoT) have been incorporated and studied in the current work, such as remote monitoring of the luminaire's health utilizing the Zigbee protocol technique of communication with the central computer. A 1 m diameter integrating sphere has been used to do a detailed photometric examination of the luminaire. The luminaire's IsoLux diagram was presented at various Pulse Width Modulation (PWM) duty cycles, which were controlled using a principal computer. It also suggests remedies to existing restrictions as well as some upgrades that could be explored in the near future to improve the system's trustworthiness.

Keywords Light emitting diode · Luminaire · Lighting devices

P. Satvaya (✉)
School of Illumination Science, Engineering and Design, Jadavpur University, Kolkata, India
e-mail: parthasatvaya@gmail.com

I. Mondal · S. Mazumdar
E.E. Department, Jadavpur University, Kolkata Pin-700032, India

© The Author(s), under exclusive license to Springer Nature Singapore Pte Ltd. 2023

S. Kumar et al. (eds.), *Sustainable Environmental Engineering and Sciences*,
Lecture Notes in Civil Engineering 323, https://doi.org/10.1007/978-981-99-0823-3_18

1 Introduction

With the world's fast-expanding energy consumption, conserving lighting energy in buildings has become increasingly crucial. According to [1], Lighting in Commercial Buildings [2], lighting accounts for a significant amount of energy consumption in commercial buildings, generally more than 20% of the total energy consumption. According to Shur and Zukauskas [3], innovative lighting technologies such as solid-state lighting(SSL) have been investigated, moreover with a more intelligent strategy for using these SSL systems. Wen and Agogino [4] discussed occupant comfort improvement and [5] discussed satisfaction with the built environment. [6, 7], and [8] discussed buildings with demand-side energy management through integrated lighting controls can improve overall performance while also increasing energy efficiency, which is good for the environment. One of the biggest obstacles, according to Alonso et al. [9], is developing SSL systems along with an advanced driver. Typically, they are Buck-boost or Fly-back topology switch mode power supply. They should be optimized for driving LEDs in terms of energy savings, according to Sauerlander et al. [10], while taking into account the following application requirements: cost, compactness, high degree of integration, safety, and smart solutions. As a result, current driver design trends strive to lower the size of the major components, such as the capacitors, transformer, and bridge rectifier, while also incorporating added passive elements within control unit.

Drivers, should be harmonious with existing adapter control and provide cutting-edge remotely controllable choices such as wireless and Zigbee, as well as capabilities such as light and color control features, along with energy management. According to Raychaudhuri and Gerla [11], the recent development of wireless technology and user application options has spurred a tremendous wireless demand, and wireless terminals have been expected to take over the Internet in the near future. The accessibility of the wireless resources as foundations, according to Rodoplu and Gohari [12], has resulted in an ever-increasing diversity of applications. According to Ackerman et al. (2011), current reports reveal that smartphone usage of the mobile Web and WiFi is rapidly expanding. In the long run, it does not appear that cellular capacity will be able to meet this expanding wireless demand.

In this project, an 18-W LED luminaire prototype has been developed with a dusk and dawn sensor for detecting night time along with turning the luminaire ON with its brightness control using a microcontroller. The luminaire's brightness has been adjusted by controlling the duty cycle of the PWM signal from the microcontroller. The system has been equipped with an occupancy sensor that detects the presence of people nearby and adjusts the brightness to full light after a certain time period. Data has been shared between two xbee routers and coordinator modules via wireless connection. Figure 1 shows, the coordinator module communicates to the Raspberry Pi system and a personal computer (PC) that serves as the local control station. Figure 2 shows, the router module has been connected to the microcontroller that serves as lighting system's brain.

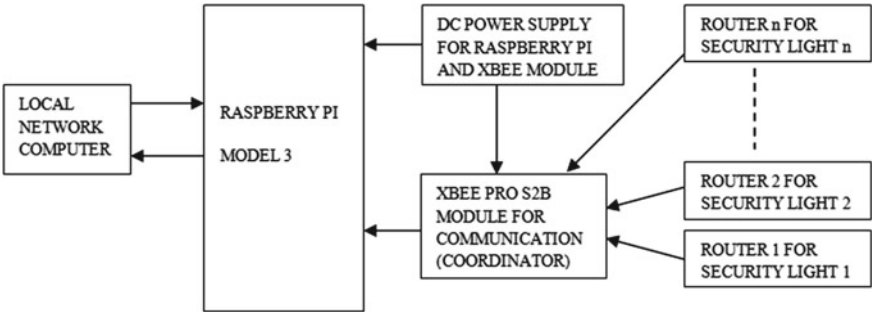

Fig. 1 Local control unit side block diagram (coordinator)

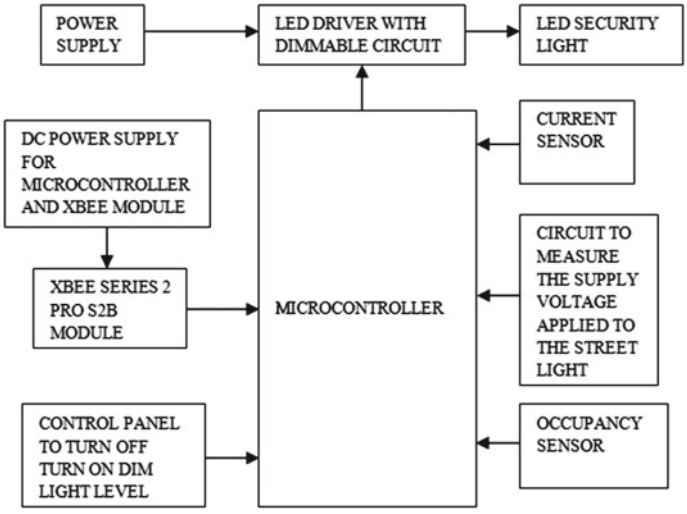

Fig. 2 Luminaire (router) side block diagram

2 Methods

In the current project, a luminaire with LED arrays has been used to create an outdoor lighting system prototype. The state of distinct situations of the luminaire was recognized with the use of several sensors. An occupancy sensor was utilized in this project to perceive the presence of any human being in front of the luminaire and alter the illuminance levels accordingly.

A Microcontroller serves as the lighting system's brain. Figure 3 shows a microcontroller with various circuits connected to the sensors, as well as a dimming circuitry and the LED driver, before being installed on the luminaire. The microcontroller's main functions are to send status information and receives command signal from the local control station unit. The microcontroller receives various data from all

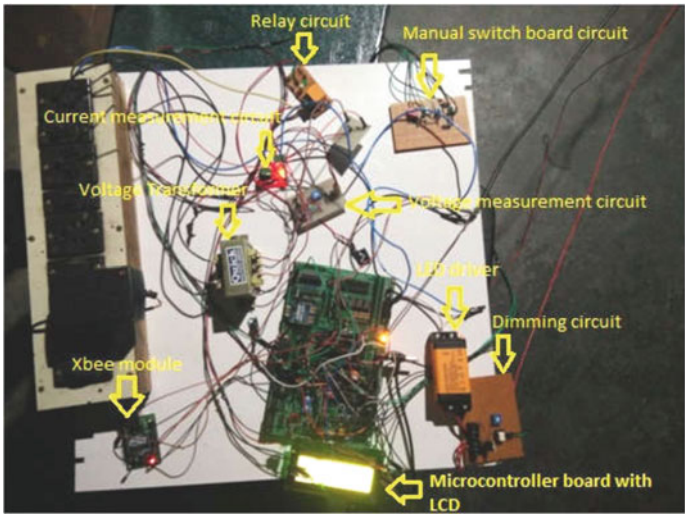

Fig. 3 Microcontroller along with various sensors

sensors for health status information accordingly communicates it via the attached xbee module. After receiving information from the xbee module unit, the microcontroller analyzes it and adjusts the luminaire's light output (brightness) accordingly. The Zigbee protocol technique has been used to communicate wirelessly in between the mentioned modules.

The microcontroller also has the ability to perceive the presence of any person nearby the luminaire. In such instance, the luminaire switches from dimmed illumination level to full brightness.

On the control unit side, the xbee module serving as a router communicates status information from the luminaire pole system to another xbee module acting as a coordinator.

The above-mentioned coordinator unit, as well as the local command and control unit, send control signals to a large number of router modules., i.e. various lighting systems, via a computer via a Raspberry Pi module. The ATMEGA32 microcontroller on the router side is connected to all of the sensors, and the xbee module is used for communication. The LED outdoor light is controlled by this block.

The data from the Luminaire has been received by this coordinator block (router side blocks). ATMEGA32, an Atmel microcontroller, has been used for controlling purposes. For serial communication, an xbee module with the Xbee Pro S2B series 2 model is utilized. On the receiver side, xbee has been used in Application Programming Interface (API) mode for broadcasting or collecting data from or to another xbee module. Figure 4 shows the microcontroller generates PWM duty cycle output. Screenshot showing the coordinator unit's xbee module receiving luminaire status information in Fig. 5. The developed prototype of the Luminaire system is displayed in Fig. 6. The illuminance at the grid points is measured using a grid mat.

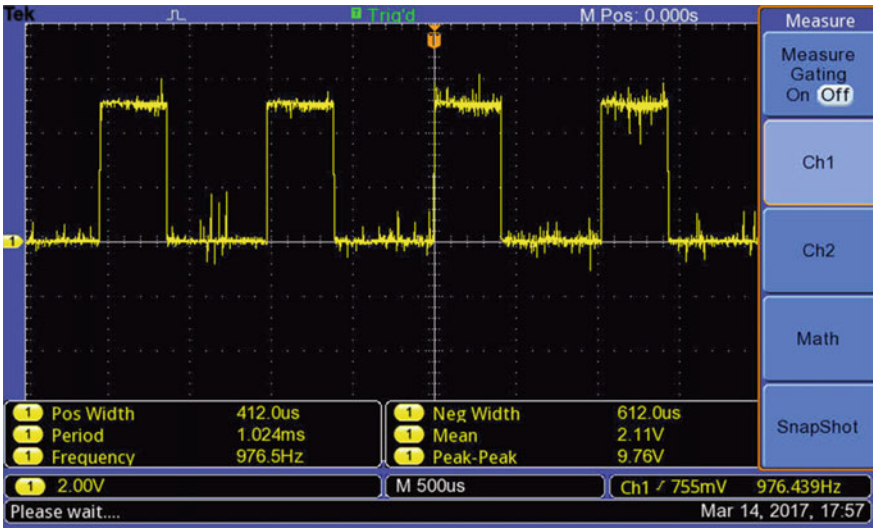

Fig. 4 PWM output from microcontroller

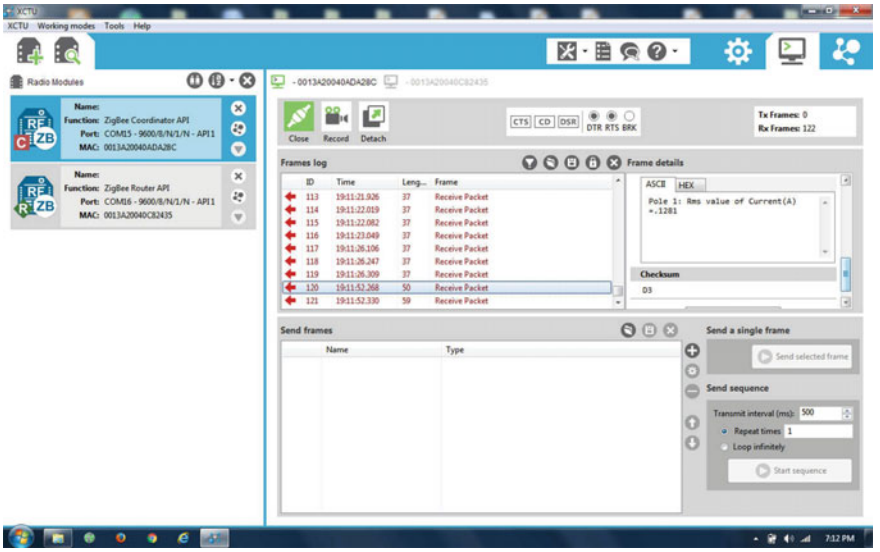

Fig. 5 Data recording by Xbee module of the luminaire

A dusk-dawn sensor detects low skylight and turns on the luminaire throughout the evening hours. As a status indicator, voltage and current sensors have been employed for detecting lamp lighting conditions. The current passing through the sensors was utilized to detect whether the luminaire was on or off. When the luminaire is dimmed,

Fig. 6 Luminaire mounted on a pole within Illumination laboratory dark room

the sensor detects a lower current. The voltage sensor measures the terminal voltage at the luminaire's connected connection. Current along with voltage sensor signals combined determine bulb failure or burnout status by using a valid voltage signal without current signal from the microcontroller. After receiving the dim signal from the microcontroller, a dimming circuit has been utilized to reduce the luminaire brightness. The luminaire will glow at full brightness for four or five hours for general lighting throughout the evening hours for a predetermined time period, after which it will be dimmed by controlling the PWM duty cycle. In presence of any human being, an interrupt signal from passive infrared (PIR) motion sensor will turn luminaire to glow to its maximum brightness level during dimmed lighting hours.

The prototype was tested in the darkroom of Jadavpur University Illumination Engineering Laboratory, and a wireless communication distance of 5.2 m has been achieved.

As an internet gateway, a Raspberry Pi Model 3 has been employed. It serves as a link to the luminaire status information that has been uploaded. The Raspberry Pi has been connected to the xbee module as shown in Fig. 7. The Raspberry Pi module has been connected to the internet via a GSM network-operated mobile phone. The Raspberry Pi Model 3 has also been used as a data collection and recording hub. Any computer with an IP address and a connection to the local network can obtain all of the information about the luminaire's state.

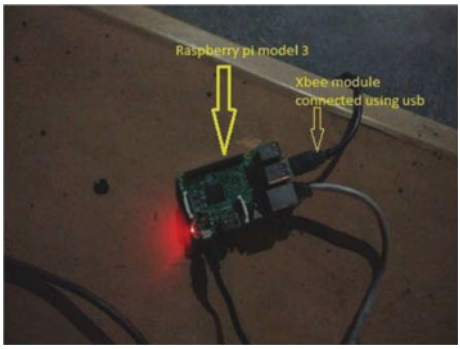

Fig. 7 Xbee module connected to raspberry Pi module

3 Results

Different illumination distribution values have been shown at various PWM duty cycles from the microcontroller to the luminaire's driver, which is passed from the local control unit for various illumination statuses.

An area of 3 m X 5.5 m has been utilized to measure illumination levels on horizontal plane from the pole for drawing isolux plot in front of the 18W LED luminaire. This space is divided into grid squares of 0.5 m X 0.5 m. apart.

For the measurement of illumination level and isolux lines diagram over the horizontal surface has been illustrated in Fig. 8. The height of the Luminaire has been kept at three (03) meter from the horizontal surface where the grid points has been drawn. Tables 1 and 2 shows the electrical and photometric parameters for the luminaire respectively.

Diameter of Integrating Sphere:	1 m
Steady State Time:	10 min
Sphere Internal Temperature:	34 °C
Communication Distance:	5.2 m

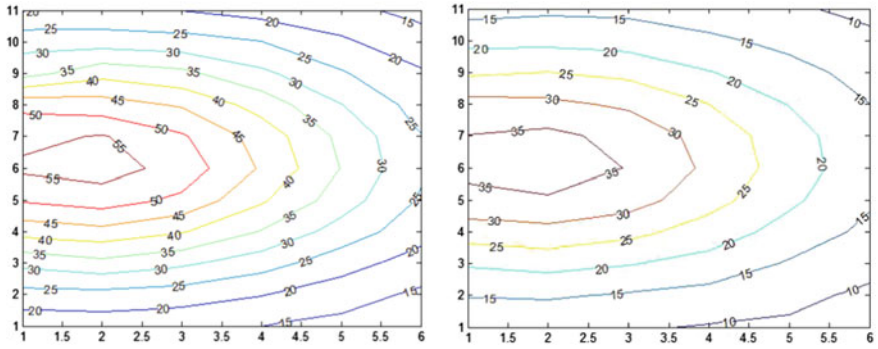

Fig. 8 Isolux lines at 100% and 30% duty cycle

Table 1 Electrical parameters of 18W Luminaire

Current (mA)	Voltage (V)	Power (W)	Frequency (Hz)	Power factor
169	230.05	18.0	49.88	0.465

Table 2 18W luminaire photometric parameters report

Lux	Luminous flux (Lumen)	CCT: (^{o}K)	x Coordinate (CIE 1931)	y Coordinate (CIE 1931)	Efficacy (lm/W)
3424	1711.60	5969.50	0.3452	0.3401	95.088

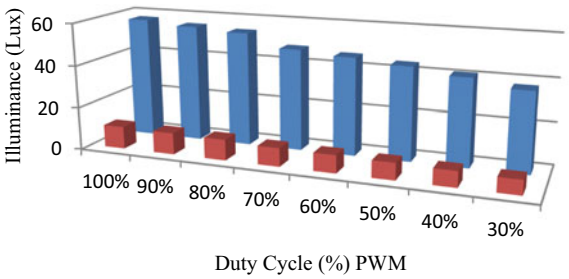

Fig. 9 Luminaire illuminance values (maximum and minimum) due to multiple duty cycles

Figure 8 shows isolux diagrams for two separate conditions for horizontally lit surface measured values: one with a PWM duty cycle of 100%, i.e. without any dimming, and the other with a duty cycle (PWM) of 30% level, i.e. when luminaire brightness has been dimmed. There have been a total of eight dimming level variations for the duty cycle shift. Figure 9 shows a bar graph with variations in minimum and maximum illuminance for changing PWM duty cycle. The output result shows the luminaire efficacy (lm/W) has been 95.88, which represents its performance is better with respect to conventional outdoor lighting systems with low environmental carbon footprint.

4 Conclusion

The goal of this project is to create a prototype for an environment-sensitive intelligent outdoor lighting system with low carbon footprint. The lighting system sends and receives data between two xbee modules using the Zigbee communication protocol, which allows the lighting system to be intelligent and self-contained. The lighting system has a communication distance limitation, which can be overcome by using a modified version of the xbee modules available in the market. It also allows for system supervisory lighting system control from a local control unit. The system is connected to a Raspberry Pi module with a specific IP address to transmit and receive data via the internet network.

References

1. Alonso, J. M. et aI, (2012) Analysis and Design of the Integrated Double Buck-Boost Converter as a High Power-Factor Driver for Power-LED Lamps. IEEE Trans on Industrial Electronics, vol. 5 9, No. 4 1689–1697.
2. Li DHW, Cheung KL, Wong SL, Lam TNT (2010) An analysis of energy-efficient light fittings and lighting controls. Appl Energy 87(2):558–567
3. Lighting in Commercial Buildings (2003) U.S. Energy Inf. Admin.,Washington, DC, USA. [Online]. Available: ttp://www.eia.gov/emeu/cbecs/cbecs2003/lighting/lighting1.html
4. Mahdavi A, Mathew P, Kumar S, Hartkopf V, Loftness V (1995) Effects of lighting, zoning, and control strategies on energy use in commercial buildings. J Illum Eng Soc 24(1):25–35
5. Raychaudhuri D and Gerla M (2005) New architectures and disruptive technologies for the future internet," Tech. Rep. GDD-05–04, NSF, http://www.geni.net/GDD/GDD-05-04.pdf
6. Rodoplu V and Gohari A. A (2008) Challenges: Automated design of networking protocols, in *Proc. ACM MOBICOM*, 271–278.
7. Roisin B, Bodart M, Deneyer A (2008) and D'Herdt P. Lighting energy savings in offices using different control systems and their real consumption Energy Buildings 40:514–523
8. Rubinstein F, Jennings J, Avery D, Blanc S (1999) Preliminary results from an advanced lighting controls testbed". J. Illuminating Eng. Soc. 28(1):130–141
9. Rubinstein F, Treado S, and Pettler P (2003) Standardizing communication between lighting control devices. in *Proc. 38th Annu. Meet. IEEE Ind.Appl. Soc.*
10. Sauerlander, G. et aI (2006) Driver electronics for LEDs, in Proc of 41'1 Conf Rec. IEEE lAS Annual Meeting, Tampa, FL, vol. 5, 2621–2626
11. Shur MS, Zukauskas A (2005) Solid-state lighting: Toward superior illumination. Proc IEEE 93(10):1691–1703
12. Wen Y-J, Agogino AM (2011) Personalized dynamic design of networked lighting for energy-efficiency in open-plan offices. Energy Buildings 43(8):1919–1924
13. Satvaya P, Mondal I, Mazumdar S (2018) Development of an Intelligent Security lighting system using wireless Communication technology published in IJETSR 5(1):1695–1701

Comparative Analysis of Water Storage Change in Ganga–Brahmaputra Basin Based on GLDAS Model Using QGIS Software

Sourav Kumar Singha, Souvik Chakraborty, Arnab Chanda, and Moumita Das

Abstract One of the most important variables for rapid expansion and urbanization is water availability. However, the water demand is growing rapidly with the increase in population as well as industrialization which has resulted in critical conditions of unsustainability and degrades the environment. As a result, data on the temporal and spatial accessibility of water will be valuable for making the best use of water resources. The water balance was can be used to calculate the seasonal and geographical availability patterns of water in order to improve water resource management. The study of water balance using the **QGIS** software with **GIS** and **remote-sensing** data is very useful for finding out the water budget for an whole basin. So the water budget is explored by GIS techniques using QGIS. The Maps have been prepared for the water budget components like Precipitation, Evapotranspiration, Strom surface runoff, and Baseflow-groundwater runoff. The water budgeting is done from the year 2005 to 2020 using the components with the help of GLDAS-2.2 or Global Land Data Assimilation System and from IMERG (The Integrated Multi-satellite Retrievals for GPM). This study indicates the variation of water storage from the year 2005 to 2020 in **Ganga–Brahmaputra river basin**. It is also observed that the water storage is increased in the entire basin from 310,134,186.8 to 538,657,359.2 km^3 from the year 2005 to 2020 which correlates with the merged satellite-gauge precipitation estimate from IMERG.

Keywords Water budget · Remote sensing · Water storage · GIS · Ganga–Brahmaputra river basin

1 Introduction

The water balance has been used to calculate irrigation demand patterns over time and space, as well as the soil moisture stressors that crops and wild plants can withstand. The water table is calculated for the total watershed or for single soil profile which

S. K. Singha · S. Chakraborty (✉) · A. Chanda · M. Das
C.E. Department, Dr. Sudhir Chandra Sur Institute of Technology and Sports Complex, Kolkata, India
e-mail: schakraborty@dsec.ac.in

© The Author(s), under exclusive license to Springer Nature Singapore Pte Ltd. 2023

S. Kumar et al. (eds.), *Sustainable Environmental Engineering and Sciences*,
Lecture Notes in Civil Engineering 323, https://doi.org/10.1007/978-981-99-0823-3_19

indicates the adjustment between the approaching of water and by outpouring of water by precipitation and evapotranspiration, respectively, groundwater revives as well as stream flow [1]. Remote sensing is a tool which has the ability to obtain orderly, fast, and repetitive coverage of natural resource management. Remote sensing has become a unique technique by geographic information systems (GIS), which have broadened the range of applications of remote sensing in natural resource management. A research was conducted at Nana Kosi watershed using TM model to find the annual surplus for the duration of June to August and the rest of the months are area deficit periods [2]. GLDAS is global for its unique qualities. It also has certain distinct characteristics like high-resolution and is used for terrestrial modeling system which consolidates ground-based and observation of satellites in order to create ideal ground surface fields of real-time states and fluxes [3]. A research was conducted over continental China and it is observed that GLDAS-1 has some genuine problems in its constraining information, with huge precipitation inaccuracy in 1996 as well as huge temperature inaccuracy in the period 2000–05 [4]. Water balance models also prepared coupling which is optimized with genetic algorithm. It is observed that coupled models performed better than the original [5]. Water budget is used to determine the quantity of water in the land required for utilization [6]. GRACE satellite observations are used to monitor groundwater resources effectively with NASA's CLSM or Catchment land surface model to derive the terrestrial storage of water globally which helps to monitor the groundwater effectively [7, 8].

Human impacts can be forecasted using the water balance on the hydrological cycle. The hydrologic impacts of climate adjustment or vegetation cover changes can be calculated at a very initial position of planning. In spite of the fact that the expectations may be approximate, they are sufficiently precise to show whether a plan is hydrologically sound or not. As a result, it's a useful tool for assessing a region's water issues.

For that reason an attempt has been made for studying the water balancing in the Ganga–Brahmaputra river basin using GLDAS and IMERG using the remote sensing and GIS techniques. Water budgeting is a process of comparing the water allowance to the estimated landscape water requirement. To estimate the water balance, it is important to collect information on precipitation (water supply) and potential evapotranspiration (climatic water need). By using evaporation data, empirical equations of the potential evaporation data can be estimated also analytical approaches can be used to calculate the water balance. In Eq. 1 the balance is expressed considering a drainage basin. The water balance of a small drainage basin carried by an impermeable rock can be expressed by Eq. 1.

$$\mathbf{Pr} = \mathbf{In} + \mathbf{AETn} + \mathbf{OFw} + \Delta\mathbf{SM} + \Delta\mathbf{GWS} + \mathbf{GWRn} \tag{1}$$

The balance of water components on a hillside or a watershed. Where, Pr = Precipitation; In = interception; AETn = actual evapotranspiration; OFw = overland flow; ΔSM = Change in soil moisture; ΔGWS—change in groundwater storage; GWRn = groundwater runoff.

Analytical Method used for Water Balancing: Water balance can be calculated by using either analytical or using empirical equations or by evaporation data. The technique founded by Thornthwaite and Mather [1] generally used for the computation of water balance potential evaporation data. This method uses lengthy average potential evopotranspiration and average monthly rainfall, and soil and vegetation features. **PET** is primarily determined by climatic circumstances (solar energy) and is unaffected by vegetation, soil water content, soil type, or ground control strategies (Mather, J., 1978). **PET** can also be estimated using some techniques like the Thornthwaite method, penman's method, etc.

Penman–Monteith Method: The FAO Penman–Monteith procedure is widely used as the standard procedure for computing reference evapotranspiration from the meteorological information. Thornthwaite Procedure: Computation of ET in this procedure is primarily depends on temperature. The model by Thornthwaite and Mather [1] (1955) was recommended for the evaluation of the spatial and temporal shape of water deficit and water surplus status of water balance.

2 Objectives

Here our primary objective is to determine the water budgeting rather we can say to determine the water budget for Ganga–Brahmaputra basin using the inflow data from snowmelt, precipitation, and the outflow by groundwater recharge, evapotranspiration, and streamflow.

3 Study Area

The drainage area of the river Ganga is located in the middle of east longitudes 73.3E, 97.8E, and north latitudes 21.5N, 31.5N which consists of four countries, they are India, Nepal, Bangladesh, and China with having major parts in India (Fig. 1).

The Ganga–Brahmaputra basin expands over an region of 1,736,903.46 km^2. The Himalayas are the source of the Ganga–Brahmaputra rivers. India has a total catchment area of 862,769 km^2. Ganga and Brahmaputra streams begin from the Himalayas. After their due course, Brahmaputra flows through other nations like Bhutan, Bangladesh, China, and Nepal. It also streams through different northern states like Rajasthan, Uttar Pradesh, Haryana, and West Bengal in India.

The Ganga–Brahmaputra basin is the largest densely populated basin also the ground is highly fertile in the sub-continent. The basin is at a junction of plains and mountains which makes this basin distinctive in its area.

The Himalayas and the Sundarbans delta are notable features located in the middle of the plains of the river Ganga and Brahmaputra river. It is enhanced with life and vegetation in both the Ganga and Brahmaputra Basin and is a proud essence of the perpetual interaction between people and environment.

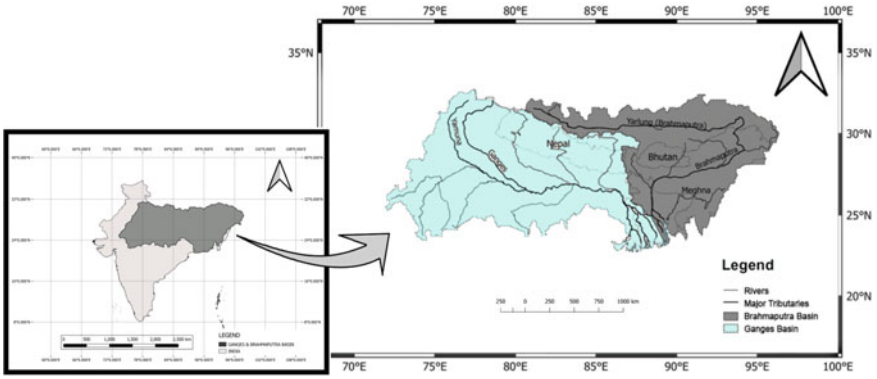

Fig. 1 Catchment area of the river Ganga and Brahmaputra

Satellites and Sensors for Water Budget Components: In Table 1, the details of Satellites, Sensors, Spectral measurements and Water budget components are given.

We have used GLDAS and IMERG as data sources for the water budget components.

In GLDAS our Inputs are rainfall from meteorological data from global reanalysis and observations, TRMM and multi-satellite, Water or Land mask, vegetation Mask, Leaf Area Index from MODIS, and Snow and Clouds from DMSP and NOAA satellites. The output data that we can get Surface/Sub-surface runoff, water content of soil, evapotranspiration and equivalent snow water.

Table 1 Satellites and sensors for water budget components

Satellites/Missions	Measurements (spectral)	Name of sensor	Water budget component
TRMM and GPM	TRMM Microwave imager: 10–85 GHz GPM-Microwave imager: (10–183) × 10^3 MHz Precipitation Radar (Ku and Ka)	Microwave Radiometer and RADAR TMI, PR GMI, DPR	Precipitation
Terra MODIS and Aqua MODIS	Visible, Near IR, Middle IR	Moderate Resolution Imaging Spectroradiometer	Snow Cover, Evapotranspiration
Landsat 7 and 8	Visible, NIR, MIR, TIR	Thematic M and ETM, OLI	Evapotranspiration
SMAP	L(Band)	Microwave Radiometer	Soil Moisture
GRACE and GRACE-FO	K(Band)	Microwave Radar	Groundwater
Jason 2, 3	C(Band) and Ku(Band)	Altimeter	Reservoir Height

Table 2 GLDAS MODEL with their Parameters

Model	Parameters	Spatial and temporal resolution
GLDAS-2.1	Evapotranspiration subsurface Runoff/Runoff Terrestrial water storage Snow water equivalent Precipitation	1° × 1°, 3 hourly/month
GLDAS-2.2	Evapotranspiration Runoff/Subsurface Runoff Terrestrial water storage Snow water equivalent	0.25° × 0.25°, daily

GLDAS-2.1 provides the data from the year of 2000 till date with a resolution (spatial) of 1° × 1° and temporal resolution of 3Hourly/Month and temporal resolution of 3Hourly/Month and GLDAS System 2.2 provides the data from the year of 2003 till date with a spatial resolution of 0.25° × 0.25°. Hence we have used GLDAS-2.2 to get our result with better accuracy in our study area.

There are primarily three components in NASA GLDAS-2: GLDAS-2.0, GLDAS-2.1, and along with that GLDAS-2.2 and 2.0 providing us a temporally consistent series from the year 1948 through 2014 with the dataset of meteorological forcing.

In Table 2 the versions of GLDAS are shown along with the parameters that we have used in our model.

Data Input: The data source of water budget components can be found in Table 3, using GPM, IMERG, and GLDAS. The data access points are Giovanni, SERVIR Global, AppEEARS, etc. We consider Giovanni as data access point to access all water budget components.

Table 3 Data sources of water budget components

Water budget component	Source	Data access
Precipitation	GPM IMERG, GLDAS	Giovanni
Evapotranspiration	ALEXI, GLDAS	SERVIR Global, Giovanni
Soil moisture	SMAP, GLDAS	AppEEARS, Giovanni
Snow melt	GLDAS	Giovanni
Runoff	GLDAS	Giovanni

Methodology Water Budget Estimation:

The unit of the ET and Precipitation is in kg/m2/sec and for Base flow and Surface runoff is in kg/m2/3 h. So the data are converted by multiplying 3600*24*365 and 8*365, respectively, to get the annual data.

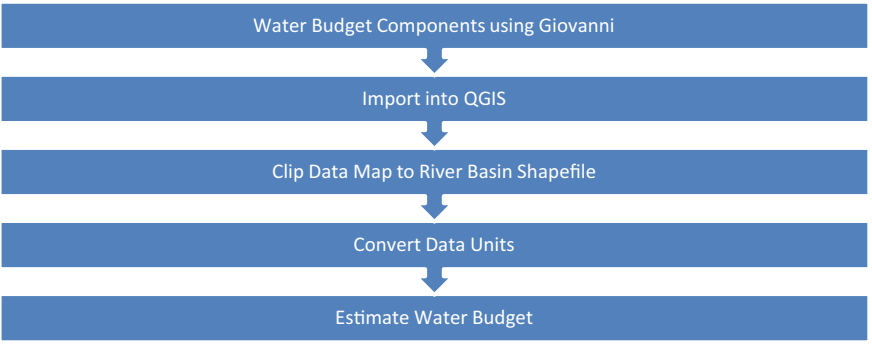

Precipitation Data (IMERG): Precipitation data from year 2000 to 2020 gathered from Giovanni (Time, Area-Averaged Merged satellite-gauge precipitation). In IMERG we get Time Averaged Map of Merged satellite-gauge precipitation estimate. (Region 73.3E,97.8E, 21.5N, 31.5N).

In Graph 1 we can see the variation in precipitation from the year 2000 to 2021. So in this study the water budget is determined and the change in total quantity of water is observed. In Fig. 2 the time series merged satellite monthly gauge precipitation estimate is shown in mm/month from the year 2000 to 2021.

Water Budget Components **(GLDAS)**: From GLDAS-2.2 Evapotranspiration, Storm surface runoff and Baseflow-groundwater runoff are used to calculate the water balance from 2005 to 2020 from Giovanni. Now using these data we will

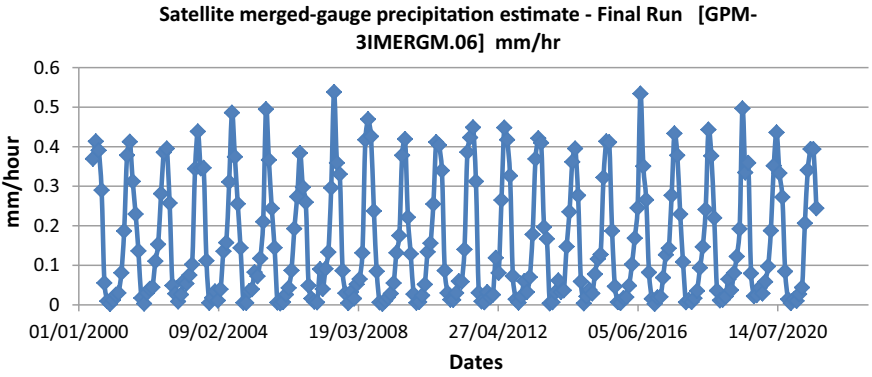

Graph 1 Satellite merged-gauge precipitation estimate—Final Run [GPM-3IMERGM.06] millimeter/hour

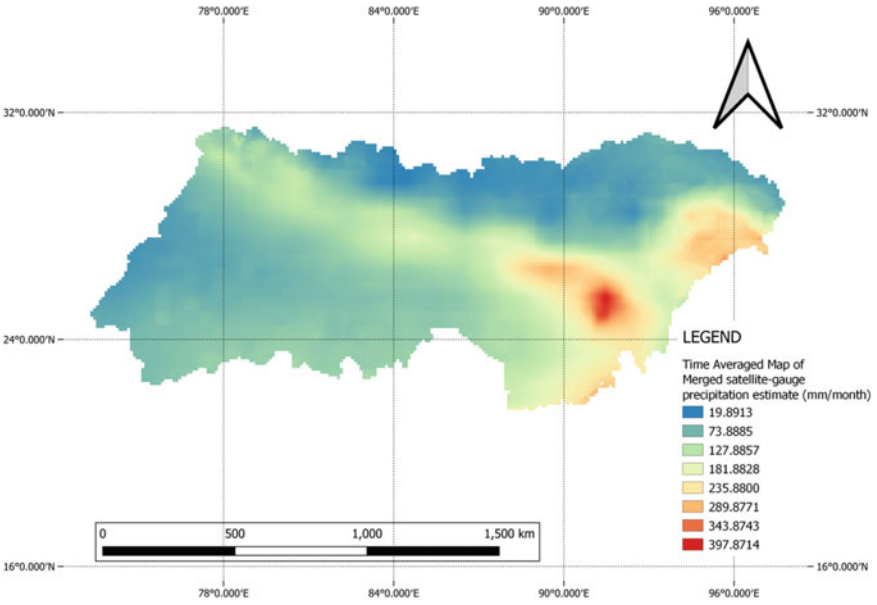

Fig. 2 Time averaged map—final run monthly 0.1 deg. [GPM GPM_3IMERGM v06] mm/month

verify the variation in water quantity for the following years using QGIS. From Tables 4, 5, 6, and 7 it is observed that the maximum precipitation is in the month of July (Figs. 3, 4, 5 and 6).

Steps for Determination of Water Budget using QGIS:

- Importing the base map.
- Importing the shape file of the river basin (Vector Layer).
- Importing the downloaded data for water budgeting.
- Clipping and Referencing the data with the shape file.
- Converting the data units using Raster Calculator.
- Generation of water balance Map using Raster Calculator.
- Determination of water quantity for the year using **Zonal Statistics**.

It is observed from the above figures that the zonal mean for evapotranspiration is highest in the year 2005 (849.328) and it is gradually decreasing from 849.328 (Fig. 7) to 765.027 (Fig. 10) from the year 2005 to 2020 (Figs. 8, 9, 11, and 12).

The water balance in mm is calculated from the year 2005 to 2020 using raster calculator in QGIS by subtracting Strom surface runoff, Evapotranspiration, and Baseflow-groundwater runoff from Precipitation data. It is observed that ET, strom surface runoff and baseflow-groundwater runoff dominates the precipitation more in the year 2005 than in the year 2010 in UP and MP regions of India (Fig. 13).

Table 4 Merged satellite-gauge precipitation estimate (2000–2004) *millimeter/hour*

Date/Month vs Year	2000	2001	2002	2003	2004
	Millimeter/hour	Millimeter/hour	Millimeter/hour	Millimeter/hour	Millimeter/hour
1st January	_	0.011892181	0.029955782	0.025921803	0.03379884
1st February	_	0.025440579	0.040313054	0.060171921	0.01097451
1st March	_	0.030093506	0.044546288	0.053829067	0.039552238
1st April	_	0.080917664	0.110300072	0.075067282	0.135566056
1st May	_	0.186904773	0.152863801	0.102338009	0.157253638
1st June	0.369475007	0.378359139	0.281148076	0.344558656	0.310876727
1st July	0.413583845	0.412702143	0.385846853	0.438621491	0.486014813
1st August	0.390814722	0.312221706	0.395440757	0.345379233	0.374506086
1st September	0.290005356	0.229606926	0.257435739	0.346616	0.255547225
1st October	0.055278156	0.136368021	0.048706364	0.111617357	0.144328594
1st November	0.00946874	0.017366409	0.028120861	0.005001716	0.005372
1st December	0.002274364	0.00300167	0.008349869	0.017711945	0.004895919

Similarly in the year 2020 we can observe the precipitation is higher compared to the year 2015 which is also dominated by the ET, strom surface runoff, and baseflow-groundwater runoff.

By using zonal statistics in QGIS the zonal mean can be determined for each year. In this study we have determined the zonal mean from the year 2005 to 2020. It is noted that the zonal mean for precipitation is gradually increasing from 178.55 (Fig. 11) to 310.12 (Fig. 14) from the year 2005 to 2020.

The volume of water storage is also determined from the year 2005 to 2020 in Table 8 which is also increased from the year 2005 to 2020 which is shown in Graph 2.

Table 9 represents the total Merged satellite-gauge precipitation which is from IMERG. Yearly Merged satellite-gauge precipitation estimate is determined from Tables 4, 5, 6, and 7 which is in millimeter/hour. It is multiplied by 24 * no of days in a month * no of months in a Year.

The correlation coefficient between the change in water storage for Ganga–Brahmaputra river with the total Merged satellite-gauge precipitation estimate (mm/month) we can find 0.812 from the year 2005 to 2020.

Table 5 Merged satellite-gauge precipitation estimate (2005–2010) *millimeter/hour*

Date/Month vs Year	2005	2006	2007	2008	2009	2010
	Millimeter/hour	Millimeter/hour	Millimeter/hour	Millimeter/hour	Millimeter/hour	Millimeter/hour
1st January	0.034301989	0.006847586	0.006155998	0.032350384	0.010698188	0.007135096
1st February	0.039555829	0.026011918	0.089996204	0.015965078	0.019484917	0.023809617
1st March	0.082692251	0.042831596	0.040107548	0.051797882	0.028453954	0.051647972
1st April	0.072278582	0.087016717	0.091305189	0.065109782	0.055027679	0.13402392
1st May	0.117207058	0.192584038	0.133267581	0.131480113	0.131637678	0.155827984
1st June	0.210303575	0.273644149	0.295968741	0.417572975	0.175205573	0.254820198
1st July	0.495007455	0.384211779	0.538280845	0.469413042	0.378323734	0.411803782
1st August	0.366541564	0.297627628	0.359173477	0.425984055	0.419580579	0.404203683
1st September	0.244153023	0.259503454	0.330684185	0.237513155	0.221578926	0.339793742
1st October	0.144652486	0.04867411	0.086402796	0.084751405	0.128825366	0.08660432
1st November	0.005882184	0.015974328	0.029418496	0.006224882	0.026773447	0.030087175
1st December	0.003712683	0.008177368	0.004300617	0.00236884	0.005308644	0.01313081

Table 6 Merged satellite-gauge precipitation estimate (2011–2015) *millimeter/hour*

Date/Month vs Year	2011	2012	2013	2014	2015
	Millimeter/hour	Millimeter/hour	Millimeter/hour	Millimeter/hour	Millimeter/hour
1st January	0.01245366	0.032290239	0.021284923	0.031764004	0.038317666
1st February	0.029897301	0.019473543	0.060059536	0.06160273	0.028939216
1st March	0.059762113	0.025649518	0.032333884	0.032479167	0.077488117
1st April	0.058392823	0.11875888	0.07010299	0.036567241	0.116044119
1st May	0.140182152	0.080690712	0.178097546	0.147240773	0.127283111
1st June	0.386355668	0.26482293	0.369015664	0.235145643	0.322048128
1st July	0.423362195	0.448272496	0.421431333	0.361473888	0.413477629
1st August	0.448769301	0.417735934	0.409916371	0.395421863	0.411269635
1st September	0.312149644	0.326535255	0.196553603	0.276800781	0.187002406
1st October	0.030826248	0.072602846	0.167084247	0.059287157	0.046738427
1st November	0.008799936	0.014153438	0.003907269	0.00384796	0.006749312
1st December	0.006474927	0.005544588	0.006722703	0.021341141	0.004574383

4 Conclusion

The study of water balance using the IMERG and GLDAS (Global Land Data Assimilation System) using RS along with GIS in QGIS software is found to be helpful to find out the duration of water surplus as well as moisture deficit for the whole river basin. We also get to know the quantity of water for each sub-basin in every year where it is observed that the water storage is increased from 2005 to 2020 as shown in Graph 3. It is also observed that total Merged satellite-gauge precipitation is also increased from 1335.68 mm/year to 1403.16 mm/year from the year 2005 to 2020. Also we can conclude that the rate of change of water storage for Ganga–Brahmaputra river is correlated with the total Satellite merged–gauge precipitation estimate in mm/month with a correlation coefficient of 0.812.

Table 7 Merged satellite-gauge precipitation estimate (2016–2021) *millimeter/hour*

Date/Month vs Year	2016	2017	2018	2019	2020	2021
	Millimeter/hour	Millimeter/hour	Millimeter/hour	Millimeter/hour	Millimeter/hour	Millimeter/hour
1st January	0.016805835	0.018631136	0.007072411	0.020893212	0.042866193	0.013478086
1st February	0.019338628	0.020475617	0.01663783	0.064693786	0.028922791	0.00991433
1st March	0.048527565	0.068767615	0.035423294	0.037346527	0.058344733	0.02725945
1st April	0.102200098	0.126800269	0.093884893	0.08038301	0.097343721	0.043942522
1st May	0.168595016	0.143017516	0.146835715	0.122419715	0.187622339	0.206536725
1st June	0.245152935	0.276985973	0.241056517	0.192199275	0.351786375	0.340544432
1st July	0.534251571	0.433547944	0.44330591	0.496711582	0.436138391	0.394055218
1st August	0.350810379	0.378056467	0.37698859	0.334787339	0.33307904	0.393714458
1st September	0.265516937	0.229408294	0.219985917	0.359010905	0.272605807	0.244388804
1st October	0.081935562	0.108505711	0.036016177	0.079579964	0.084499165	_
1st November	0.015409766	0.006584809	0.011267202	0.021946596	0.013968456	_
1st December	0.002594557	0.012359277	0.012696205	0.024560008	0.004391333	_

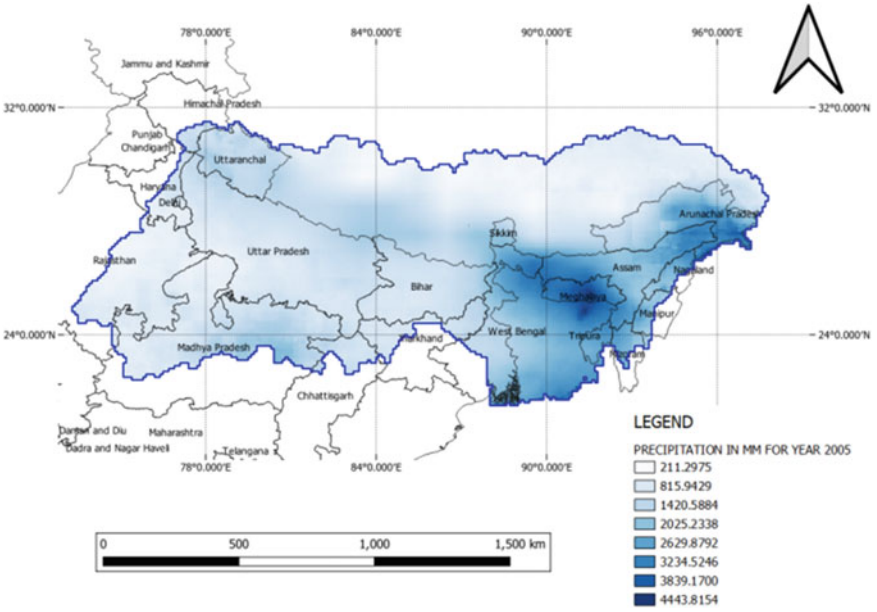

Fig. 3 Total precipitation 2005 (annual)

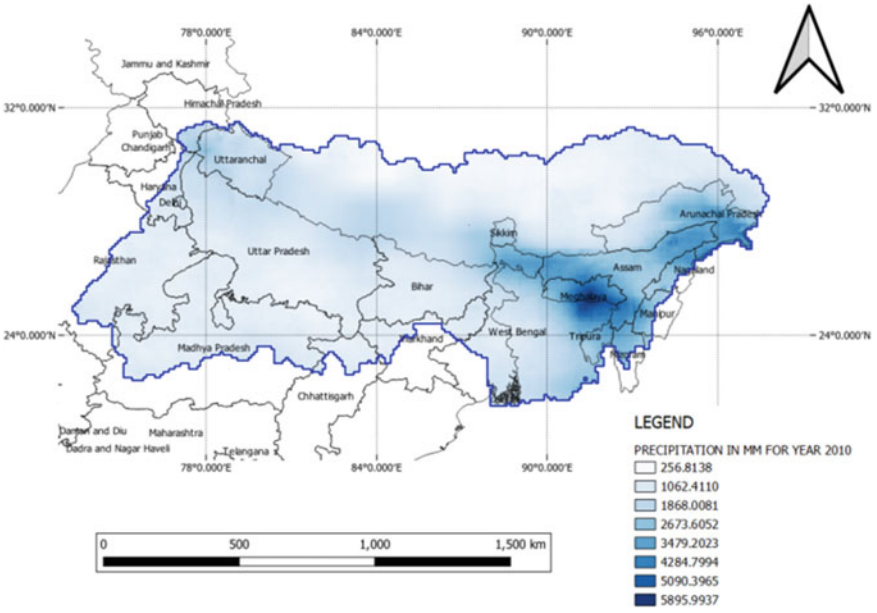

Fig. 4 Total precipitation 2010 (annual)

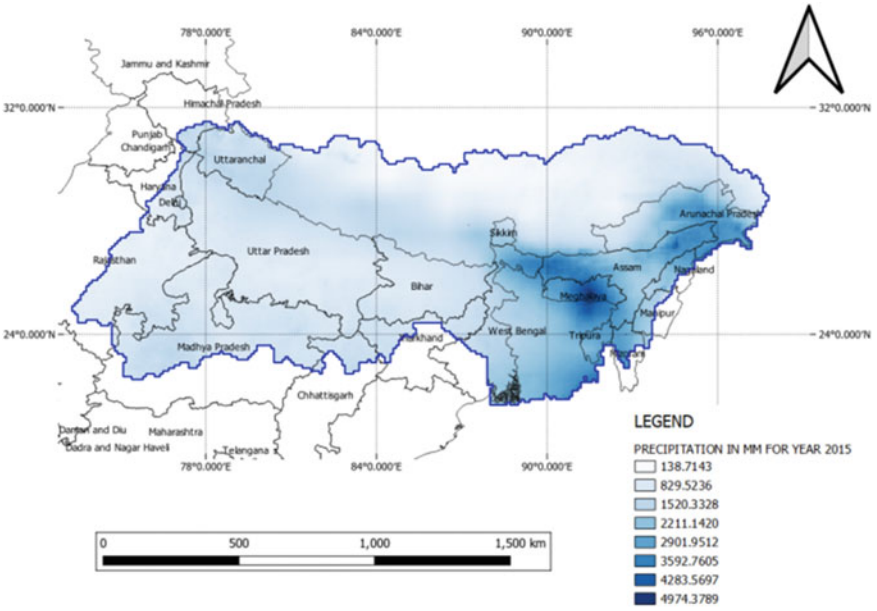

Fig. 5 Total precipitation 2015 (annual)

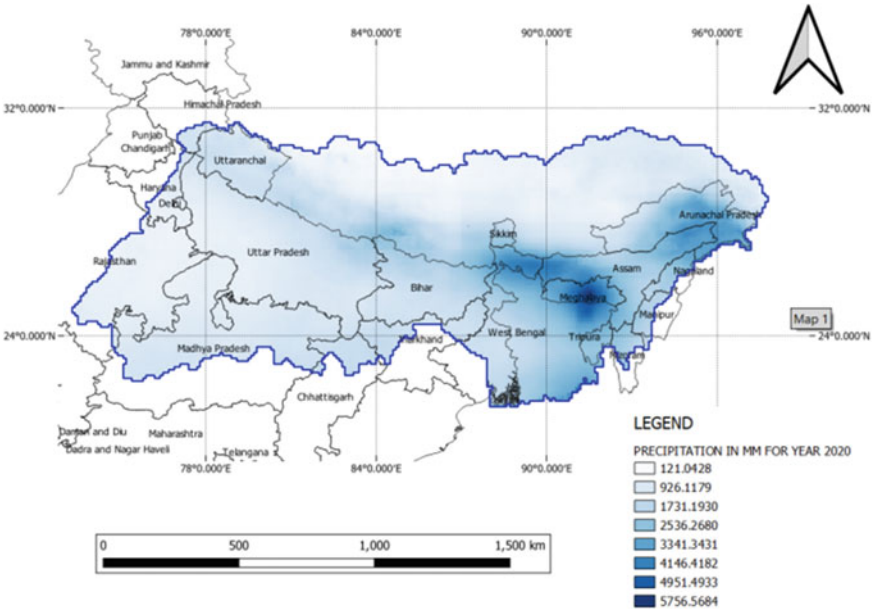

Fig. 6 Total precipitation 2020 (annual)

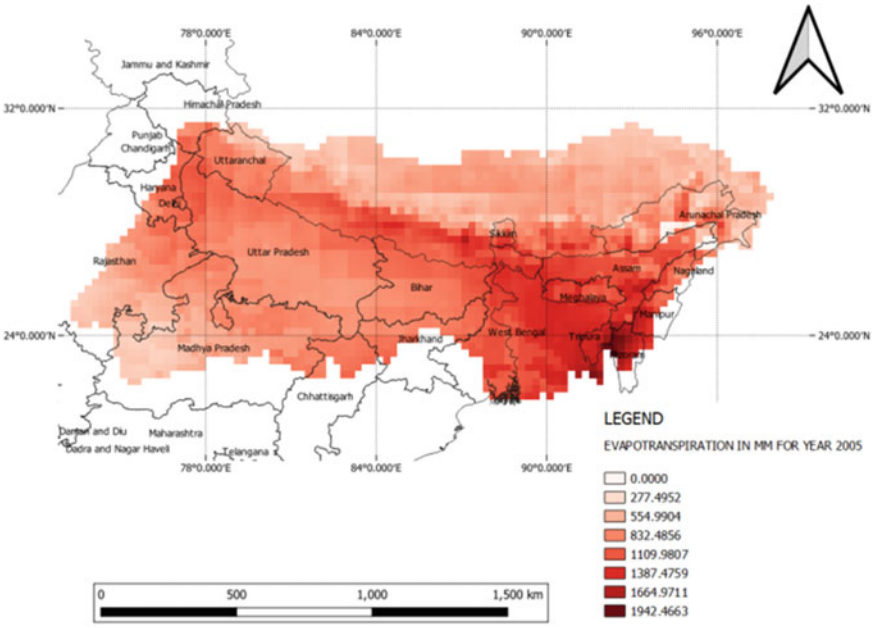

Fig. 7 Evapotranspiration in mm for the Year 2005

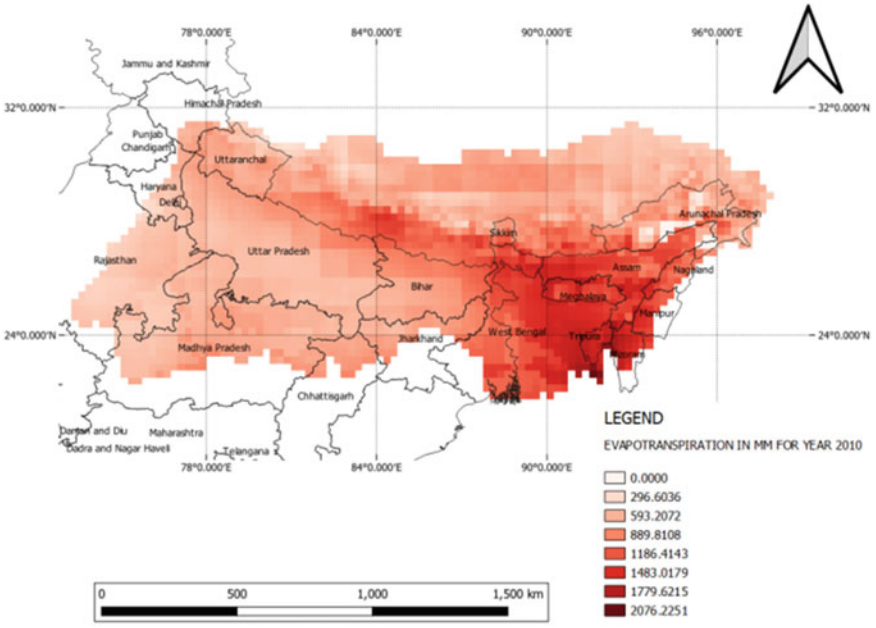

Fig. 8 Evapotranspiration in mm for the Year 2010

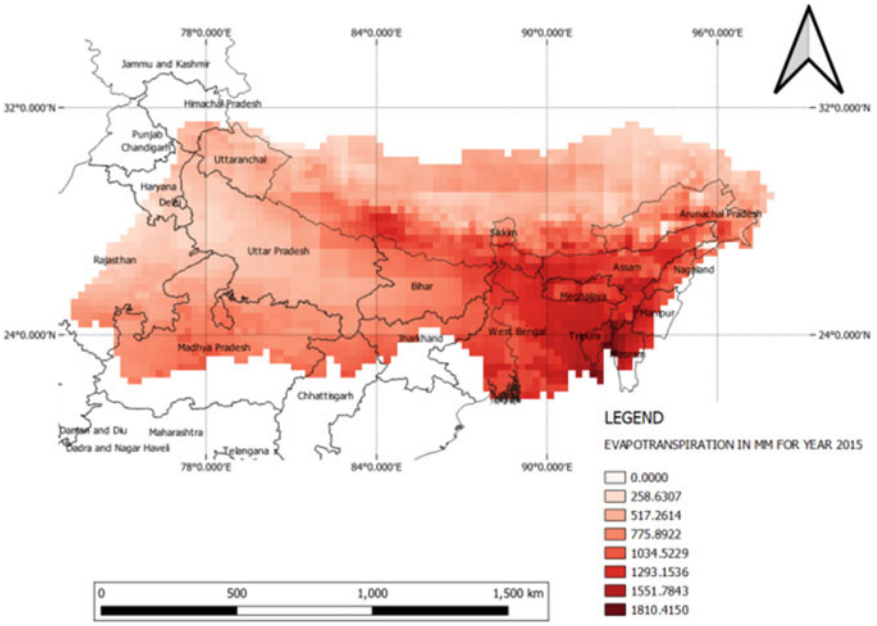

Fig. 9 Evapotranspiration in mm for the Year 2015

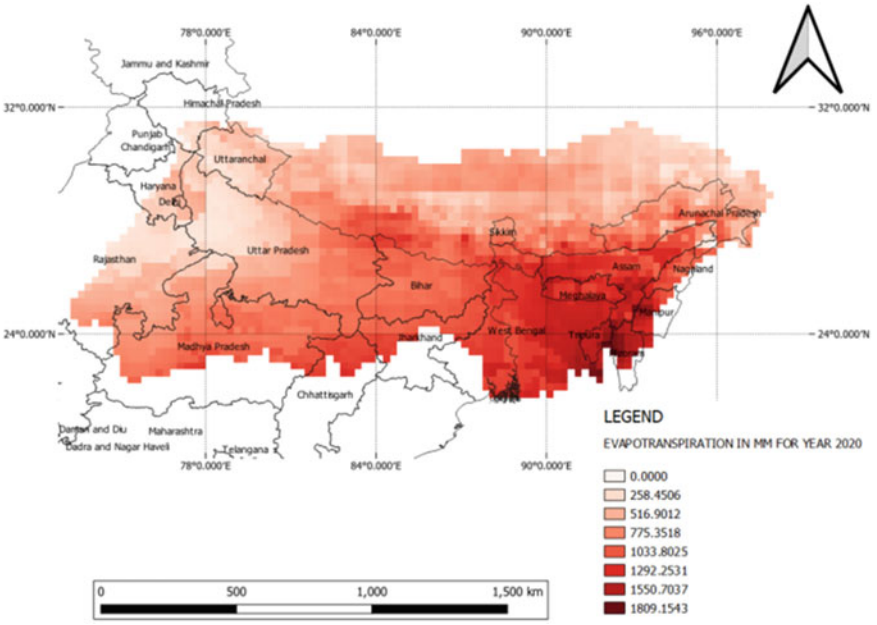

Fig. 10 Evapotranspiration in mm for the Year 2020

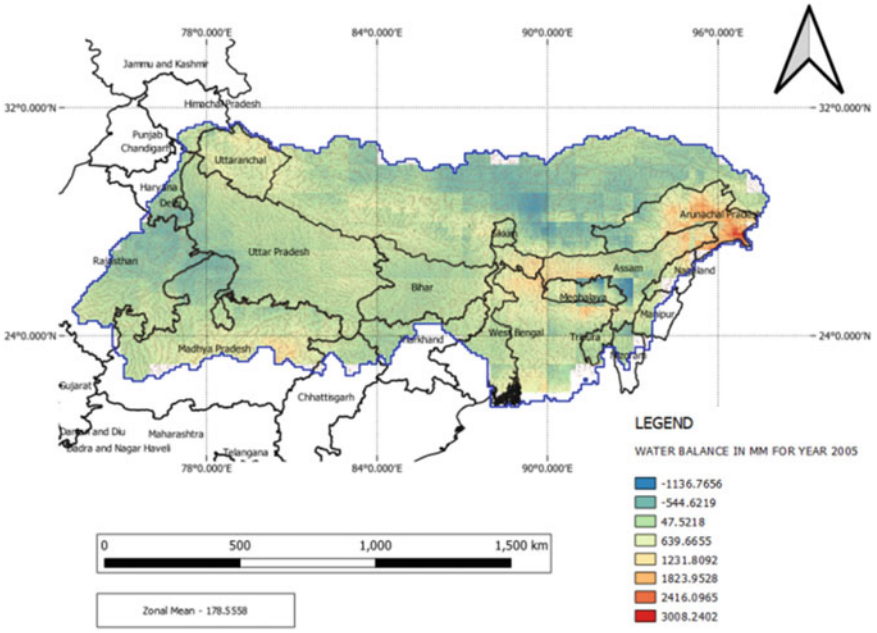

Fig. 11 Water balance in mm for the Year 2005

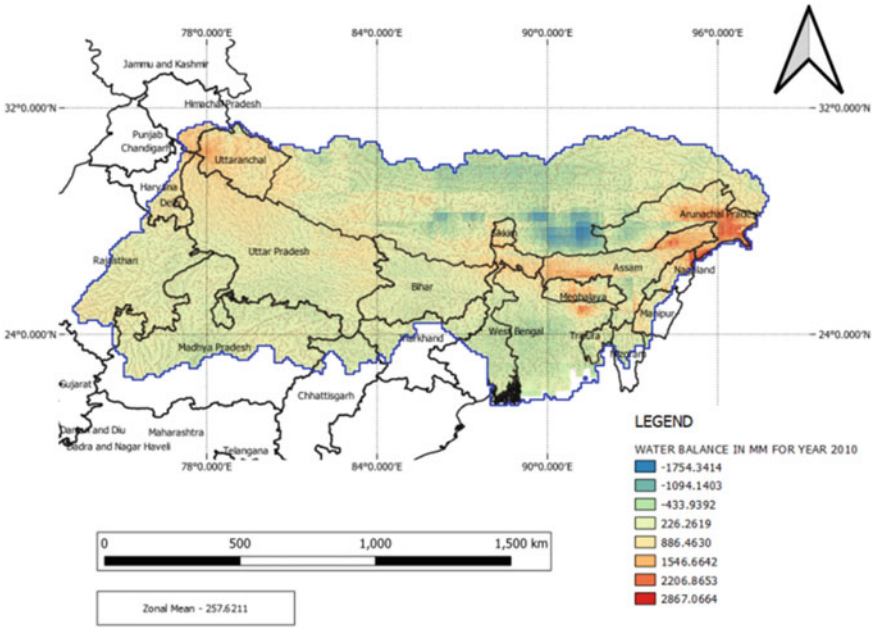

Fig. 12 Water balance in mm for the Year 2010

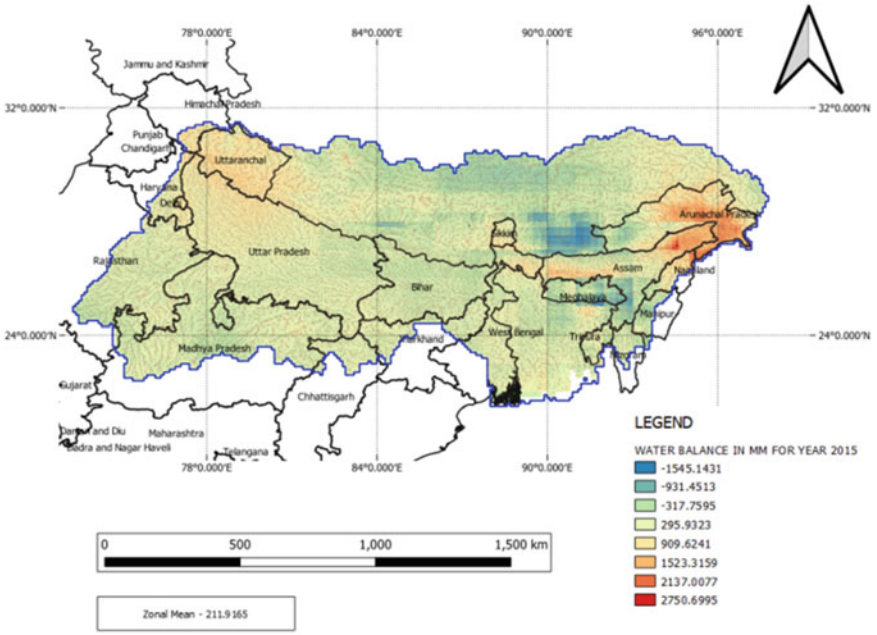

Fig. 13 Water balance in millimeter for the Year 2015

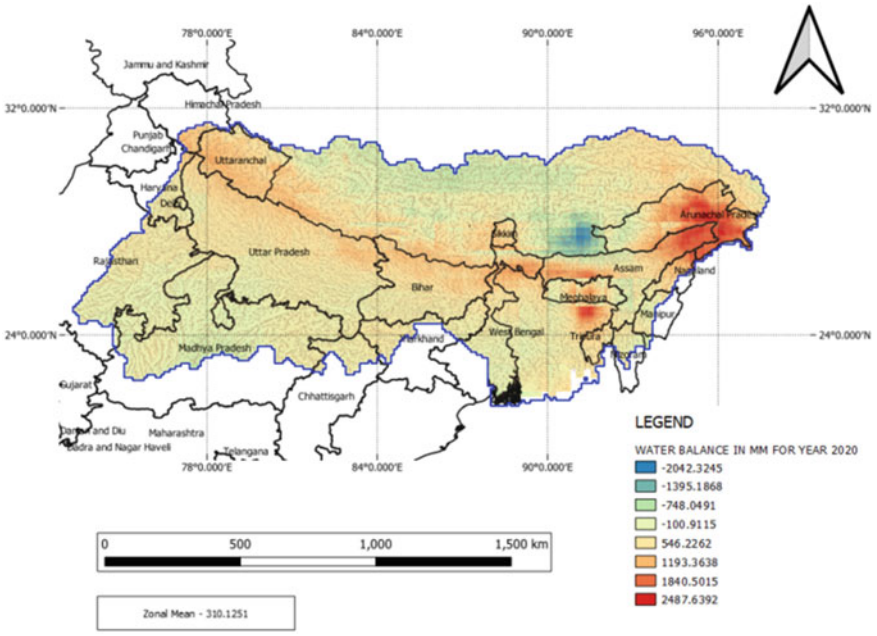

Fig. 14 Water balance in millimeter for the Year 2020

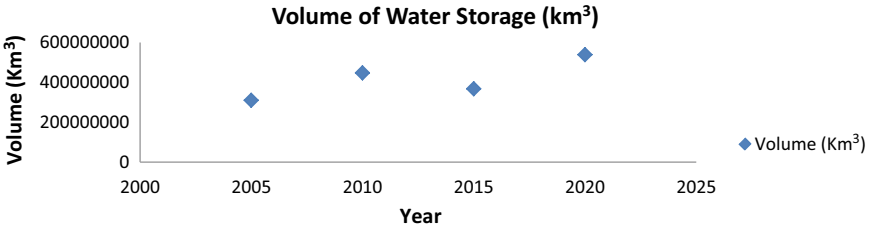

Graph 2 Variations of water storage with year in Ganga–Brahmaputra basin

Table 8 Quantity of water for each year

Year	Basin area (km^2)	Zonal mean (km)	Volume (km^3)
2005	1,736,903.46	178.5558	310,134,186.8
2010	1,736,903.46	257.6211	447,462,980
2015	1,736,903.46	211.9165	368,078,502.1
2020	1,736,903.46	310.1251	538,657,359.2

Table 9 Variations of total merged satellite-gauge precipitation with year in Ganga–Brahmaputra basin

Year	Basin area (Km^2)	Zonal mean (Km)	Volume (Km^3)	Total Satellite merged-gauge precipitation estimate in mm/hr	Total Satellite merged-gauge precipitation estimate in mm/Month
2005	1,736,903.46	178.5558	310,134,186.8	1.8162	1335.687932
2010		257.6211	447,462,980	1.9128	1403.265194
2015		211.9165	368,078,502.1	1.7799	1307.021641
2020		310.1251	538,657,359.2	1.9115	1403.161659

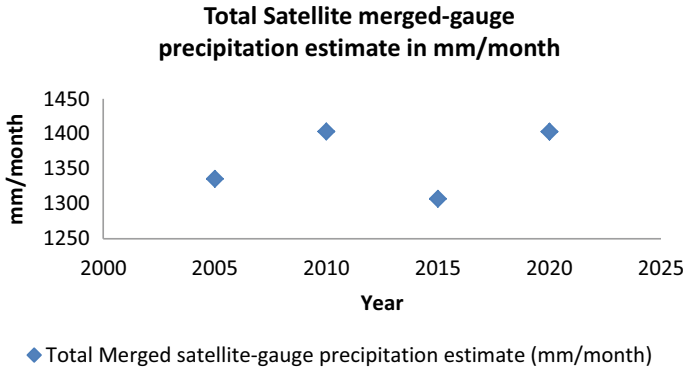

Graph 3 Variations of Total Merged satellite-gauge precipitation with year in Ganga–Brahmaputra basin

References

1. Thornthwaite CW, Mather JR (1957) Instructions and tables for computing potential evapotranspiration and water balance, Laboratory of Climatology, Publication No. 10, Centerton, NJ
2. Singh R, Vajja H, P., Bhatt, C M. (2004) Remote sensing and GIS approach for assessment of the water balance of a watershed/evaluation par télédétection et SIG du bilan hydrologique d'un bassin versant. Hydrol Sci J/Journal des Sciences Hydrologiques 49:131–141. https://doi.org/10.1623/hysj.49.1.131.53997
3. Rodell M, Houser PR, Jambor U, Gottschalck J, Mitchell K, Meng C, Arsenault K, Cosgrove B, Radakovich J, Bosilovich M, Entin JK, Walker JP, Lohmann D, Toll D (2004) The global land data assimilation system. Bull Am Meteor Soc 85:381–394. https://doi.org/10.1175/BAMS-85-3-381
4. Wang W, Cui W (2016) "Evaluation of GLDAS-1 and GLDAS-2 Forcing Data and Noah Model Simulations over China at the Monthly Scale". https://doi.org/10.1175/JHM-D-15-0191.1
5. Neskili NT, Zahraie B, Saghafian B (2017) Coupling snow accumulation and melt rate modules of monthly water balance models with the Jazim monthly water balance model. Hydrol Sci J 62(14):2348–2368
6. Birylo M, Rzepecka Z, Nastula J (2018) "Assessment of the Water Budget from GLDAS Model," 2018 Baltic Geodetic Congress (BGC Geomatics), pp 86–90. https://doi.org/10.1109/BGC-Geomatics.2018.00022
7. Li B, Beaudoing H, Rodell M, (2020) NASA/GSFC/HSL, GLDAS Catchment Land Surface Model L4 daily 0.25 x 0.25 degree GRACE-DA1 V2.2. https://doi.org/10.5067/TXBMLX370XX8
8. Mammoliti E, Fronzi D, Mancini A, Valigi D, Tazioli A (2021) WaterbalANce, a webapp for thornthwaite-mather water balance computation: comparison of applications in two European watersheds. Hydrology 8:34. https://doi.org/10.3390/hydrology8010034